frontiers | Research Topics

New molecular approaches to improve gynecological cancer management

Edited by
Sara Ricardo, Carla Bartosch and Gabriella Lillsunde Larsson

Published in
Frontiers in Oncology

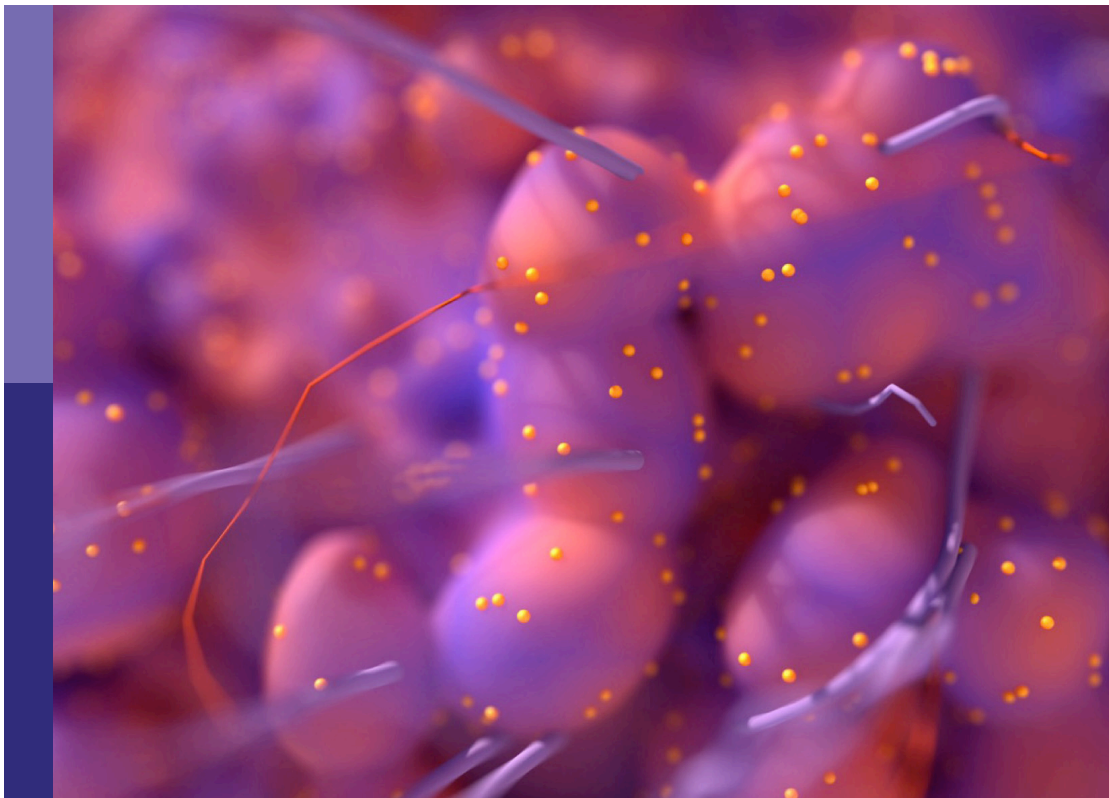

ISSN 1664-8714
ISBN 978-2-8325-2920-1
DOI 10.3389/978-2-8325-2920-1

About Frontiers

Frontiers is more than just an open access publisher of scholarly articles: it is a pioneering approach to the world of academia, radically improving the way scholarly research is managed. The grand vision of Frontiers is a world where all people have an equal opportunity to seek, share and generate knowledge. Frontiers provides immediate and permanent online open access to all its publications, but this alone is not enough to realize our grand goals.

Frontiers journal series

The Frontiers journal series is a multi-tier and interdisciplinary set of open-access, online journals, promising a paradigm shift from the current review, selection and dissemination processes in academic publishing. All Frontiers journals are driven by researchers for researchers; therefore, they constitute a service to the scholarly community. At the same time, the *Frontiers journal series* operates on a revolutionary invention, the tiered publishing system, initially addressing specific communities of scholars, and gradually climbing up to broader public understanding, thus serving the interests of the lay society, too.

Dedication to quality

Each Frontiers article is a landmark of the highest quality, thanks to genuinely collaborative interactions between authors and review editors, who include some of the world's best academicians. Research must be certified by peers before entering a stream of knowledge that may eventually reach the public - and shape society; therefore, Frontiers only applies the most rigorous and unbiased reviews. Frontiers revolutionizes research publishing by freely delivering the most outstanding research, evaluated with no bias from both the academic and social point of view. By applying the most advanced information technologies, Frontiers is catapulting scholarly publishing into a new generation.

What are Frontiers Research Topics?

Frontiers Research Topics are very popular trademarks of the *Frontiers journals series*: they are collections of at least ten articles, all centered on a particular subject. With their unique mix of varied contributions from Original Research to Review Articles, Frontiers Research Topics unify the most influential researchers, the latest key findings and historical advances in a hot research area.

Find out more on how to host your own Frontiers Research Topic or contribute to one as an author by contacting the Frontiers editorial office: frontiersin.org/about/contact

New molecular approaches to improve gynecological cancer management

Topic editors
Sara Ricardo — Universidade do Porto, Portugal
Carla Bartosch — IPO-Porto Research Centre, Portuguese Oncology Institute, Portugal
Gabriella Lillsunde Larsson — Örebro University, Sweden

Topic Coordinator
Miguel Abreu — Portuguese Oncology Institute, Portugal

Citation
Ricardo, S., Bartosch, C., Larsson, G. L., eds. (2023). *New molecular approaches to improve gynecological cancer management*. Lausanne: Frontiers Media SA.
doi: 10.3389/978-2-8325-2920-1

Table of contents

frontiers | Frontiers in Oncology

TYPE Editorial
PUBLISHED 21 June 2023
DOI 10.3389/fonc.2023.1235035

OPEN ACCESS

EDITED AND REVIEWED BY
Sophia George,
University of Miami, United States

*CORRESPONDENCE
Sara Ricardo
sricardo@i3s.up.pt

RECEIVED 05 June 2023
ACCEPTED 07 June 2023
PUBLISHED 21 June 2023

CITATION
Abreu MH, Lillsunde-Larsson G, Bartosch C and Ricardo S (2023) Editorial: New molecular approaches to improve gynecological cancer management. *Front. Oncol.* 13:1235035. doi: 10.3389/fonc.2023.1235035

Editorial: New molecular approaches to improve gynecological cancer management

Miguel Henriques Abreu[1,2], Gabriella Lillsunde-Larsson[3,4], Carla Bartosch[2,5,6] and Sara Ricardo[7,8,9]*

[1]Department of Medical Oncology, Portuguese Oncology Institute of Porto (IPO-Porto), Porto, Portugal, [2]Porto Comprehensive Cancer Center Raquel Seruca (PCCC), Porto, Portugal, [3]Department of Laboratory Medicine, Faculty of Medicine and Health, Örebro University, Örebro, Sweden, [4]School of Health Sciences, Örebro University, Örebro, Sweden, [5]Department of Pathology, Portuguese Oncology Institute of Porto (IPO-Porto), Porto, Portugal, [6]Cancer Biology & Epigenetics Group, Research Center of Portuguese Oncology Institute of Porto (CI-IPO-Porto)/ Health Research Network (RISE@CI-IPO-Porto), Portuguese Oncology Institute of Porto (IPO-Porto), Porto, Portugal, [7]Differentiation and Cancer Group, Institute for Research and Innovation in Health (i3S) of the University of Porto, Porto, Portugal, [8]1H-TOXRUN – One Health Toxicology Research Unit, University Institute of Health Sciences (IUCS), CESPU, CRL, Gandra, Portugal, [9]Department of Pathology, Faculty of Medicine from University of Porto (FMUP), Porto, Portugal

KEYWORDS

gynecology oncology, cervical cancer, ovarian cancer, endometrial cancer, vaginal cancer, vulvar cancer

Editorial on the Research Topic
New molecular approaches to improve gynecological cancer management

Gynecological cancers are major contributors to women cancer burden. Deaths estimatives for 2040, stratified by countries income level (Figure 1), unveils the lack of access to early diagnosis and inequalities in management in countries with low Human Development Index (HDI). In these countries, the average risk of death by gynecological cancers in 2040 is 100% whereas in very high HDI countries the risk raises in average 33%. This estimatives illustrates an accentuation of discrepancies related to the risk of death from gynecological cancer. In countries with less economic resources, cervical cancer continues to be the major cause of death, whereas in very high HDI countries ovarian and endometrial cancer are the ones that contribute most to the mortality index. Developed countries have the responsibility to promote and make available the treatments already implemented that will make the difference for patients' survival.

In very-high HDI countries, ovarian cancer is the most common cause of gynecological cancer death, the epithelial type being the most frequent. The maximization of the success of the treatment requires expert multidisciplinary care provided in specialised institutions. In these dedicated hospitals, epithelial ovarian cancer patients' therapies are nowadays guided, at least in part, by genomic tests, such as detection of mutation in BRCA1/BRCA2 and homologous recombination deficiency genes, which improve effectiveness of therapy (1). In this Research Topic, Abbas-Aghababazadeh et al. identified two markers, ADRB2 and FAP,

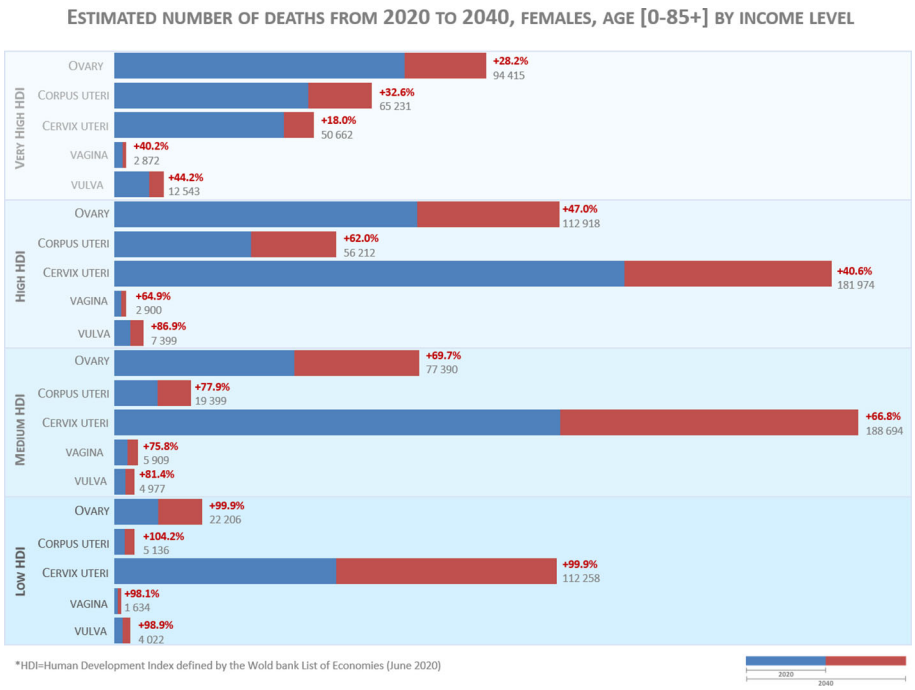

FIGURE 1
Estimated number of deaths from 2020 to 2040. The data source for graphic construction is Ferlay J, Laversanne M, Ervik M, Lam F, Colombet M, Mery L, Piñeros M, Znaor A, Soerjomataram I, Bray F (2020). Global Cancer Observatory: Cancer Tomorrow. Lyon, France: International Agency for Research on Cancer. Data available from: https://gco.iarc.fr/tomorrow, accessed on May 31th 2023.

that were associated with increased odds of optimal debulking. Liang et al. proposes a signature based on adenosine metabolism related genes that could be used as a prognostic biomarker to stratify ovarian cancer patients and Roering et al. demonstrated that Wee1 inhibition can affects several critical functions related to proliferation, cell cycle and division, apoptosis and invasion.

Endometrial Cancer is the second cause of death for gynecological cancer in very high HDI countries but the estimative of deaths are raising in less developed economies. One of the main factors contributing to this trend is obesity. Despite the prevalence of obesity, management of endometrial cancer in very-high HDI countries have the advantage of having well-equipped health services, and most endometrial cancers can be cured by surgery with modern techniques of intraoperative staging. Advances in our understanding of the molecular biology of endometrial cancer have changed the way that we stratify the patients in risk groups for relapse and, because of that, altered the definition of adjuvant therapies (2). However, new biomarkers are still needed to further stratify patients, particularly within non-specific molecular profile group. Regarding this point, Parrish et al. made an elegant review dissecting the role of mutant b-catenin in endometrial cancer progression, describing how its functions may change and drive endometrial cancer progression in CTNNB1 mutant patients.

The deaths estimatives for 2040 show that cervical cancer will be the biggest contributor for gynecological cancers deaths. High-risk subtypes of human papilomavirus (HPV) are the main cause of the disease making this type of gynecological cancer preventable. It is therefore alarming that this available preventive method of vaccination is still far from being implemented in countries with lower incomes. Decrease in cervical cancer mortality is a powerful example of how investment in research translates into gains in terms of patient survival. In very high HDI countries, the mortality risk in 2040 will increase 18% mainly because of metastatic or recurrent disease in which the overall prognosis remains poor. Nevertheless, the incorporation of the anti-VEGF agent bevacizumab (3), and most recent immunotherapy agents like pembrolizumab in 1st line with/without bevacizumab and cemiplimab in 2nd line had extend patients overall survival. In this Research Topic, Zou et al. explored the value of miR-326 as a predictive biomarker for response to neoadjuvant chemotherapy in locally advanced cervical cancer. Another promising auxiliary marker was depicted by Li et al. that found that PAX1 methylation status is highly suggestive of invasive cervical cancer and could be useful before conization clinical decision. Finally, Rai et al. elegantly presented a distinct mechanism of cervical cancer cell death caused by Drug SHetA2.

Primary vaginal cancer is rare, representing only 10% of all vaginal malignant neoplasms and only 1–2% of all gynecological cancers (4). Vaginal cancer, like cervical cancer, is strongly associated with the HPV (4) infection. In this section, Shi et al. performed a longitudinal study where it was observed a potential role of vaginal microbiota in the persistent high-risk HPV infections.

Vulvar squamous cell cancer accounts for 90% of vulvar cancers. Next-generation sequencing studies of Vulvar squamous cell cancer imply human papillomavirus and p53 status play separate roles in carcinogenesis and prognosis (5). As many as 40% of patients with Vulvar squamous cell cancer who are initially managed surgically will have a recurrence, which is often fatal.

Patients who are not candidates for locoregional treatments, have poor overall survival (5). Non epithelial tumours of the vulva are rare and encompassed several histological types. Kong et al. reported a very rare case of a patient with recurrent vulvovaginal paraganglioma with SDHB gene mutation and review of the literature of a recurrent paraganglioma of the vulva.

Gestational trophoblastic disease encompasses a range of pregnancy-related disorders, consisting of premalignant disorders including complete and partial hydatidiform mole, and malignant disorders such as invasive mole and choriocarcinoma (6). Patients' management has long been based on FIGO risk score stratification, but additional studies to further improve management have been limited by the rarity of these tumours. In this regard, Wang et al. studied the serum peptide signatures of 65 gestational trophoblastic neoplasia patients and, in combination with FIGO risk score, they showed its potential to predict outcome in these patients after first-line chemotherapy.

Despite current knowledge of the molecular and genetic events behind gynecological cancers, the field still has a lot to improve. Development of new molecular approaches is essential to early detect and treat in a personalised way these diseases. Another important challenge is to guarantee equal access to gynecological cancer treatments. The concept of global health was evidenced in the recent COVID19 pandemic and will have to be a priority to reduce cancer mortality rate worldwide.

Author contributions

All the authors contributed to the conception and revision of the editorial. SR performed the data analysis and graphical design of Figure 1. All authors contributed to the article and approved the submitted version.

Conflict of interest

The authors declare that the research was conducted in the absence of any commercial or financial relationships that could be construed as a potential conflict of interest.

Publisher's note

References

1. Lheureux S, Gourley C, Vergote I, Oza AM. Epithelial ovarian cancer. *Lancet (London England)* (2019) 393(10177):1240–53. doi: 10.1016/S0140-6736(18)32552-2

2. Crosbie EJ, Kitson SJ, McAlpine JN, Mukhopadhyay A, Powell ME, Singh N. Endometrial cancer. *Lancet (London England)* (2022) 399(10333):1412–28. doi: 10.1016/S0140-6736(22)00323-3

3. Cohen PA, Jhingran A, Oaknin A, Denny L. Cervical cancer. *Lancet (London England)* (2019) 393(10167):169–82. doi: 10.1016/S0140-6736(18)32470-X

4. Jhingran A. Updates in the treatment of vaginal cancer. *Int J Gynecological Cancer* (2022) 32(3):344–51. doi: 10.1136/ijgc-2021-002517

5. Te Grootenhuis NC, Pouwer A-FW, de Bock GH, Hollema H, Bulten J, van der Zee AGJ, et al. Prognostic factors for local recurrence of squamous cell carcinoma of the vulva: a systematic review. *Gynecol Oncol* (2018) 148(3):622–31. doi: 10.1016/j.ygyno.2017.11.006

6. Seckl MJ, Sebire NJ, Berkowitz RS. Gestational trophoblastic disease. *Lancet (London England)* (2010) 376(9742):717–29. doi: 10.1016/S0140-6736(10)60280-2

frontiers | Frontiers in Oncology

TYPE Original Research
PUBLISHED 23 August 2022
DOI 10.3389/fonc.2022.954430

OPEN ACCESS

EDITED BY
Sara Ricardo,
Universidade do Porto, Portugal

REVIEWED BY
Jenny-Maria Jonsson,
Lund University, Sweden
Xiaoyong Fu,
Baylor College of Medicine,
United States
Deborah J. Marsh,
University of Technology Sydney,
Australia

*CORRESPONDENCE
Pia Roering
piaroe@utu.fi
Olli Carpénn
olli.carpen@helsinki.fi

SPECIALTY SECTION
This article was submitted to Gynecological Oncology, a section of the journal Frontiers in Oncology

RECEIVED 27 May 2022
ACCEPTED 27 July 2022
PUBLISHED 23 August 2022

CITATION
Roering P, Siddiqui A, Heuser VD, Potdar S, Mikkonen P, Oikkonen J, Li Y, Pikkusaari S, Wennerberg K, Hynninen J, Grenman S, Huhtinen K, Auranen A, Carpén O and Kaipio K (2022) Effects of Wee1 inhibitor adavosertib on patient-derived high-grade serous ovarian cancer cells are multiple and independent of homologous recombination status. *Front. Oncol.* 12:954430. doi: 10.3389/fonc.2022.954430

Effects of Wee1 inhibitor adavosertib on patient-derived high-grade serous ovarian cancer cells are multiple and independent of homologous recombination status

Pia Roering[1*], Arafat Siddiqui[1], Vanina D. Heuser[1], Swapnil Potdar[2], Piia Mikkonen[3], Jaana Oikkonen[4], Yilin Li[4], Sanna Pikkusaari[1], Krister Wennerberg[5], Johanna Hynninen[6], Seija Grenman[6], Kaisa Huhtinen[1,4], Annika Auranen[7], Olli Carpén[8*] and Katja Kaipio[1]

[1]Institute of Biomedicine and Finnish Cancer Center (FICAN) West Cancer Centre, University of Turku and Turku University Hospital, Turku, Finland, [2]High Throughput Biomedicine Unit, Institute for Molecular Medicine Finland (FIMM), University of Helsinki, Helsinki, Finland, [3]Helsinki Institute of Life Science (HiLIFE), Institute for Molecular Medicine Finland (FIMM), University of Helsinki, Helsinki, Finland, [4]Research Program in Systems Oncology, University of Helsinki and Helsinki University Hospital, Helsinki, Finland, [5]Biotech Research and Innovation Centre (BRIC), University of Copenhagen, Copenhagen, Denmark, [6]Department of Obstetrics and Gynecology, Turku University Hospital and University of Turku, Turku, Finland, [7]Department of Obstetrics and Gynecology and Tays Cancer Centre, Tampere University Hospital, Tampere, Finland, [8]Department of Pathology, Precision Cancer Pathology, University of Helsinki and Helsinki University Hospital, Helsinki, Finland

Objective: A major challenge in the treatment of platinum-resistant high-grade serous ovarian cancer (HGSOC) is lack of effective therapies. Much of ongoing research on drug candidates relies on HGSOC cell lines that are poorly documented. The goal of this study was to screen for effective, state-of-the-art drug candidates using primary HGSOC cells. In addition, our aim was to dissect the inhibitory activities of Wee1 inhibitor adavosertib on primary and conventional HGSOC cell lines.

Methods: A comprehensive drug sensitivity and resistance testing (DSRT) on 306 drug compounds was performed on three patient-derived genetically unique HGSOC cell lines and two commonly used ovarian cancer cell lines. The effect of adavosertib on the cell lines was tested in several assays, including cell-cycle analysis, apoptosis induction, proliferation, wound healing, DNA damage, and effect on nuclear integrity.

Results: Several compounds exerted cytotoxic activity toward all cell lines, when tested in both adherent and spheroid conditions. In further cytotoxicity tests, adavosertib exerted the most consistent cytotoxic activity. Adavosertib affected cell-cycle control in patient-derived and conventional HGSOC cells, inducing G2/M accumulation and reducing cyclin B1 levels. It induced

apoptosis and inhibited proliferation and migration in all cell lines. Furthermore, the DNA damage marker γH2AX and the number of abnormal cell nuclei were clearly increased following adavosertib treatment. Based on the homologous recombination (HR) signature and functional HR assays of the cell lines, the effects of adavosertib were independent of the cells' HR status.

Conclusion: Our study indicates that Wee1 inhibitor adavosertib affects several critical functions related to proliferation, cell cycle and division, apoptosis, and invasion. Importantly, the effects are consistent in all tested cell lines, including primary HGSOC cells, and independent of the HR status of the cells. Wee1 inhibition may thus provide treatment opportunities especially for patients, whose cancer has acquired resistance to platinum-based chemotherapy or PARP inhibitors.

KEYWORDS

adavosertib, patient-derived cell line, high-grade serous ovarian cancer (HGSOC), homologous recombination (HR), drug screen, platinum-resistant ovarian cancer, homologous recombination deficiency (HRD), homologous recombination proficient

Introduction

There is an urgent need for effective therapies for patients with platinum-resistant high-grade serous ovarian cancer (HGSOC). While most HGSOC patients initially respond to the standard first-line platinum–taxane combination chemotherapy, relapse within 18 months is common followed by chemoresistance (1, 2). Reasons for relapse and treatment failure vary, and the progress in improving clinical care has been rather slow. The heterogeneity as well as adaptability of the HGSOC genome to chemotherapy requires new approaches to improve the outcome of the disease (3). A molecular indicator of platinum sensitivity is homologous recombination deficiency (HRD), through either genetic or epigenetic alterations (4). PARP inhibitors have been recently shown to provide a significant clinical benefit for HGSOC patients, but they are effective only on HRD tumors (5, 6). Therefore, there is a special need to identify compounds that are efficient regardless of the homologous recombination status.

In vitro models are essential for identifying effective oncology compounds or drug combinations for any type of cancer, including HGSOC. Until recently, most of the *in vitro* studies have been conducted using publicly available ovarian cancer cell lines that may not represent the HGSOC subtype and that may have undergone a variety of *in vitro* alterations during extensive passaging (7). To overcome this potential hurdle, we created patient-derived HGSOC cell lines and demonstrated that the cells can be cultured and tested under conditions that mimic their stemness properties (8). The cell lines can provide a valuable model of the heterogenous disease and identify personalized treatment options.

Here we tested a panel of 306 drug compounds on HGSOC cells and identified potential effective compounds for further studies (9, 10). Altogether, three patient-derived and two conventional HGSOC cell lines, containing both HRD and HR proficient (HRP) cell types, were screened using the panel, to reveal interesting pharmacologically active substances for further investigation.

In this study, we have focused on drug candidates that have shown effectiveness in most cell models and under both traditional and stemness-like growth conditions. Our rationale was that the selected compounds had the potential for a broader and fast clinical translation. Another criterion was that the candidates must and have been included in clinical trials with any type of cancer and shown promising results in early studies. Of the tested compounds, the Wee1 inhibitor adavosertib (AZD1775) showed the most consistent inhibitory results. Wee1 kinase plays a crucial role in cell-cycle regulation and DNA damage identification and repair in malignant and non-malignant cells, and its inhibition has shown promising results in early phase clinical trials (11–14), including HGSOC. Therefore, we carried out a more detailed analysis on its effects on all five cell lines.

Material and methods

Patients

Tumor and ascites material and clinical information was collected from consenting patients treated at the Department of Obstetrics and Gynecology, Turku University Hospital, Turku,

Finland, as described previously (8, 15). The patients participated in a clinical trial (NCT01276574) and were diagnosed with stage III or IV HGSOC, verified by histopathological evaluation and imaging. Treatment-naive ascites was collected during diagnostic laparoscopy. Patients who were considered primarily inoperable received three cycles of neoadjuvant chemotherapy (NACT), and new samples were taken during the interval debulking surgery (IDS). For this study, we used cell lines from three patients (OC002, M022i, and M048i). The patients' age range at the time of the diagnosis was between 61 and 66 years. Progression-free survival (PFS) was 3.1 to 10.1 months and overall survival (OS) 4.0 to 35.8 months. Detailed clinical information is presented in Table S1.

Cell culture

Two patient-derived cell lines were established from ascites (OC002 and M022i), of which OC002 was treatment-naive and M022i was from IDS. One cell line originated from omental metastasis (M048i) and was from IDS (8). The cell lines were characterized by DNA sequencing (see *DNA/RNA sequencing and functional assessment of homologous recombination capacity*). In addition to these patient-derived cell lines, two conventional HGSOC cell lines were explored: CAOV3 (RRID:CVCL_0201, American Type Culture Collection, ATCC, USA) and OVCAR8 (RRID:CVCL_1629, National Cancer Institute, NCI, USA).

Cells were grown at 37°C, at 5% CO_2. The OVCAR8 cell line was cultured in an RPMI medium; OC002, M022i, M048i, and CAOV3 cells were cultured in a DMEM-F12-based spheroid medium as described previously (8). To sustain adherent cell cultures for IncuCyte experiments and immunostainings, a modified OCMI medium was used instead of a spheroid medium: 1:1 of medium 199 (Gibco) and DMEM/F-12 (Lonza) supplemented with 5% FBS (Lonza), 2% ITS (Corning), 100 µg/ml penicillin/streptomycin (Gibco Life Technologies), 0.5 ng/ml 17 beta-estradiol (Merck), 0.2 pg/ml triiodothyronine (Sigma), 0.025 µg/ml all-trans retinoic acid (Merck), 13.75 µg/ml insulin (Sigma), 25 ng/ml cholera toxin (Sigma), 0.5 µg/ml hydrocortisone (Sigma), and 10 ng/ml EGF (Gibco Life Technologies).

DNA/RNA sequencing and functional assessment of homologous recombination capacity

To genetically characterize tumors and identify patient-specific *TP53* mutations, we sequenced available fresh frozen tissue or ascites samples, whole-blood buffy coat samples (germline reference), and/or cells from the cultures. Germline reference was available for M022i and M048i, fresh frozen tumor tissue or ascites for M048i (N = 4) and OC002 (N = 1), and cultured cells for M022i and M048i. DNA/RNA was extracted from samples with AllPrep DNA/RNA Mini Kit (Qiagen). Sequencing was performed in the BGI (Beijing Genomics Institute) as whole-genome sequencing (WGS) with HiSeq X Ten or with whole exome sequencing (WES) with Agilent SureSelect Human All Exon V5 using HiSeq 2000.

Data were aligned to GRCh38.d1.vd1 (median coverage 48, Table S2), and mutations were called with Mutect2 [GATK4 (16)]. Mutation pathogenicity was evaluated using COSMIC (17), ClinVar (18), and CADD (19) for exonic non-synonymous mutations, indels, and splicing. Cell identity was confirmed with contamination test (GATK4) for M022i and M048i where sequencing data from both cells and germline reference were available. All patients were identified with high variant allele frequency, pathogenic *TP53* mutations, which were used to verify cell identity in the cultures (Table S2). In addition, the mutational status of other HR-related genes was identified (list of genes in Table S3). Mutational signatures were fitted with COSMIC v3.1 SBS signatures based on SigProfiler attribution (20) to assess HRD mutational signature SBS3.

Functional homologous recombination status was analyzed for OC002 and M048i cells as described in (21). Epithelial cells (cytokeratin positive) in the G2 phase (cyclin A2 positive) were stained with RAD51 to distinguish between RAD51-positive and -negative cells. HR-score was obtained by calculating the percentage of RAD51-positive cells. At least 300 cells were counted per sample. HR-scores below 35% were considered HRD (Table S2).

To investigate whether the cell lines were different regarding multidrug resistance (MDR), we analyzed RNA expression data of the ABC transporters (ATP-binding cassette transporters). The results are provided as reads per kilobase per million (RPKM) values, normalized to GAPDH expression. A heatmap was produced using Log2+1 values at the publicly available web software Heatmapper (heatmapper.ca) (22).

High-throughput drug sensitivity and resistance testing

The five cell lines were subjected to high-throughput screening (HTS) with a panel of 306 clinical FDA- and/or EMA-approved and emerging oncology drug compounds (Table S4). Screening was performed at the Institute for Molecular Medicine Finland (FIMM) as described previously (9, 10). While a part of the drug screen data has been published earlier (8), here two additional patient-derived HGSOC cell lines are presented: M048i and OC002. Cells were tested in five different drug concentrations spanning a relevant 10,000-fold concentration range for each individual drug in conventional adherent and stem-like spheroidal cell culture conditions as was described earlier (8). Cell viability was measured with CellTiter-Glo (Promega, Madison, Wisconsin, USA) after 72 h of exposure to the drugs in at least five separate experiments with triplicate wells.

The data were analyzed with the quantitative scoring approach, where a multiparameter area under a curve sensitivity calculation called the drug sensitivity score (DSS) was used (9, 10). This integration combines the model-based and area-based drug response calculations. The DSS was calculated for each drug, and responses were compared to human healthy bone marrow-averaged controls to evaluate the specific selective DSS (sDSS) as previously described (9, 10). Previously reported cutoff values of sDSS were used: sDSS >5 for effective drugs and sDSS >10 for highly effective drugs (23). The drug sensitivity and resistance testing (DSRT) data were analyzed using the web-based pipeline BREEZE (https://breeze.fimm.fi/) (24).

The cytotoxic effect of adavosertib (Selleckchem, Munich, Germany) was further validated with a CellTiter-Glo® (Promega) cell viability test. To test cells' sensitivity to cisplatin, 5,000 cells/well were plated on a 96-well plate in triplicates. Cisplatin was added in concentrations of 0.01–100 μM, and cell viability was measured after 72 h of incubation. Luminescence was detected with a Victor2 luminometer (Wallac, Turku, Finland). The IC50 value of adavosertib for each cell culture was calculated, and a dose of 500 nM was selected to be used for the functional experiments. The IC50 value for cisplatin was calculated using log-transformed data and logarithmic trend line.

Flow cytometry

The M048i, OC002, CAOV3, and OVCAR8 cells were investigated with a BD LSRFortessa™ flow cytometer (BD Biosciences, NJ, USA). For each measurement, 10,000–30,000 events were assessed. The flow cytometry data were analyzed with Flowing Software 2.5.1 (Mr. Perttu Terho, Turku Bioscience Centre, Turku, Finland). Duplicates of each sample were tested, and the experiment was repeated a minimum of three times.

Early and late apoptoses were detected after 48 and 72 h of treatment with adavosertib with an Annexin V-FITC Apoptosis Detection Kit (ab14085, Abcam). Samples were processed according to the kit's protocol.

Cell-cycle phases were detected with a Click-iT EdU Flow Cytometry Assay Kit Pacific Blue (C10425, Invitrogen). Cell-cycle progression was studied in vehicle- and adavosertib-treated cells at time points 24, 48, and 72 h. Samples were collected, and the protocol was performed according to the manufacturers' instructions.

Cell proliferation

Cell proliferation of the HGSOC cell lines was inspected for 72 h at 2-h intervals with an IncuCyte S3 high-content imager (Essen BioScience, Ann Arbor, MI). Cells were plated in 96-well plates (Greiner Bio-One) to be 10% confluent and treated with 500 nM adavosertib. Cells treated with vehicle (DMSO) were used as control in all the experiments. Each sample was measured in triplicate, and the experiments were repeated a minimum of three times. Proliferation was measured by confluence area by IncuCyte software (Essen BioScience).

Wound healing assay

Wound healing of the HGSOC cells was measured for 72 h at 2-h intervals with an IncuCyte S3 high-content imager (Essen Bioscience, Ann Arbor, MI). Experiments were performed on 96-well plates (ImageLock, Essen BioScience) with adavosertib (500 nM) or vehicle (DMSO). Each sample was measured in triplicate, and the experiments were repeated a minimum of three times. Relative wound density was analyzed by IncuCyte software (Essen BioScience). The wells were precoated with Geltrex (Gibco) for migration experiments and with Matrigel (100 μg/ml, Corning, Bedford, MA, USA) for invasion experiments. Wells were pretreated for 24 h with adavosertib (500 nM) before wound making with a wound-maker provided with IncuCyte S3 (Essen Bioscience). In the invasion experiments after wound making, the cells were covered with 50 μl Matrigel (2 mg/ml) for 30 min in the incubator; thereafter, adavosertib was added.

Western blotting

The effect of adavosertib on the cell cycle was investigated in the cell cultures treated for 72 h. Cells were grown in a DMEM/F-12 or RPMI medium and harvested and lysed with a RIPA Buffer supplemented with protease inhibitors. Protein concentrations were measured using a Bio-Rad protein assay kit according to the manufacturer's instructions. Equal amounts of proteins in the Laemmli buffer were separated in 4%–20% polyacrylamide PROTEAN® TGX™ Precast Protein Gels (Bio-Rad) and transferred to the 0.2-μm PVDF membrane using the Trans-Blot Turbo Transfer System (Bio-Rad). Membranes were blocked with 5% BSA (bovine serum albumin) in Tris-buffered saline with 0.05% Tween 20 (TBST) and probed with primary antibodies diluted in the same solution. Primary antibodies used in the Western blotting were rabbit monoclonal anti-Cyclin B1 (D5C10, 1:1,000, Cell Signaling), rabbit monoclonal anti-Cyclin E1 (EP435E, 1:500, Abcam), mouse anti-PCNA (PC10, 1:2,000, Cell Signaling), and mouse monoclonal anti-γH2AX (phospho S139, 1:1,000, Abcam). GAPDH-HRP-conjugated (1:5,000, Abcam) or mouse monoclonal anti-α-Tubulin (B-5-1-2, 1:1,000, Sigma) was used as control for protein loading. The secondary antibodies were HRP-conjugated swine anti-rabbit and rabbit anti-mouse immunoglobulins (1:2,500, Dako, Glostrup, Denmark) diluted in a blocking solution. Membranes were washed three times with TBST between antibody incubations. Bound proteins were detected by enhanced chemiluminescence using ChemiDoc™ Gel Imaging System (Bio-Rad), and the signals were quantified using ImageJ.

Immunostaining and nuclear morphology analysis

Cells were grown on glass slides with a Geltrex (Gibco) coating and a modified OCMI or RPMI medium. After 72 h of incubation with 500 nM adavosertib, the cells were fixed for 10 min in 4% paraformaldehyde and washed with PBS. Blocking was performed with 5% BSA and 0.5% Triton X-100 in PBS for 30 min. Slides were incubated at room temperature for 60 min with a primary antibody diluted in a blocking buffer and thereafter for 60 min with a secondary antibody. The slides were washed twice after the antibody incubations with PBS and embedded in a mounting medium containing DAPI for staining nuclei (ProLong Gold Antifade Mountant with DAPI, Thermo Fisher). The following primary antibodies were diluted in the blocking buffer: mouse monoclonal anti-α-Tubulin (B-5-1-2, 1:100, Sigma) and mouse monoclonal anti-γH2AX (phospho S139, 1:500, Abcam). Alexa Fluor 555 Donkey anti-Mouse (1:400, Invitrogen) was used as a secondary antibody together with Alexa Fluor 488-conjugated phalloidin (1:300, Invitrogen, Carlsbad, CA) for actin filament visualization.

Nuclear morphology was assessed after 72 h after treatment with vehicle or 500 nM adavosertib by staining the tubulin for cell structure and embedding in mounting medium containing DAPI for the cell nucleus staining. At least 100 cells were counted in each sample, and the nuclei were categorized as normal, abnormal, or multinuclear. Images were taken with a Nikon Eclipse Ni fluorescence microscope, and different channels were merged using ImageJ v1.53a software (http://rsbweb.nih.gov/ij/).

Statistics

The IC50 values for the adavosertib cytotoxicity validation were acquired using a sigmoidal dose–response curve. The differences in proliferation, wound healing, cell cycle, apoptosis, nuclear abnormalities frequencies, and protein levels between vehicle- and adavosertib-treated cells were compared using the two-sided *t*-test on freely available *VassarStats: Website for Statistical Computation* (www.vassarstats.net). *P* values ≤0.05 were considered statistically significant.

Results

Several compounds effectively kill HGSOC cells

The drug sensitivity testing was performed under two growth conditions, i.e., conventional adherent and spheroid conditions inducing stemness features and mimicking the environment of the malignant cells in ascitic fluid. We employed a correlation plot analysis for sDSS to assess the condition-related variations in drug sensitivity (Figure S5). The number of effective (sDSS >5) drugs from the whole screen of 306 drug compounds varied between screened cell lines and was partially dependent on growth conditions. Of the primary HGSOC cell lines, M048i was sensitive to 28 compounds in adherent cell culture conditions, OC002 to 59 compounds, and M022i to 72 compounds. Of the conventional cell lines, OVCAR8 showed sensitivity to 74 compounds and CAOV3 to 102 compounds (Figure 1A and Table S6). The results demonstrate that compounds target cancer cells from individual patients differently, possibly reflecting the variability of individual patients' response to chemotherapy/targeted therapy. While there was variation between the patient-derived cell lines, they were generally more resistant than the conventional HGSOC cell lines.

Ten clinically interesting drug compounds from the initial screen were selected for further investigation according to two criteria: literature search and ongoing clinical studies in HGSOC or other cancers (Figure 1A). In more detailed cytotoxicity assays, the cellular responses to these 10 drug compounds were variable (Figure 1B). The patient-derived M048i cells were relatively resistant to all of the 10 oncology compounds. Similarly, M048i cells were extremely resistant to cisplatin (IC50 >100 μM) while in other cell lines IC50 varied between 1.3 and 11.7 μM (Figure S7 and Table S8). Five of the drug compounds were categorized as highly effective (sDSS ≥10) in the majority of the HGSOC lines: Wee1 inhibitor adavosertib and four Hsp90 (heat shock protein 90) inhibitors BIIB021, tanespimycin, luminespib, and alvespimycin (Figure 1B). Of these compounds, the Wee1 inhibitor adavosertib was chosen for further research due to its ongoing clinical interest and the validation results. Table S9 shows the sDSS values for the 10 investigated compounds tested in adherent or spheroid culture conditions. Adavosertib was cytotoxic for all cells except M048i, with IC50s between 578 and 785 nM (Figure 2A and Table S9).

Adavosertib induces apoptosis and causes G2/M arrest in HGSOC cells

To study whether adavosertib induces apoptosis, HGSOC cells were treated for 48–72 h before labeling with Annexin V. Adavosertib-induced apoptosis was evident in all of the examined cell lines, surprisingly also including M048i, the most resistant cell line in viability tests (Figures 2B, C, Table S10). The total number of apoptotic cells after a 72-h treatment with adavosertib (500 nM) increased from 8.9% to 26.7% in OVCAR8, from 12.6% to 31.5% in CAOV3, and from 11.9% to 25.2% in the M048i cell line.

The effect of adavosertib on the cell cycle was examined after treatment for 24, 48, and 72 h. When compared with control cells, significant G2/M accumulation and a reduction in the G1 cell-cycle phase were found in all four evaluated cell lines (Figure 3B). As compared to vehicle-treated cells, adavosertib

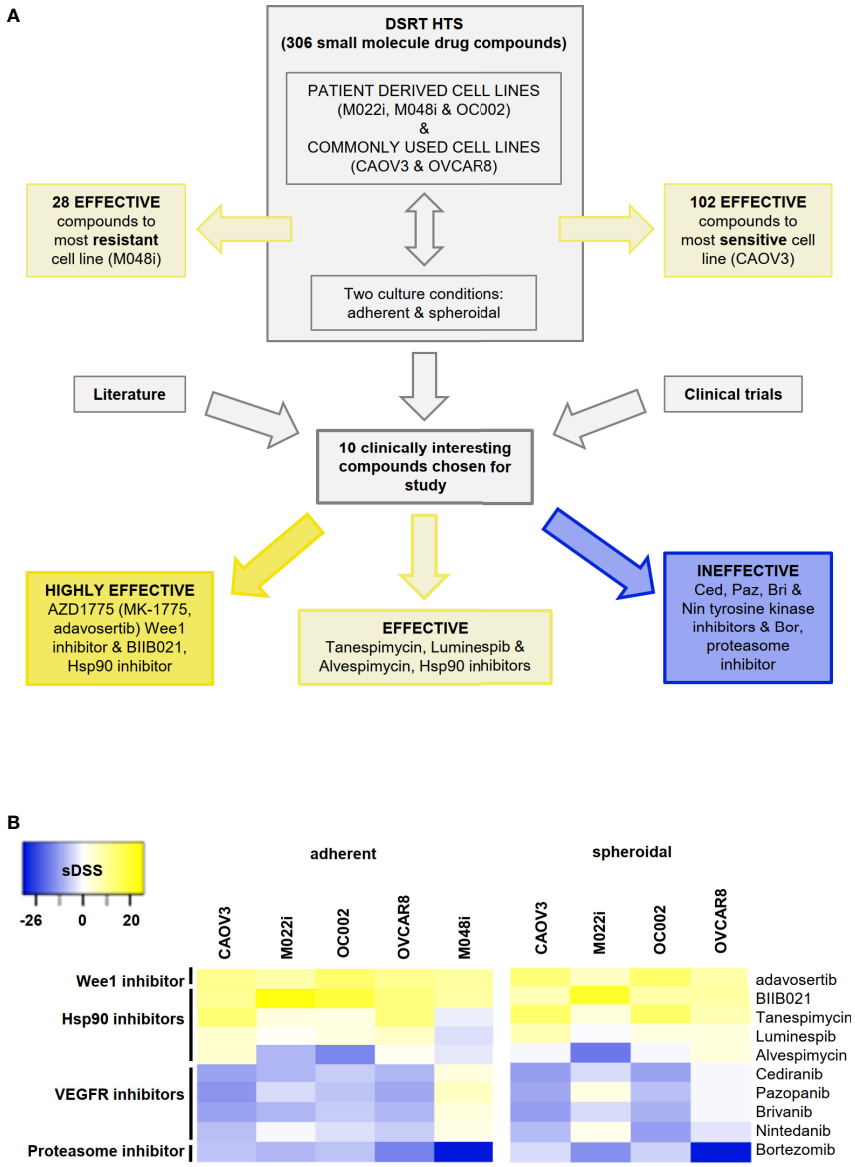

FIGURE 1
High-throughput drug sensitivity and resistance testing (DSRT) with 306 drug compounds. **(A)** Study design and basis for selection of small molecules for further analyses. DSRT was performed with five HGSOC cell lines in adherent and spheroidal culture conditions. The number of effective compounds varied between 28 (M048i) and 102 (CAOV3). Based on literature search and ongoing clinical trials, 10 compounds were selected for further cytotoxicity tests, which divided compounds into three categories: highly effective, effective, and ineffective. **(B)** Heatmap of the selected drug compounds based on sDSS (selective drug sensitivity score) values tested in adherent and spheroidal conditions. Bright yellow = sensitive, dark blue = resistant; sDSS >5 effective, sDSS ≥10 highly effective. M048i spheroidal data not available.

diminished the proportion of G1 cells by 27%–54%, dependent on the cell line. The accumulation of G2 cells was clear in all tested cell lines. In OVCAR8, the percentage of G2 cells of total cell amount after adavosertib treatment was 58.3% as compared to 14.4% in untreated cells. In CAOV3, M048i, and OC002 cell lines, the percentages of G2 cells in treated cells and vehicle were 45.3% and 16.0%; 54.0% and 23.9%; and 57.2% and 24.8%, respectively. In addition, a trend toward a reduced S phase was seen in all cell lines, but the difference was statistically significant only in CAOV3 and OC002 (Figure 3B, Table S11).

Interestingly, the cell-cycle regulation of the most resistant cell line M048i appeared abnormal. In the untreated samples, very few cells were in the S phase and the same trend was observed in the adavosertib-treated cells (Figure 3B). However, a drift from G1 to G2/M in the treated cells was detected, as expected. Although the result of the cell viability test showed

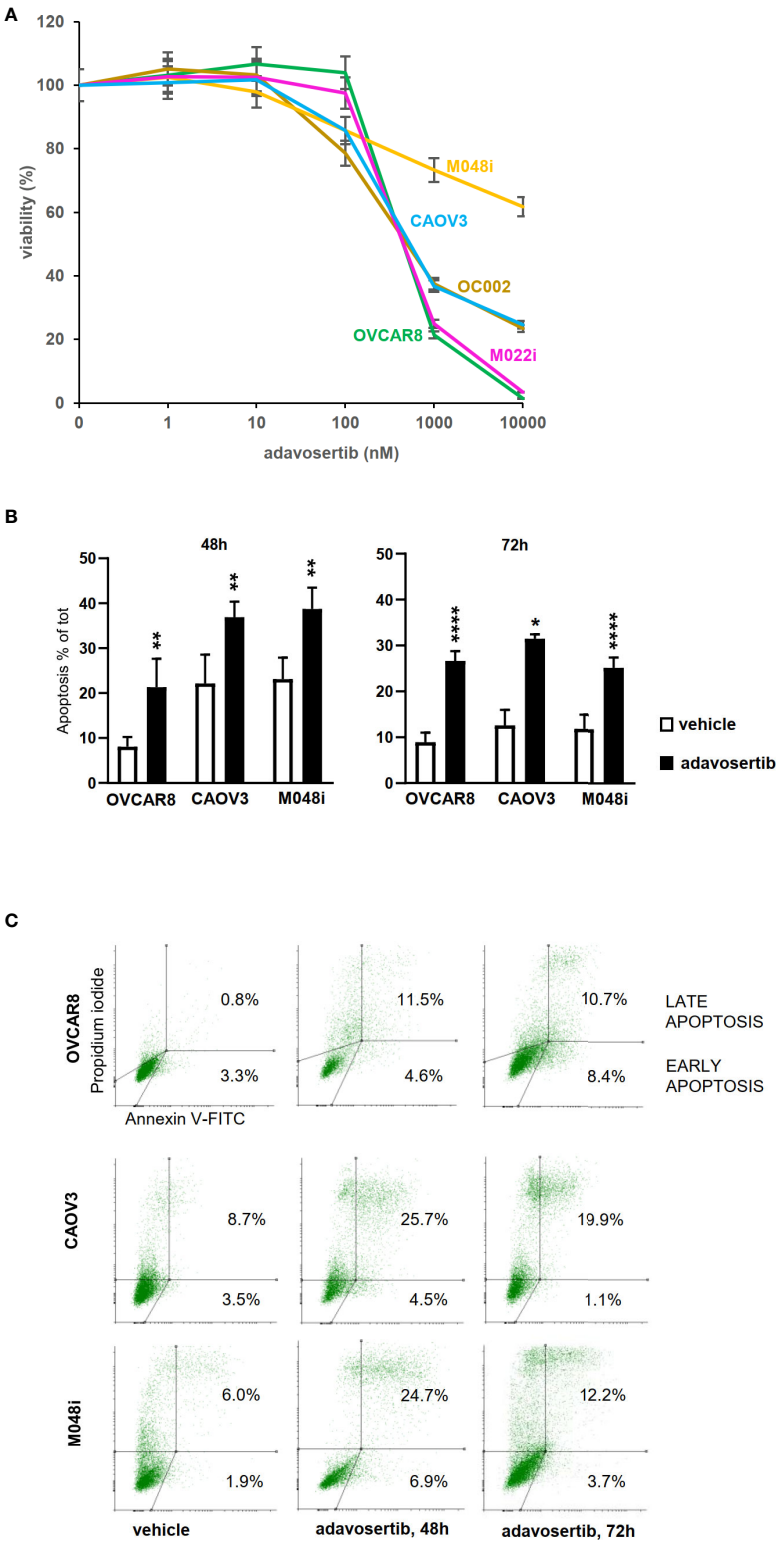

FIGURE 2
Effects of adavosertib on cell viability and apoptosis. **(A)** Viability was assessed after a 72-h treatment with adavosertib in five different concentrations (1–10,000 nM) (±SD). **(B)** Apoptosis was measured in three HGSOC cell lines (OVCAR8, CAOV3, and M048i) with annexin V staining detected by flow cytometry. Apoptotic cell populations (% of total cell amount, ±SD) were significantly elevated in all cell lines after 48 and 72 h of treatment with 500 nM adavosertib as compared with the control cells (p-value: ns = $p > 0.05$, *$p \leq 0.05$, **$p \leq 0.01$, and ****$p \leq 0.0001$). **(C)** Distribution of early and late apoptotic cell populations (% of total number of cells).

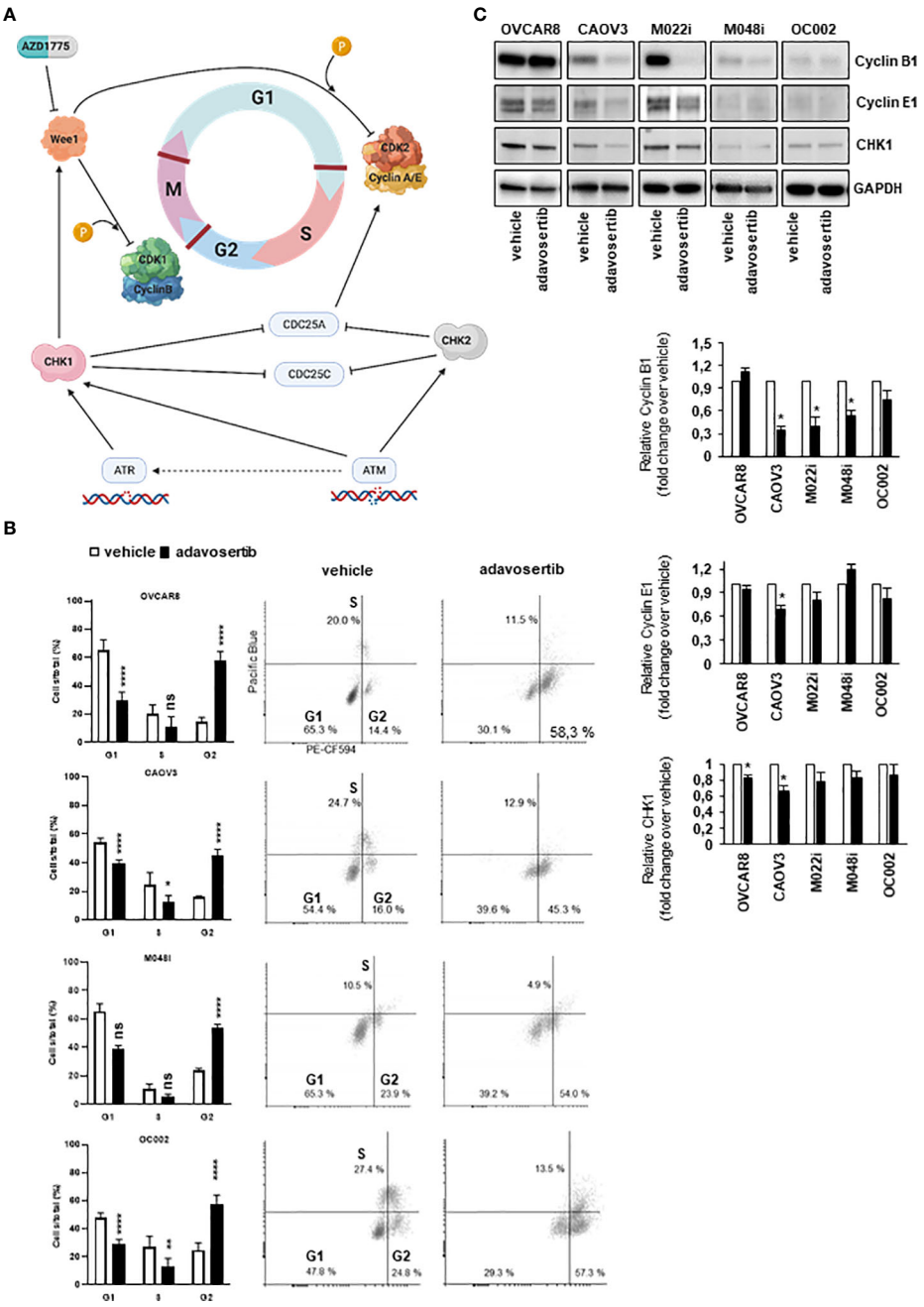

FIGURE 3
Effect of adavosertib on the cell cycle. **(A)** Illustration of cell-cycle checkpoints involved in DNA-damage response (DDR) pathways, including the role of Wee1. In HGSOC cells, the G1/S checkpoint is dysfunctional due to p53 mutation, while the G2/M checkpoint remains functional in DNA-damage repair. Inhibition of Wee1 by adavosertib (AZD1775) disables the G2/M checkpoint, thereby enabling a cell with damaged DNA to enter mitosis. Created with BioRender.com. **(B)** HGSOC cells were labeled with 5-ethynyl-2-deoxyuridine (EdU), and cell-cycle phases were monitored with flow cytometry. The distribution of cells in the G1, S, and G2/M phases is shown after 72 h of treatment with adavosertib (500 nM) or vehicle. White bars = vehicle and black bars = adavosertib treated (average, ±SD). Dot blots present the distribution of cells with EdU staining. **(C)** Western blot analysis of cyclin B1, cyclin E1, and Wee1 pathway regulating CHK1 protein in adavosertib- (500 nM) and vehicle-treated cells after 72 **(h)** The bars show quantitative analysis of cyclin B1, cyclin E1, and CHK1, normalized to GAPDH, using ImageJ software. The values shown are the mean ± SE of three separate experiments. Significant difference between vehicle and adavosertib treatment was determined by the *t*-test at ns = $p > 0.05$, *$p \leq 0.05$, **$p \leq 0.01$ and ****$p \leq 0.0001$.

relative resistance of M048i cells to adavosertib (Figure 2A), the increased apoptosis and G2/M accumulation suggest that adavosertib has some beneficial effect on these patient-derived HGSOC cells.

The cell-cycle alterations were further explored by Western blot analysis of cyclin E1 and cyclin B1, which regulate the G1/S and G2/M transition, respectively (Figure 3A). The level of cyclin B1 was reduced in most cell lines after adavosertib treatment, although it remained normal in OVCAR8 cells (Figure 3C). Cyclin E1 expression was reduced in CAOV3 and M022i following 72 h of adavosertib treatment (Figure 3C). Similarly, the CHK1 protein, which is a key regulator upstream of the Wee1 pathway (Figure 3A), was studied. After adavosertib therapy, there was a reduction in CHK1 expression (Figure 3C) in all cell lines. It is worth noting that the amounts of both cyclins and CHK1 differed greatly among the studied cell types, with M048i and OC002 expressing very low levels (Figure 3C).

Adavosertib reduces proliferation and migration in HGSOC cells

Proliferation was studied by measuring the confluence area of cell cultures at 2-h intervals. Adavosertib significantly reduced proliferation in all the tested cells ($P < 0.0001$; *t*-test) (Figure 4A). Although two of the patient-derived cell lines (M022i and OC002) proliferated very slowly, a clear (58.1% and 67.0%) inhibition of proliferation was observed after 72 h of treatment. For the faster proliferating M048i, CAOV3, and OVCAR8, the reduction was 55.2%, 38.0%, and 82.3%, respectively. Here, again we were not able to show any difference in proliferation between the adavosertib-resistant cell model M048i as compared to the more sensitive HGSOC lines.

The expression of the proliferation marker PCNA (proliferating cell nuclear antigen) was detected with Western blotting to confirm the confluence area-based proliferation result. The amount of PCNA decreased after 72 h of adavosertib treatment in the tested HGSOC lines (Figure 4B), except for OVCAR8 in which PCNA remained unchanged.

Wee1 inhibition reduced the mobility of all HGSOC lines as evaluated by both migration and invasion assays (Figure 4C and Figure S12), with migration showing a greater reduction than invasion through the extracellular matrix.

Adavosertib induces DNA damage regardless of HR status

The impact of Wee1 inhibition on DNA damage and nuclear morphology was further addressed. Apart from M022i, adavosertib induced a significant increase in the number of aberrant nuclei (multinucleated, bud, and micronuclei) in the HGSOC lines (Figure 5A). Similarly, using both Western and immunofluorescence imaging, the DNA-damage marker γH2AX (phospho S-139) was clearly upregulated in all the tested cells (Figures 5B, C).

The efficacy of many current HGSOC drugs depends on the homologous recombination DNA repair capacity of the cancer cells. Therefore, we wanted to evaluate whether this is also the case for adavosertib. The HGSOC lines were evaluated for homologous recombination (HR) capacity using both genomic (Table S2) and functional (Figure S13 and Table S14) tests. Of the cell lines, OC002 and OVCAR8 were HR-deficient (HRD) while M022i, M048i, and CAOV3 were HR-proficient (HRP) (Table S2, Figure S13, and Table S14). The result suggests that the effects of adavosertib are independent of the HR status of the cells.

Discussion

Despite the advances in understanding the molecular background of HGSOC, patients who do not initially respond or acquire resistance to platinum compounds or PARP inhibitors have limited treatment options. Based on the high-throughput screen of HGSOC cell lines, and with a focus on compounds in the clinical development, we identified two compound groups cytotoxic to HGSOC independent of the cell culture method: Wee1 inhibitor (adavosertib, AZD1775) and Hsp90 inhibitors (BIIB021, alvespimycin, luminespib, and tanespimycin). In a further validation using three patient-derived and two conventionally available HGSOC cell lines, adavosertib provided the best cytotoxicity result. Wee1 has already proven to be a potential target in genomically unstable cancers, including HGSOC, due to its role in cell-cycle control and DNA-damage response (DDR) pathways [reviewed in (25–28)]. Our findings presented here indicate that adavosertib inhibits HGSOC cell growth at multiple levels. Importantly, the effect in our study material is independent of the homologous recombination capacity of the cells and thus potentially effective in patients who do not benefit from current treatments.

We also noticed generally similar effects on the three HRP and two HRD cell lines. Additionally, adavosertib inhibited equally well patient-derived HGSOC cells and the publicly available HGSOC cell lines. One of the patient-derived HGSOC cell lines, M048i, was less responsive than the other cell lines in the high-throughput cytotoxicity assay to most of the 306 drugs including adavosertib for reasons that remain unclear. No significant difference was found in the DNA sequencing or RNA expression data of the multidrug resistance (MDR) ABC transporters (ATP-binding cassette transporters) compared to other cell lines (Figure S15). ABC transporters are known to play a role in the MDR mechanism in cancer, and they are responsible for the increased efflux rate of anticancer drugs in the MDR phenomena (29, 30). In spite of the relative resistance in the conventional cytotoxic assay, M048i responded to

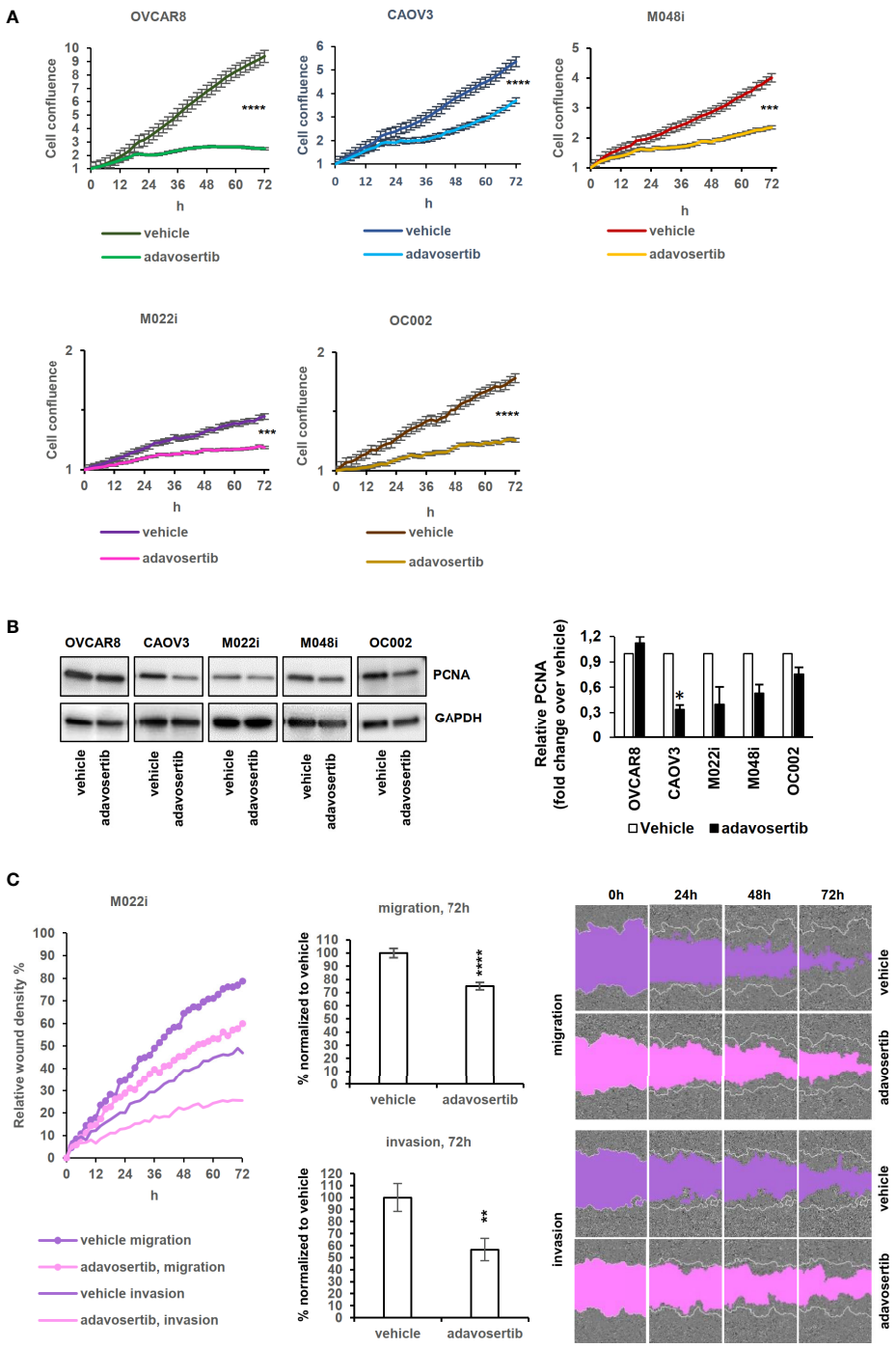

FIGURE 4
Effects of adavosertib on proliferation and wound healing. **(A)** Proliferation of HGSOC cells treated with adavosertib (500 nM) or vehicle was monitored in IncuCyte every 2 h for 72 h (normalized to time point 0 h). **(B)** Expression of the proliferation marker PCNA (proliferating cell nuclear antigen) protein at 72 (h) The bars show quantitative analysis of PCNA normalized to GAPDH using ImageJ software. The values shown are the mean ± SE of three separate experiments. **(C)** Wound healing experiment of the M022i HGSOC primary cells treated with adavosertib (500 nM) for 72 (h) Data of the four other HGSOC cells (M048i, OC002, OVCAR8, and CAOV3) are presented in Figure S8. Significant difference between vehicle and adavosertib treatment was determined by the *t*-test at ns = $p > 0.05$, *$p \leq 0.05$,**$p \leq 0.01$, ***$p \leq 0.001$, and ****$p \leq 0.0001$).

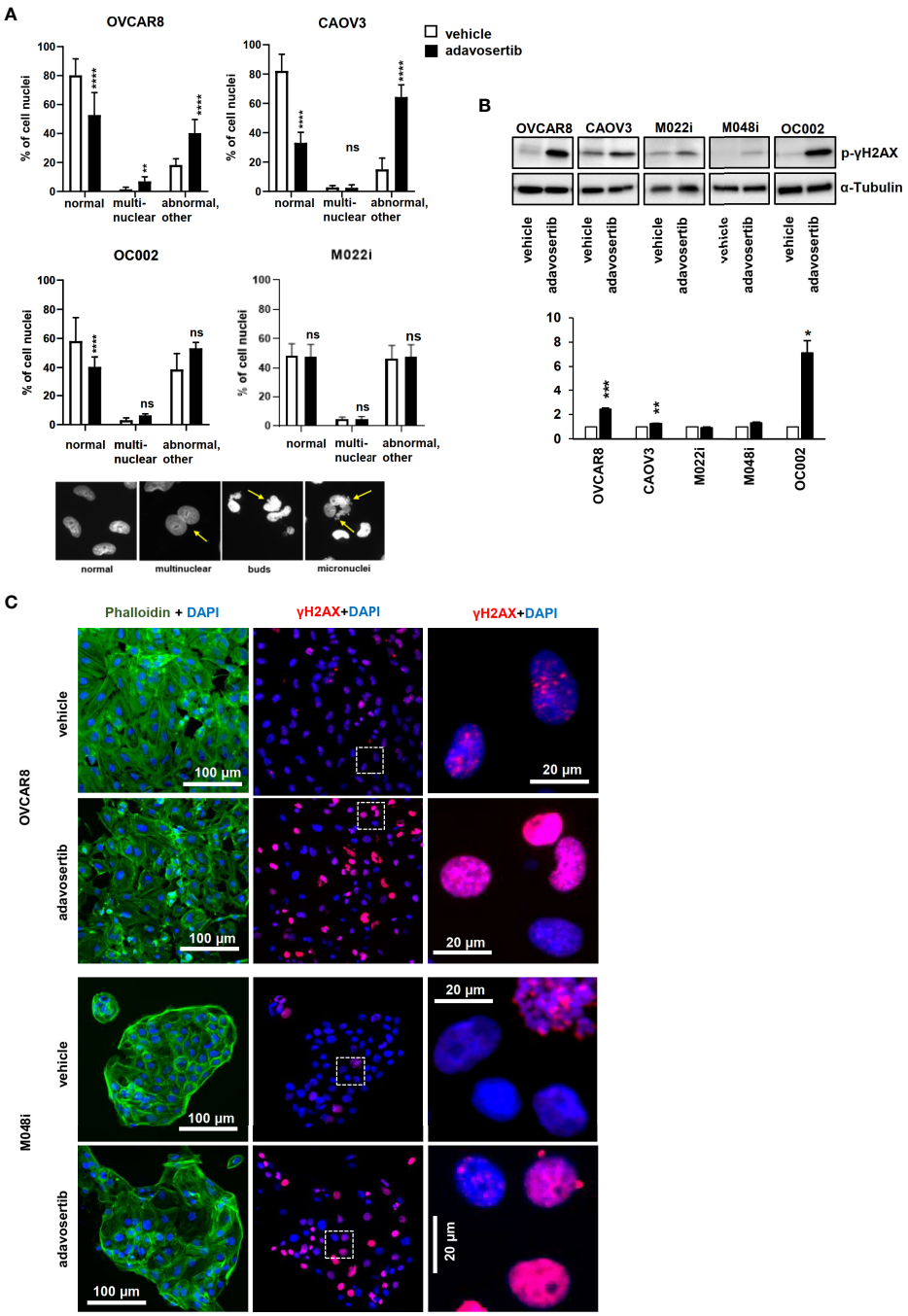

FIGURE 5
Adavosertib induces nuclear abnormalities and DNA damage **(A)** Nuclear morphology of cells treated with adavosertib or vehicle. Percentage of normal, multinucleated, and abnormal nuclei (micronucleus and buds of OVCAR8, CAOV3, OC002, and M022i cell cultures). Examples of nuclear abnormalities present in the samples: first picture of cells with normal nuclei, the second of a multinuclear cell, the third with a cell with nuclear buds, and the fourth of a cell with several micronuclei caused by the adavosertib treatment. **(B)** Protein levels of DNA-damage marker γH2AX (phosphor S-139) after 72 h of treatment with adavosertib (500 nM). The bars show quantitative analysis of PCNA normalized to α-tubulin using ImageJ software. The values shown are the mean ± SE of three separate experiments. Significant difference between vehicle and adavosertib treatment was determined by the *t*-test at ns = $p > 0.05$, *$p \leq 0.05$,**$p \leq 0.01$, ***$p \leq 0.001$, and ****$p \leq 0.0001$). **(C)** OVCAR8 and M048i cells were cultured on coverslips and treated with 500 nM adavosertib for 72h. Cells were fixed and stained with γH2AX (phosphor S-139) for DNA damage, DAPI for cell nuclei, and phalloidin for the actin filament (green, actin; blue, nucleus; and red, DNA damage).

adavosertib in other assays, indicating that none of the investigated cell lines were unresponsive to Wee1 inhibition.

Our study supports several mechanisms of action for adavosertib. Mechanistically, Wee1 regulates the G2/M checkpoint *via* inhibiting CDK1 and delays the mitosis entry of cells with DNA damage. Its inhibition in cells with DNA damage allows these cells to enter mitosis prematurely, which leads to mitotic catastrophe and apoptosis. Wee1 is also involved in regulating the G1/S checkpoint *via* CDK2 and thereby DNA replication by phosphorylating CDK2-bound cyclin A/E during the S phase (31, 32). The exact mechanisms of Wee1 inhibition in addition to the G2/M checkpoint is not yet completely understood. Heijink et al. (2015) found in their study that Wee1 inhibitor sensitivity is controlled by the status of several S-phase entry genes including CDK2 (33). In line with our results, they correspondingly report elevated γH2AX after Wee1 inhibition. We also found that adavosertib induced increased levels of the γH2AX DNA damage marker and shortened the S phase together with the abnormalities in the nuclei, which are indicators of increased replication stress. We found a reduction in CHK1 and an increase in γH2AX following adavosertib therapy, which was consistent with two earlier investigations using breast cancer, pancreatic, and osteosarcoma cell lines (34, 35).

In our study, Wee1 inhibition effectively reduced proliferation and increased apoptosis of all the tested cell lines including the less sensitive patient-derived cell line M048i. An exception was the OVCAR8 cell line that had no change in the PCNA levels compared to the other cells. PCNA plays an important role in replication and interacts with the cell-cycle progression machinery (36). We observed an accumulation of cells in the G2/M phases and a decrease in the S phase after adavosertib treatment. This is also in line with Heijink et al.'s study where they observed a shortened S phase (33). In addition, a similar increase in the G2/M phase has been shown in OVCAR8 cells in a recent study (37). A decreased cyclin B1 expression in all cell lines except in OVCAR8 might indicate the cytotoxic effect to be in the S phase rather than at the G2/M checkpoint. In a normal cell cycle, cyclin B expression peaks in the late G2 phase and radically declines in mitosis (38). The unchanged levels of PCNA and cyclin B1 expression in OVCAR8 cells might indicate that the cytotoxic effect in this cell line lies more in the mitotic catastrophe than in the S phase, compared to the other cells investigated.

Our study demonstrates that adavosertib treatment impairs migration and invasion in HGSOC cell lines, which could in part be interpreted as a consequence of cell-cycle arrest. Other studies have shown similar results in gastric cancer cell lines after Wee1 siRNA-mediated knockdown (39) or adavosertib treatment, although the mechanism of action was not elucidated (40). More recently, Bi et al. (2019) described that targeting Wee1 by shRNA or adavosertib significantly diminished the migration and invasion in esophageal squamous cell carcinoma by suppression of metalloproteinases MMP-2 and MMP-9 (41).

Several clinical trials have shown encouraging cytotoxic efficacy by adavosertib both as a single agent treatment and as a combination therapy in several solid tumors (11–14, 42–45). Thus, a combination therapy approach with platinum compounds or PARP inhibitors has been taken into clinical trials (NCT01357161, NCT03579316, NCT03345784, NCT02272790) (12–14). However, patients that are HRP and platinum resistant do not benefit from these drug combinations. Several other drug combinations have been studied in both *in vitro* and clinical trials. A recent clinical trial reported promising results with adavosertib in combination with nucleoside analog gemcitabine in treatment of platinum-resistant ovarian cancer (14). In an *in vitro* study, a similar result was reported that suggested that Wee1 inhibition sensitizes cells to gemcitabine but also reduced the ATR/CHK1 activity (35).

According to our knowledge, a thorough validation and mechanistic evaluation of Wee1 inhibition mechanisms in patient-derived HGSOC cells has been lacking. The current findings and our previous results showing that adavosertib is also effective against HGSOC cells with stemness features and had an observed cytotoxic effect in all of the studied HGSOC lines including the generally quite resistant M048i cells have increased our understanding of its broad mechanisms of action during the cell cycle.

Importantly, we observed that adavosertib inhibits HGSOC cells regardless of their HR status. A study by Garcia and others (2017) found that adavosertib impairs HR and may work as a combination therapy with PARP inhibitor olaparib in BRCA1/2-mutant leukemias (46). Another study with HRD and HRP murine cell lines demonstrated that Wee1 inhibitor in combination with olaparib had no difference in effectiveness between the HR-deficient and -proficient cells (47). Both of these studies were performed in combination with PARP inhibitor olaparib. We were able to demonstrate that adavosertib has efficacy toward HRP cells also as a single agent.

Our findings lay the basis for treatment of HRP patients, with whom treatment strategies are scarce. It is especially important to find an effective DNA-damaging agent to be used in combination with adavosertib for the platinum-resistant HGSOC patients. In this regard, gemcitabine has already shown promising results.

In conclusion, our study suggests Wee1 inhibitor adavosertib as a candidate compound to treat HGSOC patients independent of the HR status of the tumor.

Data availability statement

The raw sequencing data are available from the European Genome-Phenome Archive (EGA). RNA data is under accession

number EGAD00001006456 and DNA data is available under same DAC (EGAC00001001760).

Ethics statement

The studies involving human participants were reviewed and approved by Ethics Committee of the Hospital District of Southwest Finland (ETMK): ETMK 53/180/2009 §238 and ETMK 69/180/2010 and The Finnish National Supervisory Authority for Welfare and Health in Finland (Valvira): DNRO 6550/05.01.06/2010 and STH507A.The patients/participants provided their written informed consent to participate in this study.

Author contributions

PR, AA, and OC conceived the project. JH, SG, and AA contributed to the material acquisition. KK and PR established and maintained patient-derived HGSOC cell lines. PR, AS, VH, SaP, and KK designed the experiments. PR, AS, VH, PM, SaP, and SwP carried out the experiments. PR, AS, VH, KH, SaP, YL, and JO analyzed the data. PR, AS, and VH generated the figures. PR prepared the original draft. All authors reviewed and commented on the article. All authors contributed to the article and approved the submitted version.

Funding

The project has received funding from EU Horizon 2020 (667403), The Academy of Finland (292606), Finnish Cancer Society, Sigrid Juselius Foundation, Finska Läkaresällskapet, and Helsinki University Hospital Research Funds. PR has received research grants from K. Albin Johanssons Stiftelse, Varsinais-Suomen rahasto (85211878), Orion Research Foundation, Lounais-Suomen Syöpäyhdistys, University of Turku Postgraduation Education Unit, and Ida Montinin Säätiö.

Acknowledgments

We thank the DDCB core facility (FIMM HTB unit) supported by the University of Helsinki and Biocenter Finland. We also thank CSC – IT Center for Science Ltd. for computational resources.

Conflict of interest

AA reports receiving honoraria and travel support from GSK and is a member in Nordic Society of Gynecologic Oncology NSGO-CTU Foundation Board. KW reports receiving payment for attending and presenting at meetings organized by Pfizer and Amgen. JH has received funding from EU Horizon 2020 (965193).

The remaining authors declare that the research was conducted in the absence of any commercial or financial relationships that could be construed as a potential conflict of interest.

Publisher's note

Supplementary material

The Supplementary Material for this article can be found online at: https://www.frontiersin.org/articles/10.3389/fonc.2022.954430/full#supplementary-material

References

1. Bast RC. Molecular approaches to personalizing management of ovarian cancer. *Ann Oncol* (2011) 22:5–15. doi: 10.1093/annonc/mdr516

2. Hennessy BT, Coleman RL, Markman M. Ovarian cancer. *Lancet* (2009) 374:1371–82. doi: 10.1016/S0140-6736(09)61338-6

3. Patch AM, Christie EL, Etemadmoghadam D, Garsed DW, George J, Fereday S, et al. Whole–genome characterization of chemoresistant ovarian cancer. *Nat* (2015) 521(7553):489–94. doi: 10.1038/nature14410

4. Konstantinopoulos PA, Ceccaldi R, Shapiro GI, D'Andrea AD. Homologous recombination deficiency: Exploiting the fundamental vulnerability of ovarian cancer. *Cancer Discov* (2015) 5:1137–54. doi: 10.1158/2159-8290.CD-15-0714

5. Audeh MW, Carmichael J, Penson RT, Friedlander M, Powell B, Bell-McGuinn KM, et al. Oral poly(ADP-ribose) polymerase inhibitor olaparib in patients with BRCA1 or BRCA2 mutations and recurrent ovarian cancer: A proof-of-concept trial. *Lancet.* (2010) 376(9737):245–51. doi: 10.1016/S0140-6736(10)60893-8

6. Franzese E, Centonze S, Diana A, Carlino F, Guerrera LP, Di Napoli M, et al. PARP inhibitors in ovarian cancer. *Cancer Treat Rev* (2019) 73:1–9. doi: 10.1016/j.ctrv.2018.12.002

7. Domcke S, Sinha R, Levine DA, Sander C, Schultz N. Evaluating cell lines as tumour models by comparison of genomic profiles. *Nat Commun* (2013) 4(1):2126. doi: 10.1038/ncomms3126

8. Kaipio K, Chen P, Roering P, Huhtinen K, Mikkonen P, Östling P, et al. ALDH1A1-related stemness in high-grade serous ovarian cancer is a negative prognostic indicator but potentially targetable by EGFR/mTOR-PI3K/aurora kinase inhibitors. *J Pathol* (2020) 250(2):159–69. doi: 10.1002/path.5356

9. Pemovska T, Kontro M, Yadav B, Edgren H, Eldfors S, Szwajda A, et al. Individualized systems medicine strategy to tailor treatments for patients with chemorefractory acute myeloid leukemia. *Cancer Discov* (2013) 3(12):1416–29. doi: 10.1158/2159-8290.CD-13-0350

10. Yadav B, Pemovska T, Szwajda A, Kulesskiy E, Kontro M, Karjalainen R, et al. Quantitative scoring of differential drug sensitivity for individually optimized anticancer therapies. *Sci Rep* (2015) 4(1):5193. doi: 10.1038/srep05193

11. Do K, Wilsker D, Ji J, Zlott J, Freshwater T, Kinders RJ, et al. Phase I study of single-agent AZD1775 (MK-1775), a wee1 kinase inhibitor, in patients with refractory solid tumors. *J Clin Oncol* (2015) 33(30):3409–15. doi: 10.1200/JCO.2014.60.4009

12. Leijen S, Van Geel RMJM, Pavlick AC, Tibes R, Rosen L, Razak ARA, et al. Phase I study evaluating WEE1 inhibitor AZD1775 as monotherapy and in combination with gemcitabine, cisplatin, or carboplatin in patients with advanced solid tumors. *J Clin Oncol* (2016) 34(36):4371–80. doi: 10.1200/JCO.2016.67.5991

13. Leijen S, Van Geel RMJM, Sonke GS, De Jong D, Rosenberg EH, Marchetti S, et al. Phase II study of WEE1 inhibitor AZD1775 plus carboplatin in patientswith tp53-mutated ovarian cancer refractory or resistant to first-line therapy within 3 months. *J Clin Oncol* (2016) 34(36):4354–61. doi: 10.1200/JCO.2016.67.5942

14. Lheureux S, Cristea MC, Bruce JP, Garg S, Cabanero M, Mantia-Smaldone G, et al. Adavosertib plus gemcitabine for platinum-resistant or platinum-refractory recurrent ovarian cancer: A double-blind, randomised, placebo-controlled, phase 2 trial. *Lancet.* (2021) 397(10271):281–92. doi: 10.1016/S0140-6736(20)32554-X

15. Isoviita V-M, Salminen L, Azar J, Lehtonen R, Roering P, Carpén O, et al. Open source infrastructure for health care data integration and machine learning analyses. *JCO Clin Cancer Inform* (2019) 3):1–16. doi: 10.1200/CCI.18.00132

16. McKenna A, Hanna M, Banks E, Sivachenko A, Cibulskis K, Kernytsky A, et al. The genome analysis toolkit: A MapReduce framework for analyzing next-generation DNA sequencing data. *Genome Res* (2010) 20(9):1297–303. doi: 10.1101/gr.107524.110

17. Tate JG, Bamford S, Jubb HC, Sondka Z, Beare DM, Bindal N, et al. COSMIC: the catalogue of somatic mutations in cancer. *Nucleic Acids Res* (2019) 47 (D1):D941–7. doi: 10.1093/nar/gky1015

18. Landrum MJ, Lee JM, Benson M, Brown GR, Chao C, Chitipiralla S, et al. ClinVar: Improving access to variant interpretations and supporting evidence. *Nucleic Acids Res* (2018) 46(D1):D1062–7. doi: 10.1093/nar/gkx1153

19. Rentzsch P, Schubach M, Shendure J, Kircher M. CADD-Splice–improving genome-wide variant effect prediction using deep learning-derived splice scores. *Genome Med* (2021) 13(1):1–12. doi: 10.1186/s13073-021-00835-9

20. Alexandrov LB, Kim J, Haradhvala NJ, Huang MN, Tian Ng AW, Wu Y, et al. The repertoire of mutational signatures in human cancer. *Nature* (2020) 578 (7793):94–101. doi: 10.1038/s41586-020-1943-3

21. Tumiati M, Hietanen S, Hynninen J, Pietila E, Farkkil A, Kaipio K, et al. A functional homologous recombination assay predicts primary chemotherapy response and long-term survival in ovarian cancer patients. *Clin Cancer Res* (2018) 24(18):4482–93. doi: 10.1158/1078-0432.CCR-17-3770

22. Babicki S, Arndt D, Marcu A, Liang Y, Grant JR, Maciejewski A, et al. Heatmapper: Web-enabled heat mapping for all. *Nucleic Acids Res* (2016) 44(W1): W147–53. doi: 10.1093/nar/gkw419

23. Pietarinen PO, Eide CA, Ayuda-Durán P, Potdar S, Kuusanmäki H, Andersson EI, et al. Differentiation status of primary chronic myeloid leukemia cells affects sensitivity to BCR-ABL1 inhibitors. *Oncotarget* (2017) 8(14):22606. doi: 10.18632/oncotarget.15146

24. Potdar S, Ianevski A, Mpindi J-P, Bychkov D, Fiere C, Ianevski P, et al. Breeze: An integrated quality control and data analysis application for high-throughput drug screening. Valencia a, editor. *Bioinformatics* (2020) 36 (11):3602–4. doi: 10.1093/bioinformatics/btaa138

25. Mirza-Aghazadeh-Attari M, Ostadian C, Saei AA, Mihanfar A, Darband SG, Sadighparvar S, et al. DNA Damage response and repair in ovarian cancer: Potential targets for therapeutic strategies. *DNA Repair* (2019) 80:59–84. doi: 10.1016/j.dnarep.2019.06.005

26. Murai J. Targeting DNA repair and replication stress in the treatment of ovarian cancer. *Int J Clin Oncol* (2017) 22:619–28. doi: 10.1007/s10147-017-1145-7

27. McMullen M, Madariaga A, Lheureux S. New approaches for targeting platinum-resistant ovarian cancer. *Semin Cancer Biol* (2020) 77:167–81. doi: 10.1016/j.semcancer.2020.08.013

28. Otto T, Sicinski P. Cell cycle proteins as promising targets in cancer therapy. *Nat Rev Cancer* (2017) 17:93–115. doi: 10.1038/nrc.2016.138

29. Szakács G, Váradi A, Özvegy-Laczka C, Sarkadi B. The role of ABC transporters in drug absorption, distribution, metabolism, excretion and toxicity (ADME-tox). *Drug Discov Today* (2008) 13(9–10):379–93. doi: 10.1016/j.drudis.2007.12.010

30. Ween MP, Armstrong MA, Oehler MK, Ricciardelli C. The role of ABC transporters in ovarian cancer progression and chemoresistance. *Crit Rev Oncol Hematol* (2015) 96(2):220–56. doi: 10.1016/j.critrevonc.2015.05.012

31. Do K, Doroshow JH, Kummar S. Wee1 kinase as a target for cancer therapy. *Cell Cycle* (2013) 12(19):3348–53. doi: 10.4161/cc.26062

32. Ghelli Luserna Di Rorà A, Cerchione C, Martinelli G, Simonetti G. A WEE1 family business: Regulation of mitosis, cancer progression, and therapeutic target. *J Hematol Oncol* (2020) 13:1–17. doi: 10.1186/s13045-020-00959-2

33. Heijink AM, Blomen VA, Bisteau X, Degener F, Matsushita FY, Kaldis P, et al. A haploid genetic screen identifies the G1/S regulatory machinery as a determinant of Wee1 inhibitor sensitivity. *Proc Natl Acad Sci USA* (2015) 112 (49):15160–5. doi: 10.1073/pnas.1505283112

34. Ha DH, Min A, Kim S, Jang H, Kim SH, Kim HJ, et al. Antitumor effect of a WEE1 inhibitor and potentiation of olaparib sensitivity by DNA damage response modulation in triple-negative breast cancer. *Sci Rep* (2020) 10(1):1–13. doi: 10.1038/s41598-020-66018-5

35. Saini P, Li Y, Dobbelstein M. Wee1 is required to sustain ATR/Chk1 signaling upon replicative stress. *Oncotarget* (2015) 6(15):13072–87. doi: 10.18632/oncotarget.3865

36. Kelman Z. PCNA: structure, functions and interactions. *Oncogene* (1997) 14 (6):629–40. doi: 10.1038/sj.onc.1200886

37. Li F, Guo E, Huang J, Lu F, Yang B, Xiao R, et al. mTOR inhibition overcomes primary and acquired resistance to Wee1 inhibition by augmenting replication stress in epithelial ovarian cancers. *Am J Cancer Res* (2020) 10 (3):908–24.

38. Lindqvist A, Rodríguez-Bravo V, Medema RH. The decision to enter mitosis: feedback and redundancy in the mitotic entry network. *J Cell Biol* (2009) 185:193–202. doi: 10.1083/jcb.200812045JCB193

39. Kim H-Y, Cho Y, Kang H, Yim Y-S, Kim S-J, Song J, et al. Targeting the WEE1 kinase as a molecular targeted therapy for gastric cancer. *Oncotarget* (2016) 7(31):49902–16. doi: 10.18632/oncotarget.10231

40. Chen D, Lin X, Gao J, Shen L, Li Z, Dong B, et al. Wee1 inhibitor AZD1775 combined with cisplatin potentiates anticancer activity against gastric cancer by increasing DNA damage and cell apoptosis. *BioMed Res Int* (2018) 2018:1–10. doi: 10.1155/2018/5813292

41. Bi S, Wei Q, Zhao Z, Chen L, Wang C, Xie S. Wee1 inhibitor AZD1775 effectively inhibits the malignant phenotypes of esophageal squamous cell carcinoma *in vitro* and *in vivo*. *Front Pharmacol* (2019) 10:864. doi: 10.3389/fphar.2019.00864

42. Mendez E, Rodriguez CP, Kao MC, Raju S, Diab A, Harbison RA, et al. A phase I clinical trial of AZD1775 in combination with neoadjuvant weekly docetaxel and cisplatin before definitive therapy in head and neck squamous cell carcinoma. *Clin Cancer Res* (2018) 24(12):2740–8. doi: 10.1158/1078-0432.CCR-17-3796

43. Cuneo KC, Morgan MA, Sahai V, Schipper MJ, Parsels LA, Parsels JD, et al. Dose escalation trial of the WEE1 inhibitor adavosertib (AZD1775) in combination with gemcitabine and radiation for patients with locally advanced pancreatic cancer. *J Clin Oncol* (2019) 37(29):2643–50. doi: 10.1200/JCO.19.00730

44. Sanai N, Li J, Boerner J, Stark K, Wu J, Kim S, et al. Phase 0 trial of azd1775 in first-recurrence glioblastoma patients. *Clin Cancer Res* (2018) 24(16):3820–8. doi: 10.1158/1078-0432.CCR-17-3348

45. Oza AM, Weberpals JI, Provencher DM, Grischke E-M, Hall M, Uyar D, et al. An international, biomarker-directed, randomized, phase II trial of AZD1775 plus paclitaxel and carboplatin (P/C) for the treatment of women with platinum-sensitive, TP53 -mutant ovarian cancer. *J Clin Oncol* (2015) 33(15_suppl):5506–6. doi: 10.1200/jco.2015.33.15_suppl.5506

46. Garcia TB, Snedeker JC, Baturin D, Gardner L, Fosmire SP, Zhou C, et al. A small-molecule inhibitor of WEE1, AZD1775, synergizes with olaparib by impairing homologous recombination and enhancing DNA damage and apoptosis in acute leukemia. *Mol Cancer* (2017) 16(10):2058–68. doi: 10.1158/1535-7163.MCT-16-0660

47. Chiappa M, Guffanti F, Anselmi M, Lupi M, Panini N, Wiesmüller L, et al. Combinations of ATR, Chk1 and Wee1 inhibitors with olaparib are active in olaparib resistant Brca1 proficient and deficient murine ovarian cells. *Cancers* (2022) 14(7):1807. doi: 10.3390/cancers14071807

frontiers | Frontiers in Oncology

TYPE Case Report
PUBLISHED 26 August 2022
DOI 10.3389/fonc.2022.961666

OPEN ACCESS

EDITED BY
Gabriella Lillsunde Larsson,
Örebro University, Sweden

REVIEWED BY
Elisa Piovano,
AOU Cittàdella Salute e della Scienza di Torino,
Italy
C. Christofer Juhlin,
Karolinska Institutet (KI), Sweden

*CORRESPONDENCE
Shiqian Zhang
r370112@126.com

SPECIALTY SECTION
This article was submitted to Gynecological Oncology, a section of the journal Frontiers in Oncology

RECEIVED 05 June 2022
ACCEPTED 03 August 2022
PUBLISHED 26 August 2022

CITATION
Kong W, Qu Q and Zhang S (2022) Recurrent paraganglioma of the vulva: A rare case report and review of the literature.
Front. Oncol. 12:961666.
doi: 10.3389/fonc.2022.961666

Recurrent paraganglioma of the vulva: A rare case report and review of the literature

Wenzhi Kong, Qingxi Qu and Shiqian Zhang*

Department of Obstetrics and Gynaecology, Qilu Hospital of Shandong University, Jinan, China

Purpose: Vulva paragangliomas are rare and usually misdiagnosed or missed, especially in juveniles. Our aim was to summarize the clinical characteristics and treatments of vulva paragangliomas.

Methods and results: We present a case of a 17-year-old Chinese patient with functional paraganglioma from the vulva that was misdiagnosed as clear cell carcinoma. She had suffered from severe headaches, palpitations, sweating, pallor and hypertension. The vaginal wall was invaded by this mass. The tumour was surgically removed smoothly. However, the disease recurred 7 years after surgery, and the patient was treated again. Personalized genetic testing was performed while recovering, and the results suggested that the patient had a germline mutation in the Succinate Dehydrogenase subunit B (SDHB) gene. Now, the patient has been discharged successfully, her blood pressure has returned to normal and some of her clinical symptoms disappeared. A review of the literature concerning the topic is also presented, there have been only 2 cases of paraganglioma of the vulva and 11 cases of vaginal paraganglioma since 1955.

Conclusion: Our case describes a recurrent vulvovaginal paraganglioma with SDHB gene mutation and the largest tumor diameter to date. The diagnosis and treatment process of this case can provide reference for the management of other similar patients.

KEYWORDS

valval paraganglioma, functional tumour, diagnosis, treatment, SDHB genes

Introduction

Pheochromocytomas (PCCs) and paragangliomas (PGLs) (together referred to as PPGLs) are endocrine tumours originating from neural crest–derived cells of the adrenal medulla or from the sympathetic or parasympathetic paraganglia. Traditionally considered a “one in a million” disease, PPGLs have shown a rising incidence during the last 40 years, from 1.4 per million person-years in 1977 to 6.6 in 2015, constituting a

4.8-fold increase (1). PPGLs have the highest reported degree of heritability among all tumors. When currently known germline mutations are taken into account, around 30% to 40% of patients with PPGLs are affected by germline mutations in various susceptibility genes, and a further 35% to 40% show somatic driver mutations (2), and 50%-70% of childhood PPGL is associated with germline mutations. More than 20 germline mutations are known to be associated with PPGLs (3), Krebs cycle–related PPGLs are currently regarded as the most aggressive paraganglionic tumours, with germline Succinate Dehydrogenase subunit B (SDHB) mutations being among the strongest genetic risk factor for in development of metastatic PPGLs. The therapy of choice is surgery whenever possible; for inoperable disease, systemic therapy options include chemotherapy, radionuclide therapy, and tyrosine kinase inhibitors. PPGLs are mostly distributed in the adrenal glands, neck, mediastinum, and retroperitoneum, but they rarely occur in the vaginal wall and vulva. They are even rarer in juveniles. According to previous reports, there have been only 2 cases of PGLs of the vulva and 11 cases of vaginal PGLs since 1955 (4–16) (Table 1). Herein, we reported a vulval functional recurrent PGL.

Case presentation

A 17-year-old girl who had regular menstrual periods and no history of marriage or sexual activity was referred to the hospital for a hard lump located on the right side of the vulva for approximately 2 years. The lump progressively increased in size, with mild pain after mild physical activity. She had suffered from severe headaches, palpitations, sweating, and pallor after intense physical activity, such as sports and physical labor. These symptoms were especially common after activities involving local compression (e.g. cycling and defecation). Upon gynaecologic examination, an immobile, solid, and involved mass with no bleeding was found on the inferior margin of the right labia majora and the lateral margin of the hymen (Figure 1). Digital rectal examination (DRE) showed this mass to be closely associated with the vaginal wall and rectal wall. At the same time, inpatient evaluation revealed a blood pressure of 140–170/100–120 mmHg and a pulse rate of 90–120 beats/minute. These issues were not relieved by either metoprolol prolonged-release tablets or nifedipine tablets.

A magnetic resonance imaging (MRI) scan of the pelvis with intravenous contrast revealed a mass on the right vulva

TABLE 1 The summarized table of all vulva and vaginal paraganglioma cases reported.

author	Year	Age	location	size	functional	symptoms	gene mutation	Recurrene during follow-up
Plate, W. P (6).	1955	66	vaginal	walnut size	nonfunctional	vaginal hemorrhage	Not run	no
Pezeshkpour G (7).	1981	22	vaginal	3*2.5*1.5 cm	nonfunctional	asymptomatic	Not run	no
Colgan,T.J (4).	1991	58	vulva	1cm	nonfunctional	vulua pain and tenderness	Not run	no
Parkes, S. E (8).	1998	11	vaginal	5cm	nonfunctional	vaginal bleeding	Not run	no
Hassan, A (9).	2003	24	vaginal	2.5 cm	functional	hypertension, tachycardia and heart failure	Not run	no
Brustmann, H (10).	2007	33	vaginal	1.9 and 1.4 cm	nonfunctional	vaginal bleeding	Not run	no
Shen, J. G (11).	2008	38	vaginal	3.0 cm	functional	Paroxysmal headaches, chest distress, palpitation	Not run	no
Akl, M. N (12).	2010	65	vaginal	2.5*2.3*2cm	nonfunctional	asymptomatic	Not run	no
Liu,Y (5).	2013		vulva	3.2*2.3*1.5 cm	nonfunctional	asymptomatic	Not run	no
Cai, T (13).	2014	17	vaginal	3.5*3.0*2.5 cm	functional	vaginal bleeding	Not run	no
Sharma, S (14).	2018	28	vaginal	3*3 cm	nonfunctional	asymptomatic	Not run	no
Wong, R. W (15).	2020	15	vaginal	3 cm	nonfunctional	Irregular heavy menses, dysmenorrha, and anemia	Finding genetic mutations	no
Wang, Z (16).	2021	44	vaginal	3.5 cm	functional	hypertension, palpitations and dizziness	No mutations were found	Under follow up
Kong W.	2022		vulva	6*4*4cm	functional	hypertension,headaches, palpitations,	Finding genetic mutations	Recurrence 7 years later

FIGURE 1
The tumour was found to be located below the right labia majora, and its surface was covered with massive, engorged blood vessels.

measuring 6.0 cm*5.5 cm*4.3 cm in size, involving the right levator ani muscle. In addition, the tumour invaded the vaginal wall and disrupted the continuity of its mucous (Figure 2). Computed tomography (CT) scanning of the abdominal and female tumour markers were normal, while plasma and catecholamine concentrations were measured and found to be significantly higher than normal (Table 2). Fine needle aspiration cytology (FNAC) of the mass performed in other centres revealed clear cell carcinoma, but our centre denied this conclusion. To make a clear diagnosis and determine a suitable care plan, the patient underwent core needle biopsy (CNB) again in our centre. The biopsy tissue was sent for pathological and immunohistochemical examination, and the diagnosis was confirmed to be PGLs, synaptophysin (Syn)+, chromogranin A (CgA)+, S100+, Desmin+, HMB45 -, MelanA -, cyto-keratin (CK)-, CD10 -, CD68 -, CD34 -, CD31 -, PAX-8 -.

After oral administration of carvedilol and phenoxybenzamine for 14 days and intravenous fluids for 5 days, the effective circulating blood volume improved. Tumour resection was performed under general anaesthesia. During the operation, the tumour was found to

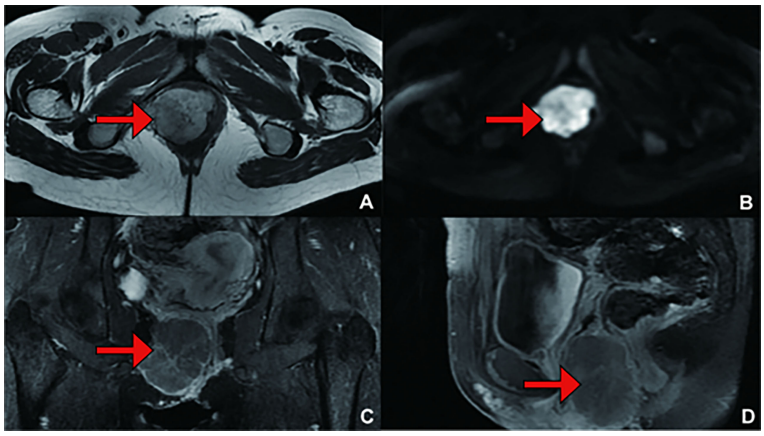

FIGURE 2
(Primary Treatment) Magnetic resonance imaging (MRI) scans: A mass on the right vulva measuring 6.0 cm*5.5 cm*4.3 cm in size, involving the right levator ani muscle, was observed. The tumour invaded the vaginal wall and disrupted the continuity of its mucous. **(A)** T1 weighted imaging (T1WI); **(B)** Diffusion Weighted Imaging (DWI); **(C)** Enhanced; **(D)** Enhanced.

TABLE 2 Plasma catecholamine concentrations (primary treatment).

Item	Result	Unit	Hint	Reference Value
E	40.23	Pg/mL		0.00–100.00
NE	3747.16	Pg/mL	↑	0.00–600.00
DA	167.85	Pg/mL	↑	0.00–100.00

E, epinephrine; NE, norepinephrine; DA, dopamine.
↑ Indicates that the result is higher than the normal reference range.

be located below the right labia majora, and its surface was covered with massive, engorged blood vessels (Figure 1). The right posterior lateral vaginal mucosa was involved. At the moment that the surgeon touched the tumour during the operation, the patient's arterial blood pressure and heart rate increased dramatically to 203/132 mmHg and 114 beats/min, respectively. However, she suffered from severe hypotension (40/30 mmHg) after complete tumour excision. This was managed by blood transfusion and vasopressor administration until her vital signs became stable. After surgery, blood pressure and heart rate were 100–110/60–70 mmHg and 90–100 beats/min, respectively, and the patient showed no manifestations suggestive of catecholamine release.

The patient did not have any active complaints in the following 2-year period. In a routine examination 7 years later, a mass was detected again at the same place, and the patient's blood pressure was increased. In the interval between the initial onset and recurrence, the patient completed childbirth. The levels of plasma catecholamines and their metabolite were examined to determine disease recurrence (Table 3). Whole-body CT examination was performed to exclude primary tumours in other sites, and pelvic scan plus enhanced MRI (Figure 3) and transanal ultrasound were used to clarify the extent of tumour invasion. The patient underwent surgery again. At this time, the resected mass was approximately 6*4*4 cm in size, hard and have a greyish white myxoma-like cut surface (Figure 4).

Comparing the pathology of the two excised tissues, the tumour cells were composed of chief cells and sustentacular cells, and they were clustered in small nests, here called zellballen, demarcated by delicate fibrous stroma and capillaries. The uninvolved margin around the neoplasm was at least 5 mm. The immunohistochemistry results at the time of primary treatment were as follows: the tumour was found to be positive for Syn, CgA, and Desmin but negative for protein S-100, human melanoma-associated antigen, MelanA, CK, CD10, CD68, CD31, and PAX-8 (Figure 5). The immunohistochemistry results at the time of recurrence treatment were as follows: CgA (+), CD56 (+), Syn (+), somatostatin receptor (SSTR2) (+), S-100 (+), SOX-10 (individual cells +), CK (-), and P53 (-), with a Ki-67 positive rate of approximately 2-3% (Figure 6). According to the Grading System for Adrenal Pheochromocytoma and Paraganglioma (GAPP) score which published in 2014 by Dr Kimura and co-workers (3), the patient can be rated 6 points, including 1 point for large and irregular cell nests, 2 points for high cellularity (> 250 cells/U), 1 point for capsular or vascular invasion, 1 point for Ki-67 labelling index 2-3%, and 1 point for catecholamine-type was NE.

After recurrence treatment, personalized genetic testing was performed during recovery, and the results suggested that the patient had a germline mutation in the SDHB gene. Assessment by Medical Genetics identifed a germline SDHB exon 7 splice site mutation (NM_003000.3(SDHB):c.765+1G>A). The minor allale frequency is 51%. According to American College of Medical Genetics and Genomics (ACMG) guidelines (17), the variation was preliminarily determined as pathogenic variation PVSI+PS4+PM2. The germline SDHB exon 7 splice site mutation described in the case has not been reported previously, which was predicted to disrupt splicing and lead to an altered and likely non-functional protein product. On this basis, genetic testing was performed for her immediate family. The genetic test results of the patient's son were normal without phenotype and did not carry the same pathogenic mutation as the patient, suggesting that the patient's son is less likely to

TABLE 3 Plasma catecholamine concentrations (recurrence treatment).

Item	Result	Unit	Hint	Reference Value
NE	35.00	nmol/L	↑	0-5.17
E	0.14	nmol/L		0-0.34
NMN	14.40	nmol/L	↑	0-0.71
MN	0.14	nmol/L		0-0.42
DA	<0.14	nmol/L		0-0.31
HVA	69.40	nmol/L		14.27-163
VMA	243.00	nmol/L	↑	0-62

NE, norepinephrine; E, epinephrine; DA, dopamine; NMN, normetanephrine; MN, metanephrine; DA, dopamine; HVA, homovanillic acid; VMA,vanillylmandelic acid.
↑ indicates that the result is higher than the normal reference range.

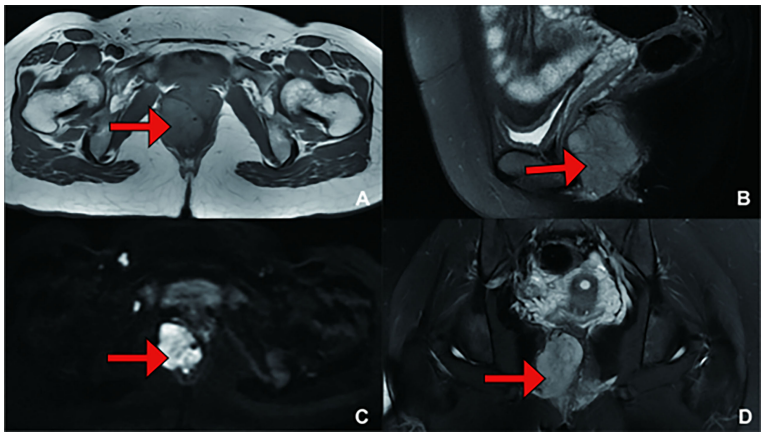

FIGURE 3
(Recurrence Treatment) Pelvic MRI showing a mass measuring 4.3 cm*3.6 cm*5.4 cm in size, suggesting that the lesion was closely related to the right posterior vaginal wall and anterior rectal wall. **(A)** T1 weighted imaging (T1WI); **(B)** T2 weighted imaging (T2WI); **(C)** Diffusion Weighted Imaging (DWI); **(D)** T2 weighted imaging (T2WI).

develop the disease. The genetic test results of the patient's mother were normal as well. As for the patient's father, he did not perform the genetic test because of some personal reasons. Since the mode of inheritance is autosomal dominant, if the patient has another child, there is a 50% chance of the offspring having the disease, and prenatal counselling is recommended for another child.

Discussion

PPGLs are rarely reported along the genital tract and are even rarer in juveniles. Only three cases of juvenile vaginal PGLs have been reported, with the patients' aged 11, 17 and 15 years (8, 13, 15). The latter involved functional tumours (13). The largest diameter of any previously reported PGL of the vagina or vulva was 5 cm, making the current case the largest functional PGL of the vulva ever reported by diameter (8). Only 2 genetic investigations were documented in the reported cases (15, 16).

The clinical manifestations of PPGLs are associated with unregulated secretion of catecholamines and with the location of the tumour. Excessive secretion of catecholamines by functional tumours is largely responsible for paroxysmal or persistent hypertension and symptoms such as palpitations, headaches, and hyperhidrosis. It can even lead to lethal cardiovascular complications, including shock and hypertensive crisis, which classically characterize these tumours (18). There have been only 4 cases of functional tumours among vaginal and vulval PGLs reported since 1955 (9, 11, 13, 16). The 2 reported patients with vaginal PGLs suffered from a cascade of events, including acute pulmonary oedema, hypertensive crisis, severe headaches, and other symptoms, after an attempted biopsy or excision of the

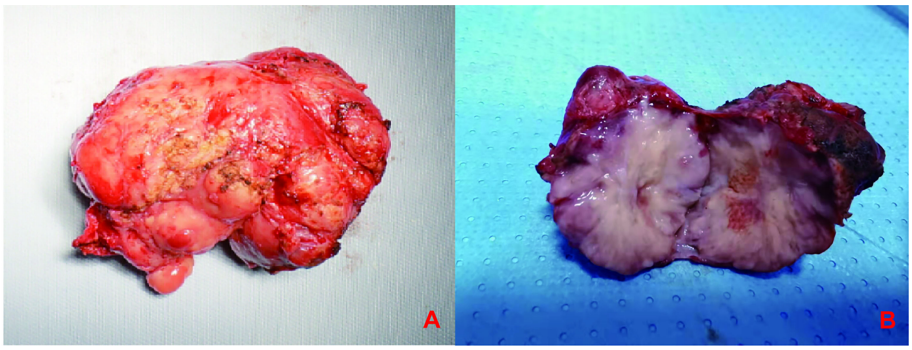

FIGURE 4
(A) The mass was dissected under the table and was approximately 6*4*4 cm in size, **(B)**The mass was hard and have a greyish white myxoma-like cut surface.

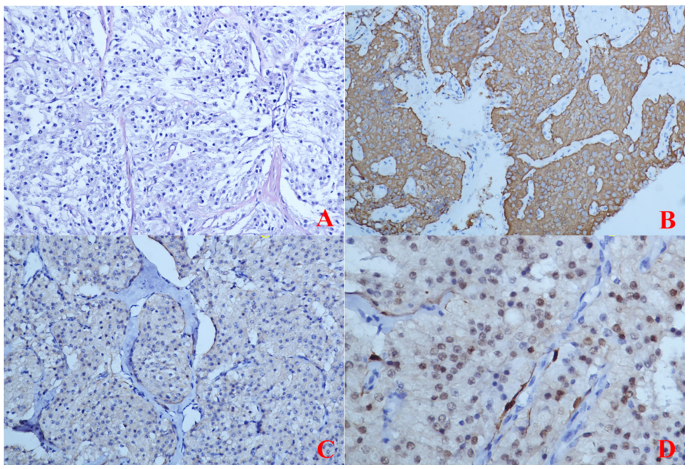

FIGURE 5
(Primary Treatment) Immunohistochemical staining: **(A)** The tumour cells were composed of chief cells and sustentacular cells, and they were clustered in small nests, here called zellballen, demarcated by delicate fibrous stroma and capillaries. **(B)** Immunohistochemical staining CgA(+); **(C)** Immunohistochemical staining SYN(+); **(D)** Immunohistochemical staining S-100(-).

mass (9, 13). Another functional case reported a 16-year history of intermittent strong paroxysmal headaches, palpitations, and chest distress. A similar episode took place during the operation that was performed to remove her tumour (11). The other functional case reported a 6-year history of paroxysmal hypertension, dizziness and palpitations (16). For these reasons, any manipulation of the tumour must be gentle, as brief as possible. This may prevent the release of catecholamines. Some cases presented with abnormal vaginal bleeding (6, 8, 10, 13).

The diagnosis of PPGLs includes qualitative and localization diagnosis. The biochemical presentation of excessive catecholamine production is an essential step in the diagnosis of functional PPGLs (19). Plasma or urine concentrations of metanephrine (MN) and normetanephrine (NMN) are preferred for biochemical examination. MNs are intermediate metabolites of catecholamines. Unlike norepinephrine (NE) and epinephrine (E), they are continuously produced in PPGL tumours, are not easily degraded by hydrolytic enzymes after secretion and can be

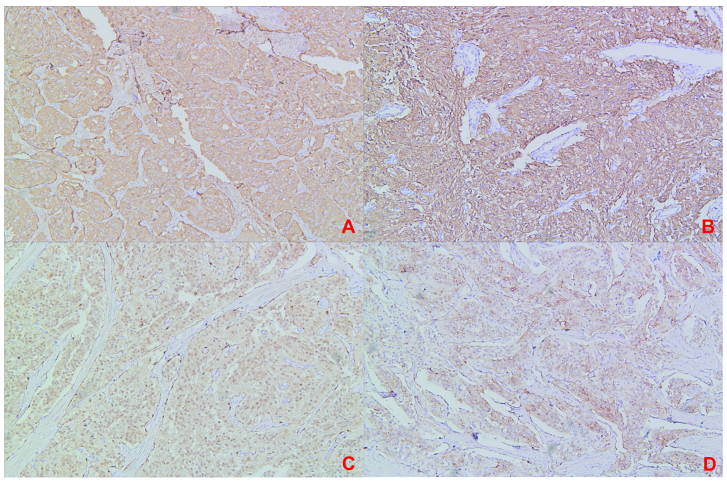

FIGURE 6
(Recurrence Treatment)Immunohistochemical staining: **(A)** Immunohistochemical staining CgA(+); **(B)** Immunohistochemical staining SYN(+); **(C)** Immunohistochemical staining S-100(+); **(D)** Immunohistochemical staining SSTR2 (+).

stably present in the blood (20, 21). For SDHB genes mutations like this patient that result of stabilization of hypoxia-inducible factors and epigenetic silencing of phenylethanolamine N-methyltransferase, the enzyme that converts NE into E, the focus should be on NMN since these tumours do not produce E (22). CT scanning and MRI are traditional positioning measurements. MRI is the preferred procedure for paediatric patients. The specificity of ^{123}I-metaiodobenzylguanidine (MIBG) scanning can be as high as 95–100%. In a report of vaginal PGL published by Zhan Wang (16), 131I-MIBG examinations revealed an obvious contractive accumulation in the perineum area. Scintigraphy of tumour somatostatin receptor (SSTR) and positron emission tomography (PET) are useful in the diagnosis of multifocal, metastatic disease and occult PGLs (19). In a report of vaginal PGL published by Tao Cai (13), two PGLs were found by PET: one was located in the vagina, and the other was located in the pelvic area.

The pathological diagnosis of PPGLs is also the gold standard for other tumours. Complete pathological examination can help distinguish PPGLs from other tumours, such as rhabdomyosarcoma, haemangioma, and leiomyoma. The diagnosis of PPGL is usually performed using histology plus immunohistochemical detection of CgA+, Syn+, GATA3+, S100 +, tyrosine hydroxylase (TH)+, dopamine beta-hydroxylase (DBH) + while being negative for CK (23). In addition to the biomarkers that confirm the diagnosis of PPGLs discussed above, there are important biomarkers that relate to the genetic background of PPGLs, that may guide genetic testing. For example, The 2022 World Health Organization(WHO) classification encourages routine use of SDHB immunohistochemistry since loss of SDHB expression is a surrogate marker in SDHx (x standing for any of the SDH genes) related pathogenesis (24). PPGLs with immunohistochemical loss of SDHB expression are classified as SDH-deficient PPGLs. This tumour is easily misdiagnosed by FNAC and intraoperative frozen sectioning. Dr. Sheila reported a vaginal PGL in an 11-year-old girl. She was misdiagnosed with rhabdomyosarcoma by frozen sectioning (8). Our patient was misdiagnosed with clear cell carcinoma by FNAC. Therefore, the pathological diagnosis of PGL should be completed by an experienced pathologist.

PPGLs does not respond well to chemotherapy or radiation, so complete surgical resection remains the standard of care (25). Sufficient preoperative preparation, including oral alpha-adrenoceptor blockade and intravenous fluids to increase blood volume, is very important. Excessive catecholamines from the tumour can lead to vasoconstriction of patients and cause a sharp rise in blood pressure. Therefore, it is necessary to expand the capacity periodically before operation to dilate the blood vessels and maintain the blood pressure of patients in a certain range, so as to prevent PGLs from being touched during operation, resulting in a rise in blood pressure of patients and resulting in dangerous surgery. The recommendations on preoperative preparation with alpha-adrenoceptor blockade are based on optimal care of patients, both before and during the surgery when a cardiovascular emergency and crisis may occur. Perioperative mortality is as high as 30% in the absence of sufficient preoperative preparation. This is due to indefinite diagnosis or misdiagnosis. This rate may drop to less than 3% if there is adequate preoperative preparation (26). In addition, the blood supply associated with PGL is extremely rich, Mohamed N. Akl MD successfully used an intervention of embolization for the uterine artery to reduce bleeding (12).

PPGLs are rare tumours and at least 30% are part of hereditary syndromes (27). PPGLs have the highest reported degree of heritability among all tumors. More than 20 germline mutations are known to be associated with PPGLs (3), about half of patients with metastatic disease harbour PPGLs susceptibility genes mutations. Germline mutations are most commonly detected in the SDHB, REarranged during Transfection (RET), von Hippel-Lindau(VHL) and NeuroFibromatosis type 1(NF1) genes. SDHB gene mutation are the most common SDHx mutations. The SDHB gene mutation is autosomal dominant and is localized at 1q36-q35 with eight exons, encoding a tricarboxylic acid cycle regulator of the mitochondrial complex II (27). The impairment of genes of the Krebs cycle leads to the accumulation of the oncometabolites succinate, fumarate, or 2-hydroxyglutarate. This in turn promotes DNA hypermethylation, inactivation of tumor suppressor genes, resulting in less hypoxia-inducible factor (HIF)-α hydroxylation and significantly lower HIF-α ubiquitination/degradation. This causes HIF-α stabilization, mitochondrial DNA impairment, collagen instability, and most likely an abnormal immune microenvironment. Only 2 genetic investigations were documented in the reported cases (15, 16). Wong, R. W (15).reported a vaginal PGL in an 15-year-old girl with a heterozygous deletion of exon 1 of the SDHB gene. Wang, Z (16). investigated 36 most common mutated genes related to PPGL through target sequencing, however, the results turned out to be negative.

Although all PPGLs and all genotypes have a potential for developing metastatic disease, mutations in the SDHB gene are associated with the highest risk of metastatic disease (30–70%). Therefore, SDHB mutations suggest that patients have a poor prognosis and should be closely monitored (28, 29). An appropriate follow-up program should be selected according to the genotype of PGL patient. Patients with SDHB gene mutations should be examined annually for blood pressure and biochemistry and every 2 years for whole-body MRI (30). A multicentric retrospective study indicated that early knowledge of genetic status had a positive impact on the management and clinical outcome of patients with a germline SDHx or VHL mutations (31). Mutation testing for the SDHB oncogene in all patients clinically diagnosed with PPGLs is beneficial not only for the confirmation of diagnosis and prognosis assessment of PPGLs patients but also for the early diagnosis and early treatment of patients' family members.

Data availability statement

The original contributions presented in the study are included in the article/supplementary material. Further inquiries can be directed to the corresponding author.

Ethics statement

The studies involving human participants were reviewed and approved by the Ethics Committee of Qilu Hospital of Shandong University KYLL-202203-018. Written informed consent was obtained from the relevant individual and minors' legal guardian, for the publication of any potentially identifiable images or data included in this article.

Author contributions

SZ screened the study subjects, participated in discussions and provided expertise and feedback. QQ assessed the patients' pathologic complications and participated in the manuscript revision. WK wrote the clinical information and manuscript. All authors contributed to the article and approved the submitted version.

Funding

This work was supported by the Natural Foundation of Shandong Province (No. ZR2021QH011).

Conflict of interest

The authors declare that the research was conducted in the absence of any commercial or financial relationships that could be construed as a potential conflict of interest.

Publisher's note

All claims expressed in this article are solely those of the authors and do not necessarily represent those of their affiliated organizations, or those of the publisher, the editors and the reviewers. Any product that may be evaluated in this article, or claim that may be made by its manufacturer, is not guaranteed or endorsed by the publisher.

References

1. Ebbehoj A, Stochholm K, Jacobsen SF, Trolle C, Jepsen P, Robaczyk MG, et al. Incidence and clinical presentation of pheochromocytoma and sympathetic paraganglioma: A population-based study. *J Clin Endocrinol Metab* (2021) 106(5): e2251–e61. doi: 10.1210/clinem/dgaa965

2. Nolting S, Bechmann N, Taieb D, Beuschlein F, Fassnacht M, Kroiss M, et al. Personalized management of pheochromocytoma and paraganglioma. *Endocr Rev* (2022) 43(2):199–239. doi: 10.1210/endrev/bnab019

3. Juhlin CC. Challenges in paragangliomas and pheochromocytomas: from histology to molecular immunohistochemistry. *Endocr Pathol* (2021) 32(2):228–44. doi: 10.1007/s12022-021-09675-0

4. Colgan TJ, Dardick I, O'Connell G. Paraganglioma of the vulva. *Int J Gynecol Pathol* (1991) 10(2):203–8. doi: 10.1097/00004347-199104000-00009

5. Liu YQ, Yue JQ. Paraganglioma of the vulva: A case report and review of the literature. *Int J Clin Exp Pathol* (2013) 6(10):2247–50.

6. Plate WP. Phaeochromo-blastoma of the vagina. *Gynaecol Int Mon Rev Obst Gynecol Rev Int Mensuelle d'obstetrique Gynecol Monatsschrift fur Geburtshilfe und Gynakol* (1955) 139(1):35–9. doi: 10.1159/000308112

7. Pezeshkpour G. Solitary paraganglioma of the vagina–report of a case. *Am J Obst Gynecol* (1981) 139(2):219–21. doi: 10.1016/0002-9378(81)90453-1

8. Parkes SE, Raafat F, Morland BJ. Paraganglioma of the vagina: the first report of a rare tumor in a child. *Pediatr Hematol Oncol* (1998) 15(6):545–51. doi: 10.3109/08880019809018317

9. Hassan A, Bennet A, Bhalla S, Ylagan LR, Mutch D, Dehner LP. Paraganglioma of the vagina: Report of a case, including immunohistochemical and ultrastructural findings. *Int J Gynecol Pathol* (2003) 22(4):404–6. doi: 10.1097/01.pgp.0000092158.33490.24

10. Brustmann H. Paraganglioma of the vagina: Report of a case. *Pathol Res Pract* (2007) 203(3):189–92. doi: 10.1016/j.prp.2007.01.002

11. Shen JG, Chen YX, Xu DY, Feng YF, Tong ZH. Vaginal paraganglioma presenting as a gynecologic mass: Case report. *Eur J Gynaecol Oncol* (2008) 29 (2):184–5.

12. Akl MN, Naidu SG, McCullough AE, Magtibay PM. Vaginal paraganglioma presenting as a pelvic mass. *Surgery* (2010) 147(1):169–71. doi: 10.1016/j.surg.2008.08.020

13. Cai T, Li Y, Jiang Q, Wang D, Huang Y. Paraganglioma of the vagina: A case report and review of the literature. *Onco Targets Ther* (2014) 7:965–8. doi: 10.2147/OTT.S62174

14. Sharma S, Chougule A, Garg R, Chopra S, Sikka P. A long-standing primary vaginal paraganglioma-coexisting with esophageal carcinoma. *Indian J Surg Oncol* (2018) 9(2):286–7. doi: 10.1007/s13193-017-0688-4

15. Wong RW, Liu APY, Choi CKM, Chan AOK. Paraganglioma of the vagina associated with germline SDHB mutation: Report of a case with review of the literature. *Int J Gynecol Pathol* (2020) 39(6):599–604. doi: 10.1097/PGP.0000000000000658

16. Wang Z, Fan H, Fan J, Seery S, Wang W, Zhang Y. Solitary vaginal paraganglioma with mature sacrococcygeal teratoma: A rare case report. *BMC Endocr Disord* (2021) 21(1):145. doi: 10.1186/s12902-021-00806-6

17. Richards S, Aziz N, Bale S, Bick D, Das S, Gastier-Foster J, et al. Standards and guidelines for the interpretation of sequence variants: A joint consensus recommendation of the american college of medical genetics and genomics and the association for molecular pathology. *Genet Med* (2015) 17(5):405–24. doi: 10.1038/gim.2015.30

18. Prejbisz A, Lenders JW, Eisenhofer G, Januszewicz A. Cardiovascular manifestations of phaeochromocytoma. *J Hypertens* (2011) 29(11):2049–60. doi: 10.1097/HJH.0b013e32834a4ce9

19. Lenders JWM, Kerstens MN, Amar L, Prejbisz A, Robledo M, Taieb D, et al. Genetics, diagnosis, management and future directions of research of phaeochromocytoma and paraganglioma: A position statement and consensus of the working group on endocrine hypertension of the european society of hypertension. *J Hypertens* (2020) 38(8):1443–56. doi: 10.1097/HJH.0000000000002438

20. Chen Y, Xiao H, Zhou X, Huang X, Li Y, Xiao H, et al. Accuracy of plasma free metanephrines in the diagnosis of pheochromocytoma and paraganglioma: A systematic review and meta-analysis. *Endocrine Prac: Off J Am Coll Endocrinol Am Assoc Clin Endocrinol* (2017) 23(10):1169–77. doi: 10.4158/ep171877.Or

21. Eisenhofer G, Prejbisz A, Peitzsch M, Pamporaki C, Masjkur J, Rogowski-Lehmann N, et al. Biochemical diagnosis of chromaffin cell tumors in patients at high and low risk of disease: Plasma versus urinary free or deconjugated o-methylated catecholamine metabolites. *Clin Chem* (2018) 64(11):1646–56. doi: 10.1373/clinchem.2018.291369

22. Eisenhofer G, Klink B, Richter S, Lenders JW, Robledo M. Metabologenomics of phaeochromocytoma and paraganglioma: An integrated approach for personalised biochemical and genetic testing. *Clin Biochem Rev* (2017) 38(2):69–100.

23. Mete O, Asa SL, Gill AJ, Kimura N, de Krijger RR, Tischler A. Overview of the 2022 WHO classification of paragangliomas and pheochromocytomas. *Endocr Pathol* (2022) 33(1):90–114. doi: 10.1007/s12022-022-09704-6

24. Oudijk L, Gaal J, de Krijger RR. The role of immunohistochemistry and molecular analysis of succinate dehydrogenase in the diagnosis of endocrine and non-endocrine tumors and related syndromes. *Endocr Pathol* (2019) 30(1):64–73. doi: 10.1007/s12022-018-9555-2

25. Somasundar P, Krouse R, Hostetter R, Vaughan R, Covey T. Paragangliomas– a decade of clinical experience. *J Surg Oncol* (2000) 74(4):286–90. doi: 10.1002/1096-9098(200008)74:4<286::aid-jso9>3.0.co;2-c

26. Wald O, Shapira OM, Murar A, Izhar U. Paraganglioma of the mediastinum: Challenges in diagnosis and surgical management. *J Cardiothorac Surg* (2010) 5:19. doi: 10.1186/1749-8090-5-19

27. Muth A, Crona J, Gimm O, Elmgren A, Filipsson K, Stenmark Askmalm M, et al. Genetic testing and surveillance guidelines in hereditary pheochromocytoma and paraganglioma. *J Intern Med* (2019) 285(2):187–204. doi: 10.1111/joim.12869

28. Albattal S, Alswailem M, Moria Y, Al-Hindi H, Dasouki M, Abouelhoda M, et al. Mutational profile and genotype/phenotype correlation of non-familial pheochromocytoma and paraganglioma. *Oncotarget* (2019) 10(57):5919–31. doi: 10.18632/oncotarget.27194

29. Currás-Freixes M, Inglada-Pérez L, Mancikova V, Montero-Conde C, Letón R, Comino-Méndez I, et al. Recommendations for somatic and germline genetic testing of single pheochromocytoma and paraganglioma based on findings from a series of 329 patients. *J Med Genet* (2015) 52(10):647–56. doi: 10.1136/jmedgenet-2015-103218

30. Plouin PF, Amar L, Dekkers OM, Fassnacht M, Gimenez-Roqueplo AP, Lenders JW, et al. European society of endocrinology clinical practice guideline for long-term follow-up of patients operated on for a phaeochromocytoma or a paraganglioma. *Eur J Endocrinol* (2016) 174(5):G1–G10. doi: 10.1530/EJE-16-0033

31. Buffet A, Ben Aim L, Leboulleux S, Drui D, Vezzosi D, Libe R, et al. Positive impact of genetic test on the management and outcome of patients with paraganglioma and/or pheochromocytoma. *J Clin Endocrinol Metab* (2019) 104 (4):1109–18. doi: 10.1210/jc.2018-02411

frontiers | Frontiers in Oncology

TYPE Original Research
PUBLISHED 20 September 2022
DOI 10.3389/fonc.2022.958536

OPEN ACCESS

EDITED BY
Sara Ricardo,
Instituto de Investigação e Inovação em Saúde, Universidade do Porto, Portugal

REVIEWED BY
Keith Pui-Kei Wu,
AbbVie, United States
Chandra Sekhar Bhol,
National Institute of Technology Rourkela, India

*CORRESPONDENCE
Doris Mangiaracina Benbrook
Doris-Benbrook@ouhsc.edu

SPECIALTY SECTION
This article was submitted to Gynecological Oncology, a section of the journal Frontiers in Oncology

RECEIVED 31 May 2022
ACCEPTED 22 August 2022
PUBLISHED 20 September 2022

CITATION
Rai R, Chandra V, Kennedy AL, Zuna RE and Benbrook DM (2022) Distinct mechanism of cervical cancer cell death caused by the investigational new drug SHetA2. *Front. Oncol.* 12:958536. doi: 10.3389/fonc.2022.958536

Distinct mechanism of cervical cancer cell death caused by the investigational new drug SHetA2

Rajani Rai[1], Vishal Chandra[1], Amy L. Kennedy[2], Rosemary E. Zuna[2] and Doris Mangiaracina Benbrook[1,2]*

[1]Gynecologic Oncology, Stephenson Cancer Center, University of Oklahoma Health Sciences Center, Oklahoma, OK, United States, [2]Department of Pathology, University of Oklahoma Health Sciences Center, Oklahoma, OK, United States

Drug-targetable vulnerabilities of cancer cells include their dependence on heat shock proteins (HSPs) to support elevated mitochondrial metabolism and counteract cell death factors. The investigational new drug SHetA2 targets these vulnerabilities in ovarian and endometrial cancer cells by disrupting complexes of the mortalin HSP with its client proteins (mitochondrial support proteins, metabolic enzymes, p53) leading to mitochondrial leakage of cytochrome c and apoptosis-inducing factor (AIF), and caspase-dependent apoptosis. Our objective was to evaluate the roles of mitochondrial damage and another SHetA2-target HSP protein, cytoplasmic heat shock cognate 70 (hsc70), in the mechanism of SHetA2 killing of cervical cancer cells. Cervical cancer cells responded to SHetA2 with excessive mitophagy that did not deter AIF leakage into the cytoplasm. Then, hsc70 was unable to prevent cytoplasmic AIF nuclear translocation and promotion of DNA damage and cell death, because SHetA2 disrupted hsc70/AIF complexes. The Cancer Genome Atlas analysis found that overexpression of hsc70, but not mortalin, was associated with worse cervical cancer patient survival. Use of specific inhibitors documented that AIF and mitophagy, but not caspases, contributed to the mechanism of SHetA2-induced cell death in cervical cancer cells. As validation, excessive mitophagy and lack of caspase activation were observed in SHetA2-inhibited xenograft tumors.

KEYWORDS

cervical cancer, SHetA2, mitochondria, mitophagy, apoptosis inducing factor, heat shock cognate 70, cell death, heat shock protein

Introduction

Globally, cervical cancer occurred in 570,000 women and caused 311,000 deaths in 2018 (1). This cancer is diagnosed primarily in middle-aged women in the age range where women commonly have productive careers and dependent families. The vast majority of cervical cancers are caused by high risk Human Papillomavirus (hrHPV) and

subsequent genomic instability. HPV vaccines have reduced cervical cancer incidence, especially in developed countries, however further reduction is not likely to be seen in the next decade due to low vaccination rates, emersion of rare oncogenic HPV variants and lack of effect of vaccines on pre-existing hrHPV infections. The standard of care therapy for cervical cancer is based on combinations of radiation and chemotherapy. These modalities are highly toxic and cause significant morbidity (2, 3). Although recent FDA approvals have added immune-based therapy to this armament, cervical cancer lags behind most other cancers in having molecular-based drugs available for therapeutic use.

Heat shock proteins (HSPs) are rational targets for development of new cancer therapeutics because cancer cells become dependent upon increased levels of HSPs to maintain their unstably-elevated proliferative and metabolic states (4). HSPs are categorized based on their molecular weights. The 70 Kd family of HSPs (HSP70s) consists of 14 members, which each have unique and redundant functions throughout the cell (5). The mortalin member of this family is localized throughout the cells, but it's primary location and function are in maintaining mitochondrial health (5, 6). Increased levels of mortalin promote carcinogenesis and cancer progression by supporting overactive mitochondria and sequestering p53 in the cytoplasm away from the mitochondria and nucleus where it can initiate apoptosis (7–10). Mortalin has also been shown to support carcinogenesis and cancer cells driven by rearranged during transfection (RET) proto-oncogene, mutant Ras and Raf oncoproteins and MEK-ERK signaling activity (11–13). These cancer supporting activities include regulation of mitochondrial bioenergetics (13) and the mitochondrial membrane potential transition pore (14, 15). The investigational new drug, SHetA2, interferes with mortalin support of cancer cells by disrupting mortalin complexes with client proteins (16). Client proteins shown to be blocked from binding mortalin by SHetA2 in endometrial cancer cells include proteins involved in mitochondrial metabolism and calcium import (17). The mitochondrial damage eventually leads to mitochondrial release of cytochrome c, which activates caspases to cause apoptotic cell death, and apoptosis-inducing factor (AIF), which translocates to the nucleus and promotes DNA damage and cell death (18). An important mortalin client protein is p53, which when released from mortalin by SHetA2 translocates to the mitochondria and nucleus where it induces apoptosis (8).

While the role of mortalin has been well established in the mechanism of SHetA2-induced ovarian and endometrial cancer cell death, the involvement of another SHetA2-binding HSP70 protein called heat shock cognate 70 (hsc70) (16) has not yet been studied. The hsc70 family member has the potential to interfere with the AIF-mediated mechanism of SHetA2-induced cell death because it sequesters AIF in cytoplasm away from the nucleus (19). It is likely that the hrHPV-driven intracellular environment of cervical cancer cells, which includes decreased p53, cause them to respond differently to SHetA2 compared to cells of other gynecologic cancers. A previous study demonstrated the cell cycle regulatory mechanism of SHetA2 and its synergistic interaction with cyclin dependent kinase 4/6 inhibitors (20), however no studies have yet been done on the mechanism of SHetA2-induced cell death of cervical cancer cells.

The objective of this study was to determine how cervical cancer cells respond to, and eventually die, from SHetA2 treatment. The known deleterious effects of SHetA2 on mitochondria in other cancers were evaluated in more depth in cervical cancer cells and tumors. The hsc70 chaperone target of SHetA2 was evaluated as a potential target for cervical cancer treatment and for its role in the mechanism of SHetA2 killing of cervical cancer cells. Specific molecular and cellular responses to SHetA2 were tested for their roles as mediators of survival versus death.

Results

SHetA2 inhibits mitochondrial function and biogenesis in cervical cancer cells

Based on the essential roles of mortalin in the import of nuclear-encoded mitochondrial proteins and maintenance of mitochondrial function (9), and the SHetA2 disruption of mortalin complexes in ovarian cancer cells (4, 5), we predicted that SHetA2 damages mitochondria in cervical cancer cells. In this study, SHetA2 effects on mitochondria were evaluated in three human cervical cancer cell lines C-33 A, Ca Ski and SiHa after 4 and 24 hours of treatment. As expected, SHetA2 reduced mitochondrial membrane potential (MMP) in all cell lines in a dose- and time-dependent manner (Figure 1A). SHetA2 also reduced total cellular ATP to similar levels at 4 and 24 hours in all three cell lines indicating decreased mitochondrial function (Figure 1B). To assess mitochondrial dysfunction, flow cytometric analysis of Mitosox was used to measure mitochondrial ROS. The results showed that SHetA2 increased mitochondrial ROS in all three cell lines, as well as the ME-180 and C-4-II human cervical cancer cell lines (Figure 1C; Supplemental Figures 1A, B). SHetA2 effects observed in all three cell lines using Mitotracker staining included reduction of mitochondrial networking (Figures 2A, B) and mitochondrial mass as measured by the ratio of Mitotracker to Hoechst nuclear staining (Figure 2C; Supplemental Figure 1C). To better visualize SHetA2 effects on mitochondria, we used transmission electron microscopy (TEM) of SiHa cultures treated with 10 μM SHetA2 or vehicle for 4 hours or 8 hours (Figure 3A upper panel). At both treatment times, SHetA2-treated cells had fewer

10.3389/fonc.2022.958536

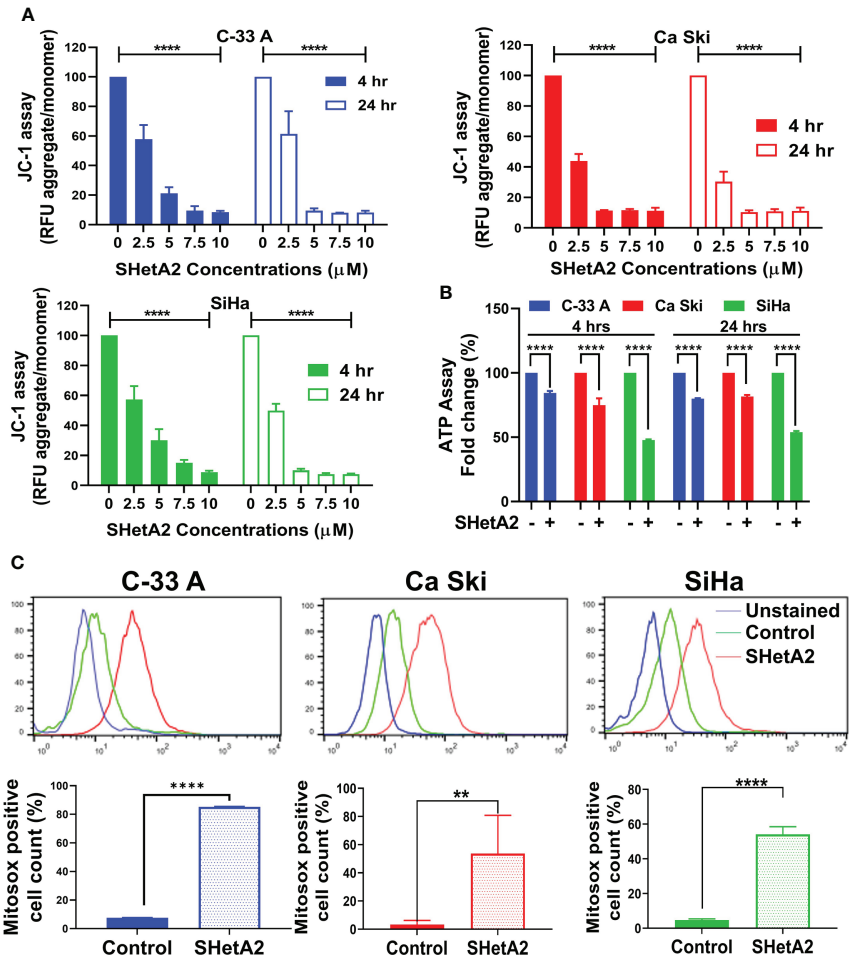

FIGURE 1
SHetA2 induces mitochondrial depolarization and loss of ATP, **(A)**: Relative fluorescence (RFU) of JC-1 dye, and ratios of JC-1 aggregate to monomer expressed as mean ± SD and analyzed using two-way ANOVA. **(B)**, ATP levels in cells treated with SHetA2 (10 μM) or vehicle analyzed using *t*-tests. **(C)**, Representative histograms from Flow cytometric analysis of MitoSOX staining of cells treated with SHetA2 (10 μM) or vehicle for 24 hours (left) and average (mean ± SD) data of three independent experiments were analyzed by t-tests (right). $^{**}p \leq 0.01$, $^{****}p \leq 0.0001$ when compared with respective control.

mitochondria, which were swollen (significantly greater length, width, and total area) (Figure 3A), and increased autophagic vesicles and chromatin condensation, in comparison to controls (Figure 3A).

To evaluate the molecular mechanism of these mitochondrial events, proteins were extracted from the cells and evaluated by western blots. SHetA2 reduced mitochondrial proteins involved in fusion (mitofusin 1/MFN1, mitofusin 2/MFN2, and long-form of outcome predictor in acute leukemia 1/OPA1L), but not those involved in fission (dynamin-related protein 1/Drp1) in the five cell lines tested (Figure 3B). Exceptions were significant reduction of Drp1 in C-33 A, and lack of significant MFN-1 reductions in Ca Ski and SiHa. The OPA1S isoform, which is dispensable for fission under stressed conditions (21), was not reduced in any of the cell lines except for C-33 A (Figure 3B). Taken together, these results demonstrate that mitochondrial biogenesis, fusion, and function are disrupted by SHetA2 in cervical cancer cells.

Cells respond to SHetA2-induced mitochondrial damage with mitophagy that contributes to the mechanism of cell death

Based on the observed mitochondrial damage, we predicted that the cervical cancer cells respond by elevating mitochondria-selective autophagy (mitophagy) (22) to eliminate the damaged mitochondria and recycle the components. In concordance with induction of mitophagy in SHetA2-treated cells, confocal imaging demonstrated increased expression of the mitophagy

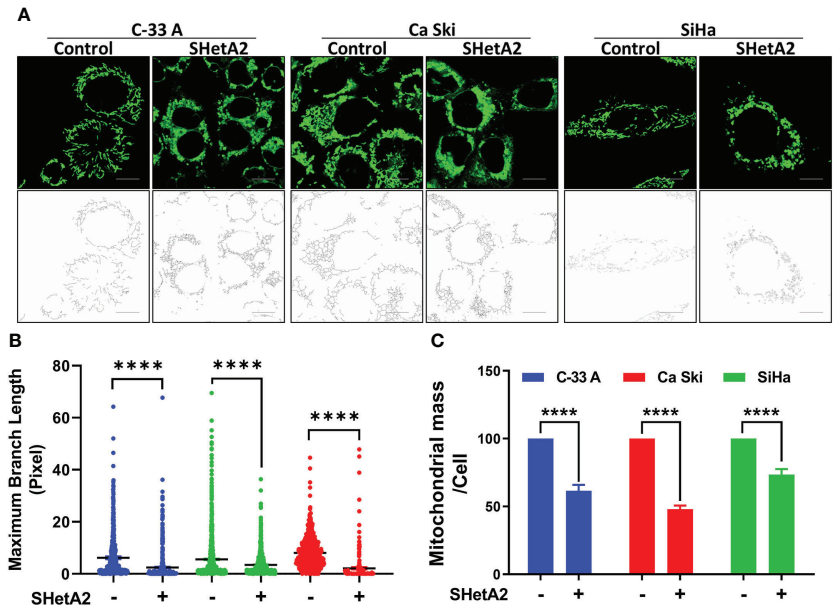

FIGURE 2
SHetA2 reduces mitochondrial networking and mass: **(A, B)**, Confocal imaging of MitoTracker™ Green staining of cells treated with 10 μM SHetA2 (**A**, upper panel). Representative imaging of mitochondrial networks analyzed using Image J software (**A**, lower panel). Maximum mitochondrial branch lengths were compared by *t*-tests **(B)**. **(C)**, C-33 A, Ca Ski and SiHa cervical cancer cells treated with 10 μM SHetA2 or vehicle for 24 hours were stained with MitoTracker™ Green and Hoechst. The fluorescence was imaged and analyzed by using the Operetta®High Content Imaging System. Mitochondrial mass in cells treated with SHetA2 or vehicle for 24 hours were measured by ratios of MitoTracker™ Green to Hoechst staining, presented as mean ± SD and analyzed using *t*-tests. ****$p \leq 0.0001$ when compared with respective control.

marker Pink1 and its co-localization with the mitochondrial marker (mitotracker red, Figure 4A and Supplementary Figure 2), in addition to colocalization of lysosome dye with mitotracker (Figure 4B).

To confirm at the molecular level that SHetA2 caused mitophagy, western blots of SHetA2-treated cultures were stained for various molecular markers of autophagy (microtubule-associated protein 1A/1B-light chain 3 (LC3)-II to the LC3-I protein modification) and mitophagy (Pink-1 and p62). In both Ca Ski and SiHa cells, SHetA2 induced increased levels Pink-1, p62, and LC3-II/LC3-I ratios (Figure 5A). For further validation of mitophagy, cytoplasmic- and mitochondria-enriched fractions of the cell extracts were collected and evaluated by western blot. In both Ca Ski and SiHa cells, SHetA2 caused recruitment of Pink1 and phosho-parkin (p-parkin, activated parkin) to mitochondria (Figure 5B).

Since mitophagy can serve as a cell survival function by eliminating and recycling damaged mitochondria, or contribute to the cell death by excessive depletion of mitochondria, we next tested if inhibition of mitophagy increased or decreased SHetA2 sensitivities of Ca Ski and SiHa cell lines using Mdivi-1, a selective cell-permeable inhibitor of mitochondrial division DRP1 (dynamin-related GTPase) and mitochondrial division Dynamin I (Dnm1). Inhibition of mitophagy by Mdivi-1 was found to partially, but significantly, reduce SHetA2 mediated cell toxicity (Figure 5C).

Ultimately, SHetA2 treatment results in AIF-induced, caspase-independent apoptosis

We next determined the mechanism of SHetA2-induced cervical cancer cell death. SHetA2 induced caspase-dependent apoptosis in ovarian, kidney, and lung cancer cells (23–26). As expected and consistent with our previous SiHa xenograft study (6), SHetA2 significantly induced caspase-3 activity in cervical cancer cell lines (Figure 6A). Inhibition of caspase activity with a pan-caspase inhibitor, as confirmed by caspase-3 assay (Figure 6A), did not significantly alter SHetA2 cytotoxicity, suggesting that SHetA2 works independently of caspase activity in cervical cancer cell lines (Figure 6B).

To evaluate a potential alternate form of mitochondrial-mediated death, SHetA2 effects on AIF localization and DNA damage were evaluated. Immunofluorescence confocal imaging documented that SHetA2 significantly increased AIF nuclear localization and nuclear staining of γH2AX, as an indicator of DNA damage (Figure 7A). Electron microscopy images

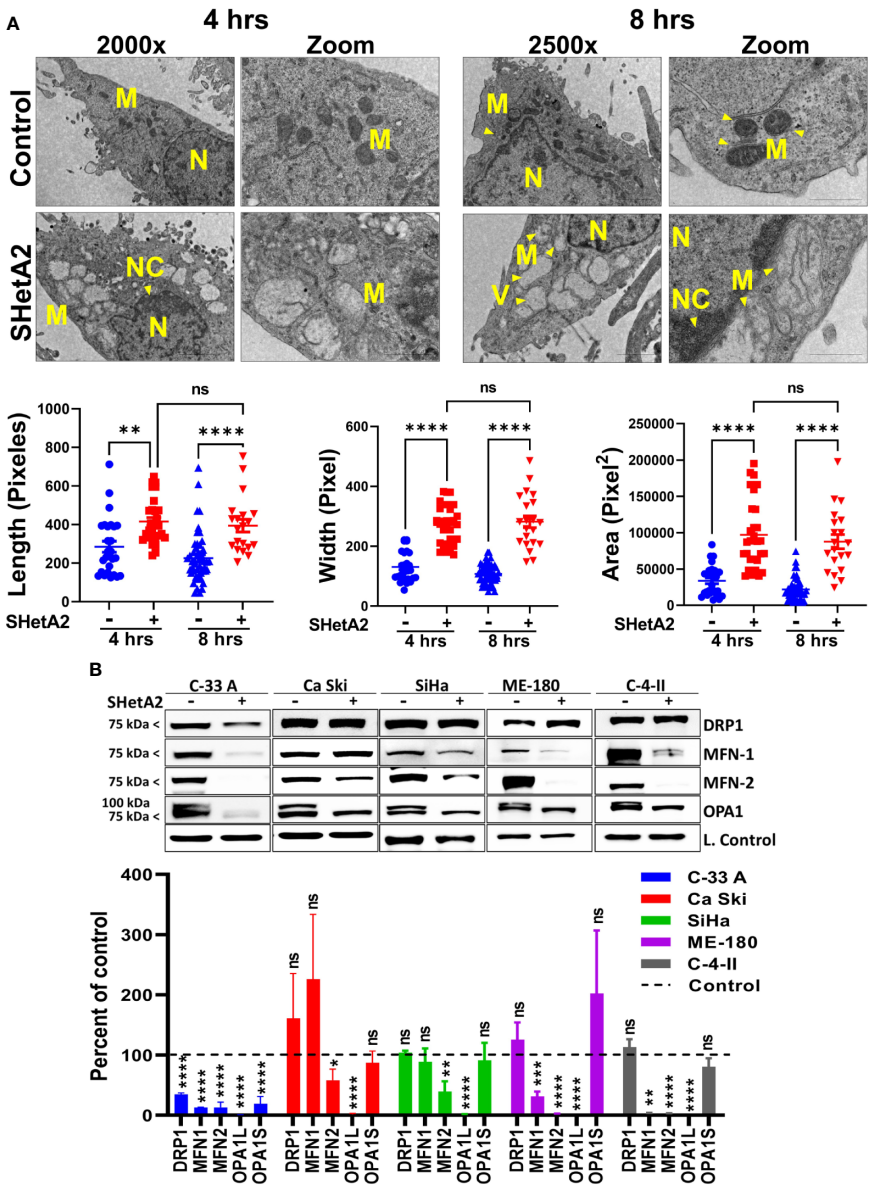

FIGURE 3
SHetA2 alters mitochondrial morphology and downregulate mitochondrial dynamics proteins: **(A)**, TEM of SiHa cells treated with SHetA2 (10 μM) or vehicle for 4 and 8 hours. Representative images showing mitochondria (M), nucleus (N), nuclear condensation (NC) and autophagic vesicles (V) are shown (**A**, upper panel). For the quantification of mitochondrial size, mitochondria with *cristae* structure were measured for length, width and total area and compared by *t*-tests (**A,** lower panel). **(B)**, Western blots of cells treated with DMSO or 10 μM SHetA2 for 48 hours (upper panel). GAPDH (for C-33 A, Ca Ski, SiHa, and C-4-II), or cyclophilin B (for SiHa**)** or α-tubulin (for ME-180) were used as loading controls (L. Control). Densitometric analysis of the bands are shown as mean ± SD and were compared using a *t*-test (lower panel). *$p \leq 0.05$, **$p \leq 0.01$, ***$p \leq 0.001$, ****$p \leq 0.0001$ NS-not significant when compared with respective control.

confirmed nuclear condensation in SHetA2-treated SiHa cells (Figure 3A). siRNA reduction of AIF, confirmed by western blot (Figure 7B), prevented SHetA2 induction of γH2AX (Figure 7B). Metabolic viability assays confirmed reduction of SHetA2 potency and efficacy by AIF siRNA in Ca Ski and SiHa (Figure 7C). Further, combined inhibition of both mitophagy by Mdivi-1 and AIF by siRNA was found to significantly counteract SHetA2-mediated cell death in cervical cancer (Figure 7D). These results document that SHetA2 treatment ultimately results in cell death through mitophagy and AIF migration from mitochondria to the nucleus where it causes DNA damage. In contrast to other cancer types, caspase activation is not required for the mechanism of SHetA2-induced death in cervical cancer.

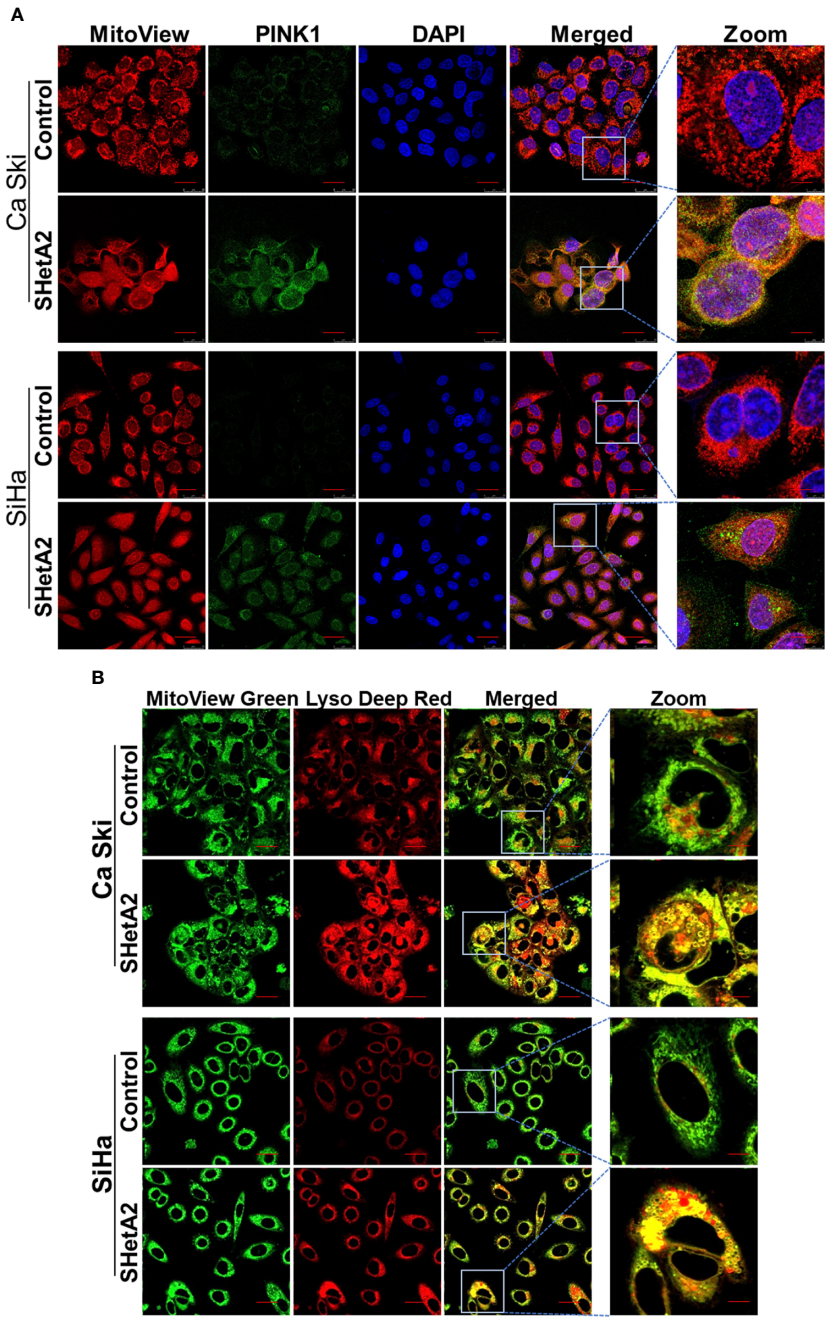

FIGURE 4
SHetA2 induces mitophagy in cervical cancer cells: **(A, B)**, Mitophagy induction was demonstrated by confocal imaging of cervical cancer cells treated with SHetA2 (10 μM) for 24 hours and stained with Pink1 (green) mitotracker red (red) and DAPI (blue) **(A)**, or with MitoView green (green) and Lyso Deep Red (red) dye **(B)**.

Role of hsc70 in cervical cancer and the SHetA2 cell death mechanism

Because hsc70 was identified as an SHetA2 binding protein (16) and can prevent AIF nuclear localization (18), we predicted that SHetA2 disrupts hsc70 binding to AIF. To test this possibility, we immunoprecipitated proteins from Ca Ski and SiHa protein extracts using hsc70 or AIF antibodies and probed the precipitates for the predicted binding proteins. Western blots of the precipitates confirmed that hsc70 co-immunoprecipitated with AIF and that AIF co-immunoprecipitated with hsc70, while SHetA2 treatment of cells for 24-hours, prevented these co-

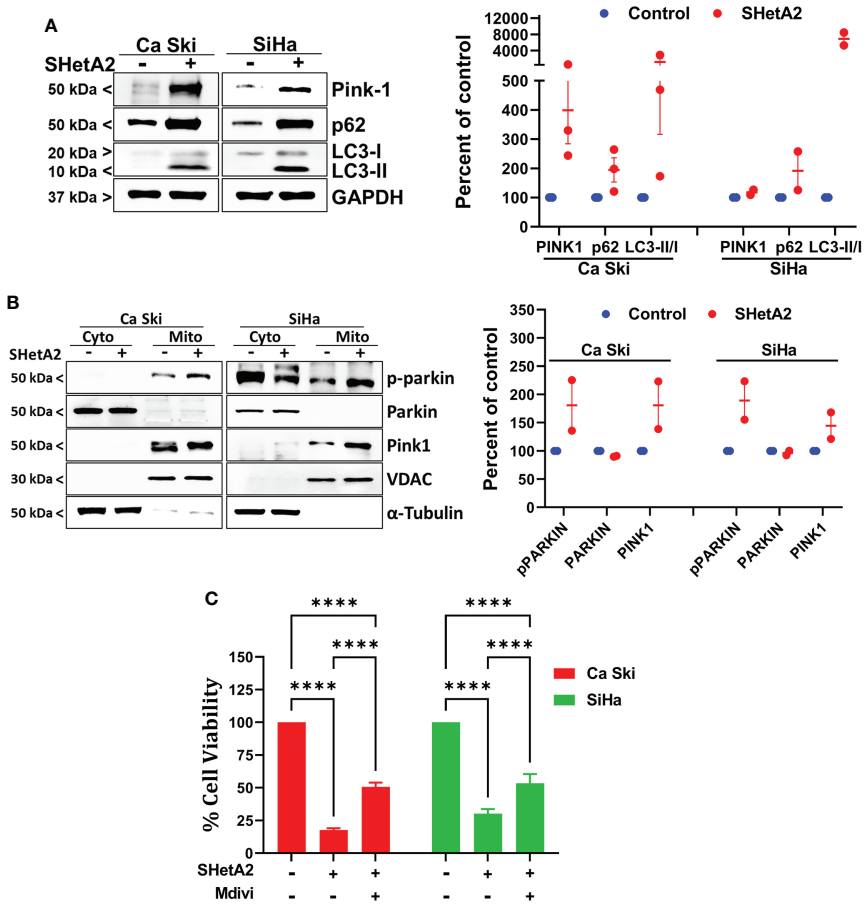

FIGURE 5
SHetA2 induced mitophagy contribute to cervical cancer cell death: **(A)**, Western blot analysis of Ca Ski and SiHa cell treated with SHetA2 (10 μM) for 48 hours (left panel). Densitometric analysis of the bands (Pink-1, p62 and LC3-II/LC3-I ratio) are shown as mean ± SD and were compared using a *t*-test (right panel). **(B)**, Western blot analysis of cytoplasmic and mitochondrial fractions of Ca Ski and SiHa cell treated with SHetA2 (10 μM) for 48 hours (left panel). Densitometric analysis of the bands are shown as mean ± SD and were compared using a *t*-test (right panel). **(C)**, Cervical cancer cells were pre-treated with 10 μM Mdivi-1 for 4 hours followed by SHetA2 (10 μM) for 72 hours and MTT assay was performed. ****$p \leq 0.0001$ when compared with respective control.

immunoprecipitations (Figure 8A). Taken together, these results demonstrate that hsc70 may interfere with SHetA2-induced nuclear AIF localization and DNA damage.

To evaluate the relevance of the SHetA2 hsc70 and mortalin targets in cervical cancer, we probed The Cancer Genome Atlas (TCGA) data using a public website (http://ualcan.path.uab.edu/index.html). This analysis demonstrated significant mortalin overexpression in cervical squamous cell carcinoma compared to healthy tissue ($p < 0.0001$), but this was not associated with patient survival (Figures 8B). Although hsc70 elevation in cervical squamous cell carcinoma was not statistically significant, there was a significant association of high hsc70 expression with reduced survival probability of patients ($p = 0.01$, Figures 8C).

SHetA2 induces mitophagy in, and inhibits growth of, Ca Ski Xenograft Tumors

We next determined if these mitochondrial effects are also caused by SHetA2 treatment in an animal model. Previously, we demonstrated that oral administration of 60 mg/kg SHetA2 significantly inhibited the growth of SiHa cervical cancer xenografts without inducing toxicity (6). In this study, two oral doses (30 and 60 mg/kg/day) of SHetA2 induced a dose-responsive reduction in Ca Ski xenograft tumor growth (Figure 9A). The 60 mg/kg/day dose was statistically significant for reduced tumor volume (ANOVA: $p = 0.0360$) and tumor

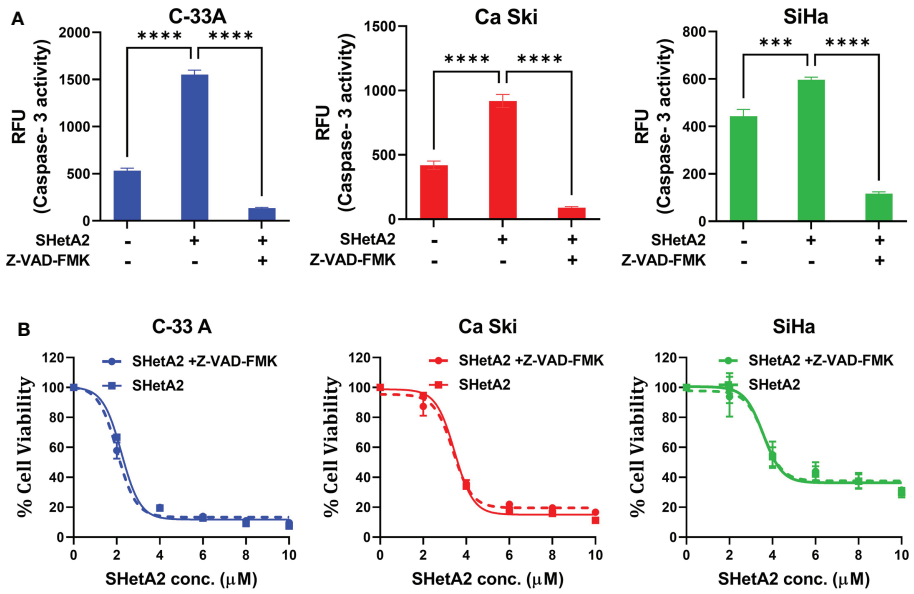

FIGURE 6
SHetA2 inhibits metabolic viability of cervical cancer cell in caspase-independent manner: **(A)**, Caspase 3 activity in cervical cancer cells treated for 48 hours with vehicle, 10 μM SHetA2, or a combination of pan-caspase inhibitor (Z-VAD-FMK, 30 μM, pre-treatment for 3 hours) and SHetA2. A one-way ANOVA was used for statistical analysis. **(B)**, Representative dose response curves of C-33 A, Ca Ski and SiHa cells pretreated with 30 μM of pan-caspase inhibitor (Z-VAD-FMK) for 3 hours followed by SHetA2 treatment at different doses for 72 hours. ***$p \leq 0.001$, ****$p \leq 0.0001$ when compared with respective control.

weight (ANOVA: p = 0.0266) compared to controls. Consistent with the caspase-independent nature of SHetA2 cell killing in cervical cancer cell line cultures, SHetA2 did not significantly alter cleaved caspase 3 expression in Ca Ski xenografts (Figure 9B). TEM of tumors from the 30 mg/kg SHetA2 treated Ca Ski xenografts revealed swollen mitochondria and accumulation of autophagic vesicles (Figure 9C). The majority of autophagic vesicles harbored mitochondria at various stages of degradation. This observation indicates that SHetA2 induced mitochondria-selective autophagy (mitophagy) in association with inhibition of cervical cancer tumor growth.

Discussion

The results of this study demonstrate that SHetA2 kills cervical cancer cells through a similar but, distinct mechanism to that demonstrated in other cancer types. Similar to observations in other cancer types, SHetA2 caused mitochondrial damage which led to activation of caspases and AIF translocation to the nucleus (17, 23–26). In contrast to the dependence on caspase activity for SHetA2 cell killing of ovarian, kidney, and lung cancer cells (21–24), the mechanism in cervical cancer cells occurred independently of caspase activation as documented by a lack of caspase inhibitor effect on SHetA2 cytotoxicity. Because cervical cancer cells are capable of undergoing caspase-dependent apoptosis (27, 28), the caspase activation we observed in SHetA2-treated cells could be contributing, but not required, for SHetA2-induced cell death, because the SHetA2-induced mitophagy and nuclear relocation of AIF could be compensating for the inhibition of caspase activity (Figure 10).

The observation of SHetA2 induction of mitophagy had not been evaluated in previous studies. The SHetA2-induced mitophagy was observed in both cell culture and xenograft tumors. In cell culture, the mitophagy was verified through upregulation of autophagy markers and co-localization of mitophagy-specific proteins with mitochondria and lysosomes. In the xenograft tumors, the levels of mitophagy were excessive with the vast majority of autophagic vesicles observed to contain single mitochondria. Thus, it was not surprising to observe that inhibition of mitophagy decreased the SHetA2 cytotoxicity. The reason for the mitophagy contributing to the mechanism of cell death instead of serving in a survival role is likely due to the excessive nature of the mitophagy eliminating too many mitochondria before more can be made. Combined inhibition of mitophagy and AIF significantly reduced, but did not completely eliminate SHetA2 cytotoxicity. Reasons for the lack of complete prevention could be that the doses and treatment times were not optimized and/or that other factors also contribute to the mechanism of cell death.

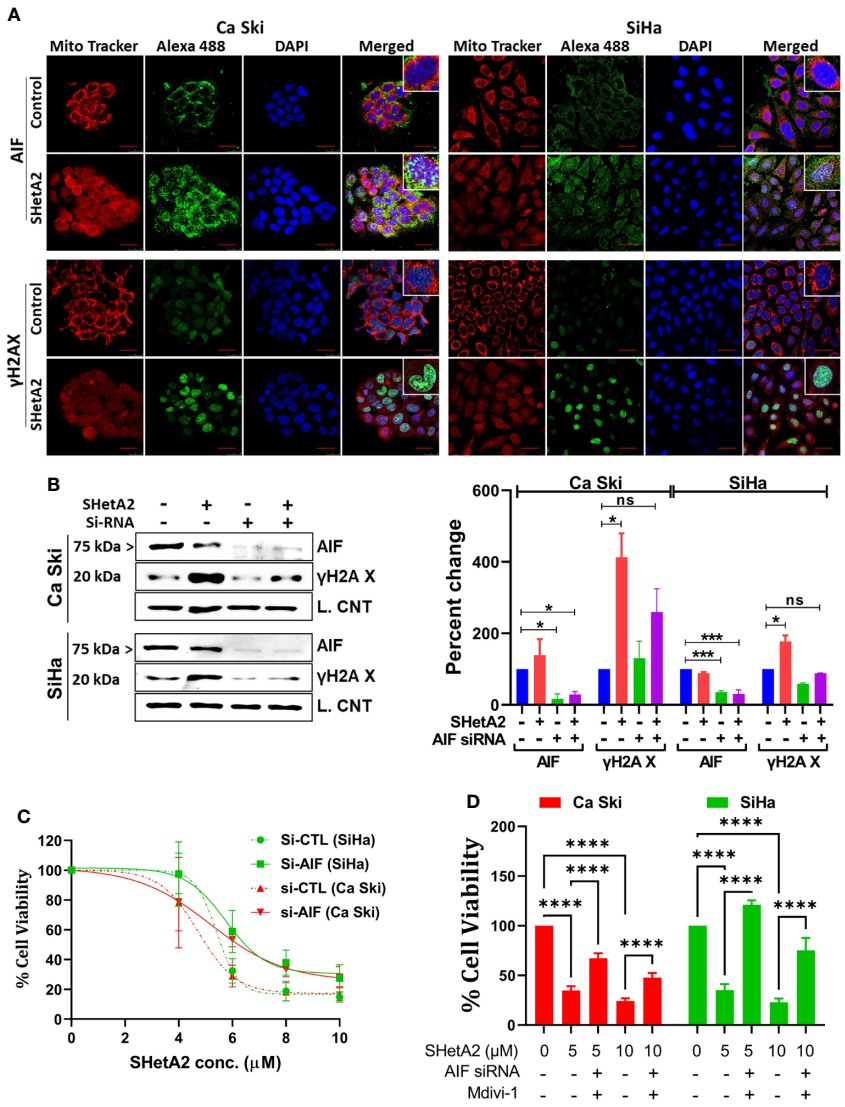

FIGURE 7
SHetA2 induces AIF mediated DNA damage contributing cell death: **(A)**, Confocal microscopy of cells stained with anti -AIF (green) or -γH2AX (green), mitotracker (red) and DAPI (blue) after treatment with 10 μM SHetA2 for 24 hours. **(B)**, Western blots of cells transfected with either non-target si-RNA (si-CTL) or si-AIF and treated with SHetA2 (10 μM) (left panel) and analyzed by densitometry analysis (right panel). GAPDH (Ca Ski, SiHa), or cyclophilin B (SiHa**)** were used as loading controls (L. Control). **(C)**, MTT assays of cells transfected with either si-CTL or si-AIF. **(D)**, cervical cancer cells were transfected with either si-CTL or si-AIF. Following pretreatment with Mdivi-1, transfected cells were treated with SHetA2 at indicated concentration for 72 hours and MTT assay was performed. *$p \leq 0.05$, ***$p \leq 0.001$, ****$p \leq 0.0001$ when compared with respective control.

The lack of caspase dependency of SHetA2-induced cell death in cervical cancer cells could be due to higher capacity of cancer cells to induce mitophagy or higher dependency on hsc70. Currently, it is not known if mitophagy or hsc70 play causative roles in the reason why caspases are not required for SHetA2-induced cell death in cervical cancer cells while they are required in other cancer types. The mitophagy capacity of cervical cancer compared to other cancer types has not been reported. TCGA data probed with the ualcan.path.uab.edu website shows that cervical cancer does not express higher levels of *HSPA8* (gene encoding hsc70) mRNA in comparison to other cancer types. Cervical cancer is one of the 5 out of 32 cancers evaluated by TCGA that have significant associations of high *HSPA8* mRNA expression with worse survival. The others are invasive breast cancer, kidney renal clear cell carcinoma, liver hepatocellular carcinoma and mesothelioma. Thus, it is possible that cervical carcinogenesis involves development of dependency on hsc70 protein expression and that hsc70 contributes to the different

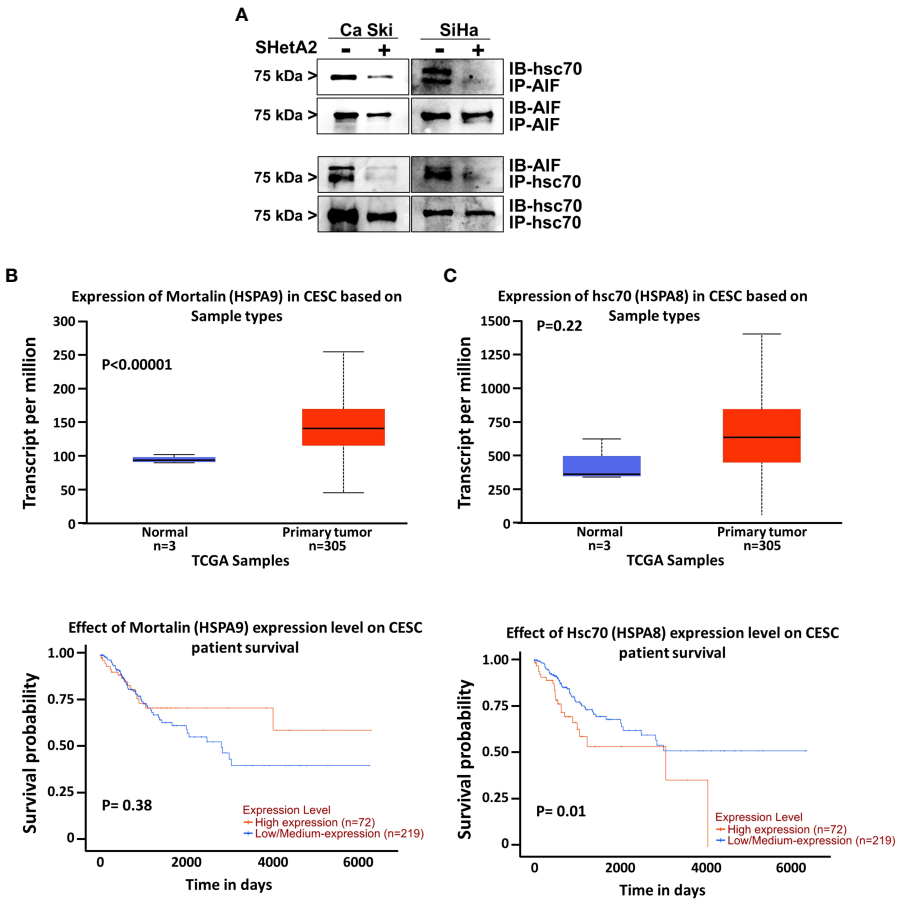

FIGURE 8
Role of hsc70 in cervical cancer and SHetA2 mediated cell death mechanism: **(A)**, Co-immunoprecipitation assays of cervical cancer cells treated with 10 μM SHetA2 for 24 hours. **(B, C)**, UALCAN analysis of TCGA data for expression of mountain (HSPA9, **B**) and hsc70 (HSPA8, **C** upper panel) mRNA in cervical squamous cell carcinoma (CESC) compared to healthy tissue and comparison of their high versus low expression with cervical squamous cell cancer patient survival probability (lower panel **B, C**).

response of cervical cancer cells to SHetA2 in comparison to other cancers. Studies of hsc70 are technically complicated by the 85% homology between hsc70 and HSP70 and cross-reactivity of antibodies to these proteins. (16)

In preclinical studies, SHetA2 was shown to act synergistically with a p53 reactivator in ovarian cancer (8) and with a CDK4/6 inhibitor in cervical cancer (20). These drug combination studies were pursued based on knowledge of the mechanism of SHetA2 as a single agent in cancer cells. The observation in this study that the SHetA2 cell killing mechanism is distinct in cervical cancer cells indicates that the efficacies of drug combinations may differ depending on the cancer type. Knowledge of drug toxicities are also important to take into consideration in designing drug combination trials. One-month long toxicity studies in rats and dogs documented that SHetA2 does not cause toxicity at doses 50 fold higher than doses which reduced tumor growth in rodent models (29). The potential for SHetA2 to be used in prevention studies is supported by its lack of mutagenicity, carcinogenicity, and skin irritancy (30–32). The preclinical SHetA2 drug combination studies conducted to-date observed no significant toxicities in any of the drug treatment groups (8, 20).

Future directions

Currently, an oral capsule formulation of SHetA2 is being evaluated in a first-in-human Phase 1 clinical trial of advanced and recurrent, ovarian, cervical and endometrial cancers (clinicaltrials.gov: NCT04928508). Pending determination of a safe recommended phase 2 dose in this trial, SHetA2 combination studies can be pursued. The caspase-independence of the SHetA2 mechanism observed in this study, suggest that SHetA2 combinations with drugs that act *via* caspases may be worth evaluating, while drugs that inhibit mitophagy or upregulate hsc70 would not be good choices for SHetA2 drug combination studies.

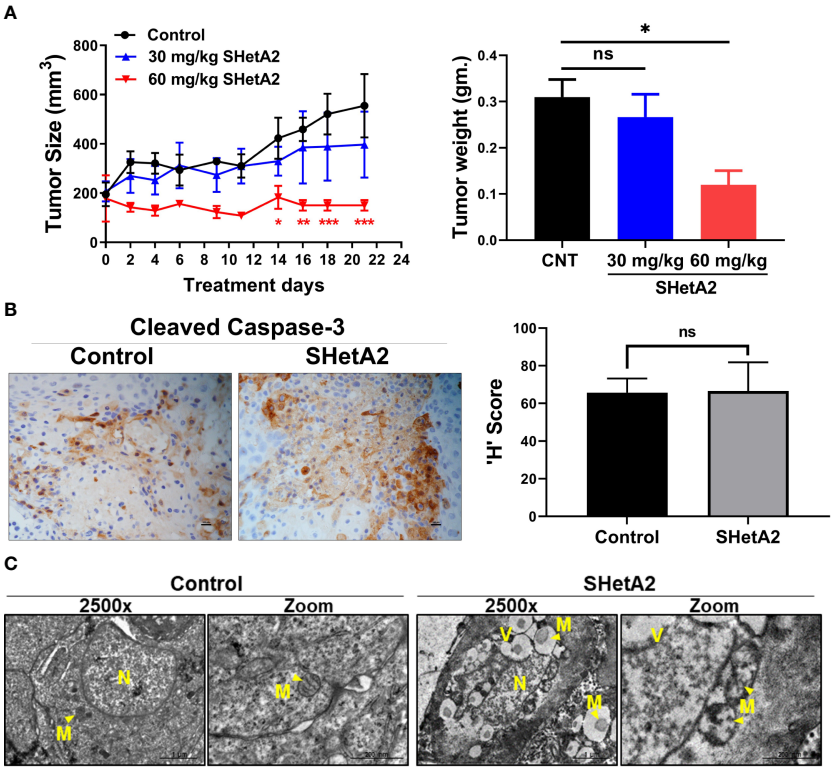

FIGURE 9
SHetA2 induces mitophagy and inhibits growth of cervical cancer tumor *in-vivo*: **(A)**, Average tumor volumes of Ca Ski xenograft in mice treated with orally SHetA2 (30 and 60 mg/kg) or vehicle for 21 days. The average tumor volume during the treatment period (left panel) and tumor weight (right panel) were compared by two-way and one-way ANOVA, respectively. **(B)**, expression of cleaved caspase-3 was measured on the xenograft tumor tissue treated with SHetA2 (60mg/kg group) or control by Immunohistochemistry and the representative images are shown (left panel). The H score was compared between both groups by using Student's *t*-tests (right panel). **(C)**, TEM images of Ca Ski xenograft tumors control or 30 mg/kg/day SHetA2 treatment groups. *$p \leq 0.05$, **$p \leq 0.01$, ***$p \leq 0.001$, ns; not significant when compared with respective control.

The minimal-to-no toxicity observed for SHetA2 to date support further development of SHetA2 as a chemoprevention drug and food additive. Women diagnosed with cervical intraepithelial neoplasia 3 (CIN3) have significant risk of developing cervical cancer and the standard of care for these patients is to have their cervical lesions removed by a loop electrosurgical excision procedure (LEEP), large loop excision of the transformation zone (LLETZ) or cold-knife conization (33). Depending on the Country, women diagnosed with CIN 2 are triaged to either active surveillance or one of these surgical procedures (34). Many women who are triaged to active surveillance feel anxiety about their risk of developing cervical cancer (35). The LEEP/LLETZ/conization procedures are only partially effective as there remains significant risk for future development of neoplasia (36) and cancer (37), especially in hrHPV positive women (38). Furthermore, these surgical procedures cause increased risk of worse obstetrics and neonatal outcomes for those pursuing reproduction after the procedure (39). This situation provides an opportunity to apply SHetA2 as a means to prevent progression of CIN to cancer. Cancer prevention studies of SHetA2 are justified by preclinical studies that documented the ability of SHetA2 to prevent development of the abnormal cancerous phenotype in organotypic cultures of endometrial epithelial cells (40) and in an animal model of colorectal cancer (41). A vaginal suppository formulation of SHetA2 has been developed, which could apply drug directly to the CIN lesion and avoid potential systemic side effects (42–45).

SHetA2 has been shown to bind three related HSP70 proteins, mortalin, Grp78 and hsc70 (16). While the role of mortalin in the mechanism of SHetA2 has been extensively studied (6), this is the first study to evaluate SHetA2 effects on hsc70. The observation that SHetA2 disrupts hsc70/AIF complexes suggests that, in addition to SHetA2 disruption of mortalin complexes, its disruption of hsc70 and potentially Grp78 complexes could contribute to the mechanism of SHetA2 cytotoxicity. Detailed studies are needed to determine which disruptions contribute to the cytotoxicity, which may

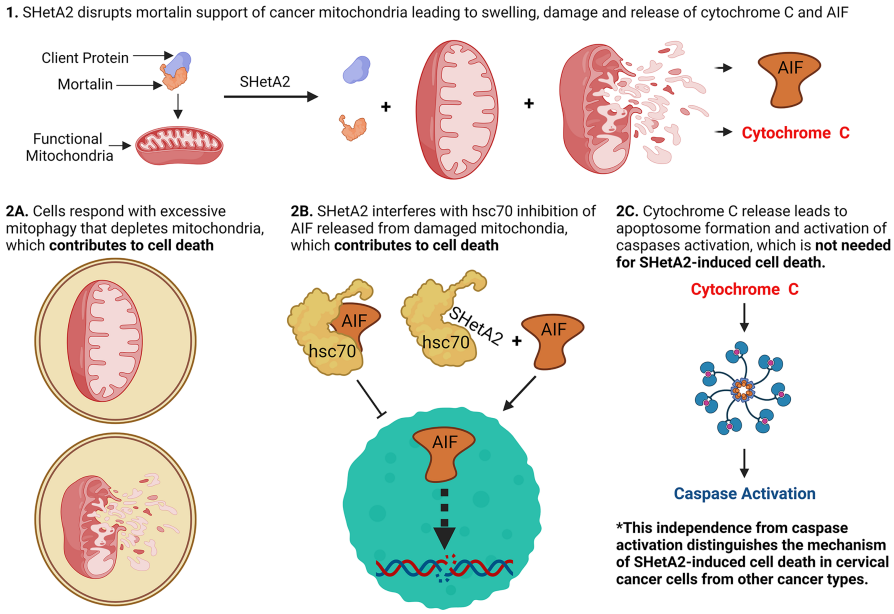

FIGURE 10
Model of SHetA2 mechanism of causing cervical cancer cell death.

counteract the cytotoxicity and/or which may have no effect. This knowledge would be valuable for the development of improved SHetA2 analogs with refined binding profiles to maximize the cytotoxicity while avoiding increased non-specific toxicity. The observation that elevated hsc70 is associated with reduced cervical cancer patient survivability suggest that hsc70 is a relevant target for cervical cancer drug development that warrants further study.

Materials and methods

Cell lines, culture conditions, and chemicals

Authenticated HPV-positive SiHa (RRID : CVCL_0032), Ca Ski (RRID : CVCL_1100), ME-180 (RRID : CVCL_1401), C-4-II (RRID : CVCL_1095), and HPV-negative C-33 A (RRID : CVCL_1094) cell lines were purchased from American Type Culture Collection (ATCC, Manassas, VA, USA) within the last three years and used within 20 passages when verified as mycoplasma-free. All the cell lines were authenticated by ATCC. SiHa, Ca Ski and C-33 A cancer cells were grown in RPMI 1640 medium (R8758, Sigma-Aldrich, Saint Louis, MO, USA), C-4 II cells were grown in Waymouth's medium (# 11220035, Fisher Scientific) and ME-180 cells were grown in McCoy's 5A Medium (#30-2007, ATCC). All the media were supplemented with 10% fetal bovine serum (Serum Source International- FBS17712) and 1% Antibiotic-Antimycotic Solution (ABL02- 100X, Caisson Labs, Smithfield, UT, USA). All experiments were performed with mycoplasma-free cells.

SHetA2 compound synthesized by K. Darrell Berlin at Oklahoma State University as published previously for product 15c in (46) was used in tissue culture studies. For all the cell culture studies, a 10 mM stock solution of SHetA2 was dissolved in dimethylsulfoxide (DMSO, Neta Scientific, Hainesport, NJ, USA). Untreated control cultures were treated with the same final volume of DMSO administered to the treated cultures. For *in vivo* studies, SHetA2 synthesized in bulk by the US National Cancer Institute RAID Program was suspended in 30% Kolliphor HS 15 (SigmaAldrich, Merck, Darmstadt, Germany) in water for use in the animal model. Untreated control animals were gavaged with the same volume of 30% Kolliphor HS 15 given to the treated animals.

Mitochondrial membrane potential assay

Alterations in the MMP were determined using the MMP assay kit (ab113850; Abcam, Cambridge, MA, USA), which utilizes the JC-1 fluorescent dye (5′,6,′-tetrachloro-1,1′,3,3′ tetraethylbenzimidazolyl carbocyanine iodide) as described by the manufacturer's instruction. In brief, cervical cancer cells (1.5×10^4 cells/well) were seeded onto 96-well black plates (#NC1463153, Perkin Elmer, Waltham, MA, USA). Following SHetA2 treatment over a range of times, cells were probed with JC-1 (20 μM) for 20

min at 37°C and washed twice. Fluorescence intensity was measured using a microplate reader for aggregates (excitation at 535 nm and emission at 590 nm) and monomer (excitation at and 475 nm and emission at 530 nm). Change in MMP ($\Delta\psi_{m.}$) was calculated as the ratio of J-aggregates to J-monomers. Depolarized mitochondria are indicated by decreased ($\Delta\psi_{m.}$).

ATP assay

CellTiter-Glo 2.0 Luminescent Cell Viability Assay (#G9241, Promega, Madison, WI, USA) was used and manufacturer's instructions were followed to measure total cellular ATP levels. Briefly, human cervical cancer cells were seeded into 96-well plates at a density of 1×10^4 and allowed to attach overnight followed by SHetA2 treatment for desired time. Afterwards, cells were incubated with CellTiter-Glo reagent and lysed. The luminescence signal was measured using a SYNERGY H1 microplate reader (BioTek, Winooski, VT, USA).

Mitochondrial ROS

Mitochondrial ROS were measured using MitoSOX (Invitrogen) staining. Cervical cells were treated with SHetA2 for 24 hours followed by incubation with MitoSox Red (2.5 μM) for 30 min at 37°C. Data were acquired with a FACS Calibur (BD Biosciences) and analyzed with Flow Jo analytical software.

Confocal microscopy for mitochondrial morphology

To assess mitochondrial morphology, cells were stained with MitoTracker™ Green FM (M7514, Invitrogen, USA). Approximately 6-8 × 10^3 cells were plated on chambered slides and treated with SHetA2 for 24 hours. Then, the cells were stained with 100 nM Mitotracker™ Green FM (Invitrogen) for 30 min at 37°C; after three times washing with PBS, the cells were incubated with 0.1 μg/mL Hoechst. Again, cells were washed twice with PBS and warm medium was administered. Live cell images were acquired with a 63X objective using a Zeiss Axio Observer. Z1 (Göttingen, Germany).

Analysis of mitochondrial mass

To assess the mitochondrial mass, approximately 6-8 × 10^3 cells were plated on 96-well black plates (#NC1463153, Perkin Elmer, Waltham, MA, USA) and treated with SHetA2 or vehicle for 24 hours. Then, the cells were stained with Mitotracker™ Green FM (100 nM, Invitrogen) for 30 min at 37°C; after three times washing with PBS, the cells were incubated with 0.1 μg/mL Hoechst. Then cells were washed twice with PBS and images were captured with the Operetta High Content Imaging System (Perkin Elmer, Waltham, MA, USA). Quantification of staining was done using Harmony Software (Perkin Elmer) to determine mitochondrial mass by the intensity of Mito Tracker green. Numbers of cells were determined by the number of nuclei as detected with Hoechst 33342 staining. The mitochondrial mass measurements were normalized to number of cells.

Transmission electron microscopy

SiHa cells grown in tissue culture in the presence or absence of 10 μM SHetA2, or solvent only, for 4- or 8-hours were fixed overnight at 4°C in 4% paraformaldehyde/2% glutaraldehyde in 0.1M Cacodylate buffer, then post-fixed with 1% OsO4 for one hour. Sample dehydration was performed using graded ethanol and propylene oxide prior to infiltration with Epon/Araldite resin, embedding, and polymerization. Ultrathin (~90nm) sections were cut on a Leica Ultramicrotome and placed on 300 mesh copper grids. Grids were stained with lead for contrast using a standard protocol (Sat. Uranyl Acetate for 30 minutes) and Lead Citrate for 15 minutes). Sections on the grids were visualized using a Hitachi H-7600 Transmission Electron Microscope (at 80 kV).

Xenograft tissues generated as described in xenograft study were processed similarly except for a addition of dehydration step with acetone and propylene oxide.

Western blot analysis

Whole-cell protein extracts of treated and control cervical cancer cells were isolated using the M-PER Mammalian Protein Extraction Reagent (#78501Thermofisher scientific, Waltham, MA, USA) supplemented with 1% phosphatase inhibitor cocktail (#4906845001 Sigma-Aldrich) and 1% protease inhibitor cocktail (#5892791001, Sigma-Aldrich). Mitochondria and cytoplasm-enriched fractions were isolated using Mitochondria/Cytosol Fractionation Kit (# ab65320, Abcam) according to the manufacturer's protocol. Protein concentrations were determined using the BCA assay reagent (#23225 Thermofisher scientific, Waltham, MA, USA). Equal amounts of protein lysates (30μg protein) were electrophoresed into a 12% sodium dodecyl sulfate-polyacrylamide gel electrophoresis (SDS-PAGE) gel (Bio Rad, California, USA), and then transferred to polyvinylidene difluoride (PVDF) membrane (Bio Rad, California, USA) using a Trans-Blot® Turbo™ Transfer System. The membranes were blocked with Tris Buffered Saline with 0.1% v/v Tween-20 (TBST) containing 10% dry skim milk for 1 hour at room temperature. Subsequently, membranes were probed with the primary antibodies overnight at 4°C. Primary antibodies; DRP1

(#5391), OPA1 (#80471), MFN1 (#14739), MFN2 (#11925), LC-3A/B (#12741), Cleaved Caspase-3 (#9664), AIF (#4642), γH2AX (#2577), Pink1 (#6946), Parkin (2132), VDAC (#4661), LC3A/B (#12741), P62/SQSTM1, GAPDH (#5174), α-Tubulin (#2125), Cyclophilin B (#43603) were purchased from Cell Signaling Technology. AIF (MA5-15880) and phospho (Ser65) Parkin (orb312554) antibodies were purchased from Thermo Fisher Scientific and Biorbyt, respectively. The primary antibody to hsc70 [EP1531Y] (ab51052) was purchased from Abcam. After three times washing with TBST, the membranes were incubated with horse radish peroxidase (HRP) conjugated anti-rabbit IgG (1:5000) or anti-mouse IgG (1:6000) for 45 min at room temperature followed by additional washing. After washing, protein bands were detected using the Enhanced Chemiluminescence (Clarity™ Western ECL Substrate #1705060S, BioRad, Hercules, CA, USA) and the Chemidoc Touch Imaging System (Bio Rad, Hercules, CA, USA) according to the manufacturer's instructions. GAPDH/cyclophilin B or α tubulin was used as loading controls. Densitometric analysis was performed using Image Lab software (BioRad, Hercules, CA, USA).

Cell viability Assay

Cell viability was measured using the 3-(4,5-dimethylthiazol-2-yl)-2, 5-diphenyl-tetrazolium bromide assay (MTT assay; #G4100, Promega Madison, WI, USA). Briefly, cells were harvested from culture dishes using 0.05% trypsin-0.02% EDTA, and cultured overnight in 96 well plates at densities of 4 000 cells/well. Then cells were treated with 0 - 10 μM of SHetA2 for 24- or 72-hours followed by addition of MTT solution (15μl). After a 2-hour incubation in the presence of MTT solution, solubilizing or STOP solution was added and the culture plate was incubated overnight. The optical density (OD) was measured at a wavelength of 570 & 620 nm using a BioTek Synergy H1 Micro Plate Reader and Gen5 2.09 Software. The average ODs of triplicate treatments were normalized to the average ODs of the cultures treated with DMSO solvent only. Prism 8 software (GraphPad, San Diego, CA, USA) was used to plot the normalized ODs against the SHetA2 concentrations used and to derive the half maximal inhibitory concentrations (IC_{50}s/potencies), and efficacies (maximal percent growth inhibition activities) using nonlinear regression. For each cell line, experiments were performed in triplicate and repeated 2-3 times with consistent results.

Caspase-3 activity assay

Caspase-3 activity was measured using Caspase 3, Caspase 8, and Caspase 9 Multiplex Activity Assay Kit (Fluorometric#ab219915, Abcam, Cambridge, MA, USA). Briefly, 1.5 X 10^4 cells were seeded in 96-well black plate for overnight and treated with SHetA2 (10 μM) for 48 hours. Then Caspase 3 substrate was added to each well and the plate was incubated at room temperature for 60 minutes in dark. The fluorescence intensity was measured with using a Bio-tek Synergy H1 Micro Plate Reader and Gen5 Software at *Ex*/*Em* of 535/620 nm for caspase-3.

Immunofluorescence microscopy

Expression and/or localization of AIF, γH2AX and PINK1 were investigated by immunofluorescence microscopy. In brief, approximately 6-8000 cervical cancer cells were seeded on 8-chambered slides, and treated with SHetA2 or vehicle for 24 hours. Then the cells were fixed with 4% paraformaldehyde and permeabilized with 0.1% TritonX-100 in PBS. Following blocking with 4% BSA in PBS, cells were incubated with and MitoTracker™ Red CMXRos (#M7512, Thermo Fisher Scientific) for 45 minutes and then by primary antibodies for AIF (#MA5-15880, Thermo Fisher Scientific) or γH2AX or PINK1 at 1:100 dilutions in 1% BSA-PBS for overnight. After washing, cells were stained with Alexa Fluor 488-labeled secondary antibody for 1 hour. DAPI (blue) was used to stain the nucleus. Cell images were acquired with a 63X objective using a Zeiss Axio Observer Z1 (Göttingen, Germany). For mitophagy detection, cervical cancer cells treated with SHetA2 or DMSO were stained with LysoTracker™ Deep Red (#L12492, Thermo Fisher Scientific) and MitoTracker™ Green FM, and live-cell imaging was performed with a 63X objective using a Zeiss Axio Observer Z1 (Göttingen).

Co-immunoprecipitation assay

For the co-immunoprecipitation assay, cervical cancer cells were treated with SHetA2 or vehicle for 24 hours and protein isolates were collected with M-PER. Approximately 500 μg of protein lysate was incubated with agarose beads (already coupled with 10 μg of hsc70 or AIF antibodies per manufacturer protocol of PierceTM Crosslink IP kit, ThermoFisher Scientific # 26147) overnight at 4°C. Then beads were washed with buffer provided in the kit and the immuno-precipitated complexes were collected, re-suspended in sample buffer and heated for 5 min at 95°C. The co-immunoprecipitation of client proteins was detected by Western blot analysis using equal volumes of immuno-precipitated proteins.

Xenograft study

The animal study was approved by the University of Oklahoma Health Sciences Center Institutional Animal Care and Use Committee (IACUC Protocol #19-009-CHI). After an acclimation period of two weeks, female athymic Hsd : Athymic Nude-*Foxn1nu* mice (four-week old, ENVIGO, Alice, TX, USA)

were subcutaneously injected with 5×10^6 Ca Ski cells suspended in 1× phosphate buffered saline (PBS). Tumor sizes were measured thrice per week with calipers. Once the tumors achieved ~200 mm^3 average tumor volume ([$width^2$ × length]/2), mice were randomized into 3 animals/treatment group based on tumor volume so that there were no significant differences between the groups (ANOVA, $p > 0.05$) and treatment was initiated. SHetA2 was orally administered daily for 21 days at doses of 30 mg/kg and 60 mg/kg while the control group was gavaged with placebo (30% Kolliphor HS 15 in water). At the end of the study period, animals were sacrificed. Tumors were collected and weighed at the time of necropsy. Tumors in the 30 mg/kg/day dose group were fixed for transmission electron microscopy analysis. Tumors in the 60 mg/kg/day dose group were fixed for immunohistochemical staining.

Statistical analysis

All the experiments were independently repeated at least twice or thrice and in triplicate wherever applicable. Data are expressed as mean ± standard deviation (SD) for experimental replicates and standard deviation of the mean (SEM) for biological replicates. The *t*-test and ANOVA were used to make comparisons between two groups or multiple groups, respectively. In situations where the data was not normally distributed, the Mann-Whitney test or Kursal-Wallis test, were used for two groups or multiple groups, respectively P <0.05 was considered statistically significant. Statistical analyses were done using GraphPad Prism 8 or 9 Software (GraphPad Software Inc., La Jolla, CA, USA).

Data availability statement

The original contributions presented in the study are included in the article/Supplementary Material. Further inquiries can be directed to the corresponding author.

Ethics statement

The animal study was reviewed and approved by University of Oklahoma Health Sciences Center Institutional Animal Care and Use Committee.

Author contributions

Conception and Design: RR and DB; Development of Methodology: RR, VC; Acquisition and analysis of data; RR for all, VC for mitochondrial network analysis and confocal imaging, AK for xenograft tumor growth, RZ for quantification of immunohistochemical staining of tumors, DB for bioinformatics; Interpretation of data: RR, VC and DB; Writing of manuscript: RR and DB; Review of manuscript: AK, VC, RR, DB; Administrative, technical or material support; RR and DB; Study Supervision: RR and DB. All authors read and approved the final manuscript.

Funding

This research was funded by the National Cancer Institute grant R01CA200126. Research reported in this publication was supported by National Cancer Institute (NCI) grant R01CA200126 (DB) and in part by the NCI Cancer Center Support Grant P30CA225520 awarded to the University of Oklahoma Stephenson Cancer Center and used the Molecular Biology and Cytometry Research and the Biospecimen and Tissue Pathology Shared Resources.

Acknowledgments

Transmission electron microscopy was performed by the Oklahoma Medical Research Foundation Imaging Core Facility. Illustration created with BioRender.com.

Conflict of interest

The authors declare that the research was conducted in the absence of any commercial or financial relationships that could be construed as a potential conflict of interest.

Publisher's note

Author disclaimer

The content is solely the responsibility of the authors and does not necessarily represent the official views of the National Institutes of Health.

Supplementary material

The Supplementary Material for this article can be found online at: https://www.frontiersin.org/articles/10.3389/fonc.2022.958536/full#supplementary-material

SUPPLEMENTARY FIGURE 1

SHetA2 induces mitochondrial ROS in cervical cancer cells: **(A, B)**, ME-180 and C-4-II cervical cancer cells were treated with 10 μM SHetA2 or vehicle for 24 hours followed by MitoSOX staining and analyzed by flow cytometry. Representative staining histogram depicting % MitoSOX positive cells are shown (left panel). Bar graphs (right panel) show the mean ±SD of three independent experiments and a t-test was used for statistical analysis. **(C)**, C-33 A, Ca Ski and SiHa cervical cancer cells treated with 10 μM SHetA2 or vehicle for 24 hours were stained with MitoTracker™ Green and Hoechst. The fluorescence was imaged and analyzed by using the Operetta®High Content Imaging System. ** $p \leq 0.01$, **** $p \leq 0.0001$ when compared with respective control.

SUPPLEMENTARY FIGURE 2

SHetA2 induces mitophagy in cervical cancer cells: Mitophagy induction was demonstrated by confocal imaging of cervical cancer cells treated with SHetA2 (10 μM) for 24 hours and stained with Pink1 (green) mitotracker red (red) and DAPI (blue). Colocalized (Yellow) spots for Mitoview and Pink1 were counted using ImageJ software.

References

1. Arbyn M, Weiderpass E, Bruni L, de Sanjosé S, Saraiya M, Ferlay J, et al. Estimates of incidence and mortality of cervical cancer in 2018: A worldwide analysis. *Lancet Glob Health* (2020) 8(2):e191–203. doi: 10.1016/s2214-109x(19)30482-6

2. Fu Z-Z, Li K, Peng Y, Zheng Y, Cao L-Y, Zhang Y-J, et al. Efficacy and toxicity of different concurrent chemoradiotherapy regimens in the treatment of advanced cervical cancer: A network meta-analysis. *Medicine* (2017) 96(2):e5853–e. doi: 10.1097/MD.0000000000005853

3. Rubinsak LA, Kang L, Fields EC, Carter JS, McGuire WP, Temkin SM. Treatment-related radiation toxicity among cervical cancer patients. *Int J Gynecol Cancer* (2018) 28(7):1387–93. doi: 10.1097/igc.0000000000001309

4. Zhang Z, Jing J, Ye Y, Chen Z, Jing Y, Li S, et al. Characterization of the dual functional effects of heat shock proteins (Hsps) in cancer hallmarks to aid development of hsp inhibitors. *Genome Med* (2020) 12(1):101. doi: 10.1186/s13073-020-00795-6

5. Rai R, Kennedy AL, Isingizwe ZR, Javadian P, Benbrook DM. Similarities and differences of Hsp70, Hsc70, Grp78 and mortalin as cancer biomarkers and drug targets. *Cells* (2021) 10(11):2296. doi: 10.3390/cells10112996

6. Benbrook DM. Sheta2 attack on mortalin and colleagues in cancer therapy and prevention. *Front Cell Dev Biol* (2022) 10:848682. doi: 10.3389/fcell.2022.848682

7. Wadhwa R, Takano S, Kaur K, Deocaris CC, Pereira-Smith OM, Reddel RR, et al. Upregulation of Mortalin/Mthsp70/Grp75 contributes to human carcinogenesis. *Int J Cancer* (2006) 118(12):2973–80. doi: 10.1002/ijc.21773

8. Ramraj SK, Elayapillai SP, Pelikan RC, Zhao YD, Isingizwe ZR, Kennedy AL, et al. Novel ovarian cancer maintenance therapy targeted at mortalin and mutant P53. *Int J Cancer* (2019) 147(4):1086–97. doi: 10.1002/ijc.32830

9. Xu M, Jin T, Chen L, Zhang X, Zhu G, Wang Q, et al. Mortalin is a distinct bio-marker and prognostic factor in serous ovarian carcinoma. *Gene* (2019) 696:63–71. doi: 10.1016/j.gene.2019.02.033

10. Lu WJ, Lee NP, Kaul SC, Lan F, Poon RT, Wadhwa R, et al. Mortalin-P53 interaction in cancer cells is stress dependent and constitutes a selective target for cancer therapy. *Cell Death Differ* (2011) 18(6):1046–56. doi: 10.1038/cdd.2010.177

11. Wu PK, Hong SK, Veeranki S, Karkhanis M, Starenki D, Plaza JA, et al. A Mortalin/Hspa9-mediated switch in tumor-suppressive signaling of Raf/Mek/Extracellular signal-regulated kinase. *Mol Cell Biol* (2013) 33(20):4051–67. doi: 10.1128/MCB.00021-13

12. Wu P-K, Hong S-K, Park J-I. Steady-state levels of phosphorylated mitogen-activated protein kinase kinase 1/2 determined by Mortalin/Hspa9 and protein phosphatase 1 alpha in kras and braf tumor cells. *Mol Cell Biol* (2017) 37(18):e00061–17. doi: 10.1128/MCB.00061-17

13. Starenki D, Hong SK, Lloyd RV, Park JI. Mortalin (Grp75/Hspa9) upregulation promotes survival and proliferation of medullary thyroid carcinoma cells. *Oncogene* (2015) 34(35):4624–34. doi: 10.1038/onc.2014.392

14. Wu PK, Hong SK, Chen W, Becker AE, Gundry RL, Lin CW, et al. Mortalin (Hspa9) facilitates braf-mutant tumor cell survival by suppressing Ant3-mediated mitochondrial membrane permeability. *Sci Signaling* (2020) 13(622):eaay1478. doi: 10.1126/scisignal.aay1478

15. Wu PK, Hong SK, Starenki D, Oshima K, Shao H, Gestwicki JE, et al. Mortalin/Hspa9 targeting selectively induces kras tumor cell death by perturbing mitochondrial membrane permeability. *Oncogene* (2020) 39(21):4257–70. doi: 10.1038/s41388-020-1285-5

16. Benbrook DM, Nammalwar B, Long A, Matsumoto A, Singh A, Bunce RA, et al. SHetA2 interference with mortalin binding to P66shc and P53 identified using drug-conjugated magnetic microspheres. *Invest New Drugs* (2013) 32):412–23. doi: 10.1007/s10637-013-0041-x

17. Chandra V, Rai R, Benbrook DM. Utility and mechanism of Sheta2 and paclitaxel for treatment of endometrial cancer. *Cancers (Basel)* (2021) 13(10):2322. doi: 10.3390/cancers13102322

18. Novo N, Ferreira P, Medina M. The apoptosis-inducing factor family: Moonlighting proteins in the crosstalk between mitochondria and nuclei. *IUBMB Life* (2021) 73(3):568–81. doi: 10.1002/iub.2390

19. Ravagnan L, Gurbuxani S, Susin SA, Maisse C, Daugas E, Zamzami N, et al. Heat-shock protein 70 antagonizes apoptosis-inducing factor. *Nat Cell Biol* (2001) 3(9):839–43. doi: 10.1038/ncb0901-839

20. Kennedy AL, Rai R, Isingizwe ZR, Zhao YD, Lightfoot SA, Benbrook DM. Complementary targeting of Rb phosphorylation and growth in cervical cancer cell cultures and a xenograft mouse model by Sheta2 and palbociclib. *Cancers (Basel)* (2020) 12(5):1269. doi: 10.3390/cancers12051269

21. Anand R, Wai T, Baker MJ, Kladt N, Schauss AC, Rugarli E, et al. The I-aaa protease Yme1l and Oma1 cleave Opa1 to balance mitochondrial fusion and fission. *J Cell Biol* (2014) 204(6):919–29. doi: 10.1083/jcb.201308006

22. Choubey V, Zeb A, Kaasik A. Molecular mechanisms and regulation of mammalian mitophagy. *Cells* (2022) 11(1). doi: 10.3390/cells11010038

23. Chengedza S, Benbrook DM. Nf-Kb is involved in Sheta2 circumvention of tnf-α resistance, but not induction of intrinsic apoptosis. *Anti-Cancer Drugs* (2010) 21:297–305. doi: 10.1097/CAD.0b013e3283350e43

24. Lin Y-D, Chen S, Yue P, Zou W, Benbrook DM, Liu S, et al. Caat/Enhancer binding protein homologous protein-dependent death receptor 5 induction is a major component of Sheta2-induced apoptosis in lung cancer cells. *Cancer Res* (2008) 68(13):5335–44. doi: 10.1158/0008-5472.CAN-07-6209

25. Liu T, Masamha CP, Chengedza S, Berlin KD, Lightfoot S, He F, et al. Development of flexible-heteroarotinoids for kidney cancer. *Mol Cancer Ther* (2009) 8(5):1227–38. doi: 10.1158/1535-7163.MCT-08-1069

26. Moxley K, Chengedza S, Benbrook DM. Induction of death receptor ligand-mediated apoptosis in epithelial ovarian carcinoma: The search for sensitizing agents. *Gynecol Oncol* (2009) 115:438–42. doi: 10.1016/j.ygyno.2009.09.007

27. Sharma S, Deep A, Sharma AK. Current treatment for cervical cancer: An update. *Anti-cancer Agents Med Chem* (2020) 20(15):1768–79. doi: 10.2174/1871520620666200224093301

28. Lagunas-Martinez A, Madrid-Marina V, Gariglio P. Modulation of apoptosis by early human papillomavirus proteins in cervical cancer. *Biochim Biophys Acta* (2010) 1805(1):6–16. doi: 10.1016/j.bbcan.2009.03.005

29. Kabirov KK, Kapetanovic IM, Benbrook DM, Dinger N, Mankovskaya I, Zakharov A, et al. Oral toxicity and pharmacokinetic studies of SHetA2, a new chemopreventive agent, in rats and dogs. *Drug Chem Toxicol* (2012) 36(3):284–95. doi: 10.3109/01480545.2012.710632

30. Benbrook D, Kamelle S, Guruswamy S, Lightfoot S, Rutledge T, Gould N, et al. Flexible heteroarotinoids (Flex-hets) exhibit improved therapeutic ratios as anti-cancer agents over retinoic acid receptor agonists. *Investigational New Drugs* (2005) 23(5):417–28. doi: 10.1007/s10637-005-2901-5

31. Doppalapudi RS, Riccio ES, Davis Z, Menda S, Wang A, Du N, et al. Genotoxicity of the cancer chemopreventive drug candidates cp-31398, SHetA2, and phospho-ibuprofen. *Mutat Res* (2012) 746(1):78–88. doi: 10.1016/j.mrgentox.2012.03.009

32. Mic FA, Molotkov A, Benbrook DM, Duester G. Retinoid activation of retinoic acid receptor but not retinoid X receptor is sufficient to rescue lethal defect in retinoic acid synthesis. *Proc Natl Acad Sci United States America* (2003) 100:7135–40. doi: 10.1073/pnas.1231422100

33. Chen RJ, Chang DY, Yen ML, Chow SN, Huang SC. Loop electrosurgical excision procedure for conization of the uterine cervix. *J Formos Med Assoc* (1994) 93(3):196–9.

34. Lycke KD, Petersen LK, Gravitt PE, Hammer A. Known benefits and unknown risks of active surveillance of cervical intraepithelial neoplasia grade 2. *Obstet Gynecol* (2022) 139(4):680–6. doi: 10.1097/AOG.0000000000004705

35. Hansen J, Kirkegaard P, Folmann B, Bungum HF, Hammer A. "I feel reassured, but there is no guarantee." how do women with a future childbearing desire respond to active surveillance of cervical intraepithelial neoplasia grade 2? a qualitative study. *Acta Obstet Gynecol Scand* (2022) 101(6):616–23. doi: 10.1111/aogs.14354

36. Kocken M, Helmerhorst TJM, Berkhof J, Louwers JA, Nobbenhuis MAE, Bais AG, et al. Risk of recurrent high-grade cervical intraepithelial neoplasia after successful treatment: A long-term multi-cohort study. *Lancet Oncol* (2011) 12 (5):441–50. doi: 10.1016/S1470-2045(11)70078-X

37. Sand FL, Frederiksen K, Munk C, Jensen SM, Kjaer SK. Long-term risk of cervical cancer following conization of cervical intraepithelial neoplasia grade 3-a Danish nationwide cohort study. *Int J Cancer* (2018) 142(9):1759–66. doi: 10.1002/ijc.31202

38. Sand FL, Frederiksen K, Kjaer SK. Risk of recurrent disease following conization of cervical intraepithelial neoplasia grade 3 according to post-conization hpv status and surgical margins. *Gynecol Oncol* (2022) 165(3):472–7. doi: 10.1016/j.ygyno.2022.03.015

39. Kyrgiou M, Athanasiou A, Paraskevaidi M, Mitra A, Kalliala I, Martin-Hirsch P, et al. Adverse obstetric outcomes after local treatment for cervical preinvasive and early invasive disease according to cone depth: Systematic review and meta-analysis. *Bmj* (2016) 354:i3633. doi: 10.1136/bmj.i3633

40. Benbrook DM, Lightfoot S, Ranger-Moore J, Liu T, Chengedza S, Berry WL, et al. Gene expression analysis in an organotypic model of endometrial carcinogenesis and chemoprevention. *Gene Regul Syst Biol* (2008) 2:21–42. doi: 10.4137/grsb.s344

41. Benbrook DM, Guruswamy S, Wang Y, Sun Z, Mohammed A, Zhang Y, et al. Chemoprevention of colon and small intestinal tumorigenesis in apcmin/+ mice by Sheta2 (Nsc721689) without toxicity. *Cancer Prev Res* (2013) 6(9):908–16. doi: 10.1158/1940-6207.capr-13-0171

42. Mahjabeen S, Hatipoglu MK, Benbrook DM, Garcia-Contreras L. Pharmacokinetics and pharmacodynamics of escalating doses of Sheta2 after vaginal administration to mice. *J Pharm Sci* (2018) 107(12):3179–86. doi: 10.1016/j.xphs.2018.08.024

43. Mahjabeen S, Hatipoglu MK, Benbrook DM, Kosanke SD, Garcia-Contreras D, Garcia-Contreras L. Influence of the estrus cycle of the mouse on the disposition of Sheta2 after vaginal administration. *Eur J Pharmaceut Biopharmaceut* (2018) 130:272–80. doi: 10.1016/j.ejpb.2018.07.004

44. Mahjabeen S, Hatipoglu MK, Chandra V, Benbrook DM, Garcia-Contreras L. Optimization of a vaginal suppository formulation to deliver Sheta2 as a novel treatment for cervical dysplasia. *J Pharm Sci* (2018) 107(2):638–46. doi: 10.1016/j.xphs.2017.09.018

45. Mahjabeen S, Hatipoglu MK, Kosanke SD, Garcia-Contreras D, Benbrook DM, Garcia-Contreras L. Vaginal suppositories containing Sheta2 to treat cervical dysplasia: Pharmacokinetics of daily doses and preliminary safety profile. *J Pharm Sci* (2020) 109(6):2000–8. doi: 10.1016/j.xphs.2020.02.016

46. Liu S, Brown CW, Berlin KD, Dhar A, Guruswamy S, Brown D, et al. Synthesis of flexible sulfur-containing heteroarotinoids that induce apoptosis and reactive oxygen species with discrimination between malignant and benign cells. *J Med Chem* (2004) 47(4):999–1007. doi: 10.1021/jm030346v

frontiers | Frontiers in Oncology

TYPE Review
PUBLISHED 29 September 2022
DOI 10.3389/fonc.2022.1009345

OPEN ACCESS

EDITED BY
Sara Ricardo,
Universidade do Porto, Portugal

REVIEWED BY
J. Omar Muñoz-Bello,
National Institute of Cancerology (INCAN), Mexico
Diego Raimondo,
University of Bologna, Italy

*CORRESPONDENCE
Andrew B. Gladden
agladden@email.unc.edu

SPECIALTY SECTION
This article was submitted to Gynecological Oncology, a section of the journal Frontiers in Oncology

RECEIVED 01 August 2022
ACCEPTED 15 September 2022
PUBLISHED 29 September 2022

CITATION
Parrish ML, Broaddus RR and Gladden AB (2022) Mechanisms of mutant β-catenin in endometrial cancer progression.
Front. Oncol. 12:1009345.
doi: 10.3389/fonc.2022.1009345

Mechanisms of mutant β-catenin in endometrial cancer progression

Molly L. Parrish[1,2], Russell R. Broaddus[1,2] and Andrew B. Gladden[1,2]*

[1]Department of Pathology and Laboratory Medicine, The University of North Carolina at Chapel Hill, Chapel Hill, NC, United States, [2]Pathobiology and Translational Science Graduate Program, The University of North Carolina at Chapel Hill, Chapel Hill, NC, United States

Endometrial carcinoma (EC) is the most diagnosed gynecological malignancy in Western countries. Both incidence and mortality rates of EC have steadily risen in recent years. Despite generally favorable prognoses for patients with the endometrioid type of EC, a subset of patients has been identified with decreased progression-free survival. Patients in this group are distinguished from other endometrioid EC patients by the presence of exon 3 hotspot mutations in *CTNNB1*, the gene encoding for the β-catenin protein. β-catenin is an evolutionarily conserved protein with critical functions in both adherens junctions and Wnt-signaling. The exact mechanism by which exon 3 *CTNNB1* mutations drive EC progression is not well understood. Further, the potential contribution of mutant β-catenin to adherens junctions' integrity is not known. Additionally, the magnitude of worsened progression-free survival in patients with *CTNNB1* mutations is context dependent, and therefore the importance of this subset of patients can be obscured by improper categorization. This review will examine the history and functions of β-catenin, how these functions may change and drive EC progression in *CTNNB1* mutant patients, and the importance of this patient group in the broader context of the disease.

KEYWORDS

endometrial cancer, β-catenin, tumor progression, cell adhesion, Wnt-signaling

Introduction

Endometrial carcinoma (EC) is the most common gynecological cancer in the industrialized world. EC poses a unique challenge, as incidence and mortality rates continue to rise despite many other major cancer types declining in recent years (1). An estimated 65,950 new cases and 12,550 deaths are predicted to arise in 2022. Strikingly, endometrial cancer mortality likelihood has risen from a 0.3% chance from 1997-2008 to a 1.9% chance from 2008-2018 (1). Endometrial cancer is primarily defined by two

histological subtypes, endometrioid and non-endometrioid, where endometrioid EC comprises approximately 80% of cases (2). Endometrioid endometrial cancers (EEC) are characterized by being low grade and having glandular histology resembling the normal endometrium. EEC is associated with intrinsic risk factors like obesity and excess estrogen and presents at a low stage at the time of diagnosis. Further, endometrial hyperplasia can be a precursor for EECs. Conversely, non-endometrioid endometrial cancers are far less common and not typically associated with environmental or life-style related risk factors. These cancers tend to be more aggressive, presenting with higher stage and higher grade non-endometrioid histological types including serous and clear cell histology.

Endometrioid and non-endometrioid endometrial cancers have different mutational signatures. Endometrioid cancers have a broader mutational spectrum than non-endometrioid cancers. Alterations in the PI3K/Akt/mTOR pathway, Wnt/β-catenin pathway, and mismatch repair genes are common in EEC while *TP53* mutations dominate non-EECs (3). Within the PI3K/Akt/mTOR pathway, the negative regulator *PTEN* is frequently mutated, as well as *PIK3CA*, the catalytic PI3K subunit. In addition to mutations in the PI3K/Akt/mTOR pathway, a subset of endometrioid cancers also harbor mutations in *CTNNB1*, which encodes for the Wnt-signaling protein β-catenin. More broadly, endometrial cancer can be divided into four molecular subtypes, as determined by The Cancer Genome Atlas: POLE (ultramutated), MSI-high (hypermutated), Copy-number low, and Copy-number high (4). The POLE, MSI-high, and Copy-number low molecular subtypes most often correspond with an endometrioid histology. Conversely, the Copy-number high molecular subtype are nearly all serous histology. Endometrioid cases with *CTNNB1* mutations are most often classified as Copy-number low, though some are classified as MSI-high.

Mutations in *CTNNB1* occur early in endometrial cancer pathogenesis, as evidenced by β-catenin dysregulation in atypical hyperplasia (5, 6). Further deletion of exon 3 of *CTNNB1* in a murine model drives endometrial hyperplasia (7). Additional investigations found that *PTEN* loss coupled with activation of β-catenin through Wnt-signaling led to an earlier onset and more aggressive endometrial cancer in a mouse model (8). This suggests *CTNNB1* mutations may drive endometrial cancer progression.

Wnt-signaling is a core developmental pathway important for cell proliferation and migration. β-catenin is a critical protein for canonical Wnt-signaling. Activation of Wnt-signaling allows β-catenin to evade the negative regulation of a cytoplasmic destruction complex promoting β-catenin translocation to the nucleus and activation of Wnt target genes (Figure 1). Alterations to β-catenin or destruction complex members are implicated in numerous cancers, namely colon and endometrial cancer (9). However, β-catenin also serves an important function at the adherens junctions, linking E-cadherin at the cell membrane to the actin cytoskeleton through α-catenin. The goal of this review is to examine the function of β-catenin as both a signaling and adhesion protein and explore how mutations may impact endometrial cancer progression.

β-catenin: History and structure

β-catenin is an evolutionarily conserved protein encoded by the *CTNNB1* gene that was first identified in the late 1980s as a binding partner of uvomorulin, later shown to be E-cadherin (10). Immunoprecipitation experiments uncovered three independent proteins bound to uvomorulin, subsequently named alpha-, beta-, and gamma-catenin. Concurrently, β-catenin was identified as a homolog of the mammalian protein plakoglobin, which itself is a homolog of the Drosophila Armadillo gene that regulates developmental polarity (11). Additional work in Drosophila identified the polarity gene, Wingless, regulates the levels of Armadillo (12). This finding began to uncover the role of β-catenin as both a signaling protein and a cell adhesion component.

In higher organisms β-catenin has two primary functions, in adherens junctions and as a member of the canonical Wnt-signaling pathway. The structure of β-catenin enables multiple functions within the cell (Figure 2). In 1996 it was discovered that β-catenin can conduct both signaling and adhesion functions through partner binding to separate regions of the protein (13) (Figure 2). The β-catenin protein is comprised of three domains: an N-terminal domain, a C-terminal domain, and a central domain comprised of 12 Armadillo (Arm) repeats. The N-terminus contains binding sites for proteins within a destruction complex that signals β-catenin for degradation. The C-terminus end serves as a binding site for members of the TCF/LEF family of transcription factors in the nucleus (14). Binding partners for both the N-terminus and C-terminus are important for Wnt-signaling function (Figure 2). The central Arm repeats form a highly conserved region sharing homology with other Armadillo family proteins. This region is made up of 12 repeating segments that form a super-helix structure with a large positively charged groove. The Arm region is the site of E-cadherin binding making this area critical for β-catenin function at the adherens junctions. Each region of the β-catenin protein allows for a unique set of binding partners to carry out numerous functions in the cell (Figure 2).

Beyond protein structure, specific amino acid residues also regulate the multiple functions of β-catenin. At the adherens junctions, E-cadherin interacts with β-catenin throughout most of the Arm region, but the core binding regions are Arm repeats 5-9 and 11-12. Within repeats 5-9 are amino acids K312 and K435, which are necessary for E-cadherin binding (15). α-catenin binds β-catenin primarily in the first Arm repeat. This binding interaction disrupts the Arm repeat near Y142 and D144 to create a hinge where both α-catenin and E-cadherin can

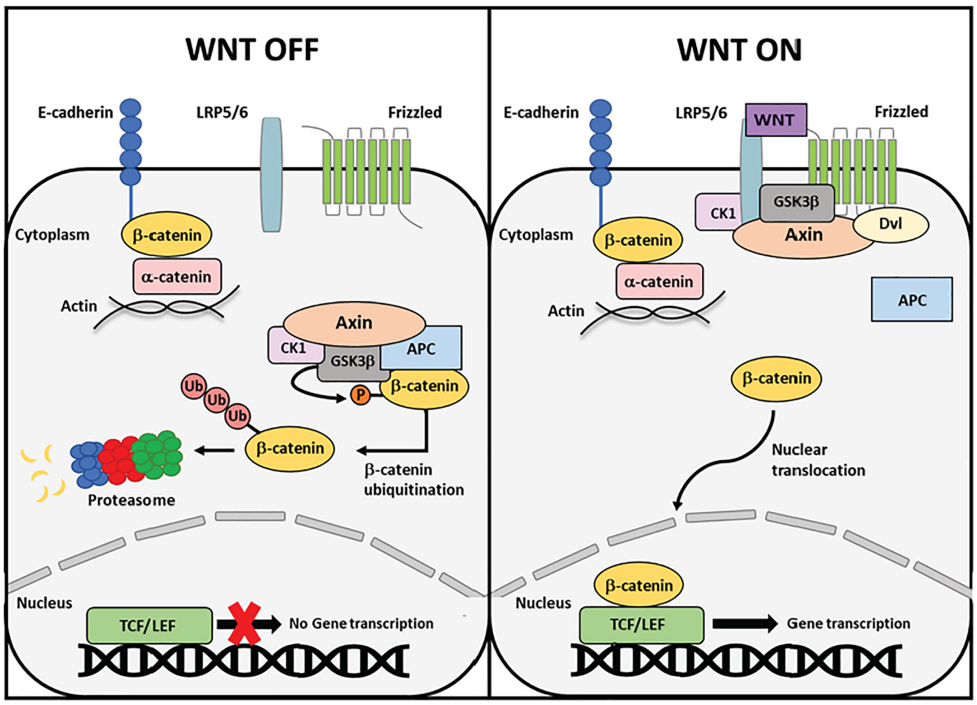

FIGURE 1
Schematic overview of canonical Wnt signaling. In the absence of a Wnt ligand, cytoplasmic β-catenin is phosphorylated in a multi-protein destruction complex comprised of scaffolding proteins Axin and APC and kinases GSK3β and CK1. Phosphorylation by the destruction complexes induces poly-ubiquitination of β-catenin and subsequent degradation by the proteasome. Upon Wnt ligand binding to the Frizzled receptor and LRP5/6 co-receptor, proteins in the destruction complex are recruited to the cell membrane, rendering the complex inoperative. Cytoplasmic β-catenin can now escape degradation and translocate to the nucleus, where it binds the TCF/LEF family of transcription factors and initiates target gene transcription.

bind β-catenin at the same time. One residue important for β-catenin regulation at the adherens junction is Y654. Phosphorylation of Y654 by Src obstructs E-cadherin binding and greatly reduces the affinity of E-cadherin for β-catenin (16).

Within the N-terminus, the stretch of amino acids 32-45 contains residues critical for β-catenin regulation in Wnt-signaling. S45 is phosphorylated by CK1 priming this region for phosphorylation of S33, S37, and T41 by GSK-3β.

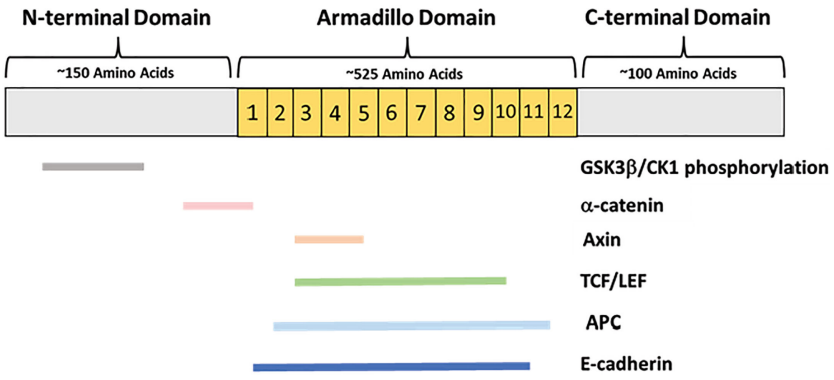

FIGURE 2
β-catenin protein domains and primary binding partners. β-catenin is comprised of an approximately 150-amino-acid N-terminal domain, a 525-amino acid central Armadillo domain containing 12 Arm repeats, and an approximately 100-amino acid C-terminal domain. The N-terminus is the site of GSK3β and CK1 phosphorylation, as well as partial α-catenin binding. The Armadillo domain contains overlapping binding sites for α-catenin, E-cadherin, Axin, APC, and the TCF/LEF transcription factors.

Phosphorylation by CK1 and GSK-3β are required prerequisites for ubiquitination and therefore regulate β-catenin levels in the cytoplasm (17). In addition to the N-terminus, phosphorylation in the C-terminus and Armadillo domain is important for β-catenin stabilization and activation of transcription. S675 can be phosphorylated by protein kinase A (PKA), inhibiting ubiquitination thereby stabilizing β-catenin (18). Additionally, phosphorylation of S552 by AKT can divert β-catenin from the adherens junctions to the cytoplasm and nucleus where it can bind to 14-3-3 ζ and increase transcriptional activity (19).

β-catenin: Duality of functions

Another important determinant of β-catenin functionality is protein localization within the cell. β-catenin is localized to the plasma membrane when bound to E-cadherin at the adherens junctions. Additionally, β-catenin resides in the cytoplasm where it can translocate to the nucleus during Wnt-signaling (Figure 1). These functions are seemingly independent of one another, as they occur by different binding interactions and subcellular locations (20).

Adherens junctions are cadherin- and catenin-based junctions that promote cell-cell adhesion. Adherens junctions are present on polarized epithelia and are important for cells to respond to extracellular signals and changes in force. They are dynamic junctions that form and re-form in response to extracellular signals. At the membrane, β-catenin is bound to the cytoplasmic tail of E-cadherin, a Ca2+ dependent transmembrane protein expressed in epithelial cells (21). The extracellular portion of E-cadherin can associate with other cadherins on adjacent cells. E-cadherin bound β-catenin binds α-catenin in the cytoplasm linking the AJ to the actin cytoskeleton of the cell. β-catenin and E-cadherin associate in the endoplasmic reticulum after being synthesized and then translocate together to the plasma membrane (22). Once at the membrane β-catenin and α-catenin can associate together with the actin cytoskeleton.

The other important function of β-catenin is in the Wnt-signaling pathway (Figure 1). Wnt-signaling is a developmental pathway important for establishing polarity in embryogenesis, inducing stem cell differentiation, and regulating adult cell proliferation and migration (23). Wnt-signaling can proceed through the canonical or non-canonical pathway. β-catenin functions in canonical Wnt-signaling to regulate gene transcription (24). The Wnt-signaling cascade is turned on by the Wnt family of secreted glycoproteins that contains 19 mammalian members. In the absence of a Wnt-signal, the pool of β-catenin in the cytoplasm is regulated by a multiprotein destruction complex (25). The destruction complex is comprised of many proteins, but the foundational members are Axin, Adenomatous Polyposis Coli (APC), Glycogen synthase kinase-3-beta (GSK3β), and casein kinase 1 (CK1). Axin is a large scaffolding protein upon which other destruction complex proteins can dock including the serine/threonine kinases GSK3β and CK1. Unbound β-catenin in the cytoplasm is targeted by the destruction complex. CK1 first "primes" β-catenin by phosphorylating S45. Next, GSK3β can phosphorylate S33, S37, and T41. Phosphorylation at the N-terminus of β-catenin creates a docking site for β-TRCP1, a member of the SCF family of E3 ubiquitin ligases. This E3 ligase recruits an E2 ligase, which polyubiquitinates β-catenin at K19 and K49, and leads to subsequent protein degradation by the proteasome (25). In this way, levels of β-catenin in the cytoplasm are kept consistently low in the absence of Wnt signaling (Figure 1).

When the Wnt-signaling pathway is turned on, Wnt ligand binds to the Frizzled (Fz) receptor at the cell membrane. The G-protein coupled receptor Fz is a seven transmembrane protein that is linked to the low-density-lipoprotein-related protein 5/6 (LRP5/6) co-receptors to carry out canonical Wnt-signaling. Upon ligand binding to Fz, the Disheveled (Dvl) phosphoprotein is recruited from the cytoplasm to bind the Fz receptor. The formation of this complex causes dissolution of the destruction complex by recruiting the Axin scaffolding protein to the plasma membrane where it docks on the cytoplasmic tail of the LRP5/6 co-receptor. After Axin docking, LRP5/6 can be phosphorylated by CK1 or GSK3β, further strengthening the destruction complex recruitment to the membrane (23). Once the destruction complex is disassembled and recruited to the membrane, cytoplasmic β-catenin is no longer targeted for degradation (23). Undegraded β-catenin can accumulate in the cytoplasm and translocate to the nucleus without restrictions. In the nucleus, β-catenin binds to and activates the T-cell factor/lymphoid enhancing factor (TCF/LEF) family of transcription factors. TCF/LEF bind β-catenin along Arm repeats 3-10, where K312 and K435 are necessary for binding to TCF/LEF (26). Without β-catenin, TCF/LEF are complexed to members of the Groucho/TLE family of transcriptional co-repressors. β-catenin displaces Groucho/TLE in the nucleus and binds TCF/LEF to activate transcription. Canonical Wnt-signaling induces the transcription of different target genes depending on the tissue type. Notable target genes are *CCND1*, which encodes the Cyclin D1 cell cycle protein, and *c-Myc* and *Jun*, which are both proto-oncogenes (27).

The exact mechanism by which β-catenin nuclear translocation occurs is not well understood, as β-catenin does not contain a nuclear localization signal (NLS) (28). Nuclear import and export are often facilitated by soluble transporter proteins like importins and exportins. Members of the importin-β family can directly bind cargo through its NLS with the help of importin-α (29). Loading and unloading of cargo are regulated by the GTPase Ran, where RanGTP levels are low in the cytoplasm and high in the nucleus to enable directional transport (30). However, it has been found that β-catenin can enter the nucleus in a RanGTP independent manner (31). Interestingly, the Arm repeats of β-catenin are structurally

similar to the HEAT repeats of importin-β (32), therefore it has been proposed that β-catenin may possess some independent transport abilities.

The questions of what prompts β-catenin to translocate from the cytoplasm to the nucleus remain. One proposed mechanism involves Rac1, a member of the Rho family of small GTPases. A previous study suggested a signaling cascade in which Wnt family member Wnt3a activates Rac1, in turn prompting c-Jun N-terminal kinase 2 (JNK2) to phosphorylate β-catenin at S191 and S605 inducing nuclear translocation (33). Further, a more recent study suggests that Wnt-mediated Rac1 activation not only induces nuclear translocation, but also enhances β-catenin and LEF-1 binding in the nucleus (34). Another proposed mechanism indicates that β-catenin nuclear translocation is influenced by its binding partners. Studies have suggested either Axin or APC as a molecular chaperone to shuttle β-catenin from the cytoplasm to the nucleus (35, 36). Additionally, α-catenin has been found to have a nuclear function. Several studies have shown that the nuclear localization and function of α-catenin is dependent on nuclear β-catenin (37, 38). Therefore, α-catenin may be mutually required for β-catenin nuclear translocation. Nevertheless, the exact mechanism driving nuclear translocation of β-catenin remains unclear.

The Wnt-signaling and adherens junction functions of β-catenin are seemingly independent, as evidenced by competition between binding partners. E-cadherin, APC, and TCF/LEF transcription factors all bind the central Arm repeats of β-catenin (Figure 2). Association with E-cadherin in the endoplasmic reticulum may be protective against cytoplasmic β-catenin being degraded by the destruction complex (39). Previous studies have shown that E-cadherin can compete with both APC and LEF-1 to bind β-catenin (39, 40). In a set of immunoblotting and affinity precipitation experiments, E-cadherin, APC, and LEF-1 were found to form independent, but competitive complexes with β-catenin. Additionally, a greater amount of β-catenin was localized to the cytoplasm or nucleus in E-cadherin deficient cells (39). In the absence of E-cadherin, there was more interaction between β-catenin and LEF-1 than in E-cadherin wild-type cells. This suggests that the localization of β-catenin is greatly determined by the presence or absence of E-cadherin.

CTNNB1 mutations and endometrial cancer

Alterations to Wnt-signaling proteins and mutations in *CTNNB1* are associated with multiple types of cancer. Additionally, loss of E-cadherin at adherens junctions is a critical step in the cellular process of the epithelial-to-mesenchymal transition (EMT). EMT is a process by which epithelial cells lose their characteristic cell-cell adhesion, polarity and transition into more migratory mesenchymal cells. This process is important for normal development, but also enables cancer cells to invade through the basement membrane promoting metastasis (41). Therefore, the cell adhesion and Wnt-signaling functions of β-catenin can be implicated in cancer progression.

A large sequencing study of cancer patients revealed *CTNNB1* mutations were most commonly observed in endometrial, liver, and colorectal tumor types, with endometrial cancer being the most prevalent (42). The majority of these *CTNNB1* gene alterations occur in the N-terminal exon 3 region. This region notably contains the phosphorylation sites for GSK3β and CK1 (Figure 3). In endometrial cancer, patients with *CTNNB1* mutations typically have missense mutations at phosphorylation sites and/or adjacent residues (Figure 3). These exon 3 mutations in endometrial cancer are thought to protect β-catenin from degradation by the destruction complex. Mutant β-catenin can accumulate in the cytoplasm and translocate to the nucleus without regulation. Consequently, TCF/LEF transcription factors can be constitutively activated. Because canonical Wnt-signaling induces transcription of genes regulating cell cycle induction and proliferation, this overactive Wnt-signaling can contribute to cancer progression.

The subset of patients with *CTNNB1* mutations almost exclusively occur in endometrioid endometrial cancer (EEC). The endometrioid histological type is the most common, with 70-80% of patients having EEC. However, this large group of tumors are incredibly heterogeneous. A multivariate analysis of 271 EEC patient's data from The Cancer Genome Atlas (TCGA) was conducted to better classify EEC tumors (43). This study identified four clusters (I, II, III, IV) with distinct molecular profiles. Notably, 87% of tumors in Cluster II harbored *CTNNB1* mutations, with most being exon 3 missense mutations. The majority of mutations were at phosphorylation sites S33, S37, T41, S45 or adjacent residues D32 and G34 (Figure 3). Cluster II comprises approximately 28% of all EEC cases analyzed in this study. Further, Gene Set Enrichment Analysis of this patient cluster revealed an association between exon 3 *CTNNB1* mutations and overexpression of other Wnt-signaling proteins. This cluster of patients is notable because it distinguishes EEC patients with *CTNNB1* mutations as a distinct group. EEC tumors typically are low stage and low grade with a favorable prognosis. Both Cluster I and Cluster II in this study are comprised of obese patients with low grade and low stage tumors. However, Cluster II is notable because these patients are younger in age and exhibit a worse overall survival rate than patients in Cluster I (43). This study suggests that *CTNNB1* mutations and alterations in other Wnt-pathway proteins may serve as a clinical marker for treatment course or patient outcome.

More recent studies have also identified a prognostic role of exon 3 *CTNNB1* mutations in EEC. A 2019 study by Imboden

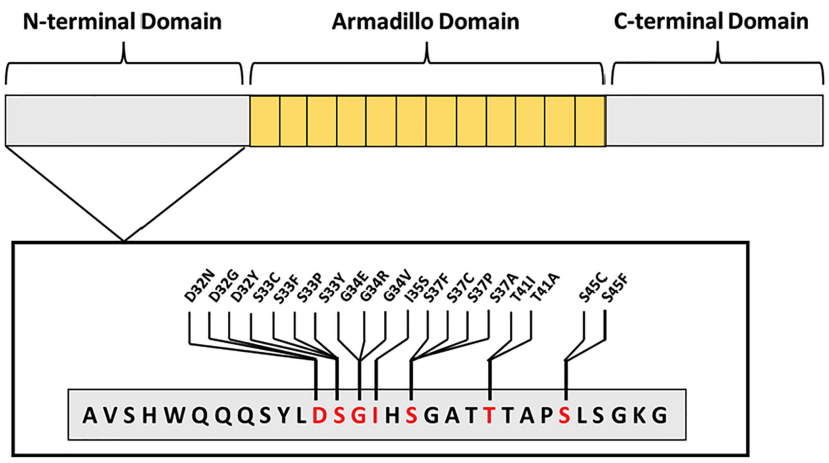

FIGURE 3
Most commonly mutated β-catenin amino acid residues occurring in endometrial cancer. All mutations occur in exon 3, found within the N-terminus, blocking GSK3β or CK1 phosphorylation sites—S33, S37, T41, S45—or adjacent residues—D32, G34, and I35.

et al. sought to determine histopathologic and genetic determinants of recurrence in early stage and low grade EEC patients to improve treatment decisions (44). Results of this study found *CTNNB1* to be the most commonly mutated gene in all early-stage and low-grade patients, including non-recurrent, recurrent, and secondary lesions. Although this study found no correlation between recurrence and exon 3 *CTNNB1* mutation, they concluded that the presence of *CTNNB1* mutations in early-stage disease combined with disease recurrence observed in other studies confers a prognostic value for these mutations.

A 2022 study by Travaglino et al. conducted a systemic review and meta-analysis of all studies examining the prognostic value of *CTNNB1* mutations in early-stage EEC (45). Following study selection, 7 studies were included comprising 1,031 early-stage EEC patients with exon 3 *CTNNB1* mutations. Out of 149 patients assessed for recurrence, 44 patients had recurrent disease (22.7%) and 23/44 recurrent patients harbored a *CTNNB1* mutation (52.3%). The significance of recurrence and mutation state increased following exclusion of patients with known molecular status other than the copy-number low/no specific molecular profile (NSMP) TCGA group. Additionally, 886 patients were evaluated for disease-free survival (DFS), of which the molecular status was known for 546. Initial analysis showed no association between *CTNNB1* mutation status and DFS, but exclusion of patients with known molecular status other than the NSMP group caused a significant association between *CTNNB1* mutation and decreased DFS. This study found an overall association between recurrence and DFS in patients with exon 3 *CTNNB1* mutations.

Given the prognostic value of exon 3 *CTNNB1* mutations in EEC, some have suggested a modification to the TCGA molecular classification of endometrial cancer. The current TCGA classification groups *CTNNB1* mutations into the copy-number low group, also known as NSMP. Studies have suggested creating an additional, fifth molecular TCGA category defined by *CTNNB1* mutations (46, 47). Tumors in the copy-number low molecular group have frequent mutations in *CTNNB1*, *PTEN*, *PIK3CA*, *ARID1A*, and *KRAS* (4). Because the mutations present in the copy-number low group are broad, the prognostic value of this molecular group is difficult to define. Further, the European Society of Gynecological Oncology (ESGO), the European Society for Radiotherapy and Oncology (ESTRO), and the European Society of Pathology (ESP) published joint guidelines in 2020 for risk stratification of endometrial cancer patients (47). These guidelines are based upon both TCGA molecular subtypes and clinical characteristics like lymph-vascular space invasion (LVSI). Under these guidelines, the copy-number low/NSMP group may fall under the low, intermediate, or high-intermediate risk category depending on the tumor stage or LVSI. For this reason, considering *CTNNB1* mutations as their own molecular group would facilitate a more accurate representation of the risk factor for patients with *CTNNB1* mutations. Further, a 2022 study by Kurnit et al. evaluated the effects of adjuvant therapy on recurrence-free survival in endometrial cancer patients with *CTNNB1* mutations (48). This study also characterized the risk category according to myometrial invasion and LVSI, integrating molecular and clinicopathologic characteristics. Results of this study indicated that patients with *CTNNB1* mutations at intermediate risk, defined as any grade endometrioid cancer with deep myometrial invasion or LVSI, had improved recurrence-free survival following adjuvant therapy. Accordingly, recurrence-free survival of low-risk patients with *CTNNB1* mutations was not impacted by

adjuvant treatment. Taken together, these studies suggest that defining endometrial cancers by both molecular characteristics and clinicopathologic features is a more effective way to assess risk factor and treatment options, particularly in the case of *CTNNB1* mutations.

Context dependence of β-catenin mutations in endometrial cancer

CTNNB1 mutations in EC represent a patient group with worse recurrence free survival rates (49, 50). However, the magnitude of the impact of *CTNNB1* mutations is context dependent. The majority of *CTNNB1* mutations in EC occur in the endometrioid histological subtype. Though *CTNNB1* mutations can occur in the non-endometrioid histological subtype, they are rare. Further, mutations in *CTNNB1* are associated with worsened survival in patients with low grade, endometrioid type cancers. Therefore, stratifying patient survival data by grade and histological type is critical to unmasking the prognostic importance of *CTNNB1* mutations in EC.

The disparity in survival between *CTNNB1* mutant and wild-type patients can be seen clearly in low grade, endometrioid type ECs. A 2021 study by Caracuel et al. examined the prognostic value of *CTNNB1* mutations in a cohort of 218 patients with low grade and low stage disease (51). Specifically, all patients in this cohort were categorized as primary endometrioid grade 1 or grade 2 ECs. The results of this study showed a significantly decreased disease-free survival (DFS) in patients with exon 3 *CTNNB1* mutations compared to those with wild-type *CTNNB1*. Further, the relationship between *CTNNB1* mutation and DFS was independent of other prognostic determinants such as age and The International Federation of Gynecology and Obstetrics (FIGO) stage. This study highlights the impact of exon 3 *CTNNB1* mutations on DFS in EEC patients.

In addition to survival, exon 3 *CTNNB1* mutations in EEC can be a marker for disease recurrence. A 2020 study by Moroney et al. evaluated a cohort of grade 1, stage 1 EEC cases to identify molecular markers associated with higher recurrence risk (52). 311 women with grade 1, stage 1 EEC were identified, of which 18 had recurrent disease and 30 were selected as matched non-recurrent controls. Molecular testing revealed that 60% of recurrent cases had exon 3 *CTNNB1* mutations whereas 28% of non-recurrent controls had exon 3 *CTNNB1* mutations. These results suggest that *CTNNB1* mutation status can serve as a clinical marker for disease recurrence in low grade and stage EEC. Grade 1 and stage 1 endometrial cancers are considered to be low risk. Because this study uses low risk patients all without adjuvant treatment, confounding variables have been controlled for and the effects of *CTNNB1* mutations on recurrence are more impactful.

Another 2020 study by Costigan et al. sought to correlate β-catenin and Cyclin D1 immunohistochemistry with exon 3 *CTNNB1* mutant EEC cases and assess the clinicopathologic features associated with these patients (53). Within the cohort of 79 patients, 34 harbored exon 3 *CTNNB1* mutations while 45 had wild-type *CTNNB1*. In contrast to the previous studies discussed, the cohort selected for this study contained grades 1, 2, and 3 EEC patients. Differences in survival and recurrence between *CTNNB1* mutant and wild-type EECs are typically observed in low grade cancers only. The present study utilized follow-up data on stage IA patients to assess disease recurrence. They found that 30% of patients with exon 3 *CTNNB1* mutations had disease recurrence whereas no patients with wild-type *CTNNB1* had recurrent disease. Because recurrence rates were defined by a low FIGO stage, all patients analyzed had grade 1 or 2 EEC. Additionally, they found no difference in recurrence rates between *CTNNB1* mutant and wild-type patients presenting with high stage EEC. These results further emphasize the significance of characterizing *CTNNB1* mutant and wild-type survival and recurrence data by grade.

The mutation status of *CTNNB1* is an important clinical marker in low grade, endometrioid type EC. However, the value of this marker can be lost when high- and low-grade EEC patients are grouped together. Studies of survival or recurrence containing cohorts of grades 1-3 EECs or both EECs and non-EECs may lose the impact of exon 3 *CTNNB1* mutations if grade 1-2 cases are not delineated. Exon 3 *CTNNB1* mutations can occur in high-grade EECs and, rarely, in non-EECs. However, a difference in survival and recurrence is not evident in these categories. Therefore, patients with grades 1-2 EEC harboring exon 3 *CTNNB1* mutations must be treated as a separate entity. While independent studies have identified low grade EEC patients with *CTNNB1* mutations as having worsened survival, none of these publications have evaluated survival according to exon 3 *CTNNB1* mutation type. One hinderance to such analysis is the high number of unique reported exon 3 *CTNNB1* mutations per study, with 15 different mutations in one report (53) and 22 different mutations in a subsequent report (54). Future studies examining the relationship between survival and type of exon 3 *CTNNB1* mutations will be valuable to further define the context of these mutations in low grade EEC patients.

Membrane and cytoplasmic pools of β-catenin and endometrial cancer

In normal epithelial cells β-catenin is primarily localized to the cell membrane associated with E-cadherin. However, β-catenin is often thought of in the context of canonical Wnt-signaling in endometrial cancer. This is due to frequent hotspot

mutations at the N-terminus region that preclude the CK1 and/or GSK3β phosphorylation sites. The membrane and cytoplasmic pools of β-catenin function differently and seemingly in an independent manner. Nonetheless, loss of cell-to-cell adhesion by way of the adherens junctions can contribute to uncontrolled cell proliferation and metastasis (55). This begs the question of how *CTNNB1* mutations found in endometrial carcinoma may affect β-catenin at the membrane as well as in the cytoplasm.

A 2001 study compared β-catenin localization in normal, hyperplastic, and endometrioid carcinoma endometrial tissue (5). The immunoreactivity score for β-catenin staining at the membrane was highest for normal samples and decreased steadily through non-atypical hyperplasia, atypical hyperplasia, and grades 1-3 carcinoma lesions. Conversely, no β-catenin nuclear localization was observed in normal samples, very little was seen in non-atypical hyperplastic lesions, and clear nuclear localization was present in atypical hyperplasia and grades 1-3 carcinoma tissues. This data suggests that β-catenin localization changes with an increasing degree of atypical hyperplasia or carcinoma grade. Additionally, they compared endometrial carcinoma cases with or without exon 3 *CTNNB1* mutations and β-catenin staining patterns. Cases with *CTNNB1* mutations had significantly lower amounts of membrane β-catenin staining and higher amounts of nuclear β-catenin staining than cases without *CTNNB1* mutations. It is known that exon 3 mutations cause evasion of the degradation complex and can lead to cytoplasmic accumulation of β-catenin. However, a correlated loss of membrane staining may indicate a change in subcellular distribution of β-catenin following *CTNNB1* mutations. Although exon 3 mutations do not overlap with E-cadherin binding sites, perhaps there is a mechanism by which the hotspot mutations affect β-catenin distribution while still within the endoplasmic reticulum. Further research is warranted to investigate the reciprocal nature of β-catenin membrane and nuclear distribution in endometrial carcinoma.

The majority of exon 3 *CTNNB1* mutations occur in low grade, endometrioid endometrial cancer. Alterations to β-catenin arise early in endometrial cancer pathogenesis. Conversely, alterations to E-cadherin can increase the metastatic potential of cells, which commonly develops only in high grade or high stage endometrial cancer (56). It is possible that *CTNNB1* mutations only affect the cytoplasmic pool of β-catenin because the membrane-bound pool is heavily dictated by E-cadherin. Thus, the dissolution of adherens junctions could rely on changes to E-cadherin, not β-catenin. A 2003 study examined cadherin and catenin levels in 149 endometrial lesions (21 endometrial atypical hyperplasia (AEH), 68 EECs, 27 non-EECs) (57). They found that non-EEC lesions like serous, clear cell, mixed serous-clear cell, or mixed endometrioid-serous types had significantly reduced E-cadherin compared to AEH and EEC lesions. Additionally, they found less membranous β-catenin in lesions with reduced E-cadherin expression than those with wild-type E-cadherin. Alterations to E-cadherin in these lesions reduces the need to inactivate β-catenin directly. Non-EEC carcinomas typically have a higher stage at diagnosis and a poorer prognosis. These results suggest that reduced E-cadherin may negatively affect the amount of β-catenin at the membrane in high grade endometrial cancer. This may be due to the co-translational relationship between E-cadherin and β-catenin in the endoplasmic reticulum.

The decreased expression of E-cadherin in endometrial cancer is not fully understood. There are various mechanisms that are thought to be causative, such as loss of heterozygosity and promoter hypermethylation. Another possibility is dysregulation of transcriptional repressors of E-cadherin. The transcription factors Twist, Snail1, Snail2, and Zeb1 all work to repress E-cadherin and are known EMT markers. Further, these transcription factors are all directly or indirectly regulated by β-catenin or Wnt-signaling (58). Thus, exon 3 *CTNNB1* mutations may not impact membranous β-catenin by interfering with E-cadherin binding, but rather indirectly affect adherens junctions by upregulating repressors of E-cadherin (Figure 4).

Clinical applications of *CTNNB1* mutations in endometrial cancer

Treatment regimens for endometrial cancer have remained relatively consistent in recent decades. The primary treatment option is surgery, typically consisting of hysterectomy, salpingectomy, and occasional lymph node dissection. One barrier to treatment is the lack of consensus on treating recurrent endometrial cancer. Radiation therapy is the current standard of care for preventing local recurrence and treating locally recurrent endometrial cancer, but further treatment options are limited (59). Currently, guidelines do not incorporate molecular biomarkers into treatment decisions for preventing recurrent disease. As previously discussed, Kurnit et al. have recently shown that incorporating the status of *CTNNB1* exon 3 mutations helps to identify stage I EEC patients who would benefit most from adjuvant radiation treatment following surgery (48).

Given the poor treatment response of advanced EC to conventional chemotherapy approaches, targeted therapies have emerged as a better treatment option for these patients. Given its role as a prognostic marker, β-catenin and the Wnt-signaling pathway have been implicated as potential targets for endometrial cancer treatment. One promising therapeutic is DKN-01, a monoclonal antibody against Dickkopf-1 (DKK-1). DKK-1 is a negative regulator of Wnt-signaling that functions by binding LRP5/6 and blocking Wnt ligands. Additionally, studies have found that overexpression of DKK-1 in some solid tumors is correlated with worsened survival (60). DKN-01 has been studied in the context of several gynecological and

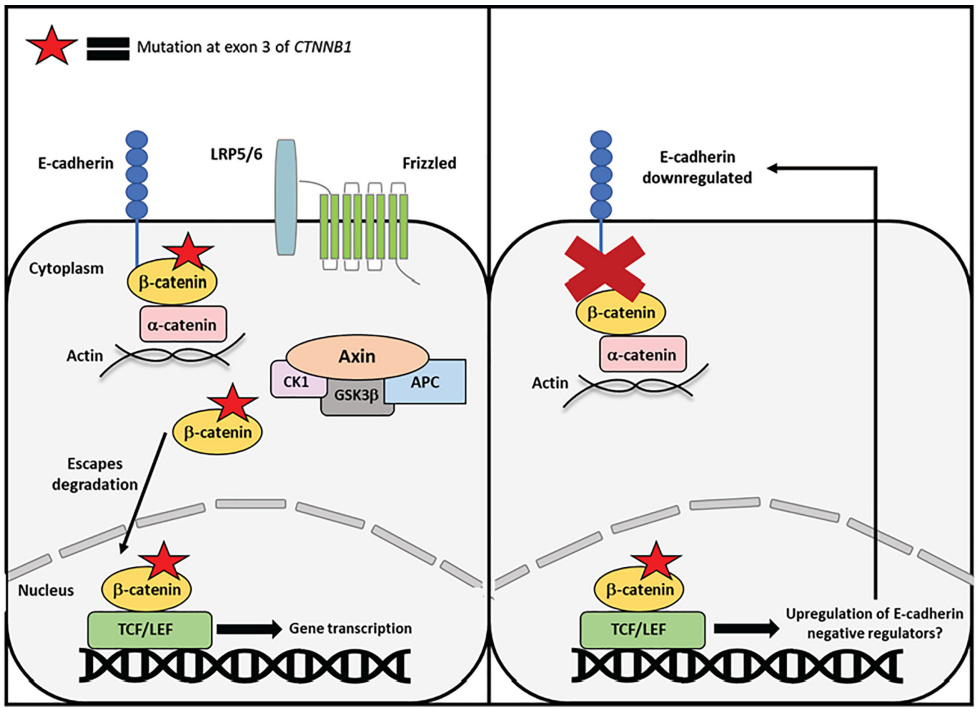

FIGURE 4
Proposed mechanism of exon 3 CTNNB1 mutations in endometrial cancer. Mutant β-catenin can escape degradation in the cytoplasm and translocate to the nucleus independent of Wnt-signaling. One mechanism by which mutant β-catenin may drive endometrial cancer is by inducing transcription of E-cadherin negative regulators or EMT genes. β-catenin mutations occur relatively early in endometrial cancer progression, whereas loss of E-cadherin occurs later in disease progression. Therefore, mutations to β-catenin may indirectly contribute to E-cadherin loss and EMT progression.

gastrointestinal cancers, which tend to have frequent alterations in Wnt-signaling pathway members. One study examining the effects of DKN-01 treatment or DKK-1 overexpression in endometrioid ovarian cancer (EOC) releveled that overexpression of DKK-1 caused a decrease in immune activity while treatment with DKN-01 did not phenotypically affect EOC cells *in vitro*, indicating that DKN-01 functions by modulating anti-tumor immunity (61). Additional studies have found that DKN-01 reverses the immunosuppressive effects of upregulated DKK-1 in several cancer types and functions by promoting natural killer cells, reducing myeloid-derived suppressor cells (MDSCs), and upregulating PD-L1 on MDSCs (62). DKN-01 may be an effective treatment in combination with other immune modulating treatments for EEC patients with aberrant Wnt-signaling caused by *CTNNB1* mutations. Additionally, DKN-01 has been tested in a phase 2 clinical trial in combination with paclitaxel treatment in epithelial endometrial and ovarian cancer patients (NCT03395080).

Another targeted treatment option for endometrial cancer patients with aberrant β-catenin/Wnt signaling is Porcupine (PORCN) inhibitors. PORCN is an enzyme residing in the endoplasmic reticulum that functions to palmitoleate Wnt ligands post-translationally at conserved serine residues. The palmitoleation of Wnts is important for both Wnt secretion and binding to the Frizzled receptor (63). Inhibition of PORCN is an effective strategy to inhibit overactive Wnt-signaling without targeting β-catenin directly. A 2016 study evaluated the efficacy of a novel, oral PORCN inhibitor, ETC-159 in colorectal cancers (CRC) harboring RSPO-translocations that increase Frizzled and LRP5/6 cell surface supply (64). Results of this study indicated that CRC patients with RSPO2/3 translocations respond well and are highly sensitive to ETC-159. Additionally, global remodeling of gene expression revealed a downregulation in Wnt-pathway target genes in ETC-159 treated tumors. Because *CTNNB1* mutations in EEC constitute an alteration to Wnt-signaling downstream of the Frizzled receptor, PORCN inhibitors may not be efficacious without combination with a molecule targeted to β-catenin specifically. A phase 1A/B clinical trial is ongoing to test the safety and tolerability of ETC-159 as a single agent or in combination with Pembrolizumab in different advanced solid tumors (NCT02521844). Therefore, additional insights are needed to evaluate the utility of ETC-159 and PORCN inhibitors in EEC.

Targeting β-catenin directly in cancer has proved challenging, despite the prognostic value of exon 3 *CTNNB1* mutations in endometrial cancer. PRI-724 is a β-catenin inhibitor that works

as an agonist for the association of β-catenin and cyclic AMP response element-binding protein (CBP), a co-activator of transcription (65). Because PRI-724 targets nuclear β-catenin and inhibits subsequent transcription through TCF/LEF, it appears as a promising option for targeting mutant β-catenin in endometrial cancer. Currently, a phase II trial for PRI-724 treatment alone or in combination with chemotherapy and Bevacizumab is ongoing to treat metastatic CRC patients (NCT02413853). CRC has frequent mutations in *APC*, another downstream Wnt-pathway protein, and therefore additional studies of PRI-724 efficacy in EEC patients with *CTNNB1* mutations may be beneficial.

Conclusion

β-catenin is an evolutionarily conserved protein encoded by the *CTNNB1* gene. It functions both at the cell membrane and the cytoplasm/nucleus in adherens junctions and Wnt-signaling, respectively. These roles are thought of as separate entities due to their distinct locations and binding partners. Mutations in exon 3 of *CTNNB1* are found in a subset of endometrioid endometrial cancer patients and studies have suggested that changes in β-catenin cellular localization in EEC are caused by exon 3 mutations (5). These mutations in endometrial cancer are typically associated with β-catenin nuclear localization. By this mechanism, exon 3 mutations directly affect the Wnt-signaling function of β-catenin by blocking CK1 and GSK3β phosphorylation sites. However, it is not well understood how these mutations may alter the functionality of β-catenin at the adherens junctions. Reduced expression of E-cadherin and β-catenin have been found in non-endometrioid endometrial cancer (56). Both reduced cadherin-catenin expression and unchecked β-catenin translocation to the nucleus can contribute to endometrial carcinoma, albeit in different ways. Similar to their separate cellular functions, perhaps the membrane and cytoplasmic pools of β-catenin are contributing to different types of endometrial carcinoma entirely. Alternatively, β-catenin mutations might affect adherens junctions indirectly by inducing transcription of negative regulators of E-cadherin. Additional research is required to uncover how the separate pools of β-catenin function following exon 3 mutations, and how they might contribute to endometrial cancer pathogenesis.

Author contributions

MP wrote manuscript and generated figures. RB edited manuscript and contributed insight. AG edited and contributed to manuscript and figures. All authors contributed to the article and approved the submitted version.

Funding

This work was supported by the NIH SPORE in Uterine Cancer NIH P50 CA098258 and a UNC Lineberger Comprehensive Cancer Center Developmental Award, which is supported in part by P30 CA016086 Cancer Center Core Support Grant.

Conflict of interest

The authors declare that the research was conducted in the absence of any commercial or financial relationships that could be construed as a potential conflict of interest.

Publisher's note

References

1. Siegel RL, Miller KD, Fuchs HE, Jemal A. Cancer statistics, 2022. *CA A Cancer J Clin* (2022) 72(1):7–33. doi: 10.3322/caac.21708

2. Murali R, Soslow RA, Weigelt B. Classification of endometrial carcinoma: More than two types. *Lancet Oncol* (2014) 15(7):e268–278. doi: 10.1016/S1470-2045(13)70591-6

3. O'Hara AJ, Bell DW. The genomics and genetics of endometrial cancer. *Adv Genomics Genet* (2012) 2012(2):33–47. doi: 10.2147/AGG.S28953

4. The Cancer Genome Atlas Research Network, Levine DA. Integrated genomic characterization of endometrial carcinoma. *Nature* (2013) 497 (7447):67–73. doi: 10.1038/nature12113

5. Saegusa M, Hashimura M, Yoshida T, Okayasu I. Beta- catenin mutations and aberrant nuclear expression during endometrial tumorigenesis. *Br J Cancer.* (2001) 84(2):209–17. doi: 10.1054/bjoc.2000.1581

6. Ashihara K, Saito T, Mizumoto H, Nishimura M, Tanaka R, Kudo R. Mutation of beta-catenin gene in endometrial cancer but not in associated hyperplasia. *Med Electron Microsc.* (2002) 35(1):9–15. doi: 10.1007/s007950200001

7. Jeong JW, Lee HS, Franco HL, Broaddus RR, Taketo MM, Tsai SY, et al. Beta-catenin mediates glandular formation and dysregulation of beta-catenin induces hyperplasia formation in the murine uterus. *Oncogene* (2009) 28(1):31–40. doi: 10.1038/onc.2008.363

8. van der Zee M, Jia Y, Wang Y, Heijmans-Antonissen C, Ewing PC, Franken P, et al. Alterations in wnt-β-catenin and pten signalling play distinct roles in endometrial cancer initiation and progression. *J Pathol* (2013) 230(1):48–58. doi: 10.1002/path.4160

9. Jung YS, Park JI. Wnt signaling in cancer: therapeutic Targeting of wnt signaling beyond β-catenin and the destruction complex. *Exp Mol Med* (2020) 52 (2):183–91. doi: 10.1038/s12276-020-0380-6

10. Ozawa M, Baribault H, Kemler R. The cytoplasmic domain of the cell adhesion molecule uvomorulin associates with three independent proteins structurally related in different species. *EMBO J* (1989) 8(6):1711–7. doi: 10.1002/j.1460-2075.1989.tb03563.x

11. Peifer M, Wieschaus E. The segment polarity gene armadillo encodes a functionally modular protein that is the drosophila homolog of human plakoglobin. *Cell* (1990) 63(6):1167–76. doi: 10.1016/0092-8674(90)90413-9

12. Riggleman B, Schedl P, Wieschaus E. Spatial expression of the drosophila segment polarity gene armadillo is posttranscriptionally regulated by wingless. *Cell* (1990) 63(3):549–60. doi: 10.1016/0092-8674(90)90451-J

13. Orsulic S, Peifer M. An *in vivo* structure-function study of armadillo, the beta-catenin homologue, reveals both separate and overlapping regions of the protein required for cell adhesion and for wingless signaling. *J Cell Biol* (1996) 134 (5):1283–300. doi: 10.1083/jcb.134.5.1283

14. Gottardi CJ, Gumbiner BM. Adhesion signaling: How β-catenin interacts with its partners. *Curr Biol* (2001) 11(19):R792–4. doi: 10.1016/S0960-9822(01) 00473-0

15. Xu W, Kimelman D. Mechanistic insights from structural studies of β-catenin and its binding partners. *J Cell Sci.* (2007) 120(19):3337–44. doi: 10.1242/ jcs.013771

16. Roura S, Miravet S, Piedra J, de Herreros AG, Duñach M. Regulation of e-cadherin/Catenin association by tyrosine phosphorylation. *J Biol Chem* (1999) 274 (51):36734–40. doi: 10.1074/jbc.274.51.36734

17. Kikuchi A, Kishida S, Yamamoto H. Regulation of wnt signaling by protein-protein interaction and post-translational modifications. *Exp Mol Med* (2006) 38 (1):1–10. doi: 10.1038/emm.2006.1

18. Hino S-I, Tanji C, Nakayama KI, Kikuchi A. Phosphorylation of beta-catenin by cyclic AMP-dependent protein kinase stabilizes beta-catenin through inhibition of its ubiquitination. *Mol Cell Biol* (2005) 25(20):9063–72. doi: 10.1128/ MCB.25.20.9063-9072.2005

19. Fang D, Hawke D, Zheng Y, Xia Y, Meisenhelder J, Nika H, et al. Phosphorylation of beta-catenin by AKT promotes beta-catenin transcriptional activity. *J Biol Chem* (2007) 282(15):11221–9. doi: 10.1074/jbc.M611871200

20. Valenta T, Hausmann G, Basler K. The many faces and functions of β-catenin. *EMBO J* (2012) 31(12):2714–36. doi: 10.1038/emboj.2012.150

21. Yap AS, Brieher WM, Gumbiner BM. Molecular and functional analysis of cadherin-based adherens junctions. *Annu Rev Cell Dev Biol* (1997) 13(1):119–46. doi: 10.1146/annurev.cellbio.13.1.119

22. Curtis MW, Johnson KR, Wheelock MJ. E-cadherin/catenin complexes are formed cotranslationally in the endoplasmic reticulum/Golgi compartments. *Cell Commun Adhes.* (2008) 15(4):365–78. doi: 10.1080/15419060802460748

23. Kim W, Kim M, hoon JE. Wnt/β-catenin signalling: From plasma membrane to nucleus. *Biochem J* (2013) 450(1):9–21. doi: 10.1042/BJ20121284

24. Ackers I, Malgor R. Interrelationship of canonical and non-canonical wnt signalling pathways in chronic metabolic diseases. *Diabetes Vasc Dis Res* (2018) 15 (1):3–13. doi: 10.1177/1479164117738442

25. Kimelman D, Xu W. Beta-catenin destruction complex: Insights and questions from a structural perspective. *Oncogene* (2006) 25(57):7482–91. doi: 10.1038/sj.onc.1210055

26. Graham TA, Weaver C, Mao F, Kimelman D, Xu W. Crystal structure of a β-Catenin/Tcf complex. *Cell* (2000) 103(6):885–96. doi: 10.1016/S0092-8674(00) 00192-6

27. Ilyas M. Wnt signalling and the mechanistic basis of tumour development. *J Pathol* (2005) 205(2):130–44. doi: 10.1002/path.1692

28. Fagotto F, Glück U, Gumbiner BM. Nuclear localization signal-independent and importin/karyopherin-independent nuclear import of β-catenin. *Curr Biol* (1998) 8(4):181–90. doi: 10.1016/S0960-9822(98)70082-X

29. Terry LJ, Shows EB, Wente SR. Crossing the nuclear envelope: Hierarchical regulation of nucleocytoplasmic transport. *Science* (2007) 318(5855):1412–6. doi: 10.1126/science.1142204

30. Güttler T, Görlich D. Ran-dependent nuclear export mediators: a structural perspective: RanGTPase-driven nuclear export. *EMBO J* (2011) 30(17):3457–74. doi: 10.1038/emboj.2011.287

31. Yokoya F, Imamoto N, Tachibana T, Yoneda Y. β-catenin can be transported into the nucleus in a ran-unassisted manner. *Silver PA editor. MBoC.* (1999) 10(4):1119–31. doi: 10.1091/mbc.10.4.1119

32. Lee SJ, Imamoto N, Sakai H, Nakagawa A, Kose S, Koike M, et al. The adoption of a twisted structure of importin-β is essential for the protein-protein interaction required for nuclear transport. *J Mol Biol* (2000) 302(1):251–64. doi: 10.1006/jmbi.2000.4055

33. Wu X, Tu X, Joeng KS, Hilton MJ, Williams DA, Long F. Rac1 activation controls nuclear localization of β-catenin during canonical wnt signaling. *Cell* (2008) 133(2):340–53. doi: 10.1016/j.cell.2008.01.052

34. Jamieson C, Lui C, Brocardo MG, Martino-Echarri E, Henderson BR. Rac1 augments wnt signaling by stimulating β-catenin-LEF-1 complex assembly independent of β-catenin nuclear import. *J Cell Sci* (2015) 128(21):3933–46. doi: 10.1242/jcs.167742

35. Henderson BR. Nuclear-cytoplasmic shuttling of APC regulates β-catenin subcellular localization and turnover. *Nat Cell Biol* (2000) 2(9):653–60. doi: 10.1038/35023605

36. Cong F, Varmus H. Nuclear-cytoplasmic shuttling of axin regulates subcellular localization of β-catenin. *Proc Natl Acad Sci USA* (2004) 101 (9):2882–7. doi: 10.1073/pnas.0307344101

37. Daugherty RL, Serebryannyy L, Yemelyanov A, Flozak AS, Yu HJ, Kosak ST, et al. α-catenin is an inhibitor of transcription. *Proc Natl Acad Sci USA* (2014) 111 (14):5260–5. doi: 10.1073/pnas.1308663111

38. Serebryannyy LA, Yemelyanov A, Gottardi CJ, de Lanerolle P. Nuclear α-catenin mediates the DNA damage response *via* β-catenin and nuclear actin. *J Cell Sci* (2017) 130(10):1717–29. doi: 10.1242/jcs.199893

39. Orsulic S, Huber O, Aberle H, Arnold S, Kemler R. E-cadherin binding prevents beta-catenin nuclear localization and beta-catenin/LEF-1-mediated transactivation. *J Cell Sci* (1999) 112(Pt 8):1237–45. doi: 10.1242/jcs.112.8.1237

40. Hülsken J, Birchmeier W, Behrens J. E-cadherin and APC compete for the interaction with beta-catenin and the cytoskeleton. *J Cell Biol* (1994) 127(6 Pt 2):2061–9. doi: 10.1083/jcb.127.6.2061

41. Tanaka Y, Terai Y, Kawaguchi H, Fujiwara S, Yoo S, Tsunetoh S, et al. Prognostic impact of EMT (epithelial-mesenchymal-transition)-related protein expression in endometrial cancer. *Cancer Biol Ther* (2013) 14(1):13–9. doi: 10.4161/cbt.22625

42. Kim S, Jeong S. Mutation hotspots in the β-catenin gene: Lessons from the human cancer genome databases. *Mol Cells* (2019) 42(1):8–16. doi: 10.14348/ molcells.2018.0436

43. Liu Y, Patel L, Mills GB, Lu KH, Sood AK, Ding L, et al. Clinical significance of CTNNB1 mutation and wnt pathway activation in endometrioid endometrial carcinoma. *J Natl Cancer Inst* (2014) 106(9):dju245. doi: 10.1093/jnci/dju245

44. Imboden S, Tapia C, Scheiwiller N, Kocbek V, Altermatt HJ, Janzen J, et al. Early-stage endometrial cancer, CTNNB1 mutations, and the relation between lymphovascular space invasion and recurrence. *Acta Obstet. Gyneco. Scand* (2020) 99(2):196–203. doi: 10.1111/aogs.13740

45. Travaglino A, Raffone A, Raimondo D, Reppuccia S, Ruggiero A, Arena A, et al. Prognostic significance of CTNNB1 mutation in early stage endometrial carcinoma: A systematic review and meta-analysis. *Arch Gyneco. Obstet.* (2022) 306 (2):423–31. doi: 10.1007/s00404-021-06385-0

46. McAlpine J, Leon-Castillo A, Bosse T. The rise of a novel classification system for endometrial carcinoma; integration of molecular subclasses: Novel classification for endometrial cancer. *J Pathol* (2018) 244(5):538–49. doi: 10.1002/ path.5034

47. Santoro A, Angelico G, Travaglino A, Inzani F, Arciuolo D, Valente M, et al. New pathological and clinical insights in endometrial cancer in view of the updated ESGO/ESTRO/ESP guidelines. *Cancers (Basel).* (2021) 13(11):2623. doi: 10.3390/ cancers13112623

48. Kurnit KC, Fellman BM, Mills GB, Bowser JL, Xie S, Broaddus RR. Adjuvant treatment in early-stage endometrial cancer: Context-dependent impact of somatic CTNNB1 mutation on recurrence-free survival. *Int J Gyneco. Cancer.* (2022) 32 (7):869–74. doi: 10.1136/ijgc-2021-003340

49. Kurnit KC, Kim GN, Fellman BM, Urbauer DL, Mills GB, Zhang W, et al. CTNNB1 (beta-catenin) mutation identifies low grade, early stage endometrial cancer patients at increased risk of recurrence. *Mod Pathol* (2017) 30(7):1032–41. doi: 10.1038/modpathol.2017.15

50. Stelloo E, Nout RA, Osse EM, Jürgenliemk-Schulz IJ, Jobsen JJ, Lutgens LC, et al. Improved risk assessment by integrating molecular and clinicopathological factors in early-stage endometrial cancer–combined analysis of the PORTEC cohorts. *Clin Cancer Res* (2016) 22(16):4215–24. doi: 10.1158/1078-0432.CCR-15-2878

51. Ruz-Caracuel I, López-Janeiro Á, Heredia-Soto V, Ramón-Patino JL, Yébenes L, Berjón A, et al. Clinicopathological features and prognostic significance of CTNNB1 mutation in low-grade, early-stage endometrial endometrioid carcinoma. *Virchows Arch* (2021) 479(6):1167–76. doi: 10.1007/ s00428-021-03176-5

52. Moroney MR, Davies KD, Wilberger AC, Sheeder J, Post MD, Berning AA, et al. Molecular markers in recurrent stage I, grade 1 endometrioid endometrial cancers. *Gyneco. Oncol* (2019) 153(3):517–20. doi: 10.1016/j.ygyno.2019.03.100

53. Costigan DC, Dong F, Nucci MR, Howitt BE. Clinicopathologic and immunohistochemical correlates of CTNNB1 mutated endometrial endometrioid carcinoma. *Int J Gynecol. Pathol* (2020) 39(2):119–27. doi: 10.1097/PGP.0000000 000000583

54. Kim G, Kurnit KC, Djordjevic B, Singh C, Munsell MF, Wang WL, et al. Nuclear β-catenin localization and mutation of the CTNNB1 gene: A context-

dependent association. *Mod Pathol* (2018) 31(10):1553–9. doi: 10.1038/s41379-018-0080-0

55. Moh MC, Shen S. The roles of cell adhesion molecules in tumor suppression and cell migration: A new paradox. *Cell Adh. Migr.* (2009) 3(4):334–6. doi: 10.4161/cam.3.4.9246

56. Schlosshauer PW, Ellenson LH, Soslow RA. Beta-catenin and e-cadherin expression patterns in high-grade endometrial carcinoma are associated with histological subtype. *Mod Pathol* (2002) 15(10):1032–7. doi: 10.1097/01.MP.0000028573.34289.04

57. Moreno-Bueno G, Hardisson D, Sarrió D, Sánchez C, Cassia R, Prat J, et al. Abnormalities of e- and p-cadherin and catenin (beta-, gamma-catenin, and p120ctn) expression in endometrial cancer and endometrial atypical hyperplasia. *J Pathol* (2003) 199(4):471–8. doi: 10.1002/path.1310

58. Heuberger J, Birchmeier W. Interplay of cadherin-mediated cell adhesion and canonical wnt signaling. *Cold Spring Harbor Perspect Biol* (2010) 2(2): a002915–a002915. doi: 10.1101/cshperspect.a002915

59. Bradford LS, Rauh-Hain JA, Schorge J, Birrer MJ, Dizon DS. Advances in the management of recurrent endometrial cancer. *Am J Clin Oncol* (2015) 38 (2):206–12. doi: 10.1097/COC.0b013e31829a2974

60. Liu Y, Tang W, Xie L, Wang J, Deng Y, Peng Q, et al. Prognostic significance of dickkopf-1 overexpression in solid tumors: a meta-analysis. *Tumor Biol* (2014) 35(4):3145–54. doi: 10.1007/s13277-013-1411-x

61. Betella I, Turbitt WJ, Szul T, Wu B, Martinez A, Katre A, et al. Wnt signaling modulator DKK1 as an immunotherapeutic target in ovarian cancer. *Gynecol. Oncol* (2020) 157(3):765–74. doi: 10.1016/j.ygyno.2020.03.010

62. Haas MS, Kagey MH, Heath H, Schuerpf F, Rottman JB, Newman W. mDKN-01, a novel anti-DKK1 mAb, enhances innate immune responses in the tumor microenvironment. *Mol Cancer Res* (2021) 19(4):717–25. doi: 10.1158/1541-7786.MCR-20-0799

63. Janda CY, Waghray D, Levin AM, Thomas C, Garcia KC. Structural basis of wnt recognition by frizzled. *Science* (2012) 337(6090):59–64. doi: 10.1126/science.1222879

64. Madan B, Ke Z, Harmston N, Ho SY, Frois AO, Alam J, et al. Wnt addiction of genetically defined cancers reversed by PORCN inhibition. *Oncogene* (2016) 35 (17):2197–207. doi: 10.1038/onc.2015.280

65. Emami KH, Nguyen C, Ma H, Kim DH, Jeong KW, Eguchi M, et al. A small molecule inhibitor of β-catenin/cyclic AMP response element-binding protein transcription. *Proc Natl Acad Sci USA* (2004) 101(34):12682–7. doi: 10.1073/pnas.0404875101

frontiers | Frontiers in Oncology

TYPE Original Research
PUBLISHED 21 October 2022
DOI 10.3389/fonc.2022.982806

OPEN ACCESS

EDITED BY
Sara Ricardo,
Universidade do Porto, Portugal

REVIEWED BY
Faraz Rashid,
Henry Ford Health System, United States
Komsun Suwannarurk,
Thammasat University, Thailand

*CORRESPONDENCE
Wei Cui
wendycuiwei@sina.cn
Feng-zhi Feng
fengfz1969@sina.com

†These authors have contributed equally to this work

SPECIALTY SECTION
This article was submitted to Gynecological Oncology, a section of the journal Frontiers in Oncology

RECEIVED 30 June 2022
ACCEPTED 06 October 2022
PUBLISHED 21 October 2022

CITATION
Wang F, Wang Z-r, Ding X-s, Yang H, Guo Y, Su H, Wan X-r, Wang L-j, Jiang X-y, Xu Y-h, Chen F, Cui W and Feng F-z (2022) Combining serum peptide signatures with International Federation of Gynecology and Obstetrics (FIGO) risk score to predict the outcomes of patients with gestational trophoblastic neoplasia (GTN) after first-line chemotherapy. *Front. Oncol.* 12:982806. doi: 10.3389/fonc.2022.982806

Combining serum peptide signatures with International Federation of Gynecology and Obstetrics (FIGO) risk score to predict the outcomes of patients with gestational trophoblastic neoplasia (GTN) after first-line chemotherapy

Fei Wang[1†], Zi-ran Wang[1†], Xue-song Ding[2†], Hua Yang[2], Ye Guo[1], Hao Su[2], Xi-run Wan[2], Li-juan Wang[3], Xiang-yang Jiang[4], Yan-hua Xu[5], Feng Chen[6], Wei Cui[6*] and Feng-zhi Feng[2*]

[1]Department of Laboratory Medicine, Peking Union Medical College Hospital, Chinese Academy of Medical Sciences & Peking Union Medical College, Beijing, China, [2]Department of Obstetrics and Gynecology, National Clinical Research Center for Obstetric & Gynecologic Diseases, Peking Union Medical College Hospital, Chinese Academy of Medical Sciences & Peking Union Medical College, Beijing, China, [3]Department of Gynecological Oncology, Sun Yat-Sen Memorial Hospital of Sun Yat-Sen University, Guangzhou, China, [4]Department of Obstetrics and Gynecology, Shanxi Provincial People's Hospital, Xian, China, [5]Department of Obstetrics and Gynecology, Jinan Maternity and Child Health Care Hospital, Jinan, China, [6]Department of Clinical Laboratory, State Key Laboratory of Molecular Oncology, National Cancer Center/National Clinical Research Center for Cancer/Cancer Hospital, Chinese Academy of Medical Sciences and Peking Union Medical College, Beijing, China

Background: Gestational trophoblastic neoplasia (GTN) is a group of clinically rare tumors that develop in the uterus from placental tissue. Currently, its satisfactory curability derives from the timely and accurately classification and refined management for patients. This study aimed to discover biomarkers that could predict the outcomes of GTN patients after first-line chemotherapy.

Methods: A total of 65 GTN patients were included in the study. Patients were divided into the good or poor outcome group and the clinical characteristics of the patients in the two groups were compared. Furthermore, the serum peptide profiles of all patients were uncovered by using weak cation exchange magnetic beads and matrix-assisted laser desorption/ionization time-of-flight mass spectrometry. Feature peaks were identified by three machine learning algorithms and then models were constructed and compared using five machine learning methods. Additionally, liquid chromatography mass spectrometry was used to identify the feature peptides.

Results: Multivariate logistic regression analysis showed that the International Federation of Gynecology and Obstetrics (FIGO) risk score was associated with poor outcomes. Eight feature peaks (*m/z* =1287, 2042, 2862, 2932, 2950, 3240, 3277 and 6626) were selected for model construction and validation by the three algorithms. Based on the panel combining FIGO risk score and peptide serum signatures, the neural network (nnet) model showed promising performance in both the training (AUC=0.9635) and validation (AUC=0.8788) cohorts. Peaks at *m/z* 2042, 2862, 2932, 3240 were identified as the partial sequences of transthyretin, fibrinogen alpha chain (FGA), beta-globin and FGA, respectively.

Conclusion: We combined FIGO risk score and serum peptide signatures using the nnet method to construct the model which can accurately predict outcome of GTN patients after first-line chemotherapy. With this model, patients can be further classified and managed, and those with poor predicted outcomes can be given more attention for developing treatment failure.

KEYWORDS

gestational trophoblastic neoplasia, serum peptide profiles, machine learning, biomarker, FIGO

Introduction

Gestational trophoblastic neoplasia (GTN) is a group of clinically rare tumors that develop in the uterus from placental tissue, including invasive mole (IM), choriocarcinoma (CC), placental site trophoblastic tumor (PSTT), and epithelioid trophoblastic tumor (ETT) (1). GTN, which had a poor outcome in the last century, can now have a cure rate of over 90% owing to the combination of different treatment regimens and the refined management for high-risk patients (2). Constant monitoring of serum human chorionic gonadotropin (hCG) levels is essential after GTN treatment and persistently elevated hCG is considered a tumor-marker of poor outcome. The International Federation of Gynecology and Obstetrics (FIGO) scoring system has been developed to predict the prognosis of GTN patients. Based on the FIGO scores, patients are divided into a low-risk group (FIGO score < 7), high-risk group (7 ≤FIGO score ≤ 12), and an ultra-high-risk group (FIGO score > 12) (3). However, more personalized biomarkers are desired to help further evaluate the outcomes of GTN patients after first-line chemotherapy.

The low molecular weight (LMW) peptides in the serum contain abundant histological information, which may be useful in the early diagnosis of disease (4). Notably, specific serum peptide patterns are strongly associated with outcomes of cancer patients (5). However, due to the diverse and complex protein/peptide composition of serum, the fractionation and identification of LMW serum peptides was incredibly challenging. With the development of technology, weak cation exchange magnetic beads (MB-WCX) method has been shown to be efficient in capturing low abundance LMW peptides in serum and matrix-assisted laser desorption/ionization time-of-flight mass spectrometry (MALDI-TOF MS) can be applied to the analysis of captured serum peptides (6). Recently, MALDI-TOF MS-based serum peptide signatures have exhibited enormous potential in identifying patients with early lung cancer (7), cervical intraepithelial neoplasia (8), colorectal cancer (9), esophageal squamous cell carcinoma (10), and coronavirus disease 2019 (COVID-19) (11).

In the present study, the serum peptide profiles of 65 patients with GTN were revealed by MALDI-TOF MS combined with MB-WCX. Simultaneously, this study was dedicated to develop a panel based on combining serum peptide signatures and clinical feature to predict the outcome of GTN patients after first-line chemotherapy using a variety of machine learning models.

Materials and methods

Study design and patients population

A prospective collection of peripheral blood of patients with treatment-naïve GTN were conducted within 7 days before the initial therapy at 5 centers from June 2017 to June 2019. Based on FIGO cancer Report and clinical practice in China about management of gestational trophoblastic disease (2, 12–14),

single-agent dactinomycin chemotherapy was prescribed as first-line treatment for low-risk GTN (FIGO score of less than 5) and multiagent chemotherapy using 5-FU based regimen or EMACO as first-treatment for low-risk GTN with FIGO score 5-6 or high-risk GTN. Chemotherapy response during first-line therapy was monitored by hCG assay at the start of each treatment cycle. Complete remission (CR) was defined as the normalization of hCG for at least 4 consecutive weeks. Chemotherapy resistance is defined by a plateau in hCG (<10% change) or a rise in hCG over two consecutive cycles, and then second-line chemotherapy is considered. The date cut-off of first-line chemotherapy response ended in completion of first-line chemotherapy for patients who have achieved CR (defined as good outcome group), or for patients who experienced chemotherapy resistance (defined as poor outcome group). And then, the data cut-off of patient survival ended in April 2022. Patients who switched to second-line therapy due to toxicity of first-line chemotherapy were excluded. Additionally, given that first-line treatment regimens for PSTT and ETT differ significantly from that for IM and CC, patients with PSTT or ETT were also excluded.

The patient's medical records including age, histology, antecedent pregnancy, hCG, FIGO score, FIGO stage, and treatment were collected. This study was approved by Chinese Academy of Medical Science, and Peking Union Medical College (approval no. 18-218/1796). The patients provided their written informed consent in accordance with the declaration of Helsinki.

Sample collection and preparation

Blood was collected from all patients in the morning and placed at 37°C for 30min to clot. Then, the blood was centrifuged at 3000 rpm for 15 minutes to obtain the serum. The serum of all patients was stored at -80°C for the next step of serum peptide analysis.

MB-WCX

Serum peptides were extracted using the serum peptide extraction kit (Bioyong Tech, Beijing, China) following the instructions. Firstly, 10μl magnetic beads, 95μl binding buffer and 10μl serum sample were mixed and incubated for 5min at room temperature. Subsequently, the supernatant derived from the mixture by using a magnetic bead separator was added to the wash buffer to remove the high molecular weight peptides/proteins. Finally, the LMW peptides were eluted by adding elution buffer and then subjected to MALDI-TOF MS analysis.

MALDI-TOF MS

The eluted peptide samples were mixed with 5mg/ml α-cyano-4-hydroxycinnamic acid (CHCA) and 1μl mixture was applied to the MALDI-TOF MS target plate then dried naturally for detection. The MALDI-TOF MS instrument (Bioyong Tech, Beijing, China) was calibrated using commercial peptide and protein calibration standards (Sigma-Aldrich, Louis, MO, USA) before assaying the samples. The spectra were automatically captured in linear mode within the range 1000 -10000 mass-to-change ratio (*m/z*). Each spectrum was normalized, baseline-corrected and smooth-applied using BioExplorer software (Bioyong Tech, Beijing, China). The assay for each sample was repeated three times and the final peak intensity was averaged from the three times.

Liquid chromatography mass spectrometry

Serum peptides were sequenced and identified by using a nano-liquid chromatography electrospray ionization-tandem mass spectrometry (nano LC/ESI-MS/MS), which consists of an Aquity UPLC system (Waters, USA) and a LTQ Orbitrap XL mass spectrometer (Thermo Fisher Scientific, USA) equipped with a nano-ESI source. Prior to LC-MS analysis of the target samples, the instrument was calibrated using the Pierce Retention Time Calibration Mixture (Thermo Fisher Scientific, USA). The peptides were desalted and then separated by UPLC system and analyzed using MS/MS instrument. The obtained raw mass spectra were analyzed by using Proteome Discoverer software (version 2.1, Thermo Fisher Scientific, USA). The UniProt database (UniProt-*homo+sapiens*.fasta, downloaded 10/08/21) was used to perform the identifications. The detailed search parameters were as follows: enzyme: trypsin, max missed cleavages: 2, fixed modifications: Carbamidomethyl, variable modifications: oxidation, protein N-terminal acetylation and deamidation, peptide mass tolerance value: 10ppm, fragment mass tolerance value: 0.02 Da.

Statistical analysis

All statistical tests were performed using R project (version 4.1.2) and SPSS 20.0 software (SPSS Inc., Chicago, IL, USA). The t-test or Wilcoxon test was used for analysis of continuous data while the chi-square test or Fisher's exact probability for analysis of categorical data. Progression free survival (PFS) were analyzed using the Kaplan-Meier method and the log-rank test. Multivariate logistic regression analysis was used to identify risk factors for patients with poor outcome. The R packages "caret", and "nnet" were used for the construction and validation of the models. Receiver operating characteristic (ROC) curves were used to evaluate the diagnostic performance of the model using MedCalc software (version 19.6.1) or Prism GraphPad (version 9.0). $P<0.05$ was considered statistically significant

Results

Clinical characteristics and outcomes

Between June 2017 and June 2019, 99 patients' samples were collected at 5 centers. Thirty-four patients were excluded, including 8 patients with non-GTN, 15 patients with the change of chemotherapy regimen due to toxicity of first-line chemotherapy, 6 patients with PSTT, 1 patient with non-gestational CC, and 4 patients with failure of serum peptide extraction. Ultimately, 65 patients met the eligibility criteria.

The clinical characteristics of the 65 GTN patients were summarized in Table 1. The median age of all patients was 32 years old, of which 27 were diagnosed with CC and 38 with IM. Patients had a median FIGO score of 3 and 91% (59 of 65) had obvious lesions located in uterus, or other organs including lung, vagina, liver, spleen, great omentum, and pelvic. Based on the status of response during first-line chemotherapy, 35 patients were classified as good outcomes group and 30 patients were classified as poor outcomes group. As shown in Figure 1A, patients in the good outcomes group had a longer PFS than those in the poor outcomes group (Hazard Ratio=0.10 (0.02-0.61), P=0.0125). Furthermore, patients in the poor outcome group had higher FIGO scores (6 vs 2, P<0.001) and higher proportion of CC (57% vs 29%, P=0.041) than those in the good outcomes group (Table 1). In addition, multivariate logistic regression analysis showed that the FIGO score (Odds Ratio=1.32(1.03-1.75), P=0.04) was associated with poor outcomes. (Figure 1B). As illustrated in Figure 1C, the FIGO risk score exhibited moderate performance in discriminating between patients with different outcomes, with the area under the curve (AUC) of the ROC being 0.749 (P<0.001). Overall, the FIGO risk score was effective in predicting outcome of GTN patients after first-line chemotherapy, but its performance could be further strengthened.

Serum peptide profiles analysis

The workflow of serum peptide profiles analysis was shown in Figure 2. Serum obtained by centrifugation of blood samples from patients contained a wide range of low and high molecular peptides/proteins. LMW serum peptides were extracted by MB-WCX method and analyzed using MALDI-TOF MS. Representative mass spectra of patients with GTN who had

TABLE 1 Clinical characteristics and treatments of GTN patients.

Variables	Total (n = 65)	good (n = 35)	poor (n = 30)	*P* value
Age, Median (Q1, Q3)	32 (28, 37)	32 (28, 36)	31.5 (27.25, 37.75)	0.707
hCG, IU/L, Median (Q1, Q3)	5513 (682, 40831)	2852 (419.06, 10471.5)	28156.5 (2985.25, 75325)	**0.007**
Lesion location, n (%)				0.594
Liver/Lung/Spleen/Great omentum	1 (2)	0 (0)	1 (3)	
Lung	13 (20)	8 (23)	5 (17)	
Lung/Pelvic	1 (2)	0 (0)	1 (3)	
Lung/Uterus	20 (31)	12 (34)	8 (27)	
Lung/Vagina/Uterus	1 (2)	0 (0)	1 (3)	
Uterus	21 (32)	9 (26)	12 (40)	
Uterus /Vagina	1 (2)	1 (3)	0 (0)	
Vagina	1 (2)	1 (3)	0 (0)	
None	6 (9)	4 (11)	2 (7)	
Antecedent pregnancy, n (%)				0.259
Abortion	10 (15)	5 (14)	5 (17)	
Hydatidiform mole	45 (69)	26 (74)	19 (63)	
Term	10 (15)	4 (11)	6 (20)	
FIGO Score, Median (Q1, Q3)	3 (1, 7)	2 (1, 4)	6 (3, 8.75)	**< 0.001**
FIGO Stage, n (%)				0.317
I	26 (40)	13 (37)	13 (43)	
II	3 (5)	3 (9)	0 (0)	
III	35 (54)	19 (54)	16 (53)	
IV	1 (2)	0 (0)	1 (3)	
Histology, n (%)				**0.041**
CC	27 (42)	10 (29)	17 (57)	
IM	38 (58)	25 (71)	13 (43)	

FIGO, International Federation of Gynecology and Obstetrics; CC, choriocarcinoma; IM, invasive mole.
Bold shows the heading of the table or the p-value <0.05.

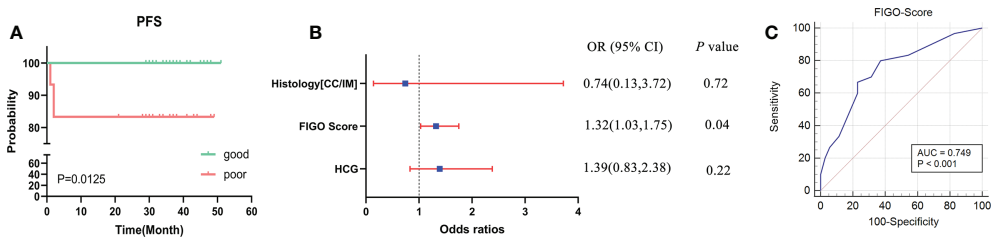

FIGURE 1
Analysis of the clinical characteristics and outcomes of patients with GTN after first-line chemotherapy **(A)**, disease-free survival (DFS) between two groups with good or poor outcomes; **(B)**, multivariate regression analysis of factors associated with outcomes; **(C)**, ROC analysis using the FIGO risk score to discriminate between different outcome groups.

good or poor outcome were shown in Figure 3A, respectively. A total of 37 peaks in the range of 1000-10000 *m/z* were detected in all 65 patients. The intensities of these peaks are shown in Figure 3B, with different patients exhibiting diverse intensity patterns.

Selection of feature peaks

To construct a robust model for predicting the outcomes of GTN patient, after normalizing the intensity of the peaks, all patients were split into training cohort (n=48) and validation cohort (n=17) with an allocation of 7:3. In training cohort, three machine learning algorithms were used to screen the feature peaks: partial least-squares-discriminant analysis (PLS-DA), recursive feature elimination (RFE) and random forest (RF). All peaks were ranked according to the relative importance score using above three algorithms and the top 20 peaks were shown in Figures 4A-C. Furthermore, 8 feature peaks (*m/z* =1287, 2042, 2862, 2932, 2950, 3240, 3277 and 6626) were selected for model construction and validation by taking the intersection of the top 20 peaks filtered by the three algorithms (Figure 4D).

Model construction and validation

Based on the fact that the FIGO score is a vital factor for poor outcome in GTN patients and the eight characteristic peaks that were screened by three machine learning algorithms, we further explored whether these features could be combined to build a powerful model to predict clinical outcomes. Thus, the above features were applied to construct five machine learning model methods, including neural network (nnet), recursive partitioning (rpart), naive bayes (nb), support vector machine (svm), logistic regression model (lm). We compared the performance of five methods by cross-validation to calculate ROC, sensitivity and specificity. As illustrated in Figure 5A, the nnet method had higher average ROC, sensitivity and specificity values. Overall, our results indicated the nnet method was superior to the other models; therefore, we chosen the nnet method for further analysis. In the training cohort, the confusion matrix of the nnet method showed that only three patients with poor outcomes were misclassified as good outcomes while no patients with good outcomes were misclassified as poor outcomes (Figure 5B). Remarkably, the nnet method reached an AUC of 0.9635 in the training cohort (Figure 5C). In the independent validation cohort, the nnet method also achieved a favorable performance: only one patient with good or poor outcome was misclassified respectively, with the AUC value reaching 0.8788 (Figures 5D, E). The accuracy, error rate, precision, recall, and F1-score of the nnet method in both the training and validation cohorts were shown in Figure 5F. Intriguingly, the AUC for the FIGO score alone to discriminate between good and poor outcome subgroups was 0.786 and 0.568 in the training and validation cohort, respectively (Figure 6). Collectively, the nnet machine learning model constructed by combining the FIGO score and serum peptide signatures had satisfactory classification performance in predicting outcomes of GTN patients after first-line chemotherapy.

Identification of peptide peaks

To further elucidate the role of serum peptide profiles in disease, we used LC-MS/MS for the identification of the peptide peaks. As depicted in Table 2, the amino acid sequences of the four peptide peaks were successfully identified. Peaks at *m/z* 2042, 2862, 2932, 3240 were identified as the partial sequences of transthyretin, fibrinogen alpha chain (FGA), beta-globin and FGA, respectively.

Discussion

Currently, most GTN patients could be cured with the preservation of their reproductive function, which benefits from timely and appropriate initial management and prognostic follow-

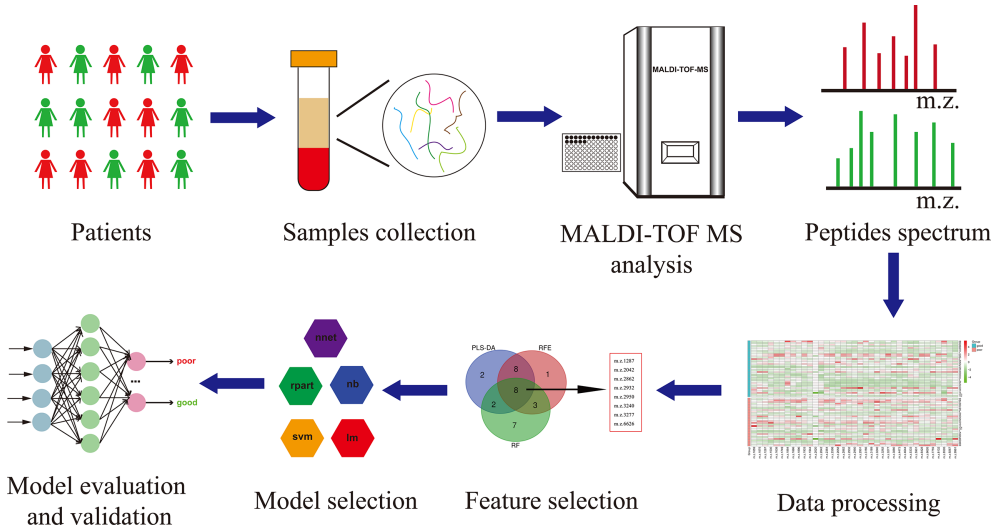

FIGURE 2
The workflow of serum peptide profiles analysis. Serum from patients containing various peptides/proteins was collected and subsequently processed for analysis using MALDI-TOF MS. The obtained peak patterns were normalized and then the machine learning algorithms were used to perform feature selection. The different machine learning methods were implemented and compared to eventually yield a robust model, which was further evaluated and validated.

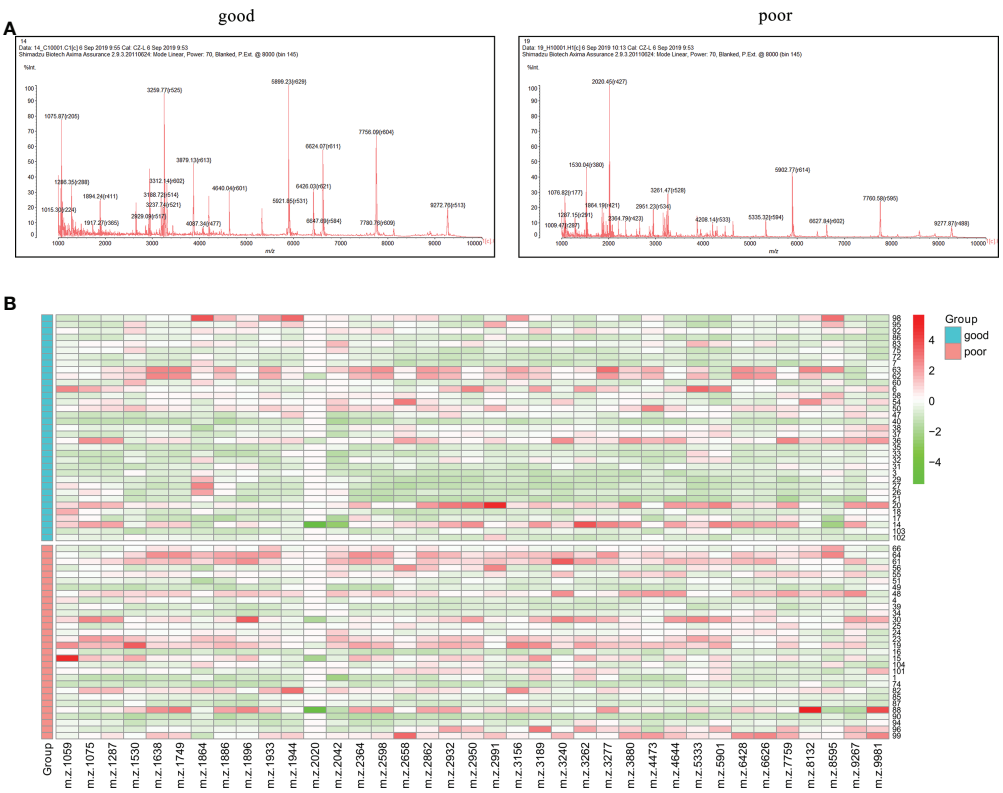

FIGURE 3
Serum peptide patterns in patients with GTN **(A)**, MALDI-TOF spectra of the serum samples from patients with good or poor outcome; **(B)**, heatmap of the intensity distribution of the 37 peptide peaks for all patients.

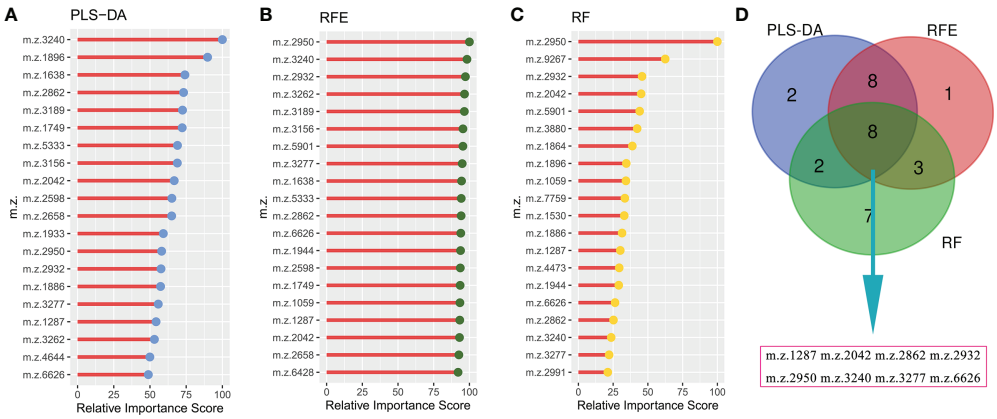

FIGURE 4
Selecting signature peptide peaks using machine learning algorithms **(A)**, top 20 features prioritized by PLS-DA ranked by the decrease in feature importance scores; **(B)**, top 20 features prioritized by RFE ranked by the decrease in feature importance scores; **(C)**, top 20 features prioritized by RF ranked by the decrease in feature importance scores; **(D)**, final 8 serum peptide features were achieved by taking the intersection of the top 20 features filtered by the three machine learning algorithms.

up. It is essential to implement less-toxic monotherapy for patients at low-risk and aggressive multiagent therapy for patients at high-risk, based on the individual risk factors (15). Constant surveillance of hCG levels is imperative and elevated hCG levels after treatment herald poor outcomes, such as relapse or resistance. In this scenario, it would be meaningful to explore individual difference-based biomarkers for predicting treatment outcomes so as to achieve individualized and refined governance for GTN patients after first-line chemotherapy. It is worth noting that the FIGO risk scoring system includes the evaluation of 8-index scale for age, antecedent pregnancy, interval months from index pregnancy, pretreatment serum hCG, largest tumor size, site of metastases, number of

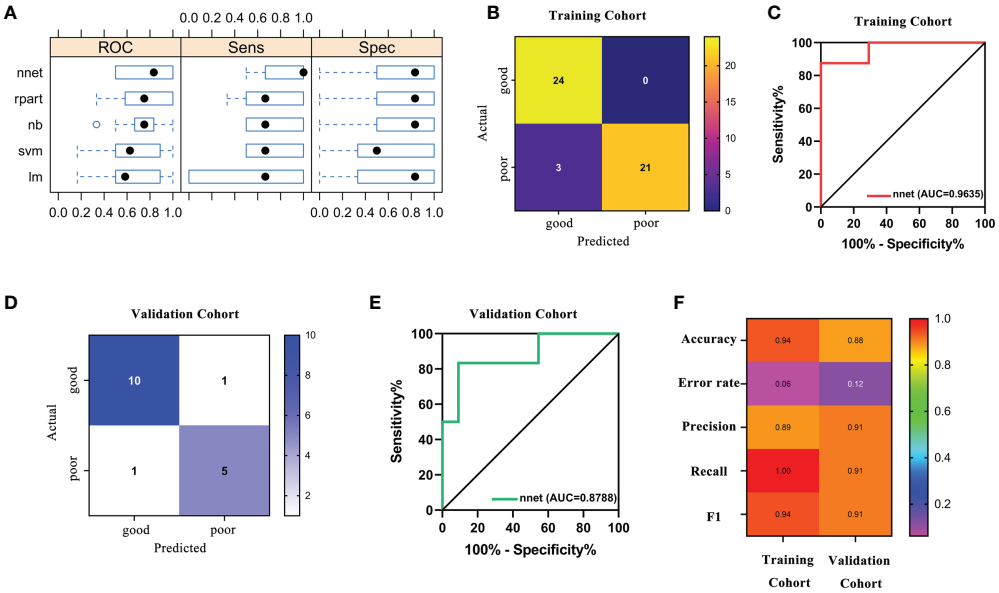

FIGURE 5
Performance of machine learning models based on FIGO risk scores and serum peptide signatures. **(A)**, comparison of the performance among 5 machine learning methods by cross-validation; **(B)**, confusion matrix of the classification results by the nnet model in training cohort; **(C)**, ROC analysis using the nnet model to discriminate between different outcome groups in training cohort; **(D)**, confusion matrix of the classification results by the nnet model in validation cohort; **(E)**, ROC analysis using the nnet model to discriminate between different outcome groups in validation cohort; **(F)**, summary of accuracy, error rate, precision, recall and F1 for the nnet model in the training and validation cohort.

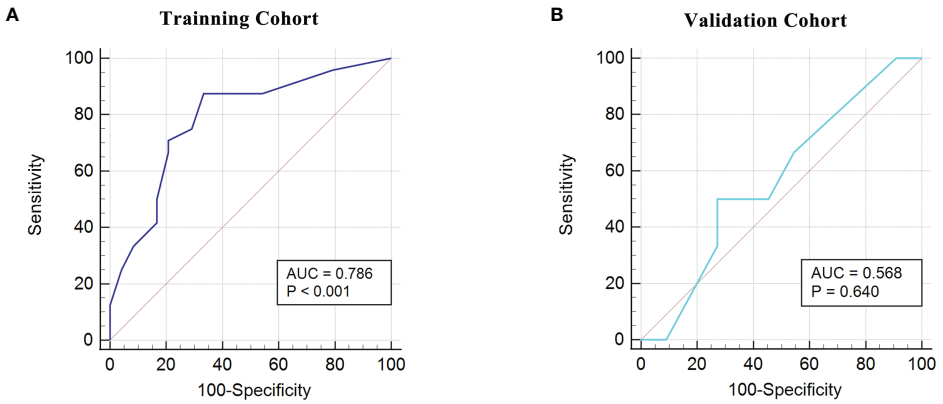

FIGURE 6
ROC analysis using the FIGO risk score to discriminate between different outcome groups. **(A)**, ROC analysis in the training cohort; **(B)**, ROC analysis in the validation cohort.

metastases and previous failed chemotherapy (15). Previous publications have highlighted the role of the FIGO risk score in assessing prognosis of patients: a higher FIGO score (≥12) forecasted increased probability of treatment failure and poor outcome (16–18). In line with the above studies, we identified the FIGO score as a vital factor for poor outcomes by multivariate logistic regression. Some studies have pointed out that the FIGO risk score is a better predictor of clinical outcomes than single indicators in it (19, 20). On this basis, we attempted to use the ROC curves to determine the power of the FIGO score to predict outcomes and obtained the AUC of 0.749 in our study cohort. It is implied that the FIGO risk score can be used as a valid predictor of outcomes for GTN patients after first-line chemotherapy but there is still room for development.

Proteases are involved in many physiological processes in the body which are crucial for maintaining homeostasis, whilst aberrant protease activity changes are closely associated with tumorigenesis and progression (21). Specifically, proteases can, on the one hand, degrade the extracellular matrix barrier to promote tumor metastasis and progression; on the other hand, cleave proteins in the serum to produce peptide fragments of variable size. In other words, the serum peptide pattern may vary in patients with disparate outcomes. Bedin et al. revealed peculiar changes in the serum peptide profile of colorectal cancer from pre-cancer lesion to metastatic disease, implying the potential usefulness of serum peptide signatures as biomarkers in early diagnosis and prognosis of patients with tumors (22). Therefore, in present study we intended to discover serum peptide signatures that are closely related to the outcome of GTN patients. For all patients, we identified 37 peptide peaks, however not all of them were meaningful. For instance, the peptide peak with m/z=2020 had minor variation in most patients. To avoid over-fitting of the constructed model, it was necessary to include only sensible features. Feature selection based on machine learning algorithms has now been reported to filter out risk factors associated with patient diagnosis and prognosis (11, 23). Hereby, we used three machine learning algorithms (PLS-DA, RFE and RF) to help us recognize valuable peptide peaks. PLS-DA is a supervised multivariate classification method that could be a variable selection method by ranking the

TABLE 2 Identified candidate peptide biomarkers.

m/z	Protein sequence	Protein name	Positions in Proteins
1287	NA	NA	NA
2042	**ALLSPYSYSTTAVVTNPKE**	**Transthyretin**	**166-184**
2862	**MADEAGSEADHEGTHSTKRGHAKSRPV**	**Fibrinogen alpha chain**	**603-629**
2932	**KEFTPPVQAAYQKVVAGVANALAHKYH**	**Beta-globin**	**121-147**
2950	NA	NA	NA
3240	**SYKMADEAGSEADHEGTHSTKRGHAKSRPV**	**Fibrinogen alpha chain**	**600-629**
3277	NA	NA	NA
6626	NA	NA	NA

NA, not available.
Bold shows the parameters of the four peptide peaks.

most important loadings in decreasing order (24). RFE is a greedy algorithm that builds gene sets by iterating continuously, removing the less important genes and selecting the optimal subset from gene sets (25). RF is an algorithm for estimating variable importance based on multiple decision trees, which measures mainly the mean decrease in accuracy or mean decrease in Gini (24). After integrating the three excellent feature selection algorithms, we have determined eight peptide signatures for further analysis.

Recently, it is a hot topic in the field of tumor diagnosis and prognosis evaluation to use selected features in the training set for model building and training by machine learning methods, and to perform the verification in the independent validation set (26–28). In this study, we combined a clinical feature (FIGO score) closely related to outcomes with serum peptide features to generate a prediction panel. Furthermore, models based on this panel were constructed and compared by five machine learning methods (nnet, rpart, nb, svm, lm). Through cross-validation, we found that the neural network (nnet) method outperformed the other methods. The nnet method is considered as a powerful tool for deep learning and artificial intelligence by simulating the functions of the brain's neural networks to help make decisions (29). The nnet method has been reported to possess enormous strengths in attaining classification of images, and it has been observed to yield a high degree of accuracy in the differentiation of bone marrow cell morphologies (30). She et al. has developed a deep learning survival neural network model which can predict the survival of lung cancer patients and test the reliability of recommended treatments (31). We found that the model constructed using the panel-based nnet method (AUC: 0.9635 in the training cohort; 0.8788 in the validation cohort) showed a substantial improvement in the efficacy of predicting outcomes compared to the FIGO score alone (AUC: 0.786 in the training cohort; 0.568 in the validation cohort).

Machine learning poses a number of challenges when it comes to building accurate models from complicated data, for instance, its complexity and uncertainty make models opaque and difficult to interpret, also known as "black box" (32). On this basis, the selected eight peptides were further identified by using MS/LS-MS to enhance the interpretability of the model. We have determined four of the eight peptides, *m/z* 2042, 2862, 2932, 3240, which were fragments of transthyretin, FGA, beta-globin and FGA, respectively. Transthyretin, also known as prealbumin, is a homotetramer plasma protein of approximately 55 KD that can transport thyroxine by binding to retinol-binding protein (33). It has been reported that transthyretin, a secreted protein downstream of STAT3, could promote oncogenic gene activation, enhance cytokine function in the tumor microenvironment as well as increase the production of reactive oxygen species to facilitate the progression of lung cancer (34). Swiatly et al. reported that transthyretin was a serum peptide biomarker that contributed to the clinical diagnosis of ovarian cancer (35). Moreover, gestational trophoblastic disease is one of the rare causes of hyperthyroidism (36). Thus, it is implied that transthyretin may be closely related to the pathological course and treatment outcome of patients with GTN. Fibrinogen is the precursor of fibrin, which is the key component of the blood coagulation system (37). Fibrinogen alpha chain (FGA) has been reported as a serum peptide signature being a hallmark of a variety of tumors, including colorectal cancer (9), esophageal squamous cell carcinoma (10), non-small cell lung cancer (38), pancreatic ductal adenocarcinoma (39). Duan et al. have revealed FGA as an attractive target for evaluating prognosis in gastric cancer by using DNA microarray analysis (40). Notably, Goldstein et al. found that patients with trophoblastic disease had increased concentration of fibrinogen along with altered fibrinolytic activity (41). In our study, two of the four successfully identified peptides were fragments of FGA, suggesting that FGA may be an important predictor of outcome for GTN patients. Certainly, the underlying mechanism of which deserves further exploration. The combination of the β globin-encoded polypeptides and the α globin-encoded polypeptides could produce distinct hemoglobin tetramers in red blood cells for oxygen transport, while aberrations in this process may lead to the development of severe hemoglobinopathies β-thalassemia (42). For patients with GTN, chemotherapy is a vital treatment, but it can also bring toxicity, such as anemia (43). Given that β globin is a regulator of the maintenance of erythrocyte function, we hypothesized that the toxicity associated with the treatment would have an imprint on it. Therefore, the β globin peptide fragment in the serum may reflect the degree of toxicity of chemotherapy which in turn provides the evidence of outcome.

Overall, the strength of this study was that combining clinical feature and serum peptide signatures constructed a robust model to predict outcomes for GTN patients after first chemotherapy through machine learning approaches. With this model, patients can be further classified and managed, and those with poor predicted outcomes can be given more attention for developing treatment failure or relapse. We were convinced that our study could provide a novel perspective on the treatment and follow-up of GTN after first chemotherapy.

There were also some limitations in this study. The major point was the limited sample size. Nevertheless, GTN as a rare disease has a low incidence. A larger cohort is desired to appraise the reliability of the model in the future. Apart from this, the amino acid sequences of the remaining four serum polypeptide signatures have not been disclosed. Moreover, since there are only 8 differentially expressed peptides identified, these peptides mass should also be verify using multiple reaction monitoring (MRM) based targeted workflow. Peptides along with two MS/MS fragments need to be targeted for absolute quantitation. However, due to the limited volume of serum retained from patients, we may not be able to perform MRM analysis at this time. In the future, we would enroll larger cohorts of patients to establish the level of these peptide during the disease progression

by using MRM technology. Notably, other confirmatory experiments could contribute to establishing the utility of these peptides in the prognostic assessment of GTN patients after first-line chemotherapy.

Data availability statement

The original contributions presented in the study are included in the article/supplementary material. Further inquiries can be directed to the corresponding authors.

Ethics statement

The studies involving human participants were reviewed and approved by the Ethics Committee of National Cancer Center/ Cancer Hospital, Chinese Academy of Medical Science, and Peking Union Medical College. The patients/participants provided their written informed consent to participate in this study.

Author contributions

WC and F-ZF contributed to the conception and design of this study. HS, X-RW and L-JW contributed to data acquisition. X-SD and X-YJ contributed to data interpretation and analysis. YX and FC contributed to study supervision. Z-RW and FW contributed to manuscript editing. HY and YG contributed to manuscript revising. All authors contributed to manuscript review.

Funding

This study was supported by the CAMS Innovation Fund for Medical Sciences (CIFMS) (No. 2017-I2M-3-005), Beijing Natural Science Foundation (No. 7202165), National Natural Science Foundation of China (No. 82072361) and the Non-profit Central Research Institute Fund of Chinese Academy of Medical Sciences(2021-PT320-001).

Conflict of interest

The authors declare that the research was conducted in the absence of any commercial or financial relationships that could be construed as a potential conflict of interest.

Publisher's note

References

1. Abu-Rustum NR, Yashar CM, Bean S, Bradley K, Campos SM, Chon HS, et al. Gestational trophoblastic neoplasia, version 2.2019, NCCN clinical practice guidelines in oncology. *J Natl Compr Canc Netw* (2019) 17(11):1374–91. doi: 10.6004/jnccn.2019.0053

2. Hoekstra AV, Lurain JR, Rademaker AW, Schink JC. Gestational trophoblastic neoplasia: Treatment outcomes. *Obstet. Gynecol.* (2008) 112(2 Pt 1):251–8. doi: 10.1097/AOG.0b013e31817f58ae

3. Ngan HYS, Seckl MJ, Berkowitz RS, Xiang Y, Golfier F, Sekharan PK, et al. Update on the diagnosis and management of gestational trophoblastic disease. *Int J Gynaecol. Obstet.* (2018) 143 Suppl 2:79–85. doi: 10.1002/ijgo.12615

4. Tirumalai RS, Chan KC, Prieto DA, Issaq HJ, Conrads TP, Veenstra TD. Characterization of the low molecular weight human serum proteome. *Mol Cell Proteomics* (2003) 2(10):1096–103. doi: 10.1074/mcp.M300031-MCP200

5. Villanueva J, Shaffer DR, Philip J, Chaparro CA, Erdjument-Bromage H, Olshen AB, et al. Differential exoprotease activities confer tumor-specific serum peptidome patterns. *J Clin Invest* (2006) 116(1):271–84. doi: 10.1172/jci26022

6. Qiu F, Liu HY, Zhang XJ, Tian YP. Optimization of magnetic beads for maldi-TOF MS analysis. *Front Biosci (Landmark Ed)* (2009) 14:3712–23. doi: 10.2741/3482

7. Widlak P, Pietrowska M, Polanska J, Marczyk M, Ros-Mazurczyk M, Dziadziuszko R, et al. Serum mass profile signature as a biomarker of early lung cancer. *Lung Cancer* (2016) 99:46–52. doi: 10.1016/j.lungcan.2016.06.011

8. Liu Y, Wei F, Wang F, Li C, Meng G, Duan H, et al. Serum peptidome profiling analysis for the identification of potential biomarkers in cervical intraepithelial neoplasia patients. *Biochem Biophys Res Commun* (2015) 465 (3):476–80. doi: 10.1016/j.bbrc.2015.08.042

9. Wang H, Luo C, Zhu S, Fang H, Gao Q, Ge S, et al. Serum peptidome profiling for the diagnosis of colorectal cancer: Discovery and validation in two independent cohorts. *Oncotarget* (2017) 8(35):59376–86. doi: 10.18632/oncotarget.19587

10. Jia K, Li W, Wang F, Qu H, Qiao Y, Zhou L, et al. Novel circulating peptide biomarkers for esophageal squamous cell carcinoma revealed by a magnetic bead-based MALDI-TOFMS assay. *Oncotarget* (2016) 7(17):23569–80. doi: 10.18632/oncotarget.8123

11. Yan L, Yi J, Huang C, Zhang J, Fu S, Li Z, et al. Rapid detection of COVID-19 using MALDI-TOF-Based serum peptidome profiling. *Anal Chem* (2021) 93 (11):4782–7. doi: 10.1021/acs.analchem.0c04590

12. Li L, Wan X, Feng F, Ren T, Yang J, Zhao J, et al. Pulse actinomycin d as first-line treatment of low-risk post-molar non-choriocarcinoma gestational trophoblastic neoplasia. *BMC Cancer* (2018) 18(1):585. doi: 10.1186/s12885-018-4512-5

13. Jiang F, Yang K, Wan XR, Xiang Y, Feng FZ, Ren T, et al. Reproductive outcomes after floxuridine-based regimens for gestational trophoblastic neoplasia: A retrospective cohort study in a national referral center in China. *Gynecol. Oncol* (2020) 159(2):464–9. doi: 10.1016/j.ygyno.2020.08.018

14. Li Y, Kong Y, Wan X, Feng F, Ren T, Zhao J, et al. Results with floxuridine, actinomycin d, etoposide, and vincristine in gestational trophoblastic neoplasias with international federation of gynecology and obstetrics scores ≥5. *Oncologist* (2021) 26(12):e2209–16. doi: 10.1002/onco.13943

15. Soper JT. Gestational trophoblastic disease: Current evaluation and management. *Obstet. Gynecol.* (2021) 137(2):355–70. doi: 10.1097/aog.0000000000004240

16. Yang J, Xiang Y, Wan X, Feng F, Ren T. Analysis of the prognosis and related factors for patients with stage IV gestational trophoblastic neoplasia. *Int J Gynecol. Cancer* (2014) 24(3):594–9. doi: 10.1097/igc.0000000000000070

17. Xiao C, Yang J, Zhao J, Ren T, Feng F, Wan X, et al. Management and prognosis of patients with brain metastasis from gestational trophoblastic neoplasia: a 24-year experience in Peking union medical college hospital. *BMC Cancer* (2015) 15:318. doi: 10.1186/s12885-015-1325-7

18. Li J, Yang J, Liu P, Ren T, Zhao J, Feng F, et al. Clinical characteristics and prognosis of 272 postterm choriocarcinoma patients at Peking union medical college hospital: a retrospective cohort study. *BMC Cancer* (2016) 16:347. doi: 10.1186/s12885-016-2383-1

19. Mortakis AE, Braga CA. "Poor prognosis" metastatic gestational trophoblastic disease: the prognostic significance of the scoring system in predicting chemotherapy failures. *Obstet. Gynecol.* (1990) 76(2):272–7.

20. Dubuc-Lissoir J, Zweizig S, Schlaerth JB, Morrow CP. Metastatic gestational trophoblastic disease: a comparison of prognostic classification systems. *Gynecol. Oncol* (1992) 45(1):40–5. doi: 10.1016/0090-8258(92)90488-5

21. Yang P, Li ZY, Li HQ. Potential roles of protease inhibitors in cancer progression. *Asian Pac. J Cancer Prev* (2015) 16(18):8047–52. doi: 10.7314/apjcp.2015.16.18.8047

22. Bedin C, Crotti S, Ragazzi E, Pucciarelli S, Agatea L, Tasciotti E, et al. Alterations of the plasma peptidome profiling in colorectal cancer progression. *J Cell Physiol* (2016) 231(4):915–25. doi: 10.1002/jcp.25196

23. Guan X, Zhang B, Fu M, Li M, Yuan X, Zhu Y, et al. Clinical and inflammatory features based machine learning model for fatal risk prediction of hospitalized COVID-19 patients: results from a retrospective cohort study. *Ann Med* (2021) 53(1):257–66. doi: 10.1080/07853890.2020.1868564

24. Gromski PS, Xu Y, Correa E, Ellis DI, Turner ML, Goodacre R. A comparative investigation of modern feature selection and classification approaches for the analysis of mass spectrometry data. *Anal Chim Acta* (2014) 829:1–8. doi: 10.1016/j.aca.2014.03.039

25. Chen Q, Meng Z, Su R. WERFE: A gene selection algorithm based on recursive feature elimination and ensemble strategy. *Front Bioeng. Biotechnol* (2020) 8:496. doi: 10.3389/fbioe.2020.00496

26. Fan NJ, Gao CF, Zhao G, Wang XL, Liu QY. Serum peptidome patterns of breast cancer based on magnetic bead separation and mass spectrometry analysis. *Diagn Pathol* (2012) 7:45. doi: 10.1186/1746-1596-7-45

27. Wang L, Tang C, Xu B, Yang L, Qu L, Li L, et al. Mass spectrometry-based serum peptidome profiling accurately and reliably predicts outcomes of pemetrexed plus platinum chemotherapy in patients with advanced lung adenocarcinoma. *PloS One* (2017) 12(6):e0179000. doi: 10.1371/journal.pone.0179000

28. Zheng D, Ding Y, Ma Q, Zhao L, Guo X, Shen Y, et al. Identification of serum MicroRNAs as novel biomarkers in esophageal squamous cell carcinoma using feature selection algorithms. *Front Oncol* (2018) 8:674. doi: 10.3389/fonc.2018.00674

29. Kriegeskorte N, Golan T. Neural network models and deep learning. *Curr Biol* (2019) 29(7):R231–r236. doi: 10.1016/j.cub.2019.02.034

30. Matek C, Krappe S, Münzenmayer C, Haferlach T, Marr C. Highly accurate differentiation of bone marrow cell morphologies using deep neural networks on a large image data set. *Blood* (2021) 138(20):1917–27. doi: 10.1182/blood.2020010568

31. She Y, Jin Z, Wu J, Deng J, Zhang L, Su H, et al. Development and validation of a deep learning model for non-small cell lung cancer survival. *JAMA Netw Open* (2020) 3(6):e205842. doi: 10.1001/jamanetworkopen.2020.5842

32. Azodi CB, Tang J, Shiu SH. Opening the black box: Interpretable machine learning for geneticists. *Trends Genet* (2020) 36(6):442–55. doi: 10.1016/j.tig.2020.03.005

33. Lim A, Sengupta S, McComb ME, Théberge R, Wilson WG, Costello CE, et al. *In vitro* and *in vivo* interactions of homocysteine with human plasma transthyretin. *J Biol Chem* (2003) 278(50):49707–13. doi: 10.1074/jbc.M306748200

34. Lee CC, Ding X, Zhao T, Wu L, Perkins S, Du H, et al. Transthyretin stimulates tumor growth through regulation of tumor, immune, and endothelial cells. *J Immunol* (2019) 202(3):991–1002. doi: 10.4049/jimmunol.1800736

35. Swiatly A, Horala A, Hajduk J, Matysiak J, Nowak-Markwitz E, Kokot ZJ. MALDI-TOF-MS analysis in discovery and identification of serum proteomic patterns of ovarian cancer. *BMC Cancer* (2017) 17(1):472. doi: 10.1186/s12885-017-3467-2

36. Lacka K, Maciejewski A. Rare thyroid non-neoplastic diseases. *Thyroid Res* (2015) 8:5. doi: 10.1186/s13044-015-0017-3

37. Kamath S, Lip GY. Fibrinogen: biochemistry, epidemiology and determinants. *Qjm* (2003) 96(10):711–29. doi: 10.1093/qjmed/hcg129

38. Song Y, Xu X, Wang N, Zhang T, Hu C. MALDI-TOF-MS analysis in low molecular weight serum peptidome biomarkers for NSCLC. *J Clin Lab Anal* (2022) 36(4):e24254. doi: 10.1002/jcla.24254

39. Huang Y, Chen F, Zhang L, Lv Q, Yan J, Cui W. MALDI-TOF-MS analysis in the discovery and identification of the serum peptide pattern of pancreatic ductal adenocarcinoma. *Lab Med* (2021) 52(6):558–66. doi: 10.1093/labmed/lmab024

40. Duan S, Gong B, Wang P, Huang H, Luo L, Liu F. Novel prognostic biomarkers of gastric cancer based on gene expression microarray: COL12A1, GSTA3, FGA and FGG. *Mol Med Rep* (2018) 18(4):3727–36. doi: 10.3892/mmr.2018.9368

41. Goldstein DP, Brakman P, Marshall JR. The plasma fibrinolytic system in patients with trophoblastic disease and undelivered hydatidiform mole. *Am J Obstet. Gynecol.* (1966) 94(1):21–8. doi: 10.1016/0002-9378(66)90375-9

42. Kiefer CM, Hou C, Little JA, Dean A. Epigenetics of beta-globin gene regulation. *Mutat Res* (2008) 647(1-2):68–76. doi: 10.1016/j.mrfmmm.2008.07.014

43. Wang M, Shen L, Xu X, Duan W, Miao J, Kong W, et al. Real-world study of cisplatin, etoposide, and bleomycin chemotherapy regimen in gestational trophoblastic neoplasia. *BioMed Res Int* (2021) 2021:6661698. doi: 10.1155/2021/6661698

frontiers | Frontiers in Oncology

TYPE Original Research
PUBLISHED 24 October 2022
DOI 10.3389/fonc.2022.955150

OPEN ACCESS

EDITED BY
Sara Ricardo,
Universidade do Porto, Portugal

REVIEWED BY
Marco Antonio Leyva Vazquez,
Autonomous University of Guerrero, Mexico
Rita Trozzi,
Agostino Gemelli University Polyclinic (IRCCS), Italy
Amanda Strickland,
Northwestern Medicine, United States

*CORRESPONDENCE
Zhen Li
zhen_li@tongji.edu.cn

†These authors have contributed equally to this work and share first authorship

SPECIALTY SECTION
This article was submitted to Gynecological Oncology, a section of the journal Frontiers in Oncology

RECEIVED 28 May 2022
ACCEPTED 27 September 2022
PUBLISHED 24 October 2022

CITATION
Shi W, Zhu H, Yuan L, Chen X, Huang X, Wang K and Li Z (2022) Vaginal microbiota and HPV clearance: A longitudinal study.
Front. Oncol. 12:955150.
doi: 10.3389/fonc.2022.955150

Vaginal microbiota and HPV clearance: A longitudinal study

Wenpei Shi[1†], Haiyan Zhu[2†], Lei Yuan[1], Xiaoyue Chen[2], Xiaojie Huang[3], Kai Wang[3] and Zhen Li[1*]

[1]Clinical Research Unit, Shanghai Key Laboratory of Maternal Fetal Medicine, Shanghai Institute of Maternal-Fetal Medicine and Gynecologic Oncology, Shanghai First Maternity and Infant Hospital, School of Medicine, Tongji University, Shanghai, China, [2]Department of Gynecology, Shanghai Key Laboratory of Maternal Fetal Medicine, Shanghai Institute of Maternal-Fetal Medicine and Gynecologic Oncology, Shanghai First Maternity and Infant Hospital, School of Medicine, Tongji University, Shanghai, China, [3]Clinical and Translational Research Center, Shanghai Key Laboratory of Maternal Fetal Medicine, Shanghai Institute of Maternal-Fetal Medicine and Gynecologic Oncology, Shanghai First Maternity and Infant Hospital, School of Medicine, Tongji University, Shanghai, China

Although vaginal microbiota (VM) may interact with human papillomavirus (HPV) infection and clearance, longitudinal data remain very limited. We aimed to investigate the association between VM at baseline and the clearance of high-risk HPV (HR-HPV) infection within 12 months. Cervical swabs were collected at diagnosis from 85 patients with HR-HPV infection and histologically confirmed cervical lesions, including cervicitis, low-grade squamous intraepithelial lesion and high-grade squamous intraepithelial lesion. Microbiome analysis was performed using 16S rRNA gene sequencing. Among the 73 women included in the analyses, HPV clearance was observed in 58.9% of the patients within 12 months. No significant difference was observed between the HPV-cleared and HPV-uncleared groups regarding age, disease stage, HPV subtype, VM community state types, and VM diversity (α and β). Women with the depletion of enterococcus ASV_62 and enrichment in *Lactobacillus iners* at baseline were less likely to have HPV clearance at month 12. Further analysis revealed a significant negative association between high abundance of *L. iners* and HPV clearance in patients who received non-operative treatment (OR = 3.94, p = 0.041), but not in those who received operative treatment (OR = 1.86, p = 0.660). Our findings provide new evidence for the potential role of VM in the persistent HR-HPV infections.

KEYWORDS

vaginal microbiota, high-risk human papillomavirus, HPV clearance, longitudinal study, cervical lesions

Introduction

Persistent infection with high-risk human papillomavirus (HR-HPV) is the major cause of cervical cancer and its precursor lesion (1–3). Although HPV infection is common worldwide, approximately 80% of the HPV infections are transient and cleared spontaneously within 2 years, and the remaining 20% of cases ensue persistent infection

and disease progression. However, the exact factors that determine infection and/or disease that will persist, progress, or spontaneously resolve are incompletely understood.

More recently, the upsurge in research on microbiome has shifted attention from known epidemiological risk factors of HPV infection, including parity, tobacco smoking, and oral contraceptive use to mucosal microbiota (4). Accumulating evidence has revealed that mucosal microbiota plays a critical role in maintaining physiological homeostasis (5). Several recent studies have highlighted the significance of the microbiome in the natural history of various viral infections and cancers (6, 7). The cervicovaginal microbiome is of particular interest in gynecology because it has been well characterized and several specific features have been associated with gynecologic diseases (8–10).

The vaginal microbiota (VM) is commonly categorized into community state types (CSTs), which were first proposed by Ravel et al. (9), and are generally defined as a dominant of a specific *Lactobacillus* spp. or a polymicrobial state with high diversity. Several cross-sectional studies (11–17) have observed distinct characteristics of VM between healthy controls and patients with HPV infection or squamous intraepithelial lesion (SIL). A link between high abundance of some types of *Lactobacillus* (*L. crispatus*, *L. jensenii*, and *L. gasseri*) and low HPV prevalence is generally supported (18). Contrary to the beneficial role of these *Lactobacillus* spp., current evidence with regard to *L. iners*, which was common in patients with HR-HPV infections and high-grade cervical lesions, remains inconsistent. In addition, high-diversity CSTs and specific anaerobes, such as *Sneathia* and *Gardnerella vaginalis*, were also found to be implicated with higher frequency and severity of disease. Nevertheless, the results of previous studies are inconsistent and sometimes contradictory, possibly because of the differences in the genetic background or environmental factors (18, 19). Additionally, it remains unclear whether features of VM influence the clearance or instead promote disease development.

Herein, we conducted a longitudinal study to assess the impact of VM composition at baseline on the clearance of HR-HPV infections at 12 months based on a treatment cohort of 85 Chinese women with a single HR-HPV infection.

Methods

Ethics statement

The study was conducted according to the guidelines of the Declaration of Helsinki and approved by the Scientific and Ethical Committee of the Shanghai First Maternity and Infant Hospital affiliated with Tongji University (protocol code: K08-018).

Study design

Patients with histologically diagnosed cervical disease were enrolled between April 2015 and October 2016 at Shanghai First Maternity and Infant Hospital and then routinely followed up every 6 months. Cervical swab specimens at diagnosis were collected from every woman for HPV testing and microbiome analysis using 16S rRNA gene sequencing after inclusion in the cohort. Detailed description of the participants can be obtained from the original publication (20). All the data were collected after obtaining written informed consent from participants.

Inclusion criteria included the following: biopsy-proven clinical lesions of the cervix, including cervicitis, low-grade SIL (LSIL), and high-grade SIL (HSIL); only infected with one HR-HPV subtype (HPV 16/52/58); follow-up data available; and patients with same diagnostic conditions were treated according to a standardized protocol. Briefly, patients with HSIL received the loop electrosurgical excisional procedure (LEEP), and other patients with a lower pathological grade lesion (cervicitis and LSIL) received conservative management rather than immediate excisional treatment. Patients with a known malignancy disease or current pregnancy were excluded from the study.

Follow-up and clinical outcome definition

Based on pathological diagnosis and the treatment undergone, patients were divided into the HPV+/LSIL group and the HSIL group. Cervical swabs and cervical biopsies were collected on each follow-up visit for HPV DNA detection and pathological examination. Clinicopathological and follow-up data, including progress notes, clinical laboratory tests, and drugs and pathological reports were captured from the hospital electronic medical record system. All laboratory examinations and inpatient and outpatient electronic medical records were reviewed.

The HPV-cleared group was defined as the presence of HPV at baseline turned negative at follow-up tests and no further positive HPV test and cytological or histological abnormality reports. The HPV-uncleared group was defined as persistent same-type HPV infection or pathological progress within a 1-year follow-up.

HPV gene type

HPV testing at each follow-up visit was performed using the HPV GenoArray test kit as previously reported (20). The absence of HPV DNA contamination was confirmed by HPV L1 and the internal control of the human a-globin in each reaction.

16S rRNA V4–V5 amplicon sequencing

Microbial genomic DNA was extracted from cervical swab samples, collected from the ectocervix and endocervix of the

uterus of every woman by baseline cervical scrapings, using the FastDNA Spin Extraction Kit (MP Biomedicals, Santa Ana, CA, USA). Then, a nested PCR protocol was employed to amplify the 16S hypervariable region V4–V5 using the 16S universal primers: 515F 5'-GTGCCAGCMGCCGCGGTAA-3' and 907R: 5'-CCGTCAATTCMTTTRAGTTT-3'. The dual-indexed amplicons were pooled according to the manufacturer's instructions (Illumina, Inc., San Diego, CA, USA) and sequenced on the Illumina MiSeq platform to produce 2 × 300 bp paired-end reads as described previously.

Bioinformatic analysis

The raw demultiplexed sequences were firstly trimmed off primers from the paired-end reads, and a preliminary quality trimming was then conducted with Cutadapt v2.10 with the setting of discard untrimmed sequences, a minimum *q*-value of 20, and a maximum *N* base of zero. Thereafter, the processed reads were subjected to quality trimming, denoising, merging, and chimera removal to generate amplicon sequence variants (ASVs) using DADA2 (21). In this step, the paired-end reads were trimmed to keep high-quality reads with a *q*-value of >20 (maxN = 0, truncQ = 2), and those with more than two or five expected errors [maxEE = c(2,5)] or derived from PhiX (rm.phix = TRUE) were discarded. After DADA2 denoising, the paired-end reads were merged with at least a 12-bp overlap. Chimera checking was conducted on the merged reads, and the recovered ASVs were summarized and used to generate the sequence table for the sequencing run. All ASVs were numbered in order.

Sequencing annotation

RESCRIPt (22) was used to compile trained naïve Bayes classifiers using the SILVA database (v132) (23) and the STIRRUPS vaginal microbiome-specific database (24). As *Lactobacillus* spp. are essential for further analysis in VM studies, the classification of the ASVs annotated as *Lactobacillus* was improved by manually BLAST searching them in the National Center for Biotechnology Information database; a maximum of one mismatch was allowed from the alignment. If ASVs could not be annotated at the species level, they were then reannotated as "genus-level ASVs order."

Diversity analysis

The ASVs table was filtered to exclude sequences annotated as chloroplasts, plastids, or non-bacterial ASVs. Low-abundance ASVs present in only one sample and with a relative abundance lower than 0.01% across all ASVs were also filtered. To reduce the sampling heterogeneity, the ASV table was rarefied to the same reads per sample 100 times using a q2-repeat-rarefy plugin (25) on the QIIME2 platform before conducting diversity analysis. The within-sample (α) diversity was calculated using Chao1 and Shannon indexes based on species richness and species frequencies. The Bray–Curtis distance between samples (β diversity) was used to evaluate differences in species complexity. Both α-diversity indexes and β-diversity distance were calculated using QIIME2 (26).

Clustering into community state types

Hierarchical clustering into CSTs based on VM composition and abundance was conducted according to the methods described by DiGiulio et al. (27). Specifically, the Bray–Curtis distance matrix between all samples was denoised by extracting the most significant principal coordinates analysis (PCoA) eigenvectors. Then, the partitioning around medoids algorithm (pam) was applied to PCoA distances. The number of clusters was determined from the gap statistic. According to this algorithm, VM composition was classified into five groups at the ASV level and two groups at the genus level.

Statistical analysis

Normality tests for continuous data were assessed by Shapiro–Wilk tests. Chi-square tests, Fisher exact tests, *t*-tests, and Wilcoxon rank-sum tests were used for two-group comparisons as appropriate. For further analysis, numerical variables such as α-diversity indexes were categorized by 75th quartile scores.

PCoA analysis was performed to interrogate the robustness of group-wise clustering. Comparisons of group-wise β diversity (Bray–Curtis distance matrix) were assessed by permutational multivariable ANOVA using the Adonis function in the vegan package (28). Logistic regression models were performed to adjust for known confounders (age, HPV subtype) and calculated adjusted odds ratios (aOR) to evaluate the relationship between CSTs and clinical outcomes. Analyses of differential taxa (species level) abundance of samples according to disease outcome were performed using a negative binomial generalized linear model in the R package DESeq2 (29) with a multifactor design. An adjusted p-value of <0.05 and an estimated fold change of >2 were considered significantly differentially abundant between groups.

P-value was adjusted for multiple tests using the Benjamini and Hochberg method. A p-value of <0.05 was considered statistically significant. Statistical analyses were performed with R statistical programming (R version 3.6.1).

Results

Characteristics of participants in the study cohort and follow-up

Eighty-five patients with a single HR-HPV infection and histologically confirmed cervical disease were enrolled in this study. Patients with incomplete clinical information (n = 2), low-quality sequence data (n = 1), or time to first follow-up visit over 1 year (n = 9) were excluded. Overall, 73 individuals were included in the analysis (Figure 1). Patient characteristics are detailed in Table 1. The mean age was 40.1 ± 11.5 years old (median = 36, range: 24–68). The majority of subjects (69.9%) had low-grade cervical lesions. All participants were infected with a single HPV subtype, of whom 37.0% were infected with HPV52, followed by 35.6% with HPV16 and 27.4% with HPV58. Sixteen (21.9%) patients had taken recombinant human interferon α-2b, and five (6.8%) had taken *Lactobacillus* capsule. No immunomodulatory medication usage was reported. At 12 months, 61.6% (45/73) of patients had cleared HPV infection, defined as the "HPV-cleared" group, and the remaining 38.4% (28/73) were classified as the "HPV-uncleared" group. The clearance rate was 54.9% among HPV+/LSIL patients and 77.3% among HSIL patients. This difference of clearance rate between the two groups was not statistically significant (p = 0.123). No differences in HPV clearance by HPV subtype were noted (HPV16, 65.4%; HPV52, 59.3%; HPV58, 60.0%; p = 0.886). Pairwise comparisons are shown in Supplementary Table S1.

Characteristics of baseline vaginal microbiota composition

A total of 2,785,739 high-quality sequences were obtained from 73 samples, with an average of 38,160 reads per sample. Following the removal of rare frequency (singletons and <0.1% total reads), nonbacterial, unclassified, mitochondrial, and chloroplast ASVs, 530 ASVs were finally generated, and then all samples were rarefied to 8,556 reads 100 times to calculate diversity indexes.

To explore CSTs and reduce dimensionality, a hierarchical clustering analysis was performed based on ASV-level data, and five major groups were identified (Figure 2 and Figures S1A–E): CST I (10/73, 13.7%) was classified as *L. crispatus* dominated, CST III was dominated by *L. iners* (15/73, 20.5%), and CST IV (12/73, 16.4%) was typified by a highly diverse microbiome rather than containing a major group.

A similar genus-level analysis demonstrated that all the samples were mainly separated into two groups, the

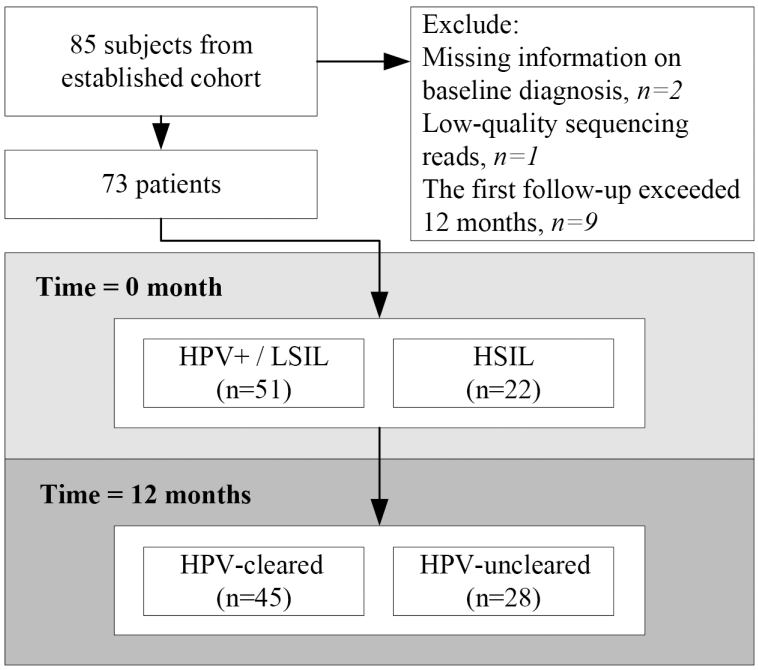

FIGURE 1
Flow chart of the study design. Seventy-three patients with histologically confirmed cervical lesion at baseline entered this study. Follow-up cytology and human papillomavirus (HPV) tests were performed every 6 months to determine whether subjects had cleared HPV infections or not at 12 months.

10.3389/fonc.2022.955150

TABLE 1 Clinical characteristics and outcomes of participants in the study.

Characteristics	HPV-cleared (N = 45)	HPV-uncleared (N = 28)	p-value	Total (N = 73)
Age at diagnosis, years			0.180	
Median [range]	35.0 [24.0–68.0]	36.5 [27.0–65.0]		40.1 (11.5)
Diagnosis at baseline			0.123	
HPV+/LSIL	28 (62.2%)	23 (82.1%)		51 (69.9%)
HSIL	17 (37.8%)	05 (17.9%)		22 (30.1%)
HPV status			0.886	
HPV16 positive	17 (37.8%)	09 (32.1%)		26 (35.6%)
HPV52 positive	16 (35.6%)	11 (39.3%)		27 (37.0%)
HPV58 positive	12 (26.7%)	08 (28.6%)		20 (27.4%)
Drug				
Recombinant human interferon α-2b			1.000	
No	35 (77.8%)	22 (78.6%)		57 (78.1%)
Yes	10 (22.2%)	06 (21.4%)		16 (21.9%)
***Lactobacillus* capsule**			1.000	
No	42 (93.3%)	26 (92.9%)		68 (93.2%)
Yes	3 (6.7%)	02 (7.1%)		5 (6.8%)
CSTs			0.216	
I	6 (13.3%)	04 (14.3%)		10 (13.7%)
II	15 (33.3%)	07 (25.0%)		22 (30.1%)
III	6 (13.3%)	09 (32.1%)		15 (20.5%)
IV	10 (22.2%)	02 (7.1%)		12 (16.4%)
V	8 (17.8%)	06 (21.4%)		14 (19.2%)
CST_genus			1.00	
1	28 (62.2%)	18 (64.3%)		46 (63.0%)
2	17 (37.8%)	10 (35.7%)		27 (37.0%)
Chao1			0.074	
Median [min, max]	36.5 [8.00, 134]	27.3 [6.00, 99.1]		29.0 [6.00, 134]
Pielou_evenness			0.863	
Mean (SD)	0.387 (0.166)	0.39 (0.164)		0.390 (0.164)
Observed_features			0.073	
Median [min, max]	32.0 [8.00, 131]	26.0 [6.00, 98.0]		
Shannon			0.664	
Median [min, max]	1.56 [0.143, 4.54]	1.77 [0.327, 3.34]		
Simpson			0.987	
Median [Min, max]	0.55 [0.028, 0.928]	0.61 [0.0850, 0.822]		

SD, standard deviation; HPV, human papillomavirus; CSTs, community state types; LSIL, low-grade squamous intraepithelial lesion; HSIL, high-grade squamous intraepithelial lesion. HSIL patients received surgical resection, and LSIL/HPV+ patients underwent non-surgical treatment.
Comparisons between groups were made using chi-square test, t-test, Wilcoxon rank-sum test, and Fisher exact test as appropriate. Age at diagnosis, Chao1, observed features, Shannon, and Simpson were non-normal distribution tested by Shapiro–Wilk test.

Lactobacillus-dominated group (CST1, 63.0%) and the non–*Lactobacillus*-dominated group (CST2, 37.0%) (Figures S1F, G). Alpha diversity analysis of the microbiota profile based on Shannon and Chao1 diversity showed that patients with HPV-16 infection or non–*Lactobacillus*-dominated CST had higher VM diversity (Tables S2 and S3). PCoA plot of Bray–Curtis distances showed a clear separation of microbial composition between different CSTs (Figure S2). Although no significant correlation was observed between VM composition (measured by Bray–Curtis) and clinical variables, including HPV subtype, age, and disease stage (Tables S4 and S5).

Overall vaginal microbiota diversity and HPV clearance

At 12 months, clearance rates appeared to be higher in HSIL patients than in patients with HPV+/LSIL, bordering on

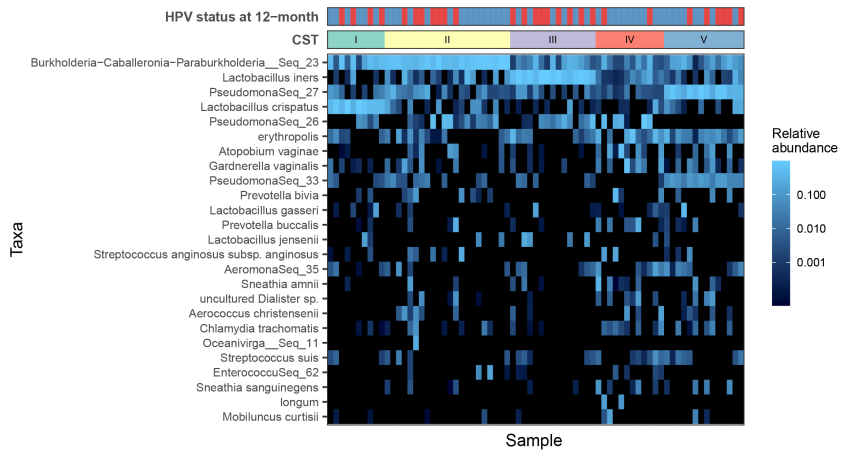

FIGURE 2
Heat map of the fractional abundance of the 25 most abundant amplicon sequence variants (ASVs) in the vaginal communities of all subjects. Clustering on the abundance profiles of individual samples using the partitioning around medoids algorithm identifies five community state types. Human papillomavirus (HPV) infection outcomes are indicated by the bar at the top: HPV negative (blue) and HPV positive (red).

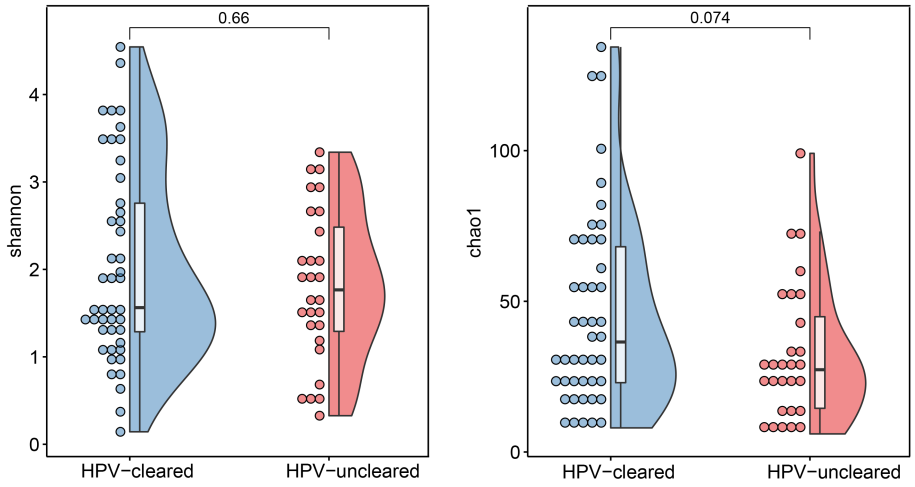

FIGURE 3
Microbial α-diversity analysis based on Shannon and Chao1 index in the HPV-cleared and HPV-uncleared groups. Statistical significance between the groups was tested by Wilcoxon rank sum tests. HPV, human papillomavirus.

significance (77.3 vs. 54.9%, p = 0.123). Both α-diversity and β-diversity analyses showed no significant difference between the HPV-cleared and HPV-uncleared groups (Figure 3). Similarly, Bray–Curtis distance showed no clear separation among samples from different HPV treatment outcome groups (Figure 4). In addition, these data were supported by the fact that no significant difference was found between VM features and HPV outcomes in univariate and multivariate logistic regression analyses (Table 2). Further stratified analysis by HPV subtype and disease stage did not reveal any significant differences between the two groups (Tables S6 and S7).

Certain bacterial species showed correlation to human papillomavirus treatment outcome

Analysis of bacterial taxonomic categories of the microbiome associated with HPV-uncleared versus HPV-

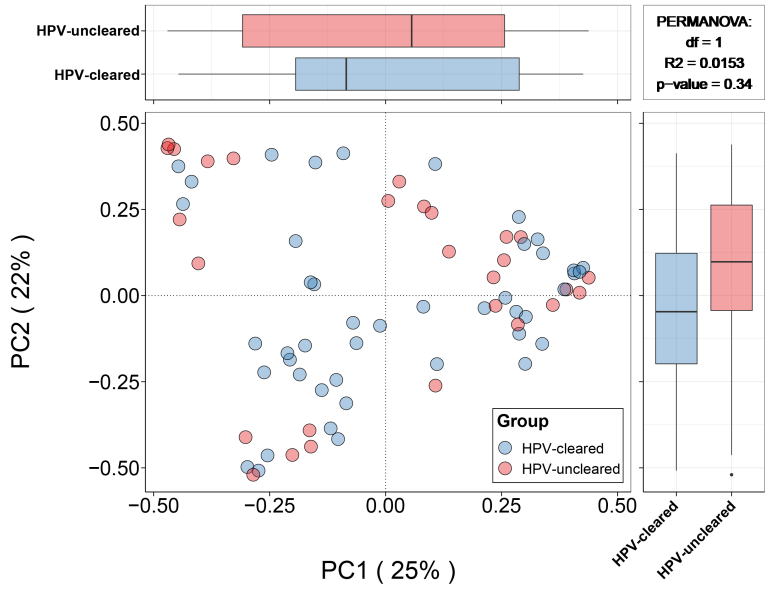

FIGURE 4
Principal coordinates analysis (for principal coordinates PCo1 and PCo2) plots with Bray–Curtis distance showing the difference in microbial community composition between the HPV-cleared and HPV-uncleared groups. Statistical significance between the groups was tested by permutational multivariable ANOVA. HPV, human papillomavirus.

cleared was performed using DESeq2, which built a generalized linear model to validate the abundance of each taxon with adjustments for disease stage, age group, and HPV subtype. DESeq2 results showed that abundances of the two species (one specie enriched and one specie depleted in HPV-cleared group) presented a significant difference between two groups. The abundance of *Enterococcus:ASV_62* (|log-fold change| = 8.84, $q < 0.001$) was significantly more prevalent among HPV-cleared patients. Interestingly, patients with higher abundance of *L. iners* at baseline were more likely to fail to clear HPV infection at 12 months (|log-fold change| = 4.16, $q < 0.001$).

To assess the robustness of the negative correlation between *L. iners* abundance and HPV clearance, a multivariable logistic regression model and stratified analyses were performed to assess the effect of *L. iners* abundance on HPV outcome status. The multivariable analysis revealed a significant risk effect of higher *L. iners* abundance (aOR = 3.34, 95% CI: 1.03–10.77) on HPV clearance (Figure 5). Further stratification logistic analysis showed that this association was only observed in patients with HPV+/LSIL (aOR = 3.94, 95% CI: 1.06–14.70), but not in those with HSIL (aOR = 1.86, 95% CI: 0.12–29.42) (Figure 5).

Discussion

To our knowledge, this longitudinal study reported for the first time that the relative abundance of specific cervicovaginal bacteria, *L. iners*, rather than the overall diversity of VM, negatively associated with the clearance of HR-HPV at month 12 after diagnosis among patients who received non-operative treatment. Our findings provide new evidence that VM may influence the clearance of HR-HPV infections and suggested a new potential therapy target that merits further investigation.

After adjustment for potential confounders, we observed the association of the enrichment of *L. iners* and depletion of *Enterococcus ASV_62* with the clearance of HR-HPV. Possibly because of the relatively limited sample size, a non-significant similar trend was seen when comparing to the CST I (*L. crispatus* dominated) state, that patients with CST III (*L. iners* dominated) state at baseline were associated with a lower rate of HPV clearance. Previously, the possible link between *L. iners* and persistent HPV infection has been reported in several cross-sectional studies (11, 17, 30, 31). A recent meta-analysis showed that VM dominated by *L. iners*, compared with VM dominated by *L. crispatus* was associated with a two- to threefold higher risk of HR-HPV infection and dysplasia (32). Although Usyk et al. (33) found that *L. iners* was the most positively associated taxon with clearance at 12 months among young adults form Costa Rica (33). The discrepancies in the findings may be related to different inclusion criteria and race differences across studies. By including patients with a single-type HR-HPV infection, this study reduced possible confounding factors related to interactions within different types of HR-HPV.

Compared to other *Lactobacillus* spp. frequently identified, such as *L. crispatus*, which is usually considered as a biomarker of healthy vaginal microenvironment, current studies support an

TABLE 2 Association between VM and HPV clearance in a 12-month follow-up.

Characteristics	Univariable model		Multivariable model 1		Multivariable model 2		Multivariable model 3		Multivariable model 4	
	OR (95% CI)	p value	aOR (95% CI)	p value	aOR (95% CI)	p value	aOR (95% CI)	p value	aOR (95% CI)	p value
Age										
<50 year	Ref.		Ref.		Ref.		Ref.		Ref.	
≥50 year	1.69 (0.96–2.98)	0.070	3.38 (0.89–12.8)	0.073	2.4 (0.71–8.08)	0.157	3.78 (0.97–14.69)	0.055	2.46 (0.73–8.32)	0.147
HPV type										
16	Ref.		Ref.		Ref.		Ref.		Ref.	
52	1.3 (0.43–3.96)	0.646	1.2 (0.33–4.38)	0.782	0.93 (0.28–3.09)	0.901	1.31 (0.36–4.82)	0.683	0.97 (0.29–3.29)	0.963
58	1.26 (0.38–4.20)	0.708	0.99 (0.25–3.94)	0.987	0.78 (0.21–2.96)	0.720	1.09 (0.27–4.43)	0.908	0.81 (0.21–3.07)	0.755
Diagnosis										
HPV+/LSIL	Ref.				Ref.		Ref.		Ref.	
HSIL	0.5 (0.22–1.15)	0.105	0.38 (0.1–1.4)	0.146	0.36 (0.11–1.24)	0.106	0.34 (0.09–1.28)	0.110	0.35 (0.1–1.2)	0.096
Shannon										
Low	Ref.		Ref.		Ref.		Ref.		Ref.	
High	0.75 (0.25–2.30)	0.614	1.14 (0.27–4.76)	0.858	0.84 (0.22–3.16)	0.794	0.87 (0.19–3.95)	0.858	0.7 (0.2–2.49)	0.577
CSTs										
I	Ref.		Ref.				Ref.			
II	0.70 (0.15–3.30)	0.652	0.38 (0.07–2.22)	0.284			0.38 (0.06–2.27)	0.288		
III	2.25 (0.44–11.52)	0.330	1.53 (0.27–8.55)	0.630			1.91 (0.31–11.62)	0.484		
IV	0.30 (0.04–2.16)	0.232	0.13 (0.01–1.25)	0.077			0.13 (0.01–1.27)	0.079		
V	1.12 (0.22–5.86)	0.889	0.6 (0.09–4.17)	0.609			0.84 (0.11–6.39)	0.863		
CST_genus										
I	Ref.				Ref.				Ref.	
II	0.92 (0.34–2.44)	0.859			0.75 (0.22–2.59)	0.649			0.73 (0.24–2.28)	0.594
Recombinant human interferon α-2b										
No	Ref.						Ref.		Ref.	
Yes	0.95 (0.3–3)	0.936					2.47 (0.57–10.78)	0.229	1.38 (0.39–4.91)	0.615
***Lactobacillus* capsule**										
No	Ref.									
Yes	1.08 (0.17–6.88)	0.938								

VM, vaginal microbiota; HPV, human papillomavirus; LSIL, low-grade squamous intraepithelial lesion; HSIL, high-grade squamous intraepithelial lesion; CSTs, community state types; aOR, adjusted odds ratios. HSIL patients received surgical resection, and LSIL/HPV+ patients underwent non-surgical treatment.

ambiguous role for *L. iners* in the vaginal niche (34, 35). *L. iners* has a relatively small genome size compared with other *Lactobacillus* spp. and has been reported as a dominant species in the transitional type of the VM (CST III) or during menses or episodes of bacterial vaginosis, suggesting that this species is very flexible and has a remarkable ability to adapt to the fluctuating vaginal environment (34). The genome of *L. iners* also encodes a number of genes, suggesting that it could may be an opportunistic pathogen, of which inerolysin (a potential cholesterol-dependent cytolysin) is well documented (36). Besides, a study examining cytokine profiles in pregnancy women showed a positive association between *L. iners* and proinflammatory cytokines in vaginal fluid (37). However, the available literature is insufficient to classify *L. iners* as a beneficial or detrimental bacterium. Because *L. iners*–dominated CST III is frequently reported as one of the most common CSTs among Asian

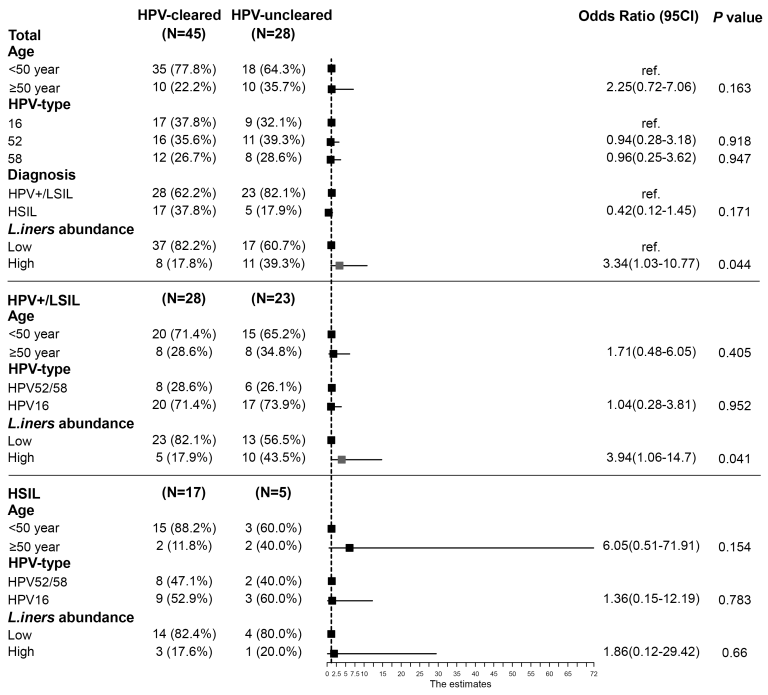

FIGURE 5
Association between *L. iners* abundance and HPV clearance in a 12-month follow-up. Forest plots were shown using data from multivariable logistic regression in total and according to disease status. HSIL patients received surgical resection, and LSIL/HPV+ patients underwent a surgical treatment. The abundance of *L. iners* was categorized by 75th quartile scores. HPV, human papillomavirus; LSIL, low-grade squamous intraepithelial lesion; HSIL, high-grade squamous intraepithelial lesion.

reproductive-age women, a more detailed approach to explore the causal relationship between *L. iners* and HPV infection clearance is warranted in future vaginal microbiome studies.

Further stratified analysis according to disease status or treatment revealed that the negative correlation between the abundance of *L. iners* and HPV clearance was only observed in HPV+/LSIL patients who received non-operative treatment. One possible reason is that, compared with non-surgical management such as anti-inflammatory or antiviral treatment, the impact of resection of the lesion on HPV clearance is immediate (38). Recently, Mitra et al. (39) found that the surgical excision for HSIL and HPV infection did not alter VM composition, which suggested that the virus is not the driver of VB alternations. In this study, women with histologically confirmed HSIL were immediately treated surgically according to clinical guidelines, whereas conservative management with regular follow-up was recommended for HPV+/LSIL patients. Previous studies (40, 41) reported that the HR-HPV clearance can reach 79.2%–97.8% (40) at 12 months after LEEP. In this study, 77.3% of HSIL patients and 54.9% of HPV+/LSIL patients were cleared of HPV infection within 12 months, which is comparable to other similar studies (41–43). It is likely that the effect of surgical treatment can mask the correlation between *L. iners* and HPV outcome in HSIL patients. These findings provide clues for future research regarding the potential targeting populations regarding the association between VM and HPV persistence.

The study has the following limitations. First, the sample size was relatively limited; thus, the negative findings need to be interpreted with caution because of potential insufficient statistical power. Considering the subtype of HPV could be a confounder factor affecting the association between VM and HPV clearance, this study enrolled patients with one of three most prevalent HR-HPV types (HPV16, HPV52, or HPV58). These were the top three subtypes with the highest HPV infection rates according to our previous study (20) and epidemiological surveys in mainland China (44, 45). Further studies with a larger sample size and more types of HPV infection would allow more detailed analyses by HPV subtypes. Second, as cigarette smoking is rare among Chinese women, we were not able to investigate the effect of smoking as a potential confounder. Reported by the Shanghai municipal center for disease control and prevention, the smoking prevalence among female was 1.03% at 2016 (46). The smoking status is not likely to change the reported associations in this study. Third, a single sampling at baseline cannot establish a definitive causal link between *L. iners* and clearance of HPV infection. Further prospective human studies

with repeated sampling and follow-up time longer than 24 months are needed to better clarify the association between VM and persistent HPV infection.

In conclusion, this study among Chinese women suggested that the relative abundance of *L. iners* at diagnosis, rather than overall bacterial diversity, was negatively correlated with HPV clearance over 12 months, particularly in patients who received non-operative treatment. Our findings provide new evidence for the potential role of VM in the persistent HR-HPV infections. Further studies are needed to clarify the mechanisms by which *L. iners* promotes persistent HPV infection or lesion progression.

Data availability statement

The raw sequence data reported in this paper have been deposited in the Genome Sequence Archive (Genomics, Proteomics & Bioinformatics 2021) in National Genomics Data Center (Nucleic Acids Res 2021), China National Center for Bioinformation / Beijing Institute of Genomics, Chinese Academy of Sciences (GSA: HRA003171) that are publicly accessible at https://ngdc.cncb.ac.cn/gsa.

Ethics statement

This study was reviewed and approved by Scientific and Ethical Committee of the Shanghai First Maternity and Infant Hospital affiliated with Tongji University. The patients/participants provided their written informed consent toparticipate in this study.

Author contributions

Conceptualization: WS, HZ, ZL and KW. Methodology: WS and XH. Software: WS and LY. Validation: HZ and XC. Formal analysis: WS and HZ. Investigation, XH, LY and WS. Resources, LY, XH and KW. Data curation: XC and HZ. Writing—original draft preparation: WS, HZ and ZL. Writing—review and editing: WS, HZ, LY, XC, XH, KW and ZL. Visualization: W.S. Supervision: HZ and ZL. Project administration: KW and ZL. All authors contributed to the article and approved the submitted version.

Funding

This study was supported by grants from the Shanghai First Maternity and Infant Hospital Science Project (WS, 2020A20) and Clinical Research Plan of SHDC (ZL, SHDC2022CRS050). The granters played no role in study design, development, data collection, or generation of this manuscript. There is no other financial support.

Acknowledgments

We thank all the participating staff for their involvement with this project.

Conflict of interest

The authors declare that the research was conducted in the absence of any commercial or financial relationships that could be construed as a potential conflict of interest.

Publisher's note

Supplementary material

The Supplementary Material for this article can be found online at: https://www.frontiersin.org/articles/10.3389/fonc.2022.955150/full#supplementary-material

References

1. Franco EL, Schlecht NF, Saslow D. The epidemiology of cervical cancer. *Cancer J* (2003) 9(5):348–59. doi: 10.1097/00130404-200309000-00004

2. Castellsagué X. Natural history and epidemiology of hpv infection and cervical cancer. *Gynecol Oncol* (2008) 110(3 Suppl 2):S4–7. doi: 10.1016/j.ygyno.2008.07.045

3. Bosch FX, de Sanjosé S. The epidemiology of human papillomavirus infection and cervical cancer. *Dis Markers* (2007) 23(4):213–27. doi: 10.1155/2007/914823

4. Mitra A, MacIntyre DA, Marchesi JR, Lee YS, Bennett PR, Kyrgiou M. The vaginal microbiota, human papillomavirus infection and cervical intraepithelial neoplasia: What do we know and where are we going next? *Microbiome* (2016) 4 (1):58. doi: 10.1186/s40168-016-0203-0

5. Young VB. The role of the microbiome in human health and disease: An introduction for clinicians. *Bmj* (2017) 356:j831. doi: 10.1136/bmj.j831

6. Sepich-Poore GD, Zitvogel L, Straussman R, Hasty J, Wargo JA, Knight R. The microbiome and human cancer. *Science* (2021) 371(6536): 1–13. doi: 10.1126/science.abc4552

7. Stefan KL, Kim MV, Iwasaki A, Kasper DL. Commensal microbiota modulation of natural resistance to virus infection. *Cell* (2020) 183(5):1312–24.e10. doi: 10.1016/j.cell.2020.10.047

8. Mendling W. Vaginal microbiota. *Adv Exp Med Biol* (2016) 902:83–93. doi: 10.1007/978-3-319-31248-4_6

9. Ravel J, Gajer P, Abdo Z, Schneider GM, Koenig SS, McCulle SL, et al. Vaginal microbiome of reproductive-age women. *Proc Natl Acad Sci U.S.A.* (2011) 108 Suppl 1:4680–7. doi: 10.1073/pnas.1002611107

10. Chen C, Song X, Wei W, Zhong H, Dai J, Lan Z, et al. The microbiota continuum along the female reproductive tract and its relation to uterine-related diseases. *Nat Commun* (2017) 8(1):875. doi: 10.1038/s41467-017-00901-0

11. Piyathilake CJ, Ollberding NJ, Kumar R, Macaluso M, Alvarez RD, Morrow CD. Cervical microbiota associated with higher grade cervical intraepithelial neoplasia in women infected with high-risk human papillomaviruses. *Cancer Prev Res (Phila)* (2016) 9(5):357–66. doi: 10.1158/1940-6207.CAPR-15-0350

12. Chen Y, Qiu X, Wang W, Li D, Wu A, Hong Z, et al. Human papillomavirus infection and cervical intraepithelial neoplasia progression are associated with increased vaginal microbiome diversity in a Chinese cohort. *BMC Infect Dis* (2020) 20(1):629. doi: 10.1186/s12879-020-05324-9

13. Cheng L, Norenhag J, Hu YOO, Brusselaers N, Fransson E, Ahrlund-Richter A, et al. Vaginal microbiota and human papillomavirus infection among young Swedish women. *NPJ Biofilms Microbiom* (2020) 6(1):39. doi: 10.1038/s41522-020-00146-8

14. Chorna N, Romaguera J, Godoy-Vitorino F. Cervicovaginal microbiome and urine metabolome paired analysis reveals niche partitioning of the microbiota in patients with human papilloma virus infections. *Metabolites* (2020) 10(1): 1–14. doi: 10.3390/metabo10010036

15. Godoy-Vitorino F, Romaguera J, Zhao C, Vargas-Robles D, Ortiz-Morales G, Vazquez-Sanchez F, et al. Cervicovaginal fungi and bacteria associated with cervical intraepithelial neoplasia and high-risk human papillomavirus infections in a Hispanic population. *Front Microbiol* (2018) 9:2533. doi: 10.3389/fmicb.2018.02533

16. Oh HY, Kim BS, Seo SS, Kong JS, Lee JK, Park SY, et al. The association of uterine cervical microbiota with an increased risk for cervical intraepithelial neoplasia in Korea. *Clin Microbiol Infect* (2015) 21(7):674.e1–9. doi: 10.1016/j.cmi.2015.02.026

17. Seo SS, Oh HY, Lee JK, Kong JS, Lee DO, Kim MK. Combined effect of diet and cervical microbiome on the risk of cervical intraepithelial neoplasia. *Clin Nutr* (2016) 35(6):1434–41. doi: 10.1016/j.clnu.2016.03.019

18. Mortaki D, Gkegkes ID, Psomiadou V, Blontzos N, Prodromidou A, Lefkopoulos F, et al. Vaginal microbiota and human papillomavirus: A systematic review. *J Turk Ger Gynecol Assoc* (2019) 21(3), 193. doi: 10.4274/jtgga.galenos.2019.2019.0051

19. Kyrgiou M, Mitra A, Moscicki AB. Does the vaginal microbiota play a role in the development of cervical cancer? *Transl Res* (2017) 179:168–82. doi: 10.1016/j.trsl.2016.07.004

20. Huang X, Li C, Li F, Zhao J, Wan X, Wang K. Cervicovaginal microbiota composition correlates with the acquisition of high-risk human papillomavirus types. *Int J Cancer* (2018) 143(3):621–34. doi: 10.1002/ijc.31342

21. Callahan BJ, McMurdie PJ, Rosen MJ, Han AW, Johnson AJ, Holmes SP. Dada2: High-resolution sample inference from illumina amplicon data. *Nat Methods* (2016) 13(7):581–3. doi: 10.1038/nmeth.3869

22. Robeson MS, O'Rourke DR, Kaehler BD, Ziemski M, Dillon MR, Foster JT, et al. Rescript: Reproducible sequence taxonomy reference database management for the masses. *PLoS computational biology* (2020) 17(11): e1009581. doi: 10.1101/2020.10.05.326504

23. Quast C, Pruesse E, Yilmaz P, Gerken J, Schweer T, Yarza P, et al. The Silva ribosomal rna gene database project: Improved data processing and web-based tools. *Nucleic Acids Res* (2013) 41(Database issue):D590–6. doi: 10.1093/nar/gks1219

24. Fettweis JM, Serrano MG, Sheth NU, Mayer CM, Glascock AL, Brooks JP, et al. Species-level classification of the vaginal microbiome. *BMC Genomics* (2012) 13(8):S17. doi: 10.1186/1471-2164-13-S8-S17

25. Xia Y. *Q2-Repeat-Rarefy: Qiime2 plugin for generating the average rarefied table for library size normalization using repeated rarefaction: GitHub repository* (2021). Available at: https://github.com/yxia0125/q2-repeat-rarefy.

26. Bolyen E, Rideout JR, Dillon MR, Bokulich NA, Abnet C, Al-Ghalith GA, et al. Qiime 2: Reproducible, interactive, scalable, and extensible microbiome data science. *PeerJ Preprints* (2018) 37(8): 2167–9843. doi: 10.1038/s41587-019-0209-9

27. DiGiulio DB, Callahan BJ, McMurdie PJ, Costello EK, Lyell DJ, Robaczewska A, et al. Temporal and spatial variation of the human microbiota during pregnancy. *Proc Natl Acad Sci U.S.A.* (2015) 112(35):11060–5. doi: 10.1073/pnas.1502875112

28. Oksanen J, B FG, Friendly M, Kindt R, Legendre P, McGlinn D, et al. *Vegan: Community ecology package. r package version 2* (2020). Available at: https://CRAN.R-project.org/package=vegan.

29. Love MI, Huber W, Anders S. Moderated estimation of fold change and dispersion for rna-seq data with Deseq2. *Genome Biol* (2014) 15(12):550. doi: 10.1186/s13059-014-0550-8

30. Mitra A, MacIntyre DA, Lee YS, Smith A, Marchesi JR, Lehne B, et al. Cervical intraepithelial neoplasia disease progression is associated with increased vaginal microbiome diversity. *Sci Rep* (2015) 5:16865. doi: 10.1038/srep16865

31. Borgdorff H, Gautam R, Armstrong SD, Xia D, Ndayisaba GF, van Teijlingen NH, et al. Cervicovaginal microbiome dysbiosis is associated with proteome changes related to alterations of the cervicovaginal mucosal barrier. *Mucosal Immunol* (2016) 9(3):621–33. doi: 10.1038/mi.2015.86

32. Njoku K, Crosbie EJ. The vaginal microbiota, human papillomavirusand cervical dysplasia a systematic review andnetwork meta-analysis. *BJOG* (2020) 127 (2):181. doi: 10.1111/1471-0528.15867

33. Usyk M, Zolnik CP, Castle PE, Porras C, Herrero R, Gradissimo A, et al. Cervicovaginal microbiome and natural history of hpv in a longitudinal study. *PloS Pathog* (2020) 16(3):e1008376. doi: 10.1371/journal.ppat.1008376

34. Petrova MI, Reid G, Vaneechoutte M, Lebeer S. Lactobacillus iners: Friend or foe? *Trends Microbiol* (2017) 25(3):182–91. doi: 10.1016/j.tim.2016.11.007

35. Zheng N, Guo R, Wang J, Zhou W, Ling Z. Contribution of lactobacillus iners to vaginal health and diseases: A systematic review. *Front Cell Infect Microbiol* (2021) 11:792787. doi: 10.3389/fcimb.2021.792787

36. Macklaim JM, Gloor GB, Anukam KC, Cribby S, Reid G. At The crossroads of vaginal health and disease, the genome sequence of lactobacillus iners ab-1. *Proc Natl Acad Sci U.S.A.* (2011) 108 Suppl 1(Suppl 1):4688–95. doi: 10.1073/pnas.1000086107

37. Fettweis JM, Serrano MG, Brooks JP, Edwards DJ, Girerd PH, Parikh HI, et al. The vaginal microbiome and preterm birth. *Nat Med* (2019) 25(6):1012–21. doi: 10.1038/s41591-019-0450-2

38. Aerssens A, Claeys P, Garcia A, Sturtewagen Y, Velasquez R, Vanden Broeck D, et al. Natural history and clearance of hpv after treatment of precancerous cervical lesions. *Histopathology* (2008) 52(3):381–6. doi: 10.1111/j.1365-2559.2007.02956.x

39. Mitra A, MacIntyre DA, Paraskevaidi M, Moscicki AB, Mahajan V, Smith A, et al. The vaginal microbiota and innate immunity after local excisional treatment for cervical intraepithelial neoplasia. *Genome Med* (2021) 13(1):176. doi: 10.1186/s13073-021-00977-w

40. Kim YT, Lee JM, Hur SY, Cho CH, Kim YT, Kim SC, et al. Clearance of human papillomavirus infection after successful conization in patients with cervical intraepithelial neoplasia. *Int J Cancer* (2010) 126(8):1903–9. doi: 10.1002/ijc.24794

41. Qin Y, Li Q, Ke X, Zhang Y, Shen X, Wang W, et al. Clearance of hr-hpv within one year after focused ultrasound or loop electrosurgical excision procedure in patients with hsil under 30. *Int J Hyperthermia* (2022) 39(1):15–21. doi: 10.1080/02656736.2021.2010817

42. Luckett R, Painter H, Hacker MR, Simon B, Seiphetlheng A, Erlinger A, et al. Persistence and clearance of high-risk human papillomavirus and cervical dysplasia at 1 year in women living with human immunodeficiency virus: A prospective cohort study. *BJOG* (2021) 128(12):1986–96. doi: 10.1111/1471-0528.16758

43. Fonn S, Bloch B, Mabina M, Carpenter S, Cronje H, Maise C, et al. Prevalence of pre-cancerous lesions and cervical cancer in south Africa–a multicentre study. *S Afr Med J* (2002) 92(2):148–56.

44. Zhang J, Cheng K, Wang Z. Prevalence and distribution of human papillomavirus genotypes in cervical intraepithelial neoplasia in China: A meta-analysis. *Arch Gynecol Obstet* (2020) 302(6):1329–37. doi: 10.1007/s00404-020-05787-w

45. Li K, Li Q, Song L, Wang D, Yin R. The distribution and prevalence of human papillomavirus in women in mainland China. *Cancer* (2019) 125(7):1030–7. doi: 10.1002/cncr.32003

46. Xiao-xia L, Hai-hong Y, Ping-ping B, Ji-ying X, Qing-hua Y, Xin-jian L, et al. Smoking and secondhand smoke exposure among registered residents in shanghai. *J Environ Occup Med* (2016) 33(10):925–30. doi: 10.13213/j.cnki.jeom.2016.16526

frontiers | Frontiers in Oncology

TYPE Original Research
PUBLISHED 09 November 2022
DOI 10.3389/fonc.2022.1036710

OPEN ACCESS

EDITED BY
Gabriella Lillsunde Larsson,
Örebro University, Sweden

REVIEWED BY
Federica Perelli,
Santa Maria Annunziata Hospital, Italy
Mauricio Rodriguez-Dorantes,
Instituto Nacional de Medicina Genómica (INMEGEN), Mexico

*CORRESPONDENCE
Zhengyu Li
zhengyuli01@126.com

†These authors have contributed equally to this work

SPECIALTY SECTION
This article was submitted to Gynecological Oncology, a section of the journal Frontiers in Oncology

RECEIVED 05 September 2022
ACCEPTED 13 October 2022
PUBLISHED 09 November 2022

CITATION
Zou K, Yang E, Cui T and Li Z (2022) Circulating miR-326 could serve as a predictive biomarker for response to neoadjuvant chemotherapy in locally advanced cervical cancer. *Front. Oncol.* 12:1036710. doi: 10.3389/fonc.2022.1036710

Circulating miR-326 could serve as a predictive biomarker for response to neoadjuvant chemotherapy in locally advanced cervical cancer

Kangni Zou[1,2†], E. Yang[1†], Tao Cui[1] and Zhengyu Li[1,2*]

[1]Department of Gynecology and Obstetrics, West China Second University Hospital, Sichuan University, Chengdu, China, [2]Key Laboratory of Birth Defects and Related Diseases of Women and Children, Sichuan University, Ministry of Education, Chengdu, China

Background: Clinically, few patients with locally advanced cervical cancer (LACC) are insensitive to neoadjuvant chemotherapy (NACT). Recent studies have reported that circulating microRNAs (miRNAs) may be involved in the response to NACT. The aim of this study was to discover the potential miRNAs that can predict the response to NACT in LACC.

Methods: Pair-matched blood samples of 39 LACC patients before and after receiving NACT were collected. Seven paired samples were used for microRNA microarray analysis. Targeted miRNAs were selected by bioinformatics analysis and were validated by quantitative reverse transcription–polymerase chain reaction (qRT-PCR). All 39 patients were assigned into either the responders group or the non-responders group after NACT. The predictive performance of selected microRNA was evaluated by sensitivity, specificity, accuracy, and the area under the receiver operating characteristic (ROC) curve.

Results: A total of 17 miRNAs downregulated before NACT and upregulated after NACT were selected according to microarray analysis in our previous study, and miR-326 and miR-376a-3p were selected for further exploration. According to the responses and the evaluation criteria, 25 patients reached partial response (PR) and 14 patients remained stable. Further qRT-PCR analysis showed that miR-326 significantly downregulated before NACT and upregulated after NACT in 12 responders (p = 0.02). The expression of miR-376a-3p showed no statistical difference before and after NACT in these 12 responders. Then, miR-326 provided an AUC-ROC of 0.75 (p = 0.04) in the discrimination between the responders and non-responders groups. The cutoff value of ROC for miR-326 to predict the response of NACT was <0.023, the sensitivity was 88.89%, and the specificity was 50%.

Conclusions: The expression of miR-326 significantly upregulated after NACT in responders. miR-326 may be a biomarker for predicting the response to NACT in LACC patients. The results may optimize individualized treatments for LACC patients.

KEYWORDS

microRNAs, locally advanced cervical cancer, neoadjuvant chemotherapy, predictive biomarker, molecular

Introduction

Cervical cancer ranks second in cancer incidence and death, following breast cancer, in women, with an estimated 570,000 cases and 311,000 deaths in 2018 worldwide (1). The majority of the cases are diagnosed as squamous cell carcinoma (SCC). Human papillomavirus (HPV) infection is the necessary but not sufficient cause of cervical cancer (2). Other important factors are young age at first coitus, multiple sexual partners, high parity, the presence of foreskin in the male partner, cigarette smoke, diet, and so on (3, 4). The risk factors associated with the development of HPV have been summarized in Table 1. After Friedlander et al. firstly reported in 1983 that cervical cancer was responsive to cisplatin-based combination chemotherapy (5), neoadjuvant chemotherapy (NACT) followed by radical hysterectomy or radiotherapy has been investigated. NACT can inhibit tumor micrometastases, improve the radiosensitivity of the tumor, and effectively shrink the tumor volume. The ovarian and vaginal functions could be reserved in patients who underwent NACT followed by radical surgery (6). However, the response of NACT varies due to individual differences and the complexity of cancer. Previous studies reported that around 30% of SCC patients were non-responsive to the chemotherapy (7). Identifying responders to NACT could improve their prognosis and optimize individualized treatment. For the non-responders, doctors could stop them from wasting precious time receiving ineffective treatments and suggest other effective treatments.

At present, the standard approach for the evaluation of response to NACT is MRI. However, the use of MRI increases the risk of false-positive results and is not a precise way for evaluating the NACT response. Diffusion-weighted MRI can measure the movement of water molecules in tissue, and this molecular imaging can identify the changes during the process of NACT (8). However, it cannot be popularized in developing countries due to the fact that it is costly. Therefore, it is important to identify effective serum biomarkers predicting the NACT response.

MiRNAs are small non-coding RNAs of 18–25 nucleotides that regulate gene expression at the posttranscriptional levels and are involved in the development of multiple malignant tumors (9). Recent studies have discovered that miRNAs may play a key role in predicting response to NACT in cancers (10, 11). The main idea of this study was to find out the potential miRNAs that can predict the response to NACT in LACC patients.

Abbreviations: LACC, locally advanced cervical cancer; NACT, neoadjuvant chemotherapy; miRNAs, microRNAs; ROC, receiver operating characteristic; qRT-PCR, quantitative reverse transcription–polymerase chain reaction; SCC, squamous cell carcinoma; HPV, human papilloma virus; CR, complete response; PR, partial response; PD, progressive disease; SD, stable disease; DLBCL, diffuse large B-cell lymphoma.

Methods

Study design

This study aimed to discover certain circulating miRNAs that could serve as markers for response to NACT in LACC patients. First, the serum samples of seven SCC patients before and after one or two cycles of NACT were collected for microRNA microarray analysis. miRNAs were selected after bioinformatics analysis and literature review. Second, the serum samples of 32 SCC patients before NACT and after one to two cycles of NACT were collected. Third, according to the response evaluation criteria for solid tumors (RECST, version 1.1), SCC patients with complete or partial response were assigned into the chemo-sensitive group (responders) and those with stable or progressive disease into the chemo-insensitive group (non-responders). Fourth, candidate miRNAs were validated both in the responders and non-responders using qRT-PCR analysis. Finally, 18 patients were randomly assigned into the testing group, and the remaining 21 patients were assigned into the validation group. Overall, the study was designed (Figure 1).

Patients and samples

All patients were recruited from the West China Second University Hospital (Chengdu, P.R. of China) between July 2014

TABLE 1 Factors linked to the development of cervical cancer.

Behavioral factors	Biological factors
Young age at first coitus (≤16 years old)	Human papillomavirus (HPV)
Multiple sexual partners	Human immunodeficiency virus (HIV)
Long-term oral contraceptive use (≥5 years)	Herpes simplex virus type-2 (HSV-2)
High parity (≥5 times)	Chlamydia trachomatis
Smoking (independent factor)	Neisseria gonorrhoeae
Diet (poor fruit and vegetable intake)	Trichomonas vaginalis
Male characteristics: Presence of foreskin ·HPV DNA positive ·Number of sexual partners ·Experience with sex workers	Treponema pallidum
Immunosuppression	Cytomegalovirus (CMV)

and June 2017. This study was approved by the Ethics Committee of West China Second University Hospital. Informed consent was obtained from all participants. All methods were performed in accordance with the relevant guidelines and regulations. All of the participants were genetically unrelated, were ethnic Han Chinese, and donated 5 ml of peripheral blood in every collection. The inclusion criteria were as follows: (1) newly diagnosed with SCC, stages IB–IIB, according to the 2009 FIGO classification; (2) had no prior hysterectomy, pelvic radiotherapy, or systemic chemotherapy; (3) had no other metabolic diseases, such as diabetes mellitus; and (4) had no any inflammations. The basic clinical information of patients is shown in Table 2. The SCC diagnosis and staging were assessed by two experienced pathologists. Once the samples were collected, tubes were kept upright at room temperature for 30 min and then stored in a 4°C refrigerator. After centrifugation at 4000 rpm, 4°C for 10 min, the serum was extracted and distributed into aliquots of 1 ml per 1.5 ml tube. Then the serum tubes were stored in a -80°C freezer.

NACT and surgery

Eligible patients received two cycles of NACT in the form of a regimen consisting of bleomycin, vincristine, and cisplatin. Once every 21 days, the patients received bleomycin at 15/30 mg intravenously (iv) on the first day and second day with vincristine at 1.5 mg iv and cisplatin at 80 mg iv on the first day. The doses and schedules of the drug administration were modified according to a drug toxicity evaluation before each course. Radical hysterectomy plus pelvic lymphadenectomy were performed after two cycles of chemotherapy.

Response evaluation

The response evaluation was based on the response evaluation criteria for solid tumors (RECST, version 1.1) (12) and was classified into four categories—CR: complete response,

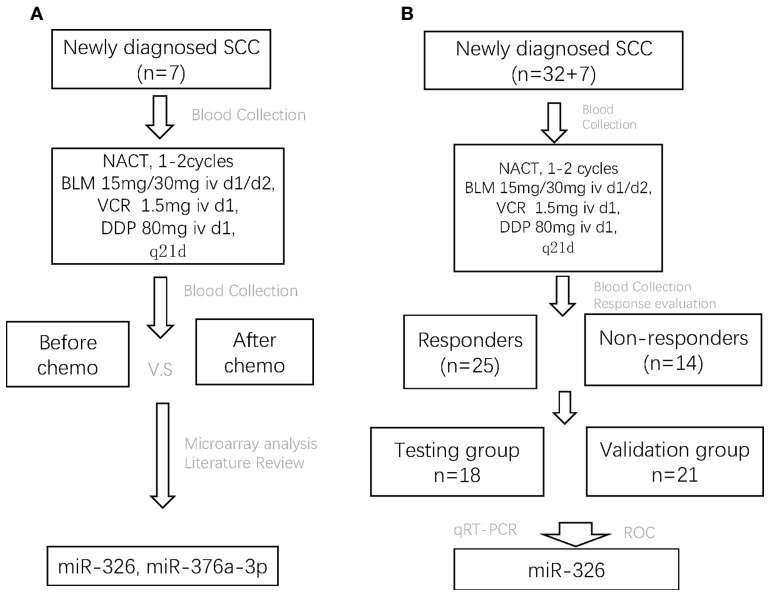

FIGURE 1
The flowchart of the whole study design. SCC, squamous cell carcinoma; NACT, neoadjuvant chemotherapy; BLM, bleomycin; VCR, vincristine; DDP, cisplatin; CR, complete response; PR, partial response; SD, stable disease; PD, progressive disease.

all the lesions disappeared (any pathological lymph nodes must have a reduction in short axis to <10mm); PR: partial response, at least a 30% decrease in the sum of diameters of lesions; PD: progressive disease, at least a 20% increase in the sum of diameters of lesions; and SD: stable disease, neither a shrinkage that qualified as the PR nor a sufficient increase that qualified as the progressive disease (PD). In our study, responders (chemo-sensitivity) were defined as CR plus PR; non-responders (chemo-insensitivity) were SD plus PD.

miRNA microarray analysis

RNA was extracted from the serum using a miRNeasy Serum/Plasma Kit (Qiagen, Hilden, Germany) according to the manufacturer's instructions. RNA was quantified and its purity evaluated by the absorption ratio at 260/280 nm using NanoDrop 2000 (Thermo Fisher Scientific, Massachusetts, USA). The ratio of 260/280 varied from 1.8 to 2.1. Then, cDNA synthesis was performed using a miScript II RT Kit (Qiagen, Hilden, Germany). The expression levels of 192 human mature miRNAs were examined using the miRCURY LNA™ Universal RT microRNA PCR system, Serum/Plasma Focus microRNA PCR Panel (Exiqon, Vedbaek, Denmark). Microarrays were scanned using the ABI PRISM7900 system (Applied Biosystems, Foster, USA), and fold changes in the miRNA expression between the two groups were calculated using the 2-ΔCt method. Raw data were normalized by quantile normalization and the robust multichip average algorithm. All miRNA level files were imported into GeneSpring 11.0 software (Agilent Technologies, Santa Clara, CA, USA).

Quantitative real-time PCR assay

The relative expression of two miRNAs was validated by qRT-PCR assay. RNA was extracted from the serum using a miRNeasy Serum/Plasma Kit (QIAGEN, Inc.) according to the manufacturer's instructions. The reverse-transcription reactions were carried out by a miScript II RT Kit (QIAGEN, Inc.). qRT-PCR was performed using a miScript SYBR Green PCR Kit (QIAGEN, Inc.). Glyceraldehyde 3-phosphate dehydrogenase (GAPDH) was used for the internal control of miRNA. Each sample was run in three independent experiments in triplicate. The reactions were amplified at 95°C for 15 min followed by 40 cycles at 94°C for 15 s and 55°C for 30 s.

Statistical analysis

Quantitative variables were expressed as mean ± SD, and categorical variables were the number of events (%). GraphPad Prism (Version 7, GraphPad Software Inc.) was applied for data analysis with all data assessed for a normal distribution and equal variance. Statistical comparisons between two groups were performed by Student's *t*-test or the chi-square test. The difference in miRNA levels between groups was evaluated using the Mann–Whitney unpaired test, and, for before/after comparison within one group, the Wilcoxon matched-pairs signed rank test was used. Receiver operating characteristic (ROC) curves were constructed to evaluate the predictive performance of the potential biomarkers. All P values were bilateral, with $P < 0.05$ being statistically significant.

Results

Demographic and clinical characteristics

Between July 2014 and June 2017, a total of 39 available SCC patients who met the inclusion criteria were enrolled in this study. Twenty-five (64%) of them were evaluated as PR and were assigned into the responders group, whereas the remaining 14 (36%) patients remained stable and were assigned into the non-responders group. Their demographic and clinical characteristics are shown in Table 2. Each characteristic was comparable in both groups.

miR-326 and miR-376a-3p were selected after microarray analysis

Pair-matched blood samples of seven SCC patients before and after receiving NACT were collected to perform microRNA microarray analysis. Seventeen significantly differentially expressed microRNAs were selected according to bioinformatics analysis in our previous study. These 17 microRNAs were significantly downregulated before NACT and upregulated after NACT (Figure 2). Combined with the literature review (13, 14), miR-326 and miR-376a-3p were selected for further explorations.

Compared with the baseline, the relative expression of miR-326 after NACT was higher and reached the statistical difference in the responders group

The pair-matched blood samples of 18 SCC patients before and after receiving NACT were used to explore the expression change of miR-326 by using qRT-PCR. According to the new response evaluation criteria in solid tumors (RECST, version 1.1), 12 patients achieved PR and were classified into the responders group, and the remaining six

10.3389/fonc.2022.1036710

TABLE 2 The clinical characteristics of SCC patients.

	Responders (n = 25)	Non-responders (n =14)	p-value
Age	44.28 ± 9.05	43.64 ± 7.12	0.82
Stage			0.17
Ib	6 (24%)	6 (43%)	
II a	15 (60%)	4 (29%)	
Iib	4 (16%)	4 (29%)	
Differentiation			0.9
Low	22 (88%)	12 (86%)	
Moderate	3 (12%)	2 (14%)	
LNM			0.54
Yes	3 (12%)	0	
No	22 (88%)	14 (100%)	
Stromal invasion			0.45
Yes	5 (20%)	5 (36%)	
No	20 (80%)	9 (64%)	
LVSI			0.72
Yes	7 (28%)	3 (21%)	
No	18 (72%)	11 (79%)	
Parametrial involvement			0.73
Yes	10 (40%)	4 (29%)	
No	15 (60%)	10 (71%)	

patients achieved SD and were classified into the non-responders group. After the qRT-PCR analysis, miR-326 was significantly downregulated before NACT and upregulated after NACT in 12 responders (p = 0.02, Figure 3A), whereas the expression before and after NACT had no statistical difference in the non-responders (Figure 3B). The expressions of miR-376a-3p before and after NACT had no statistical difference neither in the responders group nor the non-responders group (Figures 3C, D).

miR-326 could be a biomarker to predict response to NACT in SCC patients

miR-326 was selected to be the candidate biomarker for predicting the NACT response and was validated by 21 SCC patients in a further analysis. Among them, 13 patients achieved PR, and the remaining eight patients were in the SD group. The predictive performance was evaluated by sensitivity, specificity, accuracy, and the area under the ROC. miR-326 provided an AUC-ROC of 0.75 (p = 0.04) in the discrimination between the PR and SD groups (Figure 4A). The cutoff value of ROC for miR-326 to predict the response of NACT was <0.023, the sensitivity was 88.89%, and the specificity was 50%. Before NACT, the relative expression of miR-326 in the responders was much lower than that in the non-responders (p = 0.02) (Figure 4B).

Discussion

In a meta-analysis, NACT followed by radical surgery showed a highly significant reduction in the risk of death compared with radiotherapy alone (hazard ratio [HR] = 0.65, 95% CI [0.53, 0.8], P = 0.0004), with an absolute improvement of 14% in survival at 5 years, increasing from 50% to 64% (15). However, many patients cannot receive follow-up surgery because of drug toxicity or insensitivity to NACT resulting to delaying the time to receive chemoradiotherapy. Therefore, it is meaningful to find some predictive biomarkers to predict the response to NACT in newly diagnosed LACC patients.

MicroRNAs are stable and detectable in the serum, and changes in the levels of specific microRNAs could allow the detection of clinical conditions (16, 17). Feng et al. reported that miR-15a, miR-16-1, miR-29c, miR-34a, and miR-155 could be novel non-invasive biomarkers for the diagnosis of diffuse large B-cell lymphoma (DLBCL) with AUC-ROCs of 0.7722, 0.7002, 0.6672, 0.8538, and 0.7157, respectively (18).

Searching for effective prevention and management of cancers has always been at the top of medical concerns list.

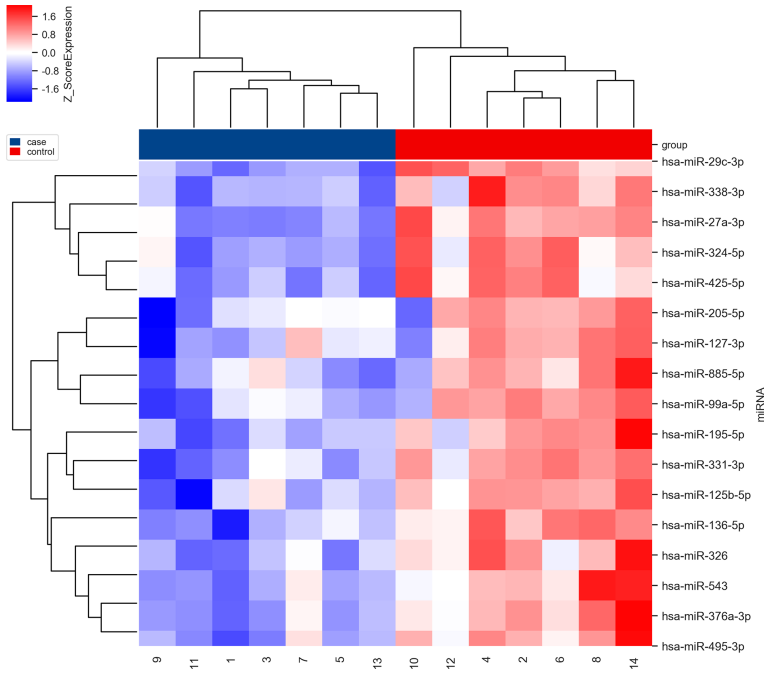

FIGURE 2
The clustering map of dysregulated microRNAs before (in blue) and after (in red) NACT in the first seven SCC patients. The blue ones mean downregulated and the red ones mean upregulated.

MicroRNAs (miRNAs), less than 22 nt small non-coding RNAs, play important roles by regulating mRNAs in cancer-related processes (9). There are still some small non-coding RNAs linked to other gynecologic cancers, which have been shown to contribute positively to the prognosis prediction of oncology patients. Piergentili et al. summarized ncRNAs with good predictive values such as miR-101, miR-152, and miR-205 in the treatment of endometrial cancer and recognized their great potential to improve risk stratification in EC (19). Cavaliere et al. also identified ncRNA pools that have a prognostic role and impact on the treatment of EC patients based on epigenetic profiles (20). However, the molecular properties of individuals may not be generalized due to the interactions between different ncRNAs. Focusing on only one molecule may not be sufficient, and combining ncRNAs with other well-known risk factors may be the key to achieving better treatment approaches. Researchers demonstrated that in luminal B HER-2 breast cancer, the miR-718 and miR-4516 expressions were lower in the group of responders than in non-responders, whereas the miR-210 expression was the opposite (21). Not come singly but in pairs, miR-195 and miR-26b were also found to be consistently upregulated after NACT (22). Todorova and colleagues found that miR-328-3p expression was downregulated before NACT and suggested that miR-127-3p is a strong predictor of NACT-positive treatment response in triple-negative breast cancer (23). Furthermore, miRNA-21 could be used as an independent predictor of chemotherapy sensitivity not only in breast cancer but also in esophageal SCC, where its levels were remarkably lower in chemotherapy-sensitive patients, whereas levels in the non-responders did not change significantly (24, 25). This indicates that miRNAs that are predictable for chemotherapy response may not only target single cancer.

Plenty of studies have proved that dysregulations of miR-326 are associated with pathological processes such as cellular proliferation and apoptosis (26), differentiation, metastasis (27, 28), and chemotherapy resistance (29, 30). Our study found that circulating miR-326 in LACC patients who were sensitive to chemotherapy significantly downregulated after NACT, whereas the expression in chemotherapy-resistant patients had no statistical difference between before NACT and after NACT. The results implied that circulating miR-326 in newly LACC patients could be a biomarker to predict the response to NACT. Liang et al. showed that miR-326 was downregulated in VP-16-resistant multidrug resistance cell lines and in a panel of advanced breast cancer tissues and consistent reversely with the expression levels of MRP-1. These results demonstrated that

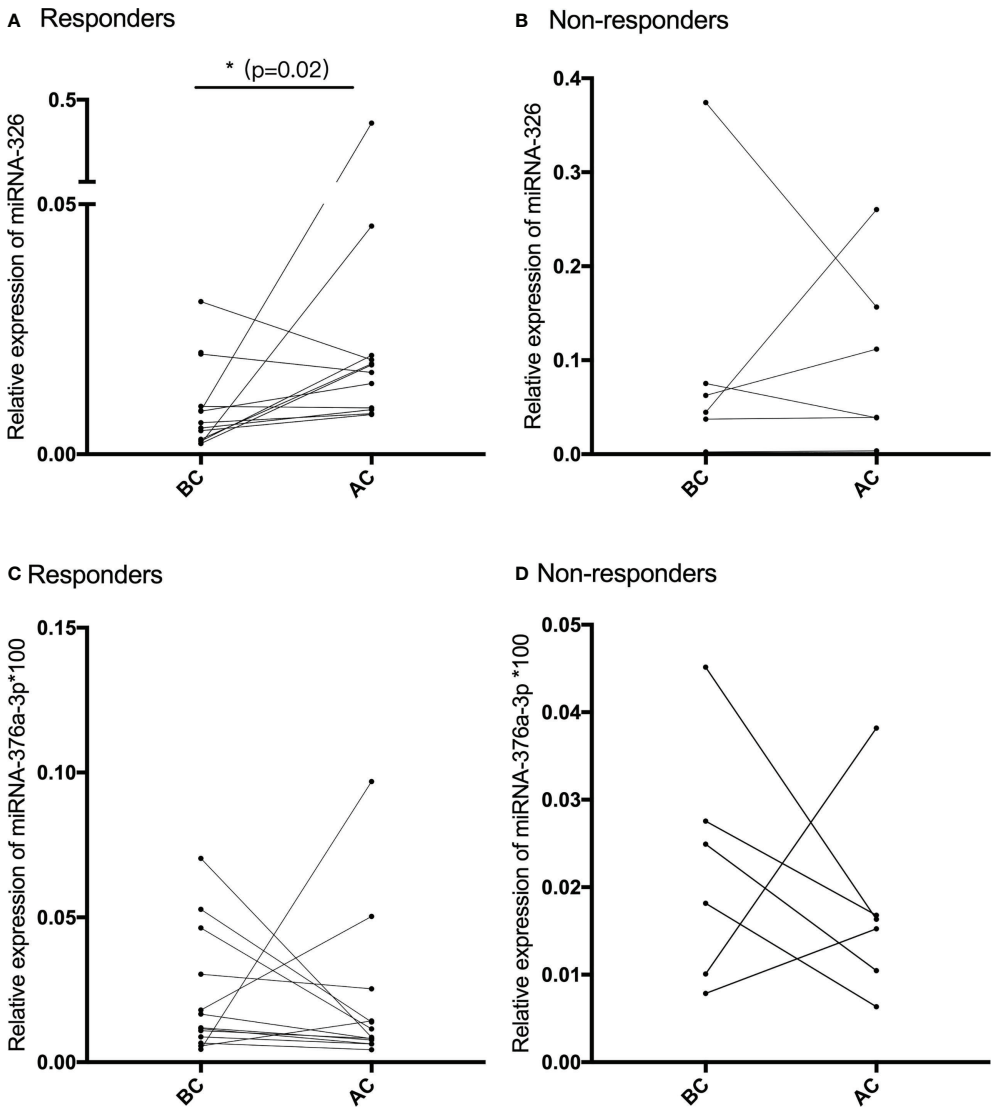

FIGURE 3
(A, B) The relative expression of miR-326 before and after NACT in chemotherapy-sensitive patients (responders) and chemotherapy-resistant patients (non-responders). **(C, D)** The relative expression of miR-376a-3p before and after NACT in chemotherapy-sensitive patients (responders) and chemotherapy-resistant patients (non-responders).

miR-326 could be an agent in the mechanism of chemotherapy resistance of breast cancer (29).

There are several studies that focus on exploring biomarkers or others to predict the response to NACT of newly diagnosed cervical cancer patients. Yan Hou et al. identified and verified L-valine and L-tryptophan as the biomarkers to predict the response to NACT by performing plasma metabolite profiling (31). Chun Fu et al. studied in a different angle and found that the axial and sagittal magnetic resonance diffusion-weighted imaging (DWI) could detect the changes in LACC patients after NACT, and the apparent diffusion coefficient values measured could be used to evaluate the response to NACT (8).

The strengths of this study are based on the meta-analysis; the target miRNAs are selected by microarray analysis, and then we screen differentially expressed miRNAs in the serum of SCC patients, which are more stable and have less influence during the collection of samples.

The limitations of our work are that we just found the potential biomarker, and we failed to find the correlation between miRNAs expression and HPV infection, as HPV infection is widely regarded as the primary cause of SCC.

Cervical adenocarcinoma patients should be included in the following relevant studies, which will benefit further clinical application. Moreover, the target gene, protein, and regulating

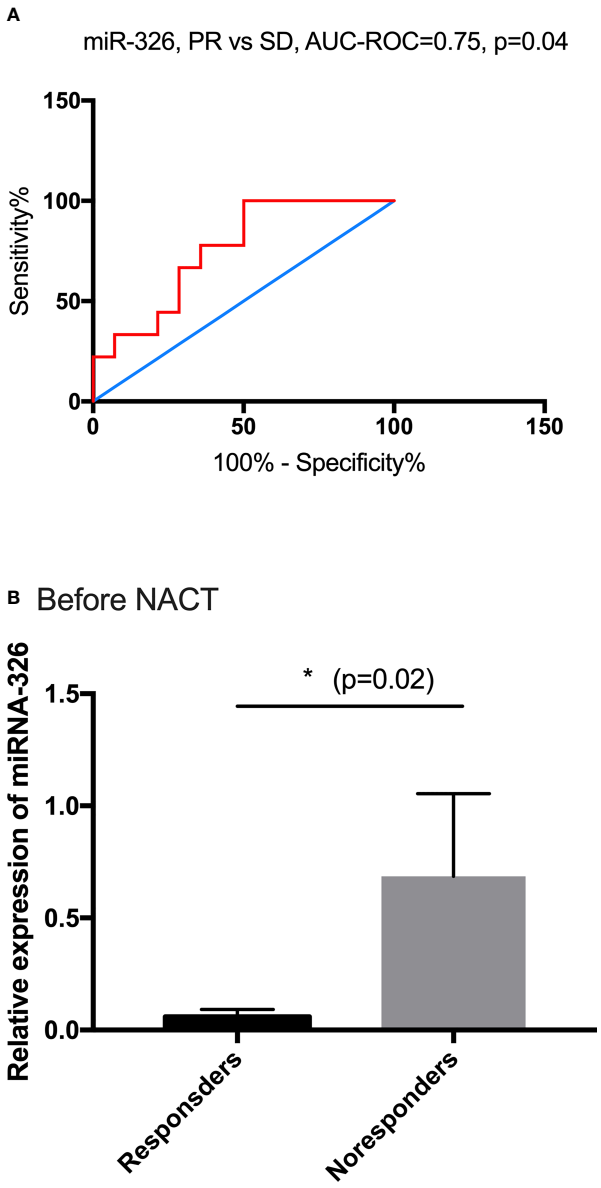

FIGURE 4
The predictive performance of miR-326. **(A)** The ROC curve for PR and SD based on the relative expression of miR-326, AUC-ROC = 0.75. **(B)** Before NACT, the baseline expressions of miR-326 in responders were much lower than those in non-responders (p = 0.02).

pathway need to be explored. Finally, a large population is also needed in future research to validate the predicted performance of miR-326 in SCC patients.

Conclusions

In summary, our present study provides the first evidence that the circulating miR-326 is significantly upregulated after receiving NACT in responders, whereas the expression has no change in non-responders. The cutoff value of ROC for miR-326 to predict the response of NACT was <0.023. It suggested that the expression of miR-326 was lower than 0.023 in patients with newly diagnosed cervical SCC, indicating that they were likely sensitive to the NACT. It seems that the circulating miR-326 may be a biomarker to predict the response of NACT in SCC patients.

Data availability statement

The raw data supporting the conclusions of this article will be made available by the authors, without undue reservation.

Ethics statement

The studies involving human participants were reviewed and approved by the Ethics Committee of West China Second University Hospital. The patients/participants provided their written informed consent to participate in this study.

Author contributions

KZ contributed to the design of the study, sample collection and preparation, interpretation of data, manuscript drafting, and final approval. EY contributed to the sample collection and preparation and bioinformatics analysis. TC contributed to sample collection and preparation. ZL contributed to the conception of the study and design, manuscript revision, and critical discussion. All authors contributed to the article and approved the submitted version.

Funding

The microarray work and analysis of the data of this study were supported by the Medical Science and Technology Project of Sichuan Province Health Commission (No.21PJ050).

Acknowledgments

We acknowledge the staff of the Key Laboratory of Birth Defects and Related Diseases of Women and Children (Sichuan University), Ministry of Education, Chengdu, People's Republic of China, for the methods instruction of the study.

Conflict of interest

The authors declare that the research was conducted in the absence of any commercial or financial relationships that could be construed as a potential conflict of interest.

Publisher's note

All claims expressed in this article are solely those of the authors and do not necessarily represent those of their affiliated organizations, or those of the publisher, the editors and the reviewers. Any product that may be evaluated in this article, or claim that may be made by its manufacturer, is not guaranteed or endorsed by the publisher.

References

1. Bray F, Ferlay J, Soerjomataram I, Siegel RL, Torre LA, Jemal A. Global cancer statistics 2018: Globocan estimates of incidence and mortality worldwide for 36 cancers in 185 countries. *CA Cancer J Clin* (2018) 68(6):394–424. doi: 10.3322/caac.21492

2. Walboomers JMM, Jacobs MV, Manos MM, Bosch FX, Kummer JA, Shah KV, et al. Human papillomavirus is a necessary cause of invasive cervical cancer worldwide. *J Pathol* (1999) 189(1):12–9. doi: 10.1002/(Sici)1096-9896(199909)189

3. Pimple S, Mishra G. Cancer cervix: Epidemiology and disease burden. *Cytojournal* (2022) 19:21. doi: 10.25259/cmas_03_02_2021

4. Moore DH. Cervical cancer. *Obstet Gynecol* (2006) 107(5):1152–61. doi: 10.1097/01.Aog.0000215986.48590.79

5. Friedlander M, Kaye SB, Sullivan A, Atkinson K, Elliott P, Coppleson M, et al. Cervical carcinoma: A drug-responsive tumor–experience with combined cisplatin, vinblastine, and bleomycin therapy. *Gynecol Oncol* (1983) 16(2):275–81. doi: 10.1016/0090-8258(83)90102-6

6. Lapresa M, Parma G, Portuesi R, Colombo N. Neoadjuvant chemotherapy in cervical cancer: An update. *Expert Rev Anticancer Ther* (2015) 15(10):1171–81. doi: 10.1586/14737140.2015.1079777

7. Kumar JV, Doval DC, Rao R, Rawal S. A retrospective study of patients with locally advanced cancer of the cervix treated with neoadjuvant chemotherapy followed by radical surgery. *Int J Gynecol Cancer* (2009) 19(3):417–22. doi: 10.1111/IGC.0b013e3181a1c6df

8. Fu C, Bian D, Liu F, Feng X, Du W, Wang X. The value of diffusion-weighted magnetic resonance imaging in assessing the response of locally advanced cervical cancer to neoadjuvant chemotherapy. *Int J Gynecol Cancer* (2012) 22(6):1037–43. doi: 10.1097/IGC.0b013e31825736d7

9. Bartel DP. Micrornas: Genomics, biogenesis, mechanism, and function. *Cell* (2004) 116(2):281–97. doi: 10.1016/s0092-8674(04)00045-5

10. Zhu W, Liu M, Fan Y, Ma F, Xu N, Xu B. Dynamics of circulating micrornas as a novel indicator of clinical response to neoadjuvant chemotherapy in breast cancer. *Cancer Med* (2018) 7(9):4420–33. doi: 10.1002/cam4.1723

11. Raychaudhuri M, Bronger H, Buchner T, Kiechle M, Weichert W, Avril S. Micrornas mir-7 and mir-340 predict response to neoadjuvant chemotherapy in breast cancer. *Breast Cancer Res Treat* (2017) 162(3):511–21. doi: 10.1007/s10549-017-4132-9

12. Eisenhauer EA, Therasse P, Bogaerts J, Schwartz LH, Sargent D, Ford R, et al. New response evaluation criteria in solid tumours: Revised recist guideline (Version 1.1). *Eur J Cancer* (2009) 45(2):228–47. doi: 10.1016/j.ejca.2008.10.026

13. Jadideslam G, Ansarin K, Sakhinia E, Babaloo Z, Abhari A, Ghahremanzadeh K, et al. Diagnostic biomarker and therapeutic target applications of mir-326 in cancers: A systematic review. *J Cell Physiol* (2019) 234 (12):21560–74. doi: 10.1002/jcp.28782

14. Wang Y, Jiang F, Xiong Y, Cheng X, Qiu Z, Song R. Lncrna ttn-As1 sponges mir-376a-3p to promote colorectal cancer progression *Via* upregulating Klf15. *Life Sci* (2020) 244:116936. doi: 10.1016/j.lfs.2019.116936

15. Benedetti-Panici P, Bermudez A, Blake P, Cardenas J, Chang TC, Chiara S, et al. Neoadjuvant chemotherapy for locally advanced cervical cancer: A systematic review and meta-analysis of individual patient data from 21 randomised trials. *Eur J Cancer* (2003) 39(17):2470–86. doi: 10.1016/S0959-8049(03)00425-8

16. Chim SS, Shing TK, Hung EC, Leung TY, Lau TK, Chiu RW, et al. Detection and characterization of placental micrornas in maternal plasma. *Clin Chem* (2008) 54(3):482–90. doi: 10.1373/clinchem.2007.097972

17. Gilad S, Meiri E, Yogev Y, Benjamin S, Lebanony D, Yerushalmi N, et al. Serum micrornas are promising novel biomarkers. *PloS One* (2008) 3(9):e3148. doi: 10.1371/journal.pone.0003148

18. Fang C, Zhu DX, Dong HJ, Zhou ZJ, Wang YH, Liu L, et al. Serum micrornas are promising novel biomarkers for diffuse Large b cell lymphoma. *Ann Hematol* (2012) 91(4):553–9. doi: 10.1007/s00277-011-1350-9

19. Piergentili R, Zaami S, Cavaliere AF, Signore F, Scambia G, Mattei A, et al. Non-coding rnas as prognostic markers for endometrial cancer. *Int J Mol Sci* (2021) 22(6):3151. doi: 10.3390/ijms22063151

20. Cavaliere AF, Perelli F, Zaami S, Piergentili R, Mattei A, Vizzielli G, et al. Towards personalized medicine: Non-coding rnas and endometrial cancer. *Healthc (Basel)* (2021) 9(8):965. doi: 10.3390/healthcare9080965

21. Zhang Z, Zhang H, Li C, Xiang Q, Xu L, Liu Q, et al. Circulating micrornas as indicators in the prediction of neoadjuvant chemotherapy

response in luminal b breast cancer. *Thorac Cancer* (2021) 12(24):3396–406. doi: 10.1111/1759-7714.14219

22. Baxter DE, Allinson LM, Al Amri WS, Poulter JA, Pramanik A, Thorne JL, et al. Mir-195 and its target Sema6d regulate chemoresponse in breast cancer. *Cancers (Basel)* (2021) 13(23):5979. doi: 10.3390/cancers13235979

23. Todorova VK, Byrum SD, Gies AJ, Haynie C, Smith H, Reyna NS, et al. Circulating exosomal micrornas as predictive biomarkers of neoadjuvant chemotherapy response in breast cancer. *Curr Oncol* (2022) 29(2):613–30. doi: 10.3390/curroncol29020055

24. McGuire A, Casey MC, Waldron RM, Heneghan H, Kalinina O, Holian E, et al. Prospective assessment of systemic micrornas as markers of response to neoadjuvant chemotherapy in breast cancer. *Cancers (Basel)* (2020) 12(7):1820. doi: 10.3390/cancers12071820

25. Kurashige J, Kamohara H, Watanabe M, Tanaka Y, Kinoshita K, Saito S, et al. Serum microrna-21 is a novel biomarker in patients with esophageal squamous cell carcinoma. *J Surg Oncol* (2012) 106(2):188–92. doi: 10.1002/jso.23064

26. Li D, Du X, Liu A, Li P. Suppression of nucleosome-binding protein 1 by mir-326 impedes cell proliferation and invasion in non-small cell lung cancer cells. *Oncol Rep* (2016) 35(2):1117–24. doi: 10.3892/or.2015.4403

27. Cai M, Wang Z, Zhang J, Zhou H, Jin L, Bai R, et al. Adam17, a target of mir-326, promotes emt-induced cells invasion in lung adenocarcinoma. *Cell Physiol Biochem* (2015) 36(3):1175–85. doi: 10.1159/000430288

28. Cheng Y, Jiang S, Yuan J, Liu J, Simoncini T. Vascular endothelial growth factor c promotes cervical cancer cell invasiveness *Via* regulation of microrna-326/Cortactin expression. *Gynecol Endocrinol* (2018) 34(10):853–8. doi: 10.1080/09513590.2018.1458304

29. Liang Z, Wu H, Xia J, Li Y, Zhang Y, Huang K, et al. Involvement of mir-326 in chemotherapy resistance of breast cancer through modulating expression of multidrug resistance-associated protein 1. *Biochem Pharmacol* (2010) 79(6):817–24. doi: 10.1016/j.bcp.2009.10.017

30. Ma J, Wang T, Guo R, Yang X, Yin J, Yu J, et al. Microrna133a and Microrna326 cocontribute to hepatocellular carcinoma 5fluorouracil and cisplatin sensitivity by directly targeting bcell lymphomaextra Large. *Mol Med Rep* (2015) 12(4):6235–40. doi: 10.3892/mmr.2015.4134

31. Hou Y, Yin M, Sun F, Zhang T, Zhou X, Li H, et al. A metabolomics approach for predicting the response to neoadjuvant chemotherapy in cervical cancer patients. *Mol Biosyst* (2014) 10(8):2126–33. doi: 10.1039/c4mb00054d

frontiers | Frontiers in Oncology

TYPE Original Research
PUBLISHED 28 November 2022
DOI 10.3389/fonc.2022.1003512

OPEN ACCESS

EDITED BY
Sara Ricardo,
Universidade do Porto, Portugal

REVIEWED BY
MIn Yu,
Sichuan University, China
Yuting Dai,
Shanghai Institute of Hematology, China
Yan Mao,
The Affiliated Hospital of Qingdao University, China

*CORRESPONDENCE
Peihai Zhang
peihaizhang@163.com

†These authors have contributed equally to this work

SPECIALTY SECTION
This article was submitted to Gynecological Oncology, a section of the journal Frontiers in Oncology

RECEIVED 26 July 2022
ACCEPTED 14 November 2022
PUBLISHED 28 November 2022

CITATION
Liang W, Zhou C, Wang J, Zhao J, Liu F, Wang G, Xu C, Zhang Y, Wang W, Cai S, Han Y, Chang L and Zhang P (2022) A prognostic signature based on adenosine metabolism related genes for ovarian cancer. *Front. Oncol.* 12:1003512. doi: 10.3389/fonc.2022.1003512

A prognostic signature based on adenosine metabolism related genes for ovarian cancer

Weifeng Liang[1], Chao Zhou[2], Jingshu Wang[3], Jing Zhao[3], Fang Liu[3], Guoqiang Wang[3], Chunwei Xu[4], Yuzi Zhang[3], Wenxian Wang[5], Shangli Cai[3], Yusheng Han[3], Lei Chang[6†] and Peihai Zhang[1*†]

[1]Department of Gynecology, Qilu Hospital (Qingdao), Cheeloo College of Medicine, Shandong University, Qingdao, Shandong, China, [2]Department of Bioinformatics and Biostatistics, Shanghai Jiao Tong University, Shanghai, China, [3]Medical Department, Burning Rock Biotech, Guangzhou, China, [4]Institute of Basic Medicine and Cancer (IBMC), Chinese Academy of Sciences, Hangzhou, Zhejiang, China, [5]Department of Clinical Trial, The Cancer Hospital of the University of Chinese Academy of Sciences (Zhejiang Cancer Hospital), Hangzhou, Zhejiang, China, [6]Department of Obstetrics and Gynecology, The First Affiliated Hospital of Zhengzhou University, Zhengzhou, Henan, China

Background: Ovarian cancer is one of the most common cause of cancer death in women due to its late diagnosis and susceptibility to drug resistance. Adenosine (ADO) signaling plays a key role in immune activity and tumor progression. In this study, we constructed a signature of ADO metabolism related genes expression in patients with ovarian cancer.

Methods: A total of 372 ovarian cancer patients from TCGA was used as training set and 1,137 patients from six GEO datasets were as validation set. The gene expression and drug response inhibitory concentration values for ovarian cancer cell line from GDSC were used for drug sensitivity analysis. The non-negative matrix factorization algorithm and ssGSVA were used to construct the ADO score.

Results: Patients with high ADO score had shorter overall survival (OS) than those with low ADO score in both training set (HR = 1.42, 95% CI, 1.06-1.88) and validation sets (pooled HR = 1.24, 95% CI = 1.02-1.51). In GSEA analysis, genes in ATP synthesis related pathways were enriched in the low ADO score group (adjusted P value = 0.02). Further, we observed that the high ADO score group had significantly higher levels of most cancer hallmark signatures (all adjusted P values < 0.01) and T cell dysfunction and exclusion signatures than the low ADO score group (all adjusted P values < 0.001). Patients with lower ADO score tended to be sensitive to common drugs including Olaparib and Paclitaxel (adjusted P values = 0.05 and 0.04, respectively).

Conclusions: In conclusion, the established ADO signature could be used as a prognostic biomarker to stratify ovarian cancer patients and had the potential to guide the drug exploitation and personalized therapy selection.

KEYWORDS

adenosine metabolism, ovarian cancer, gene expression, prognostic analysis, signature

Introduction

Ovarian cancer is one of the most common and lethal cancers (1), which ranks the eighth leading cause of cancer-related female deaths worldwide, accounting for 3.4% of all cancer deaths in women (2). Due to the non-specific symptoms at early stage, about 70% of ovarian cancer patients were diagnosed at advanced stage (3). The standard treatment for ovarian cancer is primary surgery and sequential platinum-based chemotherapy (4). In addition, targeted therapies are remarkable options for patients including PARP inhibitors targeting BRCA germline mutations, VEGF inhibitors targeting tumor angiogenesis (5). However, because of late diagnosis and susceptibility to drug resistance, the recurrence rate is still high and the 5-year survival rate is only 49% (6). Therefore, it is necessary to identify the patients who have a higher probability to relapse and require advanced cancer intervention and managements.

Previous studies have demonstrated that adenosine (ADO) signaling has immunosuppressive effects by suppressing the activity of natural killer cells (NK) and CD8+ cells and enhancing the polarization of dendritic cells and the proliferation of myeloid-derived suppressor cells (MDSC) (7, 8). In ovarian cancers, CD39 and CD73, responsible for adenosine production are over-expressed in tumor tissues and associated with worse prognosis (9). Besides, based on a murine model and patients cohort of ovarian cancer, it was found that CD73 expression on ovarian tumor cells and cancer associated fibroblast cells (CAFs) promoted cancer cell survival and immune escape (10). Further, accumulated extracellular ADO induces immunosuppressive effects, mainly through interacting with four G protein-coupled receptors: ADORA1, ADORA2A, ADORA2B, and ADORA3 (11). For example, ADORA2B activation in MDSCs significantly induces VEGF secretion and angiogenesis (12). In addition, ADORA1 antagonist tended to reduce the cisplatin resistance in ovarian cell lines (13). Therefore, ADO metabolism played an important role in ovarian cancer. In consideration that ADO metabolism is not only regulated by different adenosine-producing enzymes, but also by counteracting ATP-regenerating pathways, adenosine degrading pathways, and cellular adenosine uptake (8), it is rational to develop a signature with the integration of multiple adenosine metabolism related genes expression for the prognosis prediction. We hypothesized that the signature characterized as the conversion from ATP to ADO might be related to immunosuppressive state and worse prognosis.

In this study, we developed and validated an ADO metabolism related signature to predict prognosis in ovarian cancer based on the expression data of TCGA and six GEO datasets. Further, in order to explore the potential mechanism and clinical utility, we analyzed the association of ADO score with immune microenvironment and drug sensitivity.

Materials and methods

Data download

Twenty-two ADO metabolism related genes (18 ADO metabolism enzymes and 4 ADO receptor) were collected from a previous study (8) and the description of their biological function is shown in Supplementary Table 1. A total of 372 ovarian cancer patients from TCGA was used as training set and 1,137 patients from 6 GEO datasets were as validation set. The RNAseq, whole-exon sequencing (WES), and corresponding clinical data of TCGA were downloaded from portal.gdc.cancer.gov, and the six GEO validation datasets (GSE14764, GSE23554, GSE26712, GSE32062, GSE49997, GSE140082) were downloaded from www.ncbi.nlm.nih.gov/gds. The basic information of these cohorts is summarized in Supplementary Table 2. The gene expression and drug response inhibitory concentration (IC50) values for 198 drugs in ovarian cancer cell lines were obtained from Genomics of Drug Sensitivity in Cancer (GDSC, www.cancerrxgene.org) (14).

Biomarker discovery and signature construction

We used the non-negative matrix factorization (NMF) algorithm to obtain adenosine related Meta genes based on the

expression data from TCGA. In detail, the R package "NMF" (15) with the default methods 'brunet' was applied. The rank was set as 2 to 10 and the number of runs for each rank set was 200. The cophenetic correlation coefficient was used to determine optimal clustering number. The factorization rank was selected once cophenetic correlation coefficient started to decrease (16). After that, we extracted the top 15 genes for each basis from the results of NMF which were used for the downstream analysis. A total of 20 genes was included in the signature construction. Two gene clusters were identified by consensus clustering algorithm with a correlation matrix of genes expression (17). Further, we calculated the enrichment score by ssGSVA method implemented in R package 'GSVA' (18) with the above two gene clusters respectively and defined the ADO score as the difference between the enrichment score of two gene clusters.

Prognostic analysis

Patients were classified into high and low ADO groups by the median of ADO score in each cohort. Kaplan-Meier survival curve and univariable/multivariable Cox regression model were used to analyze the association between ADO score and overall survival (OS). In order to explore the interaction effects of BRCA1/BRCA2 mutation and Homologous Recombination Deficiency (HRD) with ADO score, hierarchical analysis was applied and interaction P value was evaluated by Wald test. The Number of Telomeric Allelic Imbalances (NtAI) count, Large-scale State Transitions (LST) count, Homologous Recombination Deficiency (HRD-LOH) score and HRD score for TCGA samples were obtained from Andrea M Marquards' article (19). In the validation set, meta-analysis with random effect was used to pool the hazard ratio (HR) of the six GEO datasets.

Molecular mechanisms and drug sensitivity analysis

To explore the molecular mechanism, the gene set enrichment analysis (GSEA) was performed in TCGA patients to analyze the significantly enriched pathways in high and low ADO score groups. In addition, the association between ADO score and ten cancer hallmark signatures related Gene Ontology (GO) terms were also analyzed (20). In order to explore the relationship between ADO score and immune microenvironment, immune infiltration signature calculated by CIBERSORT (21), ESTIMATE (22), MCPcounter (23), single-sample gene set enrichment analysis (ssGSEA) (24), TIMER (25) and TIDE (26) were compared between two ADO groups using Wilcoxon rank-sum test. The gene expression of immune checkpoint was similarly analyzed. For drug sensitivity, drugs with missing value in more than 80% of the samples were removed from the analysis. Finally, 180 drugs involving 23 pathways were used for Pearson correlation analysis between ADO score and IC50. Benjamini-Hochberg was used for P value correction for multiple comparisons.

Statistical analysis

The flowchart of this study is demonstrated in Figure 1A. All analyses were performed with R version 4.0.3. The Wilcoxon rank-sum test was used to test difference for all the calculated score or the gene expression between two groups if not specifically described. The P value less than 0.05 was regard as statistically significant and all the tests were two-side.

Results

Construction of the prognostic signature in TCGA dataset

For the 22 ADO related genes, only 38 of 434 (8.76%) ovarian cancer samples had non-silent mutation in these genes (Supplementary Figure 1A). Among them, mutation frequency of ENPP1 was the highest, which occurred in 5 of 434 samples (1.46%). There was no mutation event in ADA2, ENTP2, ENTPD8, and NME1 (Supplementary Figure 1A). For the copy number variants, it showed that the copy number variants were ubiquitous for ADO genes which indicated the mRNA expression of ADO genes might be discrepant among samples (Supplementary Figure 1B). According to the expression data of ADO genes, patients could be classified into four clusters in consensus cluster analysis (Figure 1B). Through NMF analysis, the optimal cluster number was set as 4 according to cophenetic correlation coefficient (Supplementary Figure 2A). The four Metagenes of ADO genes had different expression patterns and showed discrepant expression in all samples (Figure 1C, Supplementary Figure 2B). Top 15 genes in each metagene were extracted and formed a gene list for the following analysis. According to the correlation among these genes, we got two ADO gene groups (Figure 1D). In gene set 1, 8 of 12 genes were involved in the generation of ADP, AMP or ADO. However, in gene set 2, expect for ADA gene, the other 7 genes were enriched in the pathways related to ADP generation or ADO degradation (Supplementary Table 1). Furthermore, the enrichment scores by ssGSVA were calculated for the two gene sets, respectively. The ADO score was defined as enrichment score of gene set 1 minus gene set 2, which was significantly different among the four sample clusters (Figure 1E).

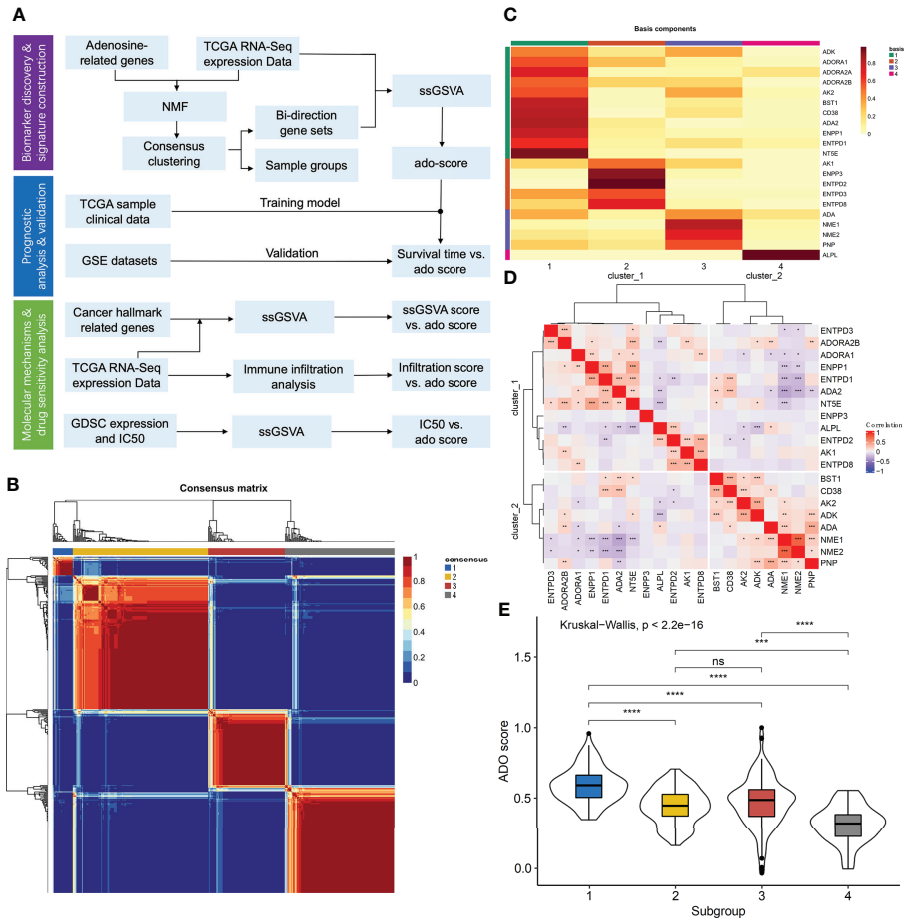

FIGURE 1
The construction of adenosine signature. **(A)** The flowchart of the study; **(B)** The consensus map of NMF clustering; **(C)** The metagenes obtained from NMF cluster; **(D)** The correlation matrix of adenosine metabolism related genes expression; **(E)** The boxplots of ADO score for different samples clusters. (ns: P > 0.05, *P < 0.05, **P < 0.01, ***P < 0.001, ****P < 0.0001).

Prognostic analysis in TCGA and GEO datasets

In TCGA cohort, patients with high ADO score had shorter OS than those with low ADO score (HR, 1.33; 95% CI, 1.02-1.72, Figure 2A). After adjusted for age, grade, stage, BRCA1/2 mutation and debulking surgery, the association was still significant (HR, 1.42; 95% CI, 1.06-1.88, Supplementary Table 3). Among the six validation cohorts, similar results were observed in GSE49997 and GSE140082 dataset (Log-rank P = 0.04 for GSE49997 and 0.01 for GSE140082, Figures 2B, C). In the meta-analysis of the six validation cohorts, the pooled HR was still significant in both univariable (HR, 1.27; 95% CI, 1.00-1.62; Figure 2D) and multivariable Cox models adjusted for age, stage, debulking surgery, histology and histological grade (HR, 1.24; 95% CI, 1.02-1.51, Figure 2E). The detailed results were reported in Supplementary Table 3. Besides, the hierarchical meta-analysis was applied stratified by serous and non-serous cancers, different grade and different stage, and the high ADO score was still significantly associated with worse OS in subgroups of stage III/IV (HR, 1.24; 95% CI, 1.01-1.52; Supplementary Table 4) and serous histology (HR, 1.23; 95% CI, 1.00-1.50; Supplementary Table 4) in the multivariable model. In grade G3/4 subgroup, the association were similar and borderline significant (HR, 1.28; 95% CI, 0.96-1.70; Supplementary Table 4).

Hierarchical analysis for BRCA1/2 mutation and HRD score in TCGA dataset

There is no significant difference in BRCA1/2 mutation frequency, NtAI count, LST count, HRD-LOH score and HRD between low and high ADO score groups (Supplementary Figures 3A, B). For BRCA1/2 mutation, the association of ADO score and OS was significant in the patients with

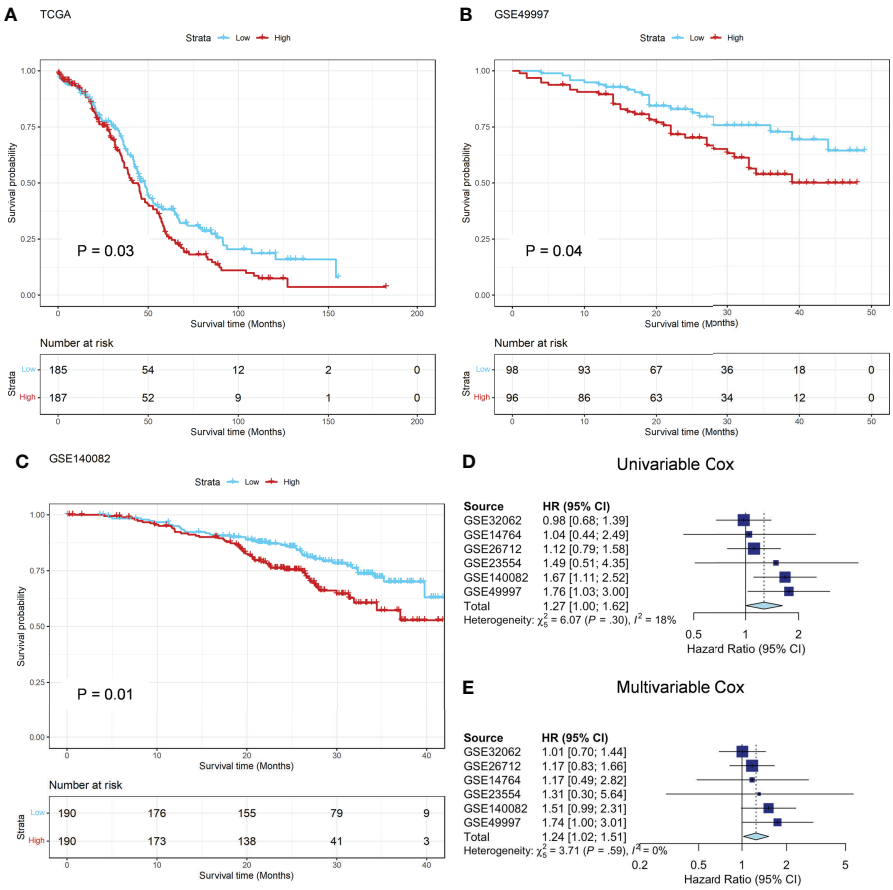

FIGURE 2
Prognostic analysis in TCGA and GEO datasets. **(A)** The Kaplan-Meier survival curves of OS between the ADO groups in the TCGA training dataset; **(B, C)** The Kaplan-Meier survival curves of OS between the two ADO groups in the GSE49997 and GSE140082 validation datasets, respectively; **(D, E)** The forest plot of the meta-analysis on the results of 6 GEO validation dataset calculated by using univariate and multivariate Cox model, respectively.

BRCA1/2 mutation, but not significant in other patients (P interaction = 0.018) (Figures 3A, B, Supplementary Table 5). Besides, the patients were classified in two subgroups based on the median of HRD score. There was a significant association between ADO score and OS in high HRD subgroup, but not in low HRD subgroup. However, the P interaction was not significant (P interaction = 0.35, Figures 3C, D, Supplementary Table 5). The results showed that ADO score tended to be significantly associated with prolonged survival only in BRCA1/2 mutant or HRD patients.

The association between ADO score and biological signatures or immune genes expression in TCGA dataset

According to GSEA analysis, we found that genes in ATP synthesis related pathways were significantly enriched in the low ADO score group (adjusted P value = 0.02, Figure 4A). The associations of ADO score with ten cancer hallmarks signatures were analyzed (Figure 4B). Patients with high ADO scores had higher tissue invasion and metastasis, sustained angiogenesis, self-sufficiency of growth signals, but lower genome instability than those with low ADO scores (all adjusted P values < 0.01, Figure 4B, Supplementary Table 6). For ovarian cancer, patients with high genome instability tend to prolong OS (27, 28). Consistently, we found that patients with high HRD score had better prognosis (Log-rank P < 0.001, Supplementary Figure 4).

In order to explore the association between ADO scores and immune microenvironment, five immune signatures algorithms were applied. The heatmap showed that the high ADO group had enriched immunosuppressive cells, including stromal cells and CAF, while the low ADO group had enriched immune activating cells, including cytotoxic cells and M1 macrophage cells (adjusted P value = 0.01 for stromal cells, <0.001 for CAF, <0.001 for cytotoxic cells, 0.03 for M1 macrophage cells,

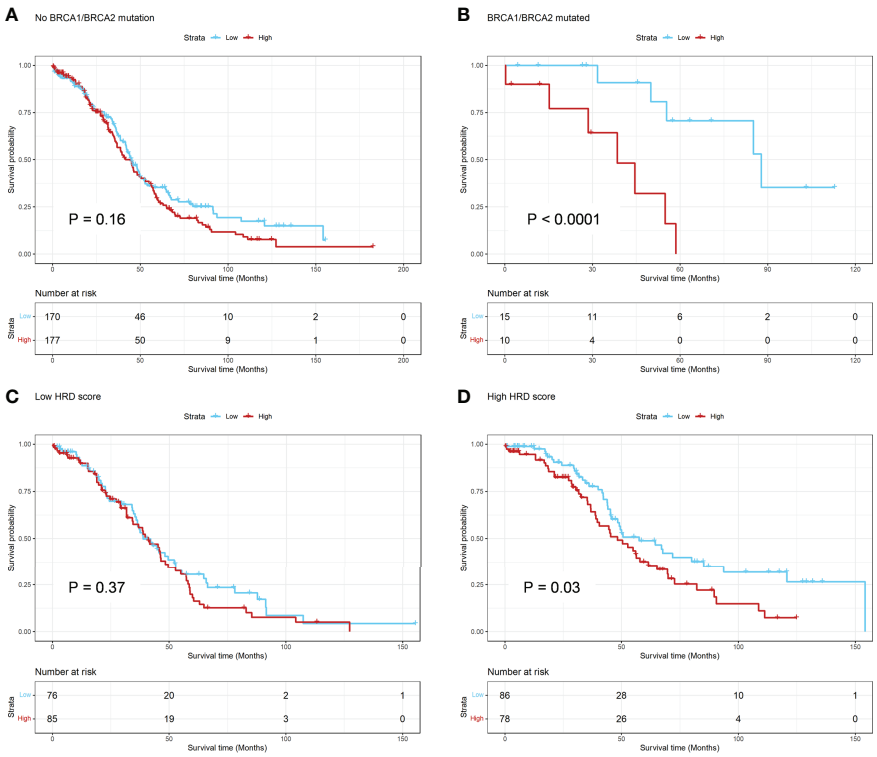

FIGURE 3
Hierarchical Analysis for BRCA1/2 mutation and HRD Score in TCGA dataset. **(A, B)** The Kaplan-Meier survival curve of OS between the ADO groups for subgroups of patients with or without BRCA1/2 mutation, respectively; **(C, D)** The Kaplan-Meier survival curve of OS between the ADO groups for subgroups of patients with low or high HRD score, respectively.

Figure 4C, Supplementary Figure 5, Supplementary Table 6). Besides, for the immune checkpoint genes, compared with low ADO group, the high ADO group had higher expression of CD276, but lower expression of other genes, including CD40, IDO1, LAG3 and TIGIT (adjusted P value = 0.001, 0.02, <0.001, 0.05 and 0.02 respectively, Figure 4D, Supplementary Table 6). Further, based on the TIDE algorithm which could estimate the overall immune status, similar results were found. In detail, IFNG, representative of immune activating status was significantly higher in low ADO group than in high ADO group, while the signatures of T cell dysfunction, T cell exclusion and CAF were significantly lower in low ADO group (all adjusted P values < 0.001, Figure 4E, Supplementary Table 6).

The association between ADO score and drug sensitivity in GDSC dataset

We constructed ADO score based on the expression data of DGSC ovarian cancer cell lines and calculated the Pearson correlation between ADO score and IC50 of 180 drugs. A total of 26 cell lines was used to obtain the IC50 (Supplementary Table 7). IC50 of 65 drugs was significantly associated with ADO score after Benjamini-Hochberg correction (adjusted P value < 0.05, Figure 5A**)**. The detailed adjusted P values are shown in Supplementary Table 8. High ADO score group had significant higher IC50 than low ADO score group for conventional drugs, including Talazoparib, Paclitaxel and Olaparib (adjusted P value = 0.04, 0.04 and 0.05 respectively, Figure 5B), while not for Cisplatin and Docetaxel (adjusted P value = 0.10 and 0.10 respectively, Figure 5B). For MK-1775 (WEE1 Inhibitor) which was researched in a phase II clinical trials (29), high ADO score group also had significant higher IC50 than low ADO score group (adjusted P value = 0.007 and 0.05, Figure 5B).

Discussion

In this study, an ADO metabolism related gene signature was constructed based on TCGA dataset to predict prognosis of ovarian cancer, and was validated in six GEO dataset. Moreover, compared with the low ADO score group, the high ADO score group with worse prognosis had lower genome instability, higher immunosuppressive signatures and tended to be insensitive to olaparide and paclitaxel.

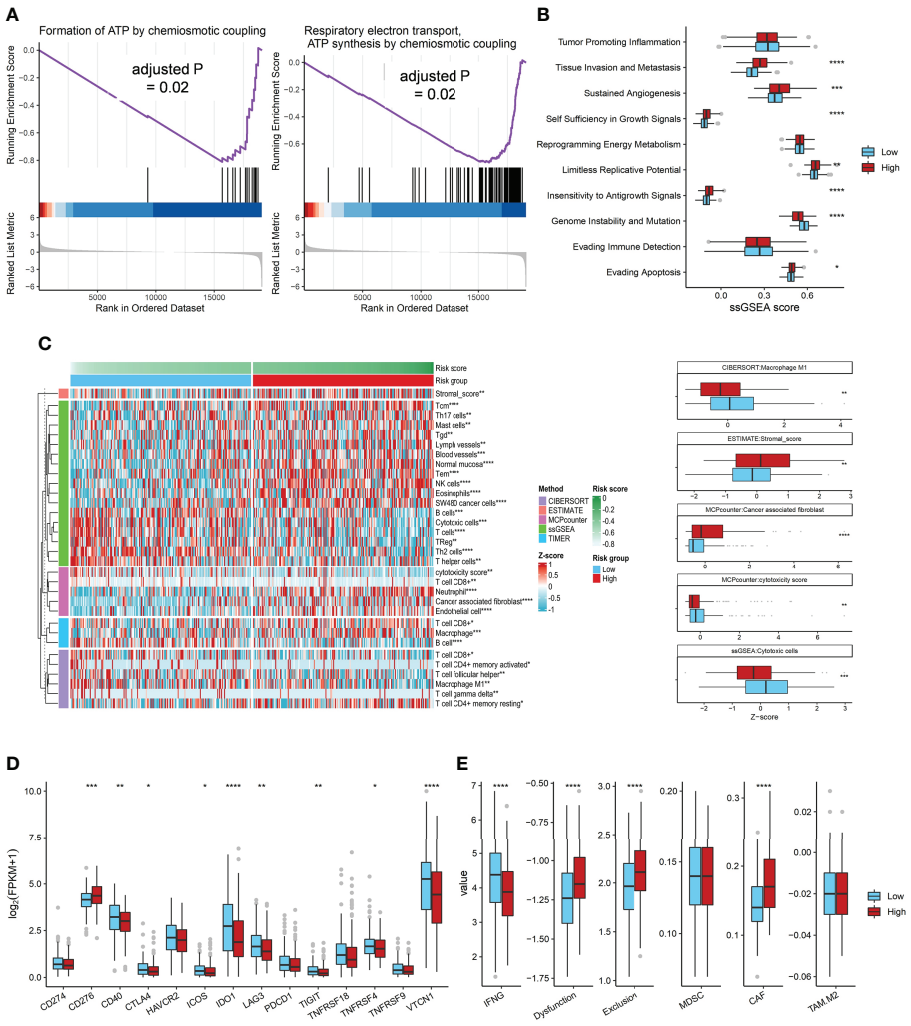

FIGURE 4
The Association of ADO score with biological signatures or immune genes expression in TCGA dataset. **(A)** Two significantly enriched ATP synthesis pathways in the low ADO group by GSEA; **(B)** Boxplots of the ssGSEA score of 10 cancer hallmarks signatures between two ADO groups; **(C)** Heatmap and boxplots of the infiltrated immune signatures score based on five algorithms; **(D)** Boxplots of immune checkpoint genes expression between two ADO groups; **(E)** Boxplots of the T cells dysfunction and exclusion signatures from TIDE algorithm between two ADO groups. (*P < 0.05, **P < 0.01, ***P < 0.001, ****P < 0.0001).

Tumor growth requires a lot of energy which mainly comes from the degradation of ATP (30). In this process, a large amount of ADO was produced due to the mediation of CD73-CD39 axis. Hypoxia, chronic inflammation and nutrient deprivation are all catalysts for the generation of ADO (31–33) which can promote tumor cell proliferation, inflammatory response, neo-angiogenesis, tumor invasion and metastasis, and EMT transformation through interplay with the corresponding G protein-coupled receptors (34–36). In this study, we observed that the low ADO score group, rather than the high ADO score group was enriched for genes in ATP synthesis related pathways which suggested that the high ADO score group tended to accumulate more ADO. Further, based on the cancer hallmarks analysis, the high ADO score group had higher signatures in tissue invasion and metastasis pathway, sustained angiogenesis pathway and the insensitivity to antigrowth signals pathway than the low ADO score group. All evidence supported that patients with high ADO score would suffer a worse prognosis.

Subsequently, we noticed that the high ADO score group showed an immunosuppressive state. Previous literature has reported that tumor cells tended to accumulate eADO in the tumor core to create an immunosuppressive microenvironment (8, 37). Interestingly, in the high ADO score group, the expression level of immune effector molecule IFNG decreased significantly, while the level of NK cells, a main member of

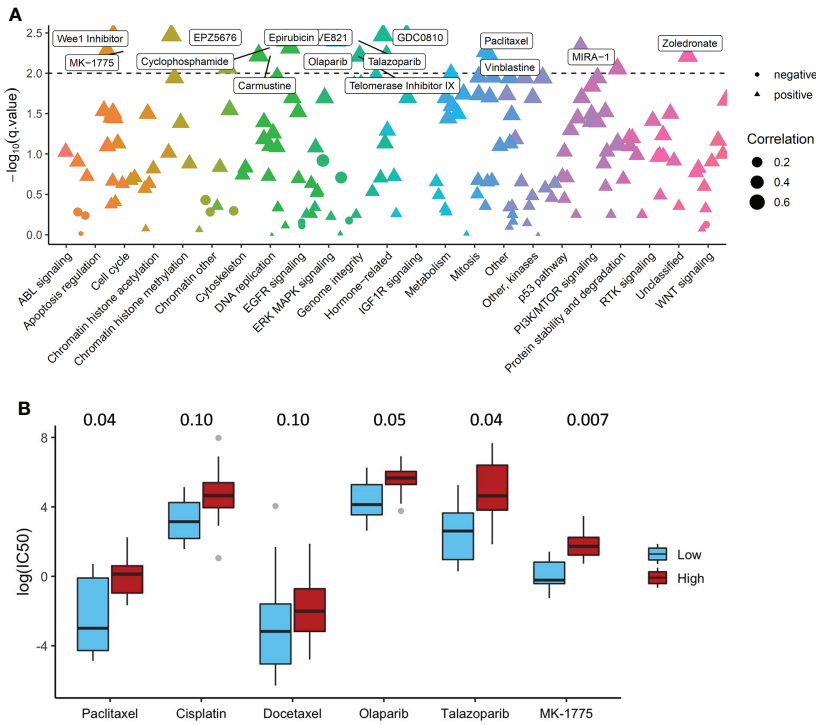

FIGURE 5
The Association of ADO score with Drug Sensitivity in GDSC dataset. **(A)** The Pearson correlation between ADO score and IC50 of the drugs in different biological pathways; **(B)** Boxplots of the IC50 for conventional and investigational drugs (P values were adjusted by Benjamini-Hochberg).

tumor killing cells, was relatively high. Molecular mechanism related studies showed that although the NK cells gathered at the tumor site, they were prevented from killing tumor cells by eADO and A2AR hindering the nutritional, promoting and cytolytic activities of NK cells, and finally inhibiting the production of IFNG (38, 39). Besides, the level of immune CAF signature was higher in the high ADO score group, which was consistent with the previous finding that CD73 was often highly expressed in the stroma of ovarian tumor tissue samples, probably CAFs (10). There have been a lot of clinical trials to develop anti-CD73 drugs to improve the effectiveness of anti-PD-1/PD-L1 immune therapy (40). Furthermore, we also observed that the high ADO score group had higher PD-L1 gene expression and might be insensitive to most conventional drugs, including chemotherapy, PARP inhibitor and other targeted drugs. Therefore, for patients with high ADO scores, the combination of anti-CD73 and anti-PD-1/PD-L1 immune therapy might be a potential treatment selection. Definitely, more molecular studies and clinical trials are needed to verify the hypothesis.

In the hierarchical analysis, it showed that ADO score tended to be significantly associated with prolonged survival only in BRCA1/2 mutant or HRD patients. As is well-known, HRD including BRCA1/2 mutation is one biomarker to measure the genomic instability (41), a hallmark of human cancer. It has been demonstrated that the ADO pathway was related to genomic instability. ENPP1, a gene with the function of hydrolyzing the extracellular cGAMP was increasingly expressed in cancer cells with genomic instability (42). Moreover, genomic errors contributed by HRD could lead to the formation of micronuclear envelopes which are highly rupture-prone and further produce cytosolic double-stranded DNA (dsDNA) (43). Then, cytosolic dsDNA is sensed by cGAS to be converted to the cyclic dinucleotide cGAMP, which could be catalyzed by ENPP1 and NT5E to form adenosine (42). Consistent with the results, in HRD subgroup, high ADO score group had higher gene expression of ENPP1 and NT5E expression and was relatively less enriched for genes in ATP synthesis, which leaded to more immunosuppressive adenosine accumulation and worse prognosis. However, the sample size in BRCA1/2 mutant or HRD patients was limited in this study and more evidence was needed to confirm this finding. Furthermore, we found that high score group seemed to be insensitive to PARP inhibitors and WEE1 inhibitors. The mechanism for both types of drugs is to inhibit DNA damages repair, increase genomic instability and trigger cell apoptosis (29, 44), which might increase cytosolic dsDNA production and promote the immunosuppressive adenosine formation in high ADO score

group featured with ATP degradation. Therefore, for high ADO score group, it was a potential research topic to explore whether combination treatment could be a more appropriate choice.

In this study, we constructed an ADO metabolism related gene signature and explore its association with prognosis, immune signatures and drug sensitivity. However, there were still some limitations in our study. Firstly, this study was a retrospective analysis of public databases. However, our findings were validated in six independent cohorts to reduce false-positive results and further explained by the association with cancer hallmarks and immune signatures to confirm the rationality of the ADO signature. Secondly, the censor rate was high in the TCGA cohort, but it was not significantly different between ADO groups (High vs Low: 34.22% vs 42.7%, P = 0.10) which reduced the impact on the survival analysis. Thirdly, although the multivariable model involved all the available clinical features as confounders, there might be other unexpected confounders. Fourthly, the mRNA expression in our study was based on different platforms, such as RNAseq or microarray, so the evidence would be more solid if it was validated with a single method, especially RT-PCR or IHC. Fifthly, the drug sensitivity analysis was based on cell lines data. Therefore, the value of ADO score in the choice of treatment strategies for ovarian cancer remains need to be further explored in clinical trials. In the future, prospective studies with large sample sizes are required to confirm the clinical utility of ADO score.

In conclusion, we studied the relationship between the expression of ADO metabolism related genes and the prognosis of patients with ovarian cancer. ADO score was constructed to predict prognosis and had the potential to guide the treatment selection. More studies are needed to further confirm the clinical value of ADO score.

Data availability statement

Publicly available datasets were analyzed in this study. This data can be found here: www.ncbi.nlm.nih.gov/gds portal.gdc.cancer.gov www.cancerrxgene.org.

Author contributions

The authors confirm contribution to the paper as follows: study conception and design: LC, PZ and WL; data collection: CZ, JW, JZ, CX, YZ, WW and YH; analysis and interpretation of results: WL, CZ, JW, JZ, FL, GW, SC, LC and PZ; and draft manuscript preparation: all authors. All authors contributed to the article and approved the submitted version.

Acknowledgments

We thank all the volunteer patients, staffs and researchers in TCGA, GEO and GDSC for their contribution to the research data.

Conflict of interest

The authors declare that the research was conducted in the absence of any commercial or financial relationships that could be construed as a potential conflict of interest.

Publisher's note

All claims expressed in this article are solely those of the authors and do not necessarily represent those of their affiliated organizations, or those of the publisher, the editors and the reviewers. Any product that may be evaluated in this article, or claim that may be made by its manufacturer, is not guaranteed or endorsed by the publisher.

Supplementary material

The Supplementary Material for this article can be found online at: https://www.frontiersin.org/articles/10.3389/fonc.2022.1003512/full#supplementary-material

SUPPLEMENTARY TABLE 1
Annotation of 22 adenosine metabolism related genes.

SUPPLEMENTARY TABLE 2
Description of clinical information for seven cohorts.

SUPPLEMENTARY TABLE 3
The detailed results of survival analysis from the univariate and multivariate Cox regression model.

SUPPLEMENTARY TABLE 4
The hierarchical meta-analysis of clinical features in GEO datasets.

SUPPLEMENTARY TABLE 5
The detailed results of the Cox regression model for hierarchical analysis based on BRCA1/2 mutation and HRD score.

SUPPLEMENTARY TABLE 6
The detailed correlation of ADO score groups and gene signatures.

SUPPLEMENTARY TABLE 7
The cell line list.

SUPPLEMENTARY TABLE 8
The correlation between the ADO signature and IC50 for 180 drugs in ovarian cell lines.

References

1. Alexandrova E, Pecoraro A, Sellitto V, Melone C, Ferravante T, Rocco , et al. An overview of candidate therapeutic target genes in ovarian cancer. *Cancers (Basel)* (2020) 12(6):1470. doi: 10.3390/cancers12061470

2. Sung H, Ferlay J, Siegel RL, Laversanne M, Soerjomataram I, Jemal A, et al. Global cancer statistics 2020: GLOBOCAN estimates of incidence and mortality worldwide for 36 cancers in 185 countries. *CA Cancer J Clin* (2021) 71(3):209–49. doi: 10.3322/caac.21660

3. Hubbell E, Clarke CA, Aravanis AM, Berg CD. Modeled reductions in late-stage cancer with a multi-cancer early detection test. *Cancer Epidemiol Biomarkers Prev* (2021) 30(3):460–8. doi: 10.1158/1055-9965.EPI-20-1134

4. Kuroki L, Guntupalli SR. Treatment of epithelial ovarian cancer. *BMJ* (2020) 371:m3773. doi: 10.1136/bmj.m3773

5. Cortez AJ, Tudrej P, Kujawa KA, Lisowska KM. Advances in ovarian cancer therapy. *Cancer Chemother Pharmacol* (2018) 81(1):17–38. doi: 10.1007/s00280-017-3501-8

6. Siegel RA-O, Miller KA-O, Fuchs HE, Jemal A. Cancer statistics. *CA Cancer J Clin* (2022) 72(1):7–33. doi: 10.3322/caac21708

7. Hardie DG. Adenosine monophosphate-activated protein kinase: a central regulator of metabolism with roles in diabetes, cancer, and viral infection. *Cold Spring Harb Symp Quant Biol* (2011) 76:155–64. doi: 10.1101/sqb.2011.76.010819

8. Boison D, Yegutkin GG. Adenosine metabolism: Emerging concepts for cancer therapy. *Cancer Cell* (2019) 36(6):582–96. doi: 10.1016/j.ccell.2019.10.007

9. Turcotte M, Spring K, Pommey S, Chouinard G, Cousineau I, George J, et al. CD73 is associated with poor prognosis in high-grade serous ovarian cancer. *Cancer Res* (2015) 75(21):4494–503. doi: 10.1158/0008-5472.CAN-14-3569

10. Gaudreau PO, Allard B, Turcotte M, Stagg J. CD73-adenosine reduces immune responses and survival in ovarian cancer patients. *Oncoimmunology* (2016) 5(5):e1127496. doi: 10.1080/2162402X.2015.1127496

11. Leone RD, Emens LA. Targeting adenosine for cancer immunotherapy. *J Immunother Cancer* (2018) 6(1):57. doi: 10.1186/s40425-018-0360-8

12. Sorrentino C, Miele L, Porta A, Pinto A, Morello S. Myeloid-derived suppressor cells contribute to A2B adenosine receptor-induced VEGF production and angiogenesis in a mouse melanoma model. *Oncotarget* (2015) 6 (29):27478–89. doi: 10.18632/oncotarget.4393

13. Bednarska-Szczepaniak K, Krzyzanowski D, Klink M, Nowak M. Adenosine analogues as opposite modulators of the cisplatin resistance of ovarian cancer cells. *Anticancer Agents Med Chem* (2019) 19(4):473–86. doi: 10.2174/1871520619666190118113201

14. Iorio F, Knijnenburg TA, Vis DJ, Bignell GR, Menden MP, Schubert M, et al. A landscape of pharmacogenomic interactions in cancer. *Cell* (2016) 166(3):740–54. doi: 10.1016/j.cell.2016.06.017

15. Gaujoux R, Seoighe C. A flexible r package for nonnegative matrix factorization. *BMC Bioinf* (2010) 11:367. doi: 10.1186/1471-2105-11-367

16. Brunet JP, Tamayo P, Golub TR, Mesirov JP. Metagenes and molecular pattern discovery using matrix factorization. *Proc Natl Acad Sci U.S.A.* (2004) 101 (12):4164–9. doi: 10.1073/pnas.0308531101

17. Wilkerson MD, Hayes DN. ConsensusClusterPlus: a class discovery tool with confidence assessments and item tracking. *Bioinformatics* (2010) 26 (12):1572–3. doi: 10.1093/bioinformatics/btq170

18. Hänzelmann S, Castelo R, Guinney J. GSVA: gene set variation analysis for microarray and RNA-seq data. *BMC Bioinf* (2013) 14:7. doi: 10.1186/1471-2105-14-7

19. Marquard AM, Eklund AC, Joshi T, Krzystanek M, Favero F, Wang ZC, et al. Pan-cancer analysis of genomic scar signatures associated with homologous recombination deficiency suggests novel indications for existing cancer drugs. *biomark Res* (2015) 3:9. doi: 10.1186/s40364-015-0033-4

20. Plaisier CL, Pan M, Baliga NS. A miRNA-regulatory network explains how dysregulated miRNAs perturb oncogenic processes across diverse cancers. *Genome Res* (2012) 22(11):2302–14. doi: 10.1101/gr.133991.111

21. Newman AM, Liu CL, Green MR, Gentles AJ, Feng W, Xu Y, et al. Robust enumeration of cell subsets from tissue expression profiles. *Nat Methods* (2015) 12 (5):453–7. doi: 10.1038/nmeth.3337

22. Yoshihara K, Shahmoradgoli M, Martínez E, Vegesna R, Kim H, Torres-Garcia W, et al. Inferring tumour purity and stromal and immune cell admixture from expression data. *Nat Commun* (2013) 4:2612. doi: 10.1038/ncomms3612

23. Becht E, Giraldo NA, Lacroix L, Buttard B, Elarouci N, Petitprez F, et al. Estimating the population abundance of tissue-infiltrating immune and stromal cell populations using gene expression. *Genome Biol* (2016) 17(1):218. doi: 10.1186/s13059-016-1070-

24. Barbie DA, Tamayo P, Boehm JS, Kim SY, Moody SE, Dunn IF, et al. Systematic RNA interference reveals that oncogenic KRAS-driven cancers require TBK1. *Nature* (2009) 462(7269):108–12. doi: 10.1038/nature08460

25. Li T, Fan J, Wang B, Traugh N, Chen Q, Liu JS, et al. TIMER: A web server for comprehensive analysis of tumor-infiltrating immune cells. *Cancer Res* (2017) 77(21):e108–10. doi: 10.1158/1538-7445.AM2017-108

26. Jiang P, Gu S, Pan D, Fu J, Sahu A, Hu X, et al. Signatures of T cell dysfunction and exclusion predict cancer immunotherapy response. *Nat Med* (2018) 24(10):1550–8. doi: 10.1038/s41591-018-0136-1

27. Persi E, Wolf YI, Leiserson MDM, Koonin EV, Ruppin E. Criticality in tumor evolution and clinical outcome. *Proc Natl Acad Sci U.S.A.* (2018) 115(47): E11101–10. doi: 10.1073/pnas.1807256115

28. Birkbak NJ, Kochupurakkal B, Izarzugaza JM, Eklund AC, Li Y, Liu J, et al. Tumor mutation burden forecasts outcome in ovarian cancer with BRCA1 or BRCA2 mutations. *PloS One* (2013) 8(11):e80023. doi: 10.1371/journal.pone.0080023

29. Lheureux S, Cristea MC, Bruce JP, Garg S, Cabanero M, Mantia-Smaldone G, et al. Adavosertib plus gemcitabine for platinum-resistant or platinum-refractory recurrent ovarian cancer: a double-blind, randomised, placebo-controlled, phase 2 trial. *Lancet* (2021) 397(10271):281–92. doi: 10.1016/S0140-6736(20)32554-X

30. Qian Y, Wang X, Li Y, Cao Y, Chen X. Extracellular ATP a new player in cancer metabolism: NSCLC cells internalize ATP in vitro and in vivo using multiple endocytic mechanisms. *Mol Cancer Res* (2016) 14(11):1087–96. doi: 10.1158/1541-7786.MCR-16-0118

31. Wu CA, Chao Y, Shiah SG, Lin WW. Nutrient deprivation induces the warburg effect through ROS/AMPK-dependent activation of pyruvate dehydrogenase kinase. *Biochim Biophys Acta* (2013) 1833(5):1147–56. doi: 10.1016/j.bbamcr.2013.01.025

32. Yin X, Motorwala A, Vesvoranan O, Levene HB, Gu W, Huang CY. Effects of glucose deprivation on ATP and proteoglycan production of intervertebral disc cells under hypoxia. *Sci Rep* (2020) 10(1):8899. doi: 10.1038/s41598-020-65691-w

33. Garcia-Faroldi G, Sanchez-Jimenez F, Fajardo I. The polyamine and histamine metabolic interplay in cancer and chronic inflammation. *Curr Opin Clin Nutr Metab Care* (2009) 12(1):59–65. doi: 10.1097/MCO.0b013e328314b9ac

34. Allard B, Turcotte M, Spring K, Pommey S, Royal I, Stagg J. Anti-CD73 therapy impairs tumor angiogenesis. *Int J Cancer* (2014) 134(6):1466–73. doi: 10.1002/ijc.28456

35. Gao ZW, Wang HP, Lin F, Wang X, Long M, Zhang HZ, et al. CD73 promotes proliferation and migration of human cervical cancer cells independent of its enzyme activity. *BMC Cancer* (2017) 17(1):135. doi: 10.1186/s12885-017-3128-5

36. Xiong L, Wen Y, Miao X, Yang Z. NT5E and FcGBP as key regulators of TGF-1-induced epithelial-mesenchymal transition (EMT) are associated with tumor progression and survival of patients with gallbladder cancer. *Cell Tissue Res* (2014) 355(2):365–74. doi: 10.1007/s00441-013-1752-1

37. Vijayan D, Young A, Teng MWL, Smyth MJ. Targeting immunosuppressive adenosine in cancer. *Nat Rev Cancer* (2017) 17(12):765. doi: 10.1038/nrc.2017.86

38. Yan J, Li XY, Aguilera Roman A, Xiao C, Jacoberger-Foissac C, Nowlan B, et al. Control of metastases via myeloid CD39 and NK cell effector function. *Cancer Immunol Res* (2020) 8(3):356–67. doi: 10.1158/2326-6066.CIR-19-0749

39. Qin L, Thompson LF, Kuzel TM, Zhang B. Requirement of NK cells for selective A2A receptor blockade to suppress CD73+ tumor metastasis. *Immunotherapy* (2014) 6(1):19–21. doi: 10.2217/imt.13.154

40. Tu E, McGlinchey K, Wang J, Martin P, Ching SL, Floc'h N, et al. Anti-PD-L1 and anti-CD73 combination therapy promotes T cell response to EGFR-mutated NSCLC. *JCI Insight* (2022) 7(3):e142843. doi: 10.1172/jci.insight.142843

41. Sokol ES, Pavlick D, Khiabanian H, Frampton GM, Ross JS, Gregg JP, et al. Pan-cancer analysis of BRCA1 and BRCA2 genomic alterations and their association with genomic instability as measured by genome-wide loss of heterozygosity. *JCO Precis Oncol* (2020) 4:442–65. 10.1200/po1900345

42. Li J, Duran MA, Dhanota N, Chatila WK, Bettigole SE, Kwon J, et al. Metastasis and immune evasion from extracellular cGAMP hydrolysis. *Cancer Discov* (2021) 11(5):1212–27. doi: 10.1158/2159-8290CD-20-0387

43. Bakhoum SF, Ngo B, Laughney AM, Cavallo JA, Murphy CJ, Ly P, et al. Chromosomal instability drives metastasis through a cytosolic DNA response. *Nature* (2018) 553(7689):467–72. doi: 10.1038/nature25432

44. Mirza MR, Coleman RL, González-Martín A, Moore KN, Colombo N, Ray-Coquard I, et al. The forefront of ovarian cancer therapy: update on PARP inhibitors. *Ann Oncol* (2020) 31(9):1148–15. doi: 10.1016/j.annonc.2020.06.004

frontiers | Frontiers in Oncology

TYPE Original Research
PUBLISHED 11 January 2023
DOI 10.3389/fonc.2022.1064722

OPEN ACCESS

EDITED BY
Gabriella Lillsunde Larsson,
Örebro University, Sweden

REVIEWED BY
Stephanie M. McGregor,
University of Wisconsin-Madison,
United States
Adriana Campaner,
Santa Casa of Sao Paulo, Brazil

*CORRESPONDENCE
Lihui Wei
weilh@bjmu.edu.cn

†These authors have contributed equally to this work and share first authorship

SPECIALTY SECTION
This article was submitted to Gynecological Oncology, a section of the journal Frontiers in Oncology

RECEIVED 08 October 2022
ACCEPTED 22 December 2022
PUBLISHED 11 January 2023

CITATION
Li M, Zhao C, Zhao Y, Li J, Wang J, Luo H, Tang Z, Guo Y and Wei L (2023) The role of PAX1 methylation in predicting the pathological upgrade of cervical intraepithelial neoplasia before cold knife conization.
Front. Oncol. 12:1064722.
doi: 10.3389/fonc.2022.1064722

The role of PAX1 methylation in predicting the pathological upgrade of cervical intraepithelial neoplasia before cold knife conization

Mingzhu Li†, Chao Zhao†, Yun Zhao, Jingran Li, Jingyuan Wang, Hongxue Luo, Zhijian Tang, Yan Guo and Lihui Wei*

Department of Obstetrics and Gynecology, Peking University People's Hospital, Beijing, China

Objective: To explore the ability of PAX1 methylation ($PAX1^m$) to predict the pathological upgrade of cervical intraepithelial neoplasia (CIN) before cold knife conization (CKC).

Methods: A total of 218 women that underwent colposcopy-directed biopsy (CDB) pathology for the confirmation of CIN2 and CIN3 between December 2020 to September 2021 were enrolled in this study. The methylation levels of PAX1 (ΔCp_{PAX1}) were determined by quantitative methylation-specific polymerase chain reaction (qMSP). Receiver operating characteristic curve was used to identify the optimal cut-off value of ΔCp_{PAX1} for predicting the pathological upgrade of disease.

Results: In the CDB-confirmed CIN2 group, 36% of CIN2 was found to have pathologically upgraded to CIN3 and 30% regressed to low-grade squamous intraepithelial lesion (LSIL) and below, and none of CIN2 upgraded to early-stage cervical cancer (ESCC) after CKC. In the CDB-confirmed CIN3 group, 19.5% (23/118) of CDB-confirmed CIN3 were pathologically upgraded to ESCC after CKC. Regardless of CIN2 or CIN3, the ΔCp_{PAX1} level of women with upgraded pathology after CKC was significantly lower than that of women with degraded pathology. The optimal $\triangle Cp_{PAX1}$ cut-off value in predicting CIN3 to be upgraded to ESCC after CKC was 6.360 and the area under the curve (AUC) was 0.814, with similar sensitivity (78.3%) and higher specificity (84.2%) than cytology≥LSIL (Se:78.3%;Sp:58.9%) and HPV16/18 positive (Se:73.9%;Sp:46.3%) patients.

Conclusions: $PAX1^m$ could be a promising auxiliary marker in predicting the pathological upgrade of CIN before CKC. We found that if the $\triangle Cp_{PAX1}$ cut-off value is lower than 6.360, it is highly suggestive of invasive cervical cancer.

KEYWORDS

cervical intraepithelial neoplasia, cold knife conization, PAX1, methylation, pathological upgrade

1 Introduction

Persistent infection of high-risk human papillomavirus (hr-HPV) is an important risk factor for the development of cervical intraepithelial neoplasia (CIN) and cervical cancer. In 2020, the World Health Organization (WHO) classification of female genital tumours was updated from the original three-level classification of cervical intraepithelial neoplasia (CIN1, CIN2, CIN3) to a two-level classification that included low-grade squamous intraepithelial lesions (LSIL/CIN1) and high-grade squamous intraepithelial lesions (HSIL/CIN2 and CIN3) (1). HSIL is recognized as the true precancer with a higher risk of progression. However, it is difficult to determine whether or when a patient with HSIL will progress to invasive cervical cancer from an individual perspective, in fact, some patients may already have occult cervical cancer when diagnosed with HSIL. HSIL are primarily treated with cervical conization, including cervical cold knife conization (CKC) or loop electrode excision procedure (LEEP). On the other hand, most CIN2 lesions (60%), particularly in young women (<30 years), regress spontaneously, indicating that active surveillance, rather than immediate intervention, is justified, especially if patients adhere to monitoring (2). However, there are some limitations in the consistency between pathological assessment *via* colposcopy-directed biopsy(CDB) and final pathological diagnosis after conization, with an upgrade rate of 23.1% and degrade rate of 33.6% post-conization pathology (3).

To date, there are no accurate tests to determine whether CIN lesions have a tendency to regress or progress. The HPV genotype present in affected patients could not provide additional information to predict high-grade disease progression (4). Although the proportion of severe lesions caused by HPV16/18 has increased over time, its potential for progression remains uncertain (5, 6). Gene methylation is a kind of epigenetic modification that can contribute to the accumulation of mutated genes over time and methylation may play an important role in tumor genesis and progression. As such, using methylation as a marker due to its high sensitivity for cancer has potential as a primary screening tool. It may also be used for the management of women with CIN lesions to prevent overtreatment of CIN2/CIN3 lesions (7).

In particular, the efficacy of paired boxed gene 1 (PAX1) methylation ($PAX1^m$) as a biomarker for the detection of CIN3 or worse (CIN3+) has been demonstrated in various studies (8–10). $PAX1^m$ can be used as a triage method for women with atypical squamous cells of undetermined significance (ASCUS) and has shown better diagnostic performance than HPV-DNA in predicting CIN2+ (11). Besides, $PAX1^m$ has a comparable clinical performance to cytology and better accuracy and specificity than HPV16/18 as a triage tool for detecting CIN3+ in women with hr-HPV (12). $PAX1^m$ has also been reported to predict the efficacy of concurrent chemo-radiotherapy in cervical cancer (13), and is a potential biomarker for monitoring the prognosis of cervical adenocarcinoma (14). However, few studies have evaluated PAX1 gene methylation before conization, it has been previously reported that $PAX1^m$ would be a suitable alternative method to conventional options and it has the ability to predict the outcome of conization in CIN3 cases (15). However, the role of $PAX1^m$ in predicting the pathological upgrade of CIN2 is unclear. In this study, we aim to investigate the predictive value of $PAX1^m$ status in determining the upgrade tendency of CIN2 and CIN3. This information would help patients and doctors make more individualized treatment decisions.

2 Materials and methods

2.1 Participants, study design, and sample collection

In total, 247 women with pathologically confirmed HSIL by CDB were included in this study at the Peking University People's Hospital between December 2020 to September 2021. The exclusion criteria were as follows: (1) CDB revealed the presence of squamous cell cancer, adenocarcinoma *in situ* (AIS), or adenocarcinoma, (2) inability to undergo CKC, (3) inadequate DNA concentration in cell samples, (3) HSIL in patients who were also pregnant, had immune system diseases, or receiving immunosuppressive therapy, (4) patients that had a history of cervical disease treatment, hysterectomy, or chemoradiotherapy. Of the 247 women with CDB-confirmed HSIL, 16 cases of CIN2 and 4 of CIN3 chose observational follow-up rather than CKC and 9 cases were determined to have AIS. Therefore, a total of 218 women with pathologically confirmed HSIL by CDB were included in this study.

Exfoliated cervical cell samples were collected after biopsy pathology had confirmed HSIL within 7 days before the CKC procedure. Briefly, a vaginal speculum was placed to expose the cervix and cervical exfoliation was performed at the squamocolumnar junction of the cervix using a sampling brush. The sampling brush was then placed into a 20mL PreservCyt1 solution (Hologic, Marlborough Mass, USA, DOC sample) for testing. All specimens were tested for cytology, HPV detection, and PAX1 methylation. We informed patients of the research programs and obtained written consent before CKC. The study was approved by the Institutional Review Board of Peking University People's Hospital (2020PHB298-01).

2.2 Quantitative methylation-specific PCR

Cervical exfoliated cells were centrifuged and stored in phosphate-buffered saline at -20°C. Genomic DNA was extracted using standard protocols and then converted to

bisulfite form using the EZ DNA Methylation-Gold kits (Zymo Research, Irvine, CA, USA). Quantitative methylation-specific PCR (qMSP) was performed using a Light Cycler LC480 system (Roche Applied Science, Penzberg, Germany) to determine the methylation level of PAX1 according to the manufacturer's instructions (Hoomya Ltd, Hunan, P.R China). Type II collagen gene (COL2A) was used as an internal reference. The △Cp is the difference between the △Cp values for PAX1 and COL2A. The methylation level (△Cp) was assessed by the following formula: △Cp=Cp target gene - Cp Col2A (16). A smaller $\triangle Cp_{PAX1}$ value denotes a higher degree of PAX1 methylation detected in the collected samples.

2.3 HPV genotyping

Type-specific HR-HPV viral genotyping was simultaneously measured using a BioPerfectus Multiplex Real-Time PCR (BMRT) assay. BMRT is a PCR-based assay for the detection of high-risk HPV strains and it was performed using a fluorescence-based multiplex HPV DNA genotyping kit (Bioperfectus Ltd, Jiangsu, P.R. China). This assay can detect 14 high-risk HPV subtypes (HPV 16, 18, 31, 33, 35, 39, 45, 51, 52, 56, 58, 59, 66, and 68) and 7 medium- and low-risk subtypes. For this study, all types specifically refer to high-risk HPV.

2.4 Pathological diagnosis of upgraded disease after conization

Colposcopic impressions were made according to the American Society for Colposcopy and Cervical Pathology (ASCCP) standard, multiple biopsies targeting all areas with acetowhitening, metaplasia, or higher abnormalities are recommended. At least 2-4 targeted biopsies from distinct acetowhite lesions should be taken (17). A circular knife cut is made 3 mm peripheral to the abnormal transformation zone (ATZ). The knife is angled toward the endocervical canal and cuts deeper into the stroma, the depth of excision depends on the type of TZ according to 2011 Colposcopic Terminology of International Federation for Cervical Pathology and Colposcopy (IFCPC) (18). Cervical biopsy and CKC specimens were histologically examined and classified according to the 2020 WHO classification of female genital tumours (1), which reported as HSIL(CIN2) and HSIL (CIN3), p16 immunohistochemistry was used only in morphologically ambiguous cases when HSIL is suspected according to the guidance provided by the Lower Anogenital Squamous Terminology (LAST) Project (19). The highest pathological grade was taken as the final pathological diagnosis. Pathological upgrade of disease is defined as $CIN2_{CDB}$ (CDB-confirmed CIN2) →$CIN3_{CKC}$ (CKC-confirmed CIN3) and pathology-confirmed $CIN3_{CDB}$ (CDB-confirmed CIN3) →$ESCC_{CKC}$ (CKC-confirmed early-stage cervical cancer). The cervical lesions were diagnosed by two professional pathologists.

2.5 Statistical analysis

The samples were characterized using descriptive statistics in two groups of biopsy diagnosis. The Mann-Whitney test was utilized to analyze the differences between $\triangle Cp_{PAX1}$ levels. We used restricted cubic spline models fitted for logistic odds ratio with 3 knots of $PAX1^m$ using statistical software (rms in R, version 4.1.2) (Supplementary Figure 1). We divided the $\triangle Cp_{PAX1}$ into 3 groups to form grade variables and assigned the group names of Low (1:△Cp >15), Moderate (2: 9 ≤ △Cp ≤ 15), and High (3:△Cp ≤ 9). Logistic regression was used to evaluate the odds ratio (OR) and control for confounding factors (e.g., HPV, cytology) (model 1). The receiver operating characteristic (ROC) curve was used to identify the optimal cut-off value of $PAX1^m$ for predicting pathological upgrade of disease. Sensitivity (Se), specificity (Sp), positive predictive value (PPV), and negative predictive value (NPV) were calculated. Confidence intervals for Se and Sp are Clopper-Pearson confidence intervals. Confidence intervals for the predictive values are the standard logit confidence intervals (20). SPSS software version (Version 26.0, SPSS, Inc, Chicago, IL) were used for statistical analysis. All differences were considered two-sided and statistically significant at $P < 0.05$.

3 Results

Among the 218 women with CDB-confirmed HSIL, 100 cases were $CIN2_{CDB}$ and 118 cases were $CIN3_{CDB}$. The mean age was 40.7 ± 10.8 years (22-69). The median $\triangle Cp_{PAX1}$ was 19.3 (10.5-20.9) and 8.9 (6.0-14.0) in $CIN2_{CBD}$ and $CIN3_{CBD}$, respectively, which was significantly different (Figure 1A). In the $CIN2_{CBD}$ group, 36% of CIN2 was pathologically upgraded to CIN3 and 30% regressed to LSIL and below, none of the CIN2 cases upgraded to SCC after CKC, and the positive margin rate was only 2%. However, in the $CIN3_{CBD}$ group, 19.5% (23/118) of CDB-confirmed CIN3 were pathologically upgraded to ESCC after CKC. The detailed characteristics are presented in Table 1.

After conization, the$\triangle Cp_{PAX1}$ level of $ESCC_{CKC}$ was significantly lower than that of $CIN3_{CKC}$, and that of $CIN3_{CKC}$ was lower than $CIN2_{CKC}$, with statistically significant differences (p<0.001) (Figure 1B). Within the $CIN2_{CDB}$ group, there was no difference in $\triangle Cp_{PAX1}$ between $CIN2_{CDB}$ that had degraded to ≤$CIN1_{CKC}$ and those that had maintained at $CIN2_{CKC}$, but there was a significant difference between those that had maintained at $CIN2_{CKC}$ and those that upgraded to $CIN3_{CKC}$. Among the $CIN3_{CDB}$ group, $\triangle Cp_{PAX1}$levels were significantly lower in those that had upgraded to $ESCC_{CKC}$ than those that had

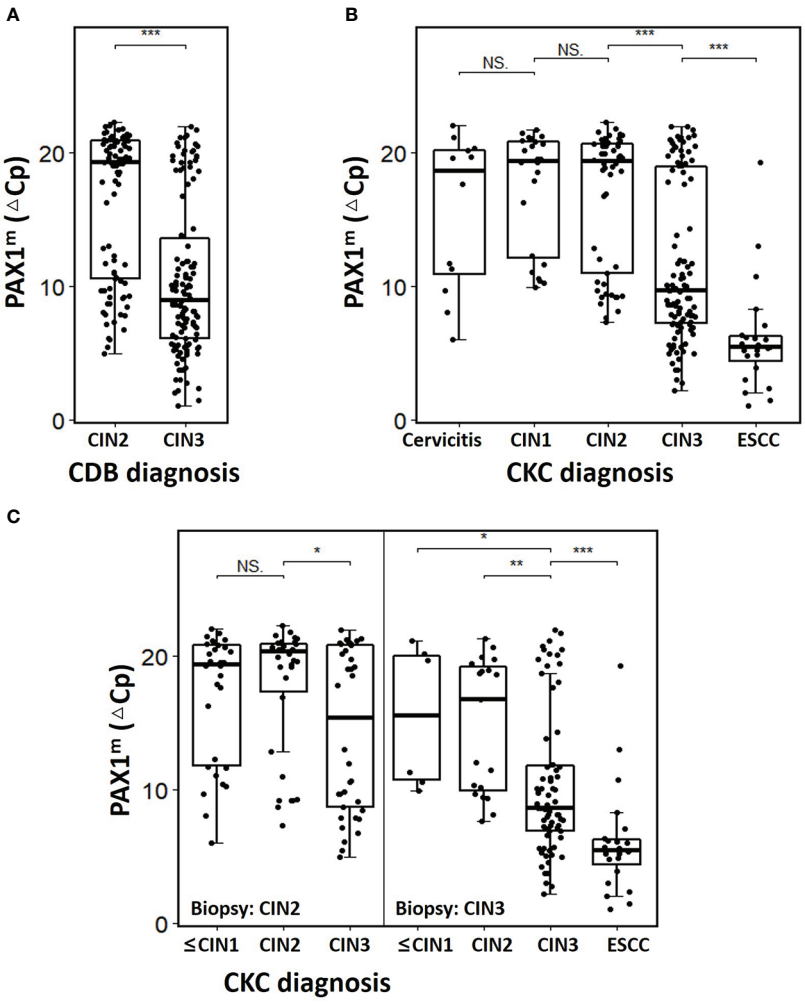

FIGURE 1
The PAX1^{m} distribution of cervical lesions diagnosed by CDB and CKC. **(A)** Comparison of ΔCp_{PAX1} levels of CIN2 and CIN3 diagnosis by CDB; **(B)** Comparison of ΔCp_{PAX1} levels of different cervical lesions diagnosed by CKC; **(C)** Comparison of ΔCp_{PAX1} levels changing in upgraded, maintained, or degraded lesions after CKC. The middle line is the median; the box shows the inter-quartile range (IQR), and the whiskers extend to, at most, 1.5 times the IQR. *p<0.05, **p<0.01, ***p<0.001, NS: not significant.

TABLE 1 Characteristics of CDB pathology-confirmed CIN2 and CIN3.

Characteristics	CIN2 $_{CBD}$ (n = 100)		CIN3 $_{CBD}$ (n = 118)	
	Frequency	Percent	Frequency	Percent
Age median (IQR)	40 (35.2-50.0)		40 (35.5-51.0)	
Cytology				
LSIL-*	79	79.0	69	58.5
ASC-H+^	21	21.0	49	41.5
HR-HPV genotype				
HPV16/18(+)	34	34.0	68	57.6
Other 12 HR-HPV(+)	59	59.0	44	37.3

(Continued)

TABLE 1 Continued

Characteristics	$CIN2_{CBD}$ (n = 100)		$CIN3_{CBD}$ (n = 118)	
	Frequency	Percent	Frequency	Percent
Negative	7	7.0	6	5.1
CKC pathology				
Cervicitis	8	8.0	4	3.4
CIN1	22	22.0	2	1.7
CIN2	34	34.0	19	16.1
CIN3	36	36.0	70	59.3
ESCC	–	–	23	19.5
Margin status				
Negative	98	98.0	90	76.3
Positive	2	2.0	28	23.7

*including negative for intraepithelial lesion or malignancy (NILM), atypical squamous cells of undetermined significance (ASCUS), and low-grade squamous intraepithelial lesion (LSIL); ^including: atypical squamous cells cannot exclude HSIL(ASC-H),atypical glandular cell(AGC), and high-grade squamous intraepithelial lesion(HSIL). CKC, cold knife conization; CIN, cervical intraepithelial neoplasia; ESCC, early-stage cervical cancer; IQR, inter quartile range.

maintained at $CIN3_{CKC}$ and downgraded to $\leq CIN2_{CKC}$ ($p<0.001$) (Figure 1C). Regardless of CIN2 or CIN3 status, $\triangle Cp_{PAX1}$ level of women with upgraded pathology after CKC was significantly lower than that of women with degraded pathology (detailed information see Supplementary Table 1).

When analyzing $PAX1^m$ at different thresholds, it was found that the risk of CIN3+ increased significantly when $\Delta Cp_{PAX1} < 7$, while the trend turns flat when $\Delta Cp_{PAX1} > 15$ (Supplementary Figure 1). We divided the different threshold levels of $PAX1^m$ according to high-, medium-, and low-risk for CIN2+, CIN3+, and ESCC. When ΔCp_{PAX1} was 6.4 (1.1-9.0), the OR values of CIN2+, CIN3+, and ESCC were 12.52 (2.85-55.00), 20.61 (8.08-52.57), and 34.07 (4.45-261.08), respectively. In order to adjust variables that would have effects on $PAX1^m$, we established $PAX1^m{}_{Model\ 1}$(shown in the "Methods" section), and further confirmed that the risk of ESCC, CIN3+, and CIN2+ was still high, and the OR values were 24.85 (3.17-194.67), 19.27 (7.39-50.22), and 11.98 (2.68-53.65), respectively (Table 2), indicating that if ΔCp_{PAX1} less than 6.4, it should be alert for the occurrence of high-grade lesions or even cervical cancer.

The optimal ΔCp_{PAX1} cut-off value in predicting whether CIN3 would upgrade to ESCC after CKC was 6.360 and the area under the curve (AUC) was 0.814 (95% CI: 0.714–0.915), with similar sensitivity (78.3%) but higher specificity (84.2%) than cytology≥ LSIL (Se:78.3%;Sp:58.9%) and HPV16/18 positive (Se:73.9%;Sp:46.3%). The optimal ΔCp_{PAX1} cut-off value in predicting whether CIN2 would upgrade to CIN3 was 10.830 and the AUC was 0.636 (95% CI: 0.515–0.756), with lower sensitivity (44.4%) but higher specificity (82.8%), compared with cytology>ASCUS (Se:44.4%;Sp:45.3%) and HPV positive (Se:97.2%;Sp:9.4%) (Figure 2 and Table 3).

TABLE 2 $PAX1^m$ levels stratified by low-, medium-, and high-risks of CIN2+, CIN3+ and ESCC.

Variable	OR/Adjusted OR (95%CI) [a]			P for trend [b]
$PAX1^m$	Low N = 93	Moderate N = 51	High N = 74	
Median (range)	20.4 (16.3-22.3)	10.6 (9.11-14.35)	6.4 (1.1-9.0)	
OR, CIN2+	1.0	1.43 (0.62-3.28)	12.52 (2.85-55.00)	<0.001
P		0.404	0.001	
OR, CIN3+	1.0	2.21 (1.10-4.44)	20.61 (8.08-52.57)	<0.001
P		0.025	<0.001	
OR, ESCC	1.0	3.76 (0.33-42.46)	34.07 (4.45-261.08)	<0.001

(Continued)

TABLE 2 Continued

Variable	OR/Adjusted OR (95%CI) [a]			P for trend [b]
PAX1 [m]	Low N = 93	Moderate N = 51	High N = 74	
P		0.285	0.001	
PAX1[m] Model 1[c]				
OR, CIN2+	1.0	1.36 (0.58-3.18)	11.98 (2.68-53.65)	<0.001
P		0.473	0.001	
OR, CIN3+	1.0	2.00 (0.98-4.08)	19.27 (7.39-50.22)	<0.001
P		0.056	<0.001	
OR, ESCC	1.0	3.20 (0.27-37.08)	24.85 (3.17-194.67)	<0.001
P		0.353	0.002	

[a] ORs and 95%CI were calculated with the use of the logistic regression.
[b] P for trend, from a 1 degree-of-freedom trend test.
[c] The following variables were included to control for the effects of PAX1[m]: hrHPV [other hrHPV (+) except HPV16/18, HPV16/18 (+)] and cytology (<LSIL, LSIL+).

4 Discussion

In our study, CDB-confirmed CIN2 and CIN3 were stratified to predict pathological progression after CKC. We found that 19.5% (23/118) of the CDB-confirmed CIN3 cases were pathologically upgraded to ESCC after CKC, which was higher than previously reported (15), indicating that CDB alone is insufficient for the diagnosis of microinvasive cervical cancer (21). In the CDB-confirmed CIN2 group, 36% of the CIN2 cases were pathologically upgraded to CIN3 and 30% regressed to LSIL and below, however, none of the CIN2 cases were pathologically upgraded to SCC after CKC. Using accurate tests to determine whether CIN lesions have a tendency to regress or progress is crucial for subsequent disease management.

Prognostic testing for CIN could dramatically alter the treatment algorithm. Underdiagnosis leads to multiple follow-up visits, and either delayed or progressed the lesion, exacerbating the potential harm to patients. Alternatively, overdiagnosis can result in unnecessary or premature treatment, especially in younger women, as inappropriate treatment significantly increases the risk of adverse outcomes in subsequent pregnancies (22). The majority of HSILs require surgery for the purpose of completely removing lesions, as well as prevent cancer, a small number of special conditions or periods (such as young or pregnant women) can be

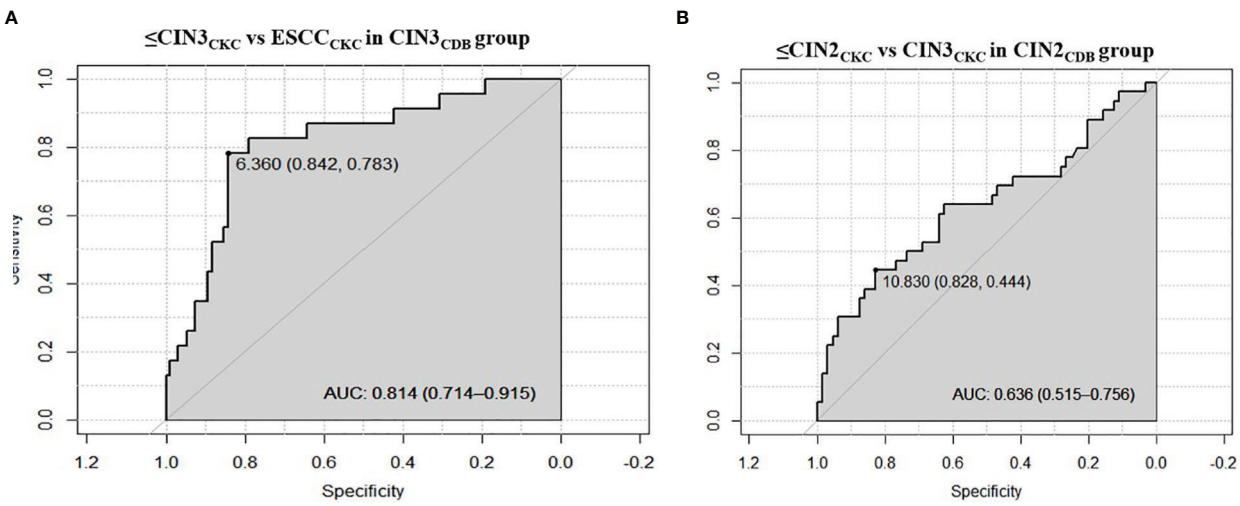

FIGURE 2
Receiver operating characteristic curves of performance of PAX1 methylation. **(A)** The optimal ΔCp_{PAX1}cut-off value in predicting whether CIN3 would be upgraded to ESCC after CKC; **(B)** The optimal ΔCp_{PAX1}cut-off value in predicting whether CIN2 would be upgraded to CIN3.

TABLE 3 The Performance of ΔCp_{PAX1} in predicting CIN2 upgrade to CIN3, and CIN3 upgrade to ESCC after conization.

Test	Sensitivity % (95%CI)	Specificity % (95%CI)	PPV % (95%CI)	NPV % (95%CI)	OR (95%CI)
$CIN2_{CDB}$ (n = 100)					
$CIN3+_{CKC}$ (n = 36)					
$\triangle Cp_{PAX1} \leq 10.83$	44.4 (27.9-61.9)	82.8 (71.3-91.1)	59.3 (43.2-73.6)	72.6 (65.9-78.4)	3.86 (1.53-9.71)
Cytology (ASCUS+)	44.4 (27.7-61.9)	45.3 (32.8-58.3)	31.4 (22.9-41.2)	59.2 (49.3-68.3)	0.66 (0.29-1.51)
hrHPV (+)	97.2 (85.5-99.9)	9.4 (3.5-19.3)	37.6 (35.4-39.9)	85.7 (42.9-98.0)	3.62 (0.42-31.34)
$CIN3_{CDB}$ (n = 118)					
$ESCC_{CKC}$ (n = 23)					
$\triangle Cp_{PAX1} \leq 6.36$	78.3 (56.3-92.6)	84.2 (75.3-90.9)	54.5 (41.8-66.7)	94.1 (88.0-97.2)	19.20 (6.18-59.67)
Cytology ≥ LSIL	78.3 (56.3-92.5)	58.9 (48.4-68.9)	31.6 (25.0-38.9)	91.8 (83.5-96.1)	5.17 (1.77-15.10)
HPV16/18 (+)	73.9 (51.6-89.8)	46.3 (36.0-56.8)	25.0 (19.7-31.2)	88.0 (78.1-93.8)	2.44 (0.89-6.74)

Estimated sensitivity and specificity of $PAX1^m$ at maximum value of Youden index.

given a short-term close follow-up (23). As recommended by the ASCCP2019 guidelines, CIN2 and CIN3 should be managed separately, and for patients with CIN 2 that are more concerned about the effects of treatment on a future pregnancy outweigh their concerns about cancer, observation without treatment is acceptable (24).

However, CIN2 and CIN3 diagnosed by CDB have limitations to some extent. For example, the diagnosis of CIN2 has historically been a gray area in pathology and it is difficult for pathologists to reproduce which might be overcalled CIN1 or under-called CIN3 (25). Some pathologists even use "CIN1–2 or CIN2–3" to equivocate the classification. Based on difficulties associated with receiving an accurate diagnosis, it is challenging to determine whether or when a patient with CIN3 will progress to invasive cervical cancer from an individual perspective. In fact, some patients may already have occult cervical cancer when diagnosed with HSIL. The rate of progression to invasive cancer after conization have been reported to be about 0.3%-15% (26–28). In our study, although none of the CIN2 cases progressed to invasive cancer, 36% of the women within the afore mentioned group did progress to CIN3, and progression to invasive cancer in the CIN3 group was as high as 20%. Relying on HPV testing alone cannot accurately predict the progression of cancer satisfactorily. A better prognostic risk evaluation for CIN2 and CIN3 is needed. The integration of molecular markers in cervical cancer screening, such as DNA methylation, might help avoid unnecessary referrals and repeatedly performing diagnostic procedures, which is a waste medical resources and generate needless worry for the patient and her family (29).

The PAX1 gene is located on chromosome 20p11 and consists of a paired domain (PD) and an octapeptide domain (OP). The expression PAX1 is associated with embryogenesis, especially the development of the skeleton, thymus, and the parathyroid glands (30, 31). In 2008, Lai et al. first reported that abnormal methylation of PAX1 was associated with cervical cancer, and that the PAX1 gene was found to be silenced by hyper-methylation and under-expressed in cervical cancer biopsies (8). PAX1 can regulate cell division and differentiation, and methylation and silencing of PAX1 is closely related to the progression of precancerous lesions into cervical cancer (32). It has been reported that the disruption between kinases and phosphatases caused by PAX1 methylation is involved in cervical carcinogenesis (33). An increasing number of studies have confirmed PAX1 methylation as a promising biomarker for cervical cancer based on its ability to discriminate between high-grade cervical lesions and normal tissues, resulting in a reduced necessity for colposcopy referral and biopsy (9, 10, 34). The current study demonstrated that the ΔCp_{PAX1} level of CIN3 determined by CDB was lower than that of CIN2 and the ΔCp_{PAX1} level of ESCC was lower than that of both CIN2 and CIN3. Regardless of CIN2 or CIN3 status, the ΔCp_{PAX1} level of women with upgraded pathology after conization was significantly lower than that of women with degraded pathology. We further stratified the $PAX1^m$ level by different thresholds and found that the risk of CIN3+ increased significantly when $\Delta Cp_{PAX1} < 7$. The optimal ΔCp_{PAX1} cut-off value in predicting whether CIN3 would be upgraded to ESCC, and whether CIN2 would be upgraded to CIN3 after CKC was

6.360 and 10.830, respectively, and is more specific than using with cytology or HPV abnormalities. This concept implies that if biopsy pathology indicates CIN2 status with a ΔCp_{PAX1} less than 10.83, then the actual pathology is more likely to be upgraded to CIN3, so it is necessary to be more careful if observation without treatment was selected. If biopsy pathology indicates CIN3 with a ΔCp_{PAX1} less than 6.36, then cervical conization is inevitable because of the increased risk of pathological upgrade to early-stage cervical cancer. On the other hand, women with negative PAX1 methylation do not need immediate colposcopy or conization because of there being a relatively low short-term progression risk for cancer. For young women with CIN2 who have fertility requirements, this approach seems to be particularly important, since only hypermethylated lesions require treatment and the risk of preterm abortion due to treatment could be reduced.

Limitation

This study has several limitations. First, since our research has not reached the follow-up endpoint, residual and recurrence of lesions have not been discussed here, and continued follow-up is needed in the future. Secondly, the sample size was not large enough and a larger longitudinal study is necessary to validate the natural history of CIN2 and CIN3 progression in relation to DNA methylation. Thirdly, only hospitalized patients with CKC were included in this study who can be followed up well, however, those patients for LEEP from outpatient were not included due to unstable follow-up. In addition, further studies are needed to explore $PAX1^m$ levels after treatment and to compare $PAX1^m$ changes before and after CKC. At last, further studies are also needed to determine the ideal interval of monitoring using $PAX1^m$ to avoid underdiagnosis and overdiagnosis.

Conclusions

In this exploratory study, we found that PAX1 methylation could be a promising auxiliary marker in the prediction of pathological upgrade risk in patients with CIN2 or CIN3 before conization, especially if $\triangle Cp_{PAX1}$ cut-off value is lower than 6.360, as we found this to be highly suggestive of invasive cervical cancer. Using PAX1 methylation as a monitoring tool could help prevent inappropriate conservative observation or ablation therapy. Further validation and prospective clinical trials are needed to confirm these findings in the future.

Data availability statement

The raw data supporting the conclusions of this article will be made available by the authors, without undue reservation.

Ethics statement

The studies involving human participants were reviewed and approved by Peking University People's Hospital Ethics Committee. The patients/participants provided their written informed consent to participate in this study.

Author contributions

Data collection, study conception, and study design was performed by ML. Personnel organization, data collection, and the cold knife conization procedure was performed by CZ. Sample collection was performed by YZ, JL, HL, ZT, JW and YG. Supervision of the research program and manuscript review and guidance during the study was provided by LW. The first draft of the manuscript was written by ML and all authors commented on previous versions of the manuscript. All authors read and approved the final manuscript.

Funding

This work was supported by The National Key Research and Development Program of China (2021YFC2701200) (2021YFC2701202) and Peking University People's Hospital Scientific Research Development Funds (RDL2020-02) (RDL2022-34).

Acknowledgments

Thanks to Hong Tao for statistics and interpretation of data, and Ching-Tung Yeh as well as Yu-ligh Liou for giving guidance and advice on statistics and interpretation of data.

Conflict of interest

The authors declare that the research was conducted in the absence of any commercial or financial relationships that could be construed as a potential conflict of interest.

Publisher's note

Supplementary material

The Supplementary Material for this article can be found online at: https://www.frontiersin.org/articles/10.3389/fonc.2022.1064722/full#supplementary-material

SUPPLEMENTARY FIGURE 1
Restricted cubic splines of odds ratio for CIN3+CKC according to ΔCp_{PAX1} levels in all participants.

References

1. World Health Organization. Female genital tumours. IARCpress. WHO classification of tumours. 5th Edition Volume 4[EB/OL]. (2020-09-09)[2021-01-25]. Available at: https: //tumourclassification.iarc.who.int/9789283245049.

2. Tainio K, Athanasiou A, Tikkinen K, Aaltonen R, Cardenas J, HernandesGlazer-Livson S, et al. Clinical course of untreated cervical intraepithelial neoplasia grade 2 under active surveillance: systematic review and meta-analysis. *BMJ* (2018) 360:k499. doi: 10.1136/bmj.k499

3. Jung Y, Lee AR, Lee SJ, Lee YS, Park DC, Park EK. Clinical factors that affect diagnostic discrepancy between colposcopically directed biopsies and loop electrosurgical excision procedure conization of the uterine cervix. *Obstet Gynecol Sci* (2018) 61(4):477–88. doi: 10.5468/ogs.2018.61.4.477

4. Louvanto K, Aro K, Nedjai B, Butzow R, Jakobsson M, Kalliala I, et al. Methylation in predicting progression of untreated high-grade cervical intraepithelial neoplasia. *Clin Infect Dis* (2020) 70(12):2582–90. doi: 10.1093/cid/ciz677

5. Guan P, Howell-Jones R, Li N, Bruni L, de Sanjose S, Franceschi S, et al. Human papillomavirus types in 115,789 HPV-positive women: a meta-analysis from cervical infection to cancer. *Int J Cancer* (2012) 131(10):2349–59. doi: 10.1002/ijc.27485

6. Moscicki AB, Ma Y, Wibbelsman C, Darragh TM, Powers A, Farhat S, et al. Rate of and risks for regression of cervical intraepithelial neoplasia 2 in adolescents and young women. *Obstet Gynecol* (2010) 116(6):1373–80. doi: 10.1097/AOG.0b013e3181fe777f

7. Steenbergen RD, Snijders PJ, Heideman DA, Meijer CJ. Clinical implications of (epi)genetic changes in HPV-induced cervical precancerous lesions. *Nat Rev Cancer* (2014) 14(6):395–405. doi: 10.1038/nrc3728

8. Lai HC, Lin YW, Huang TH, Yan P, Huang RL, Wang HC, et al. Identification of novel DNA methylation markers in cervical cancer. *Int J Cancer* (2008) 123(1):161–7. doi: 10.1002/ijc.23519

9. Luan T, Hua Q, Liu X, Xu P, Gu Y, Qian H, et al. PAX1 methylation as a potential biomarker to predict the progression of cervical intraepithelial neoplasia: A meta-analysis of related studies. *Int J Gynecol Cancer* (2017) 27(7):1480–8. doi: 10.1097/IGC.0000000000001011

10. Xu J, Xu L, Yang B, Wang L, Lin X, Tu H. Assessing methylation status of PAX1 in cervical scrapings, as a novel diagnostic and predictive biomarker, was closely related to screen cervical cancer. *Int J Clin Exp Pathol* (2015) 8(2):1674–81.

11. Li SR, Wang ZM, Wang YH, Wang XB, Zhao JQ, Xue HB, et al. Value of PAX1 methylation analysis by MS-HRM in the triage of atypical squamous cells of undetermined significance. *Asian Pac J Cancer Prev* (2015) 16(14):5843–6. doi: 10.7314/apjcp.2015.16.14.5843

12. Chang CL, Ho SC, Su YF, Juan YC, Huang CY, Chao AS, et al. DNA Methylation marker for the triage of hrHPV positive women in cervical cancer screening: Real-world evidence in Taiwan. *Gynecol Oncol* (2021) 161(2):429–35. doi: 10.1016/j.ygyno.2021.02.011

13. Li X, Zhou X, Zeng M, Zhou Y, Zhang Y, Liou YL, et al. Methylation of PAX1 gene promoter in the prediction of concurrent chemo-radiotherapy efficacy in cervical cancer. *J Cancer* (2021) 12(17):5136–43. doi: 10.7150/jca.57460

14. Zhao Z, Zhang X, Zhao X, Cai J, Wu NY, Wang J. SOX1 and PAX1 are hypermethylated in cervical adenocarcinoma and associated with better prognosis. *BioMed Res Int* (2020) 2020:3981529. doi: 10.1155/2020/3981529

15. Fu K, Lei M, Wu LS, Shi JC, Yang SY, Yang WQ, et al. Triage by PAX1 and ZNF582 methylation in women with cervical intraepithelial neoplasia grade 3: A multicenter case-control study. *Open Forum Infect Dis* (2022) 9(5):c13. doi: 10.1093/ofid/ofac013

16. Kan YY, Liou YL, Wang HJ, Chen CY, Sung LC, Chang CF, et al. PAX1 methylation as a potential biomarker for cervical cancer screening. *Int J Gynecol Cancer* (2014) 24(5):928–34. doi: 10.1097/IGC.0000000000000155

17. Wentzensen N, Massad LS, Mayeaux EJ, Khan MJ, Waxman AG, Einstein MH, et al. Evidence-based consensus recommendations for colposcopy practice for cervical cancer prevention in the united states. *J Low Genit Tract Dis* (2017) 21(4):216–22. doi: 10.1097/LGT.0000000000000322

18. Bornstein J, Bentley J, Bosze P, Girardi F, Haefner H, Menton M, et al. 2011 colposcopic terminology of the international federation for cervical pathology and colposcopy. *Obstet Gynecol* (2012) 120(1):166–72. doi: 10.1097/AOG.0b013e318254f90c

19. Darragh TM, Colgan TJ, Cox JT, Heller DS, Henry MR, Luff RD, et al. The Lower Anogenital SquamousTerminology standardization project for HPV-associated lesions:background and consensus recommendations from the College of American Pathologists and the American Society for Colposcopy andCervical Pathology. *J Low Genit Tract Dis* (2012) 16:20542.

20. Mercaldo ND, Lau KF, Zhou XH. Confidence intervals for predictive values with an emphasis to case-control studies. *Stat Med* (2007) 26(10):2170–83. doi: 10.1002/sim.2677

21. Xiao FY, Wang Q, Zheng RL, Chen M, Su TT, Sui L. [Diagnosis and treatment value of colposcopy and loop electrosurgical excision procedure in microinvasive cervical cancer: analysis of 135 cases]. *Zhonghua Fu Chan Ke Za Zhi* (2016) 51(3):186–91. doi: 10.3760/cma.j.issn.0529-567X.2016.03.005

22. Kyrgiou M, Athanasiou A, Kalliala I, Paraskevaidi M, Mitra A, Martin-Hirsch PP, et al. Obstetric outcomes after conservative treatment for cervical intraepithelial lesions and early invasive disease. *Cochrane Database Syst Rev* (2017) 11(11):CD012847. doi: 10.1002/14651858.CD012847

23. Massad LS, Einstein MH, Huh WK, Katki HA, Kinney WK, Schiffman M, et al. 2012 updated consensus guidelines for the management of abnormal cervical cancer screening tests and cancer precursors. *Obstet Gynecol* (2013) 121(4):829–46. doi: 10.1097/AOG.0b013e3182883a34

24. Perkins RB, Guido RS, Castle PE, Chelmow D, Einstein MH, Garcia F, et al. 2019 ASCCP risk-based management consensus guidelines for abnormal cervical cancer screening tests and cancer precursors. *J Low Genit Tract Dis* (2020) 24(2):102–31. doi: 10.1097/LGT.0000000000000525

25. Carreon JD, Sherman ME, Guillen D, Solomon D, Herrero R, Jeronimo J, et al. CIN2 is a much less reproducible and less valid diagnosis than CIN3: results from a histological review of population-based cervical samples. *Int J Gynecol Pathol* (2007) 26(4):441–6. doi: 10.1097/pgp.0b013e31805152ab

26. McIndoe WA, McLean MR, Jones RW, Mullins PR. The invasive potential of carcinoma *in situ* of the cervix. *Obstet Gynecol* (1984) 64(4):451–8.

27. Milojkovic M. Residual and recurrent lesions after conization for cervical intraepithelial neoplasia grade 3. *Int J Gynaecol Obstet* (2002) 76(1):49–53. doi: 10.1016/s0020-7292(01)00523-9

28. Temkin SM, Hellmann M, Lee YC, Abulafia O. Dysplastic endocervical curettings: a predictor of cervical squamous cell carcinoma. *Am J Obstet Gynecol* (2007) 196(5):461–9. doi: 10.1016/j.ajog.2006.11.018

29. Lai HC, Ou YC, Chen TC, Huang HJ, Cheng YM, Chen CH, et al. PAX1/SOX1 DNA methylation and cervical neoplasia detection: a Taiwanese gynecologic oncology group (TGOG) study. *Cancer Med* (2014) 3(4):1062–74. doi: 10.1002/cam4.253

30. Paixao-Cortes VR, Salzano FM, Bortolini MC. Origins and evolvability of the PAX family. *Semin Cell Dev Biol* (2015) 44:64–74. doi: 10.1016/j.semcdb.2015.08.014

31. Yamazaki Y, Urrutia R, Franco LM, Giliani S, Zhang K, Alazami AM, et al. PAX1 is essential for development and function of the human thymus. *Sci Immunol* (2020) 5(44):eaax1036. doi: 10.1126/sciimmunol.aax1036

32. Da SM, De Albuquerque B, Allyrio T, De Almeida VD, Cobucci R, Bezerra FL, et al. The role of HPV-induced epigenetic changes in cervical carcinogenesis (Review). *BioMed Rep* (2021) 15(1):60. doi: 10.3892/br.2021.1436

33. Su PH, Lai HC, Huang RL, Chen LY, Wang YC, Wu TI, et al. Paired box-1 (PAX1) activates multiple phosphatases and inhibits kinase cascades in cervical cancer. *Sci Rep* (2019) 9(1):9195. doi: 10.1038/s41598-019-45477-5

34. Fang C, Wang SY, Liou YL, Chen MH, Ouyang W, Duan KM. The promising role of PAX1 (aliases: HUP48, OFC2) gene methylation in cancer screening. *Mol Genet Genomic Med* (2019) 7(3):e506. doi: 10.1002/mgg3.506

frontiers | Frontiers in Oncology

TYPE Original Research
PUBLISHED 24 January 2023
DOI 10.3389/fonc.2023.1090092

OPEN ACCESS

EDITED BY
Sara Ricardo,
Universidade do Porto, Portugal

REVIEWED BY
Mikel Gorostidi,
University of the Basque Country, Spain
Marion Curtis,
Mayo Clinic Arizona, United States

*CORRESPONDENCE
Brooke L. Fridley
Brooke.Fridley@moffitt.org

†These authors have contributed equally to this work and share first authorship

SPECIALTY SECTION
This article was submitted to Gynecological Oncology, a section of the journal Frontiers in Oncology

RECEIVED 04 November 2022
ACCEPTED 06 January 2023
PUBLISHED 24 January 2023

CITATION
Abbas-Aghababazadeh F, Sasamoto N, Townsend MK, Huang T, Terry KL, Vitonis AF, Elias KM, Poole EM, Hecht JL, Tworoger SS and Fridley BL (2023) Predictors of residual disease after debulking surgery in advanced stage ovarian cancer.
Front. Oncol. 13:1090092.
doi: 10.3389/fonc.2023.1090092

Predictors of residual disease after debulking surgery in advanced stage ovarian cancer

Farnoosh Abbas-Aghababazadeh[1,2†], Naoko Sasamoto[3†], Mary K. Townsend[4], Tianyi Huang[5], Kathryn L. Terry[3], Allison F. Vitonis[3], Kevin M. Elias[3], Elizabeth M. Poole[6], Jonathan L. Hecht[7], Shelley S. Tworoger[4] and Brooke L. Fridley[1*]

[1]Department of Biostatistics & Bioinformatics, H. Lee Moffitt Cancer Center and Research Institute, Tampa, FL, United States, [2]University Health Network, Princess Margaret Cancer Center, Toronto, ON, Canada, [3]Department of Obstetrics and Gynecology, Brigham and Women's Hospital and Harvard Medical School, Boston, MA, United States, [4]Department of Cancer Epidemiology, H. Lee Moffitt Cancer Center and Research Institute, Tampa, FL, United States, [5]Department of Medicine, Channing Division of Network Medicine, Brigham and Women's Hospital, Boston, MA, United States, [6]Sanofi Genzyme, Global Medical Affairs, Cambridge, MA, United States, [7]Department of Pathology, Beth Israel Deaconess Medical Center, Boston, MA, United States

Objective: Optimal debulking with no macroscopic residual disease strongly predicts ovarian cancer survival. The ability to predict likelihood of optimal debulking, which may be partially dependent on tumor biology, could inform clinical decision-making regarding use of neoadjuvant chemotherapy. Thus, we developed a prediction model including epidemiological factors and tumor markers of residual disease after primary debulking surgery.

Methods: Univariate analyses examined associations of 11 pre-diagnosis epidemiologic factors (n=593) and 24 tumor markers (n=204) with debulking status among incident, high-stage, epithelial ovarian cancer cases from the Nurses' Health Studies and New England Case Control study. We used Bayesian model averaging (BMA) to develop prediction models of optimal debulking with 5x5-fold cross-validation and calculated the area under the curve (AUC).

Results: Current aspirin use was associated with lower odds of optimal debulking compared to never use (OR=0.52, 95%CI=0.31-0.86) and two tissue markers, ADRB2 (OR=2.21, 95%CI=1.23-4.41) and FAP (OR=1.91, 95%CI=1.24-3.05) were associated with increased odds of optimal debulking. The BMA selected aspirin, parity, and menopausal status as the epidemiologic/clinical predictors with the posterior effect probability ≥20%. While the prediction model with epidemiologic/clinical predictors had low performance (average AUC=0.49), the model adding tissue biomarkers showed improved, but weak, performance (average AUC=0.62).

Conclusions: Addition of ovarian tumor tissue markers to our multivariable prediction models based on epidemiologic/clinical data slightly improved the model performance, suggesting debulking status may be in part driven by tumor characteristics. Larger studies are warranted to identify those at high risk of poor surgical outcomes informing personalized treatment.

KEYWORDS

ovarian cancer, debulking, residual disease, prediction model, immunohistochemistry, tissue microarray

Introduction

Ovarian cancer has a 5-year survival <50%, as most cases are diagnosed at late stages (1). Optimal debulking with no or minimal residual disease during cytoreductive surgery is predictive of survival (2). Randomized trials showed 20% higher risk of death and 25% higher risk of progression among patients with residual tumor >10mm versus 1-10mm (3). Identifying women who may have poor surgical outcomes is critical to defining appropriate treatment, including use of neo-adjuvant chemotherapy to reduce tumor burden (4).

Studies of preoperative predictors of suboptimal debulking had not led to a reproducible model. For example, findings are mixed regarding the predictive value of preoperative blood CA125 (5) and radiologic features from computed tomography scans (6). Data is limited regarding epidemiologic factors related to debulking, with mixed results for obesity and hormone therapy (7, 8). Furthermore, prior studies observed that tumor molecular characteristics can predict residual disease, identifying gene expression signatures in migration, invasion, and stromal activation pathways (9–13). However, no studies to date have assessed a comprehensive prediction model for debulking outcomes. Thus, our objectives were to identify epidemiological characteristics and tumor markers associated with residual disease and build a prediction model of optimal debulking status after primary debulking surgery in treatment naïve, advanced stage, invasive epithelial ovarian cancer patients.

Materials and methods

The Nurses' Health Study (NHS) is a prospective cohort study established in 1976 enrolling 121,000 female nurses ages 30-55 years from 11 US states (14). NHSII was established in 1989 enrolling 116,429 female nurses ages 25-42 years from 14 US states (15). Women provided demographic, lifestyle, reproductive, and medical information biennially. Self-reported ovarian cancer diagnosis were confirmed by pathology report review (94%) or linkage to tumor registries. A gynecologic pathologist abstracted information from pathology and surgical reports on stage, histology, grade, and residual tumor (optimal debulking: residual tumor <2cm; suboptimal debulking: residual tumor ≥2cm; unknown). This definition was used because most cases were diagnosed when this threshold was used to define optimal debulking. The study protocol was approved by the institutional review boards of the Brigham and Women's Hospital and Harvard T.H. Chan School of Public Health, and those of participating registries as required.

The New England Case-Control Study (NECC) is a population-based case control study of ovarian cancer enrolling over three phases (1992-1997, 1998-2002, 2003-2008) from New Hampshire and Eastern Massachusetts (16); 2,203 (71%) of eligible cases identified using area hospital registries agreed to participate. Participants completed in-person interviews on demographics, lifestyle, reproductive factors, and medical history one year prior to ovarian cancer diagnosis. Surgical and pathological reports were reviewed to confirm diagnosis and abstract stage, histology, and grade. Optimal vs. suboptimal debulking was defined as residual disease <1cm vs. ≥1cm or unknown. The study was approved by the Institutional Review Board of Brigham and Women's Hospital, Boston, Massachusetts and Dartmouth College, Hanover, New Hampshire.

Epidemiologic factors included age (years, continuous), body mass index (BMI; kg/m^2, continuous), smoking (never, current, former), duration of smoking (pack-years, continuous), oral contraceptive use (OC; never, ever), parity (0, 1, 2+), menopausal status (premenopausal, postmenopausal never used hormone therapy [HT], postmenopausal ever used HT), aspirin use (never, current, past), family history of breast or ovarian cancer (no, yes), and history of hysterectomy, tubal ligation or Cesarean section (ever, never) at least one year before diagnosis.

Details on ovarian tumor block collection has been described previously (17). We retrieved formalin fixed paraffin embedded (FFPE) blocks with primary ovarian tumor from 631 invasive cases (330 NHS, 86 NHSII, 215 NECC). Blocks were reviewed for histology, invasiveness, and grade by a gynecologic pathologist, using 2014 WHO diagnostic criteria, circling areas of tumor for tissue microarrays (TMA) with two 1.0mm or three 0.6mm cores per case (17). We used histology, invasiveness, and grade from the slide review and record abstraction otherwise.

Immunohistochemistry (IHC) staining was performed on TMA slides within two weeks of sectioning (Supplementary Table S1). IHC markers, except pSMAD2/3, were evaluated by a gynecologic pathologist based on the proportion of cells staining positive (0-3+) or mutant/abnormal or wild type (TP53). For pSMAD 2/3, we assessed H-score (18) based on intensity and percent staining area, calculated *via* Definiens Tissue Studio v4.2 suite (Definiens Inc, Germany) with scans from Aperio™ ScanScope AT2 or AT Turbo (Leica Biosystems, Vista, CA) at Moffitt Cancer Center. All IHC markers were evaluated in the tumor epithelial component. For this study, we included IHC markers that have previously been reported to be associated with debulking status (i.e. ADH1B, COL11A1, CXCL14, FABP4, FAP, POSTN, pSmad2/3) and other IHC markers in which data were generated as part of pprior studies (i.e. ADRB2 (19), CD163 (20), CD68 (20), PTGS1 (20), PTGS2 (20), ESR1 (17, 21), ESR2n (22), MAPK (23), MUC1, MUC16, TP53 (23), PGR (17, 21), STAT1, VDRc, VDRn).

Statistical analysis

Imputation

Imputation of missing IHC scores was conducted using *k*-Nearest Neighbors (*k*NN; k=5) since some markers were missing in selected TMAs (Supplementary Figure S1). Imputed data had more symmetrical distribution and slightly higher median values versus observed data (Supplementary Figure S2).

Clinical and tissue biomarker predictors of debulking status

Mean and standard deviation (SD) for continuous variables and frequencies and percentage for categorical variables were used to summarize the predictors. Tissue markers were treated continuously. The primary outcome was coded as optimal versus suboptimal debulking. Analyses were conducted including all cases and restricted to type II ovarian tumors (high-grade serous, endometrioid, mixed or poorly differentiated, Transitional/Brenner,

carcinosarcoma) (24). Logistic regression was used to examine the association of epidemiologic characteristics and normalized IHC scores with debulking status, adjusting for study site (NECC, NHS/NHSII). Cox proportional hazards regression was used to assess the relationship of debulking status with overall survival to ensure the validity of our debulking measure.

Prediction modeling

Bayesian model averaging (BMA) with logistic regression was used to develop the prediction model for debulking status with only additive effects (i.e., no interaction effects) using the BMA R package (25). BMA was fit using five 5-fold cross-validations (CV), resulting in different training and test sets for each run to improve estimated performance. For each predictor, we present the average posterior mean (APM) and average posterior SD (APSD) across the five 5-fold CV. The receiver operating characteristics curve was calculated from the posterior probabilities. For each fold, we evaluated the discriminatory accuracy using the area under curve (AUC) and calculated the mean for each CV, and the overall AUC by averaging the average AUCs of the 5 CVs and computing the associated standard deviation (SD). We conducted BMA for epidemiological/clinical variables with debulking status (n=593). Then, after creating a single predictive score from the epidemiologic variables, we conducted BMA adding the tumor marker data. Analyses were performed using R, version 4.0.2.

Results

In NHS/NHSII, of the 1,550 incident invasive ovarian cancer cases (1,227 in NHS and 323 in NHSII) diagnosed from 1976-2017, we excluded those with unknown debulking status (n=1,307; 1,067 in NHS and 240 in NHSII) and stage I or II disease (n=75, 33 in NHS and 42 in NHSII). In NECC, of the 1,650 invasive epithelial ovarian cancer cases, we excluded those who did not have information on debulking status (n=1,054) and stage I or II disease (n=171) (Figure 1). As a result, the epidemiologic model included 593 invasive epithelial ovarian cancer cases (NHS=127, NHSII=41, NECC=425), of which 464 (78%) were optimally debulked (type II n=537 and 419 optimally debulked; Table 1). Average age at diagnosis was 56.9 years (SD 12.6) with the majority (>90%) being type II tumors. Characteristics of cases by debulking status were similar

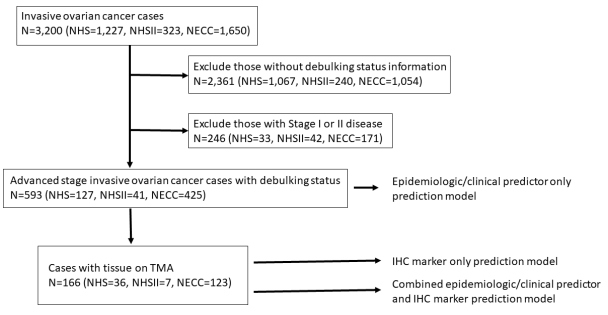

FIGURE 1
Flow chart of the exclusion criteria and study population included in the various prediction modeling.

(Supplementary Table S2). Cases with optimal versus suboptimal debulking had better overall survival (all: HR=0.60, 95%CI=0.48-0.75; type II: HR=0.63, 95%CI=0.50-0.80). Current vs. never aspirin use was significantly associated with lower odds of optimal debulking (OR=0.52, 95%CI=0.31-0.86), which remained significant for type II tumors (OR=0.47, 95%CI=0.28-0.81; Supplementary Table S3).

Tissue IHC markers were available in 166 cases with data on debulking status, of which 135 (81%) were optimally debulked. Distribution of clinical and epidemiologic characteristics were similar to all cases (Supplementary Table S4; Supplementary Table S5). ADRB2 (OR=2.21, 95%CI=1.23-4.41) and FAP (OR=1.91, 95% CI=1.24-3.05) were associated with optimal debulking (Figure 2). Results were similar for type II tumors (Supplementary Figure S3).

Prediction modeling of optimal debulking status using epidemiologic and clinical predictors

We first sought to develop a prediction model using epidemiologic and clinical predictors only. The BMA results for all models are presented in Supplemental File 1. Three predictors had a posterior effect probability ≥20% for selection into the prediction model: current vs. never aspirin use (APM=-0.12, APSD=0.21), parity=1 vs. nulliparous (APM=0.05, APSD=0.16), and postmenopausal ever HT vs. premenopausal (APM=0.05, APSD=0.12 (Figure 3A). For type II tumors, 3 predictors were identified (current aspirin use, APM=-0.18, APSD=0.28; smoking pack-years, APM=-0.001, APSD=0.002, and menopausal status/ever HT use, APM=0.04, APSD=0.15; Supplementary Figure S4). The mean AUC of 0.49 (SD 0.02) for all invasive ovarian cancer (Figure 3B) and 0.53 (SD 0.03) for type II tumors (Supplementary Figure S4).

Prediction modeling of optimal debulking status using tissue markers

Next, we developed a prediction model using tissue IHC markers only. There were 8 biomarkers with posterior effect probability of ≥20% including ESR1 and CD8+ T cells, which were associated with higher odds of optimal debulking (APM from -0.72 to 0.04), while p-SMAD2/3, PTGS2, and ADRB2 had lower odds of optimal debulking (APM of -0.72 to -0.02) (Figure 4A). For type II tumors, there were 7 biomarkers with positive posterior means (APM of 0.02 to 0.2) and 6 biomarkers with negative posterior means (APM of -0.14 to -0.02) (Supplementary Figure S5). These IHC markers resulted in a mean AUC of 0.62 (SD 0.03) for advanced stage invasive cases, and 0.47 (SD 0.1) for type II tumors (Figures 4B; Supplementary Figure S5).

Combined prediction model with epidemiologic variables and tissue biomarkers

Lastly, we developed a prediction model including both epidemiologic/clinical predictors and tissue biomarkers. Among the

TABLE 1 Association between demographic/clinical characteristics and debulking status (1=optimally debulked, 0 = sub-optimally debulked) among advanced stage invasive epithelial ovarian cancer cases in NHS/NHSII/NECC.

	Total (n=593)	Optimally debulked (n=464)	Sub-optimally Debulked (n=129)	OR (95% CI) optimally vs. sub-optimally debulked
Age at diagnosis (years), Mean (SD)	56.9 (12.6)	56.9 (12.6)	56.7(12.8)	1.00 (0.99 to 1.02)
BMI (kg/m^2), Mean (SD)	26.2 (5.7)	26.2 (5.7)	26.1 (5.6)	1.00 (0.97 to 1.04)
Smoking status, n (%)				
never	270 (45.5%)	213 (45.9%)	57 (44.2%)	1 (ref.)
current	87 (14.7%)	64 (13.8%)	23 (17.3%)	0.74 (0.43 to 1.32)
former	236 (39.8%)	187 (40.3%)	49 (38.0%)	1.02 (0.67 to 1.57)
Smoking (pack-years), Mean (SD)	11.7 (19.6)	11.2 (19.2)	13.5 (21.0)	1.00 (0.99 to 1.00)
Aspirin, n (%)				
never	391 (65.9%)	317 (68.3%)	74 (57.4%)	1 (ref.)
current	93 (15.7%)	64 (13.8%)	29 (22.5%)	0.52 (0.31 to 0.86)
past	109 (18.4%)	83 (17.9%)	26 (20.2%)	0.75 (0.45 to 1.25)
Oral Contraceptive use, n (%)				
never	294 (49.6%)	224 (48.3%)	70 (54.3%)	1 (ref.)
ever	299 (50.4%)	240 (51.7%)	59 (45.7%)	1.27 (0.86 to 1.88)
Parity, n (%)				
0	122 (20.6%)	97 (20.9%)	25 (19.4%)	1 (ref.)
1	60 (10.1%)	51 (11.0%)	9 (7.0%)	1.46 (0.65 to 3.52)
2 +	411 (69.3%)	316 (68.1%)	95 (73.6%)	0.86 (0.51 to 1.39)
Menopausal status, n (%)				
premenopausal	155 (26.1%)	120 (25.9%)	35 (27.1%)	1 (ref.)
postmenopausal never used PMH	242 (40.8%)	190 (40.9%)	52 (40.3%)	1.07 (0.65 to 1.73)
postmenopausal ever used PMH	196 (33.1%)	154 (33.2%)	42 (32.6%)	1.07 (0.64 to 1.78)
Family history of breast or ovarian cancer, n (%)				
No	512 (86.3%)	396 (85.3%)	116 (89.9%)	1 (ref.)
Yes	81 (13.7%)	68 (14.7%)	13 (10.1%)	1.53 (0.84 to 2.99)
History of surgery [a], n (%)				
Ever	206 (34.7%)	159 (34.3%)	47 (36.4%)	1 (ref.)
Never	387 (65.3%)	305 (65.7%)	82 (63.6%)	1.10 (0.73 to 1.65)
Tumor Type [b], n (%)				
type 1	56 (9.4%)	193 (27.7%)	11 (8.5%)	1 (ref.)
type 2	537 (90.6%)	504 (72.3%)	118 (91.5%)	0.87 (0.42 to 1.67)

BMI, Body mass index; CI, Confidence interval; NHS, Nurses' Health Study; NHSII, Nurses' Health Study II; NEC, New England Case-Control Study; OR, Odds ratio; PMH, postmenopausal hormone use.

All models were adjusted for study sites (NHS/NHSII and NEC). Odds ratios represent the odds of optimally debulked surgery.

(a) Cases with history of hysterectomy or tubal ligation or Cesarean section.

(b) Type 1 tumors: low-grade serous, mucinous, endometrioid, clear cell, low grade mixed; type 2 tumors: high-grade serous or poorly differentiated, Transitional/Brenner, Carcinosarcoma, high grade mixed.

10.3389/fonc.2023.1090092

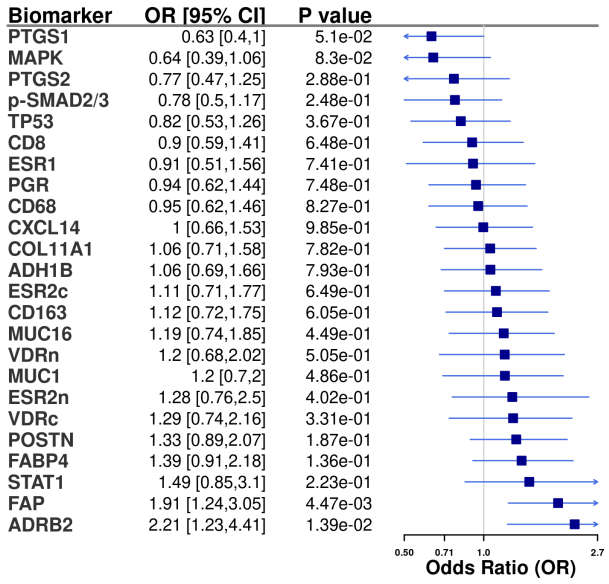

FIGURE 2
Tissue marker associations (odds ratio [OR] and 95% confidence intervals [CI]) with optimal debulking status among advanced stage invasive epithelial ovarian cancer cases in NHS/NHSII/NECC (n=166). All models were adjusted for study (NHS/NHSII and NEC). In the logistic regression models 1 = optimally debulked and 0 = sub-optimally debulked.

subset of cases with biomarker data, the model with only the clinical prediction score had a mean AUC of 0.58 (SD 0.07) for all cases and 0.62 (SD 0.01) for type II tumors. When tissue biomarkers were added, positive posterior mean was observed for 8 markers including ESR1 (APM=0.67, APSD=0.38) and CD8+ T cells (APM=0.03, APSD=0.12) and a negative posterior mean for p-SMAD2/3 (APM=-0.71, APSD=0.35) and PTGS2 (APM=-0.13, APSD=0.23) (Figure 5A). The clinical prediction score had an average posterior mean of 1.58 (APSD=7.94). The resultant mean AUC was 0.62 (SD 0.04) (Figure 5B). We observed similar results for type II tumors, although the model resulted in an AUC=0.47 (SD 0.1; Supplementary Figure S6).

Discussion

We simultaneously examined a wide range of potential epidemiologic and molecular predictors of optimal debulking in advanced stage invasive ovarian cancer patients undergoing primary debulking surgery in a population-based study. Relatively few epidemiologic predictors were identified, and they did not have predictive capacity. However, four tumor markers (POSTN, pSMAD2/3, CXCL14, ADH1B, FAP) that have previously been reported to predict suboptimal debulking were selected in our model, although only p-SMAD2/3 was in the same direction but with lower discriminatory performance compared to prior reports. Seven other tumor markers predicted optimal debulking. However, the multivariable prediction model showed discriminatory performance that is not clinically actionable.

Several studies have previously identified ovarian tumor tissue markers that predict debulking status (9–13), with some studies reporting high discriminatory performance (11–13). One recent study sought to validate 20 previously reported molecular signatures using gene expression data and all combinations resulted in poor performance with AUC < 0.65 (10), which is consistent with our observation of poor performance for a tissue marker only prediction model. Notably, the direction of association reported in prior gene expression studies often showed opposite associations using IHC markers as in our study (11, 12). This may be due to the use of protein markers, which do not always correlate with gene expression, and the use of a population-based sample in our study. It is unclear if the protein markers do not provide the same predictive capacity as gene expression or if the high dimensionality of gene expression data is led to overfitting of results. Overall, our work and others support that biologic features of the tumor may differ between optimally and sub-optimally debulked tumors.

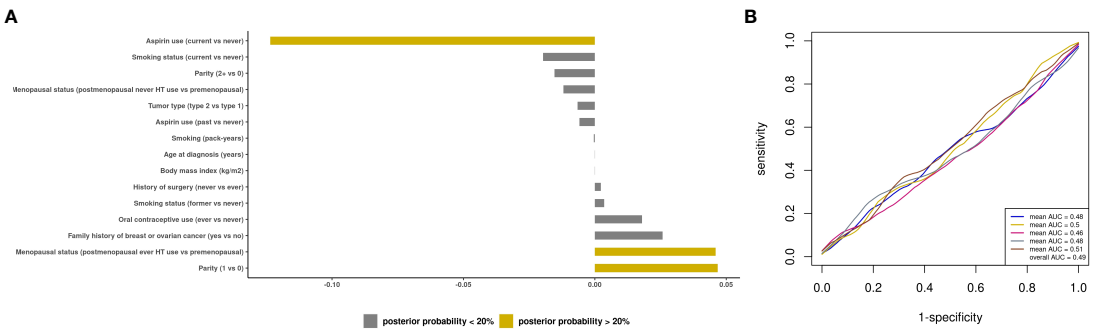

FIGURE 3
Prediction modeling of optimal debulking status using epidemiologic and clinical predictors. Average posterior means and associated average posterior probabilities of epidemiologic and clinical predictors being selected in the final prediction model of optimal debulking status and area under the curve (AUC) of the prediction models using Bayesian model averaging among invasive epithelial ovarian cancer cases (n=593) in NHS/NHSII/NEC. We assessed the posterior probability of 11 predictors for possible selection in the final model and conducted five 5-fold cross-validations. The bar chart **(A)** presents the average posterior mean across the 25 models that were run in total; grey bars denote predictors with average posterior probabilities <20% and yellow bars denote predictors with average posterior probability ≥ 20%. **(B)** presents the five average AUCs from the five 5-fold cross-validations and in the legend overall AUC, which is the average of the average AUCs from the 5-fold CV, is presented. Type 2 tumors include high-grade serous or poorly differentiated, Transitional/Brenner, Carcinosarcoma, high grade mixed histology.

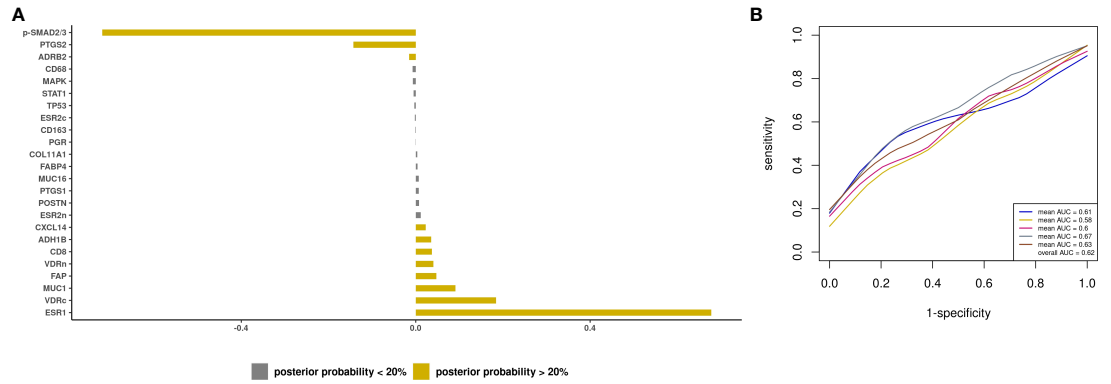

FIGURE 4
Prediction modeling of optimal debulking status using tissue markers. Average posterior means and associated average posterior probabilities of tissue markers being selected in the final prediction model of optimal debulking status and area under the curve (AUC) of the prediction models using Bayesian model averaging among invasive epithelial ovarian cancer cases (n=166) in NHS/NHSII/NEC. We assessed the posterior probability of 24 tissue marker predictors for possible selection in the final model and conducted five 5-fold cross-validations. The bar chart **(A)** presents the average posterior mean across the 25 models that were run in total; grey bars denote predictors with average posterior probabilities <20% and yellow bars denote predictors with average posterior probability ≥ 20%. **(B)** presents the five average AUCs from the five 5-fold cross-validations and in the legend overall AUC, which is the average of the average AUCs from the 5-fold CV, is presented.

Even though aspirin use has been associated with a lower ovarian cancer risk (26), pre-diagnostic current aspirin use was associated with decreased odds of optimal debulking. This is inconsistent with reported null associations between pre-diagnostic aspirin use and ovarian cancer survival (27). Complications during surgery may be one reason for this observation (10) as aspirin users may be more likely to develop hemorrhage-related surgical complications. Parous women had increased odds of optimal debulking, in line with studies reporting modest inverse associations between parity and ovarian cancer survival or risk of aggressive disease (28, 29). HT use also increased odds of optimal debulking, consistent with an international case-control consortium reporting that pre-diagnosis HT was associated with lower risk of having macroscopic residual disease and improved survival among postmenopausal patients (8). Interestingly, pre-diagnostic smoking was associated with decreased odds of optimal debulking among type II tumors, which is consistent its association with worse survival (30) and increased risk of aggressive rapidly fatal disease in high-grade serous tumors (29). Smoking increases systemic inflammation (31) and also has been reported to accelerate migration and invasion of ovarian cancer cells, promoting progression and metastasis (32), which may result in tumors that are more likely to be sub-optimally debulked. Future work, with larger sample sizes, should further explore these relationships to validate our observations.

With respect to the biomarkers, we identified new potential predictors of debulking, including CD8+ T cells and ESR1, which increased odds of optimal debulking. CD8+ T cell infiltration has been associated with improved ovarian cancer survival (33). It is possible that an immune-activated tumor microenvironment results in tumors that are easier to surgically resect, possibly by reducing

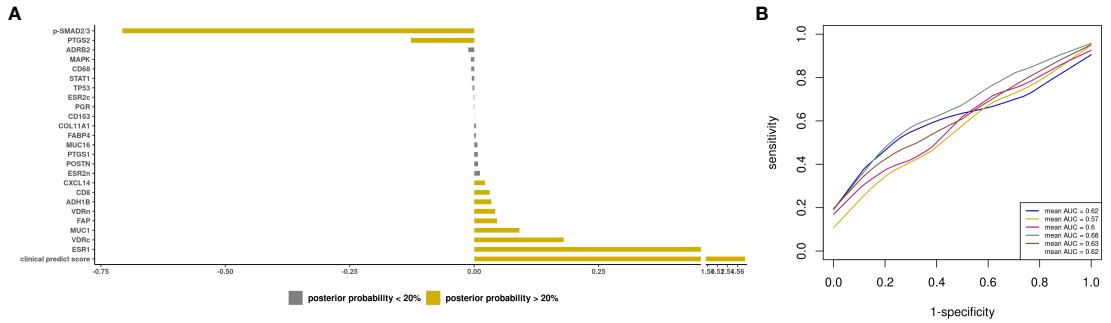

FIGURE 5
Prediction modeling of optimal debulking status using epidemiologic/clinical predictors and tissue markers. Average posterior means and associated average posterior probabilities of epidemiologic/clinical predictors and tissue markers being selected in the final prediction model of optimal debulking status and area under the curve (AUC) of the prediction models using Bayesian model averaging among invasive epithelial ovarian cancer cases (n=166) in NHS/NHSII/NEC. We assessed the posterior probability of 24 tissue markers in addition to our base model of clinical predict score, which included epidemiologic/clinical variables that had ≥ 20% posterior probability of being selected in the final prediction model of optimal debulking status (i.e. aspirin, parity, and menopausal status), for possible selection in the final model and conducted five 5-fold cross-validations. The bar chart **(A)** presents the average posterior mean across the 25 models that were run in total; grey bars denote predictors with average posterior probabilities <20% and yellow bars denote predictors with average posterior probability ≥ 20%. **(B)** presents the five average AUCs from the five 5-fold cross-validations and in the legend overall AUC, which is the average of the average AUCs from the 5-fold CV, is presented.

metastatic spread (34). ESR1 expression has been associated with improved ovarian cancer survival and lower risk of macroscopic residual disease in endometrioid tumors (35). Conversely, PTGS2 and ADRB2 were associated with lower odds of optimal debulking. Both PTGS2, which drives prostaglandin synthesis in the tumor microenvironment, and ADRB2 activation can increase cell migration, enhance cell survival (36), and promote cancer growth and metastasis (37). One study reported that concurrent increased expression of ADRB2 and PTGS2 in ovarian cancer was associated with poor survival (37), suggesting activation of this axis should be explored as a biological pathways driving disease spread, leading to residual disease. Additional large-scale, population-based studies are needed to evaluate the biologic differences between tumors that were optimally versus sub-optimally debulked and evaluate and validate the predictive capacity of these biomarkers above that of clinical and epidemiologic measures.

The strength of our study is that we had detailed epidemiologic/clinical and tumor tissue marker data and applied BMA to develop a multivariable prediction model. Limitations include the number of sub-optimally debulked patients and different definitions of optimal debulking across studies due to change in the criteria over time. We also were unable to evaluate complete cytoreductive surgery, although many prior studies used 1cm of residual disease as the cutoff for defining optimal debulking status. In NHS/NHSII and NECC, many ovarian cancer cases were missing data on debulking status (84% in NHS/NHSII; 64% in NECC), which may not be missing at random and possibly biased the observed results. However, the distribution of epidemiologic factors in our analytic sample were similar between those with and without data on debulking status, suggesting a representative sample. Furthermore, there could be reporting bias of debulking status particularly as many women in NHS/NHSII were treated in community settings, which may explain the high percentage of optimally debulked cases (83%) in our study compared to prior studies (range~40%-90%) (38), although debulking status was strongly associated with survival in our population. In NECC, nearly all cases received surgical care by subspecialist gynecologic oncologists at tertiary academic hospitals, likely leading to improved surgical outcomes (39). Our study was limited by not have an independent validation cohort to validate our prediction models, so conducted internal validation using 5x5-fold cross-validation. We did not have a measure of surgical skills by individual surgeons, which may vary widely due to the population-based nature of our study, or detailed laparoscopic data on tumor spread, both of which have been shown to be related to debulking status. While there were some IHC markers that are known to be more present in the stromal component (e.g. POSTN, COL11A1), our ovarian TMA was created to maximize the tumor epithelial tissue and the IHC scoring was based on the expression in the tumor epithelial compartment. Further studies are necessary to evaluate protein expression in the stromal compartments. Finally, we could not study laparoscopy-based scores, which have reported discriminatory performance ranging widely (AUCs~0.69-0.98), depending on outcome definition (complete and/or optimal cytoreduction) and the proportion of cases undergoing neo-adjuvant chemotherapy (40). Adding molecular factors to existing laparoscopy-based scores could enhance discriminatory ability in the primary debulking setting, which is most critical time to determine the need for neoadjuvant chemotherapy.

Overall, combining information on ovarian tumor tissue markers and epidemiologic/clinical data led to the best model performance, although it is not yet clinically actionable. Our results further support that debulking status may be in part driven by tumor characteristics. Future studies are warranted to validate our findings and integrate these variables into currently used clinical models based on disease spread to identify those at high risk of poor surgical outcomes, which will inform personalized treatment for ovarian cancer.

Data availability statement

The datasets presented in this article are not publicly available because of participant confidentiality and privacy concerns. Further information including the procedures to obtain and access data from the Nurses' Health Studies is described at https://www.nurseshealthstudy.org/researchers (contact email: nhsaccess@channing.harvard.edu). The NEC data that support the findings of this study are available upon request and review by study leadership.

Ethics statement

The study protocol was approved by the institutional review boards of the Brigham and Women's Hospital and Harvard T.H. Chan School of Public Health, and those of participating registries as required. The patients/participants provided informed consent to participate in the study.

Author contributions

FA-A: Conceptualization, Data curation, Formal analysis, Writing-Original draft, Writing – review & editing. NS: Conceptualization, Data curation, Writing-Original draft, Writing – review & editing. MT: Data curation, Writing – review & editing. TH: Data curation, Writing – review & editing. KT: Data curation, Writing – review & editing. AV: Data curation, Writing – review & editing. KE: Writing – review & editing. EP: Funding acquisition, Data curation, Writing – review & editing. JH: Data curation, Writing – review & editing. ST: Conceptualization, Funding acquisition, Supervision, Writing – review & editing. BF: Conceptualization, Methodology, Supervision, Writing – review & editing. All authors contributed to the article and approved the submitted version.

Funding

This study was funded by the National Cancer Institute grants UM1 CA186107, P01 CA87969, U01 CA176726, R01 CA054419, P50 CA105009, and the Marsha Rivkin Center for Ovarian Cancer Research Skacel Family Scholar Award. NS was supported by the Department of Defense award W81XWH-21-1-0320 and Marsha Rivkin Center for Ovarian Cancer Research Rivkin Scientific Scholars

Award. The content is solely the responsibility of the authors and does not necessarily represent the official views of the National Institutes of Health. Dana-Farber/Harvard Cancer Center is supported in part by an NCI Cancer Center Support Grant # NIH 5 P30 CA06516. This work has been supported in part by the Biostatistics and Bioinformatics Shared Resource and the Analytic Microscopy Core Facility at the H. Lee Moffitt Cancer Center & Research Institute, an NCI designated Comprehensive Cancer Center (P30-CA076292).

Acknowledgments

The authors would like to acknowledge the contribution to this study from central cancer registries supported through the Centers for Disease Control and Prevention's National Program of Cancer Registries (NPCR) and/or the National Cancer Institute's Surveillance, Epidemiology, and End Results (SEER) Program. Central registries may also be supported by state agencies, universities, and cancer centers. Participating central cancer registries include the following: Alabama, Alaska, Arizona, Arkansas, California, Colorado, Connecticut, Delaware, Florida, Georgia, Hawaii, Idaho, Indiana, Iowa, Kentucky, Louisiana, Massachusetts, Maine, Maryland, Michigan, Mississippi, Montana, Nebraska, Nevada, New Hampshire, New Jersey, New Mexico, New York, North Carolina, North Dakota, Ohio, Oklahoma, Oregon, Pennsylvania, Puerto Rico, Rhode Island, Seattle SEER Registry, South Carolina, Tennessee, Texas, Utah, Virginia, West Virginia, Wyoming. We thank Dana-Farber/Harvard Cancer Center in Boston, MA, for the use of the Specialized Histopathology Core, which provided histology and immunohistochemistry service.

Conflict of interest

NS reports grants from NCI, DOD, Marsha Rivkin Center for Ovarian Cancer Research. TH report grants from NHLBI. KLT reports grants from NIH. KE reports funding from Abcam; royalties from Aspira Women's Health; consultant of Bluestar Genomics; personal fees from Expert Institute; and is a member of the Enhanced Recovery After Surgery USA unpaid. EP reports grants from NIH. SST reports grants from NIH/NCI, DOD, Rivkin Center, State of Florida, BMS; personal fees from AACR, Ponce Health Science University, Ovarian Cancer Research Alliance, German Cancer Research Center, Harvard T.H. Chan School of Public Health, and NIH outside of submitted work; and is a member of external advisory committee of California Teachers Study City of Hope and The Tomorrow Project Alberta Cancer Center.

The remaining authors declare that the research was conducted in the absence of any commercial or financial relationships that could be construed as a potential conflict of interest.

Publisher's note

Supplementary material

The Supplementary Material for this article can be found online at: https://www.frontiersin.org/articles/10.3389/fonc.2023.1090092/full#supplementary-material

SUPPLEMENTARY FIGURE 1
Aggregation plots show all combinations of missing (yellow) and non-missing (blue) values across biomarkers, from the highest to lowest frequency among Invasive epithelial ovarian cancer cases in **(A)** NECC and **(B)** NHS/NHSII. Imputation was conducted using *k*-Nearest Neighbors (*k*NN; k=5) with the *VIM* R package. Data were assumed to be missing at random or completely at random. To avoid scaling issues and ensure comparability across markers and studies, we applied *z*-score transformation. The horizontal bars to the right of the grid show the frequencies of the corresponding combinations, while the vertical bars on top of it present the proportions of missing values in each variable.

SUPPLEMENTARY FIGURE 2
Box plots represent the distribution of average immunohistochemistry (IHC) scores before (top row) and after (bottom row) applying imputation method among the invasive epithelial ovarian cancer cases in **(A)** NECC and **(B)** NHS/NHSII.

SUPPLEMENTARY FIGURE 3
Tissue marker associations (odds ratio [OR] and 95% confidence intervals [CI]) with optimal debulking status among invasive epithelial ovarian cancer cases in NHS/NHSII/NECC (n=204) in Type 2 tumors. All models were adjusted for study (NHS/NHSII and NEC). In the logistic regression models 1 = optimally debulked and 0 = sub-optimally debulked. Type 2 tumors include high-grade serous or poorly differentiated, Transitional/Brenner, Carcinosarcoma, high grade mixed histology.

SUPPLEMENTARY FIGURE 4
Prediction modeling of optimal debulking status using epidemiologic and clinical predictors in Type 2 tumors. Average posterior means and associated average posterior probabilities of epidemiologic and clinical predictors being selected in the final prediction model of optimal debulking status and area under the curve (AUC) of the prediction models using Bayesian model averaging among invasive epithelial ovarian cancer cases (n=537) in NHS/NHSII/NEC. We assessed the posterior probability of 11 predictors for possible selection in the final model and conducted five 5-fold cross-validations. The bar chart **(A)** presents the average posterior mean across the 25 models that were run in total; grey bars denote predictors with average posterior probabilities <20% and yellow bars denote predictors with average posterior probability ≥ 20%. **(B)** presents the five average AUCs from the five 5-fold cross-validations and in the legend overall AUC, which is the average of the average AUCs from the 5-fold CV, is presented. Type 2 tumors include high-grade serous or poorly differentiated, Transitional/Brenner, Carcinosarcoma, high grade mixed histology.

SUPPLEMENTARY FIGURE 5
Prediction modeling of optimal debulking status using tissue markers in Type 2 tumors. Average posterior means and associated average posterior probabilities of tissue markers being selected in the final prediction model of optimal debulking status and area under the curve (AUC) of the prediction models using Bayesian model averaging among invasive epithelial ovarian cancer cases (n=150) in NHS/NHSII/NEC. We assessed the posterior probability of 24 tissue marker predictors for possible selection in the final model and conducted five 5-fold cross-validations. The bar chart **(A)** presents the average posterior mean across the 25 models that were run in total; grey bars denote predictors with average posterior probabilities <20% and yellow bars denote predictors with average posterior probability ≥ 20%. **(B)** presents the five average AUCs from the five 5-fold cross-validations and in the legend overall AUC, which is the average of the average AUCs from the 5-fold CV, is presented. Type 2 tumors include high-grade serous or poorly differentiated, Transitional/Brenner, Carcinosarcoma, high grade mixed histology.

SUPPLEMENTARY FIGURE 6

Prediction modeling of optimal debulking status using epidemiologic/clinical predictors and tissue markers in Type 2 tumors. Average posterior means and associated average posterior probabilities of epidemiologic/clinical predictors and tissue markers being selected in the final prediction model of optimal debulking status and area under the curve (AUC) of the prediction models using Bayesian model averaging among invasive epithelial ovarian cancer cases (n=150) in NHS/NHSII/NEC. We assessed the posterior probability of 24 tissue markers in addition to our base model of clinical predict score, which included epidemiologic/clinical variables that had ≥ 20% posterior probability of being selected in the final prediction model of optimal debulking status (i.e. aspirin, pack-years of smoking, and menopausal status), for possible selection in the final model and conducted five 5-fold cross-validations. The bar chart **(A)** presents the average posterior mean across the 25 models that were run in total; grey bars denote predictors with average posterior probabilities <20% and yellow bars denote predictors with average posterior probability ≥ 20%. **(B)** presents the five average AUCs from the five 5-fold cross-validations and in the legend overall AUC, which is the average of the average AUCs from the 5-fold CV, is presented. Type 2 tumors include high-grade serous or poorly differentiated, Transitional/Brenner, Carcinosarcoma, high grade mixed histology.

References

1. American Cancer Society. *Cancer facts & figures 2021*. Atlanta: American Cancer Society, American Cancer Society (2021).

2. Elattar A, Bryant A, Winter-Roach BA, Hatem M, Naik R. Optimal primary surgical treatment for advanced epithelial ovarian cancer. *Cochrane Database Syst Rev* (2011) 8): CD007565. doi: 10.1002/14651858.CD007565.pub2

3. du Bois A, Reuss A, Pujade-Lauraine E, Harter P, Ray-Coquard I, Pfisterer J. Role of surgical outcome as prognostic factor in advanced epithelial ovarian cancer: a combined exploratory analysis of 3 prospectively randomized phase 3 multicenter trials: by the arbeitsgemeinschaft gynaekologische onkologie studiengruppe ovarialkarzinom (AGO-OVAR) and the groupe d'Investigateurs nationaux pour les etudes des cancers de l'Ovaire (GINECO). *Cancer* (2009) 115(6):1234–44. doi: 10.1002/cncr.24149

4. Wright AA, Bohlke K, Armstrong DK, Bookman MA, Cliby WA, Coleman RL, et al. Neoadjuvant chemotherapy for newly diagnosed, advanced ovarian cancer: Society of gynecologic oncology and American society of clinical oncology clinical practice guideline. *J Clin Oncol* (2016) 34(28):3460–73. doi: 10.1200/jco.2016.68.6907

5. Kang S, Kim TJ, Nam BH, Seo SS, Kim BG, Bae DS, et al. Preoperative serum CA-125 levels and risk of suboptimal cytoreduction in ovarian cancer: a meta-analysis. *J Surg Oncol* (2010) 101(1):13–7. doi: 10.1002/jso.21398

6. Rutten MJ, van de Vrie R, Bruining A, Spijkerboer AM, Mol BW, Kenter GG, et al. Predicting surgical outcome in patients with international federation of gynecology and obstetrics stage III or IV ovarian cancer using computed tomography: a systematic review of prediction models. *Int J Gynecol Cancer* (2015) 25(3):407–15. doi: 10.1097/igc.0000000000000368

7. Fotopoulou C, Richter R, Braicu EI, Kuhberg M, Feldheiser A, Schefold JC, et al. Impact of obesity on operative morbidity and clinical outcome in primary epithelial ovarian cancer after optimal primary tumor debulking. *Ann Surg Oncol* (2011) 18 (9):2629–37. doi: 10.1245/s10434-011-1637-z

8. Brieger KK, Peterson S, Lee AW, Mukherjee B, Bakulski KM, Alimujiang A, et al. Menopausal hormone therapy prior to the diagnosis of ovarian cancer is associated with improved survival. *Gynecol Oncol* (2020) 158(3):702–9. doi: 10.1016/j.ygyno.2020.06.481

9. Torres D, Kumar A, Bakkum-Gamez JN, Weaver AL, McGree ME, Wang C, et al. Mesenchymal molecular subtype is an independent predictor of severe postoperative complications after primary debulking surgery for advanced ovarian cancer. *Gynecol Oncol* (2019) 152(2):223–7. doi: 10.1016/j.ygyno.2018.11.019

10. Heitz F, Kommoss S, Tourani R, Grandelis A, Uppendahl L, Aliferis C, et al. Dilution of molecular-pathologic gene signatures by medically associated factors might prevent prediction of resection status after debulking surgery in patients with advanced ovarian cancer. *Clin Cancer Res* (2020) 26(1):213–9. doi: 10.1158/1078-0432.CCR-19-1741

11. Liu Z, Beach JA, Agadjanian H, Jia D, Aspuria PJ, Karlan BY, et al. Suboptimal cytoreduction in ovarian carcinoma is associated with molecular pathways characteristic of increased stromal activation. *Gynecol Oncol* (2015) 139(3):394–400. doi: 10.1016/j.ygyno.2015.08.026

12. Tucker SL, Gharpure K, Herbrich SM, Unruh AK, Nick AM, Crane EK, et al. Molecular biomarkers of residual disease after surgical debulking of high-grade serous ovarian cancer. *Clin Cancer Res* (2014) 20(12):3280–8. doi: 10.1158/1078-0432.CCR-14-0445

13. Riester M, Wei W, Waldron L, Culhane AC, Trippa L, Oliva E, et al. Risk prediction for late-stage ovarian cancer by meta-analysis of 1525 patient samples. *J Natl Cancer Institute* (2014) 106(5). doi: 10.1093/jnci/dju048

14. Colditz GA, Hankinson SE. The nurses' health study: lifestyle and health among women. *Nat Rev Cancer* (2005) 5(5):388–96. doi: 10.1038/nrc1608

15. Rockhill B, Willett WC, Hunter DJ, Manson JE, Hankinson SE, Spiegelman D, et al. Physical activity and breast cancer risk in a cohort of young women. *J Natl Cancer Institute* (1998) 90(15):1155–60. doi: 10.1093/jnci/90.15.1155

16. Vitonis AF, Titus-Ernstoff L, Cramer DW. Assessing ovarian cancer risk when considering elective oophorectomy at the time of hysterectomy. *Obstetr Gynecol* (2011) 117(5):1042–50. doi: 10.1097/AOG.0b013e318212fcb7

17. Shafrir AL, Rice MS, Gupta M, Terry KL, Rosner BA, Tamimi RM, et al. The association between reproductive and hormonal factors and ovarian cancer by estrogen-alpha and progesterone receptor status. *Gynecol Oncol* (2016) 143(3):628–35. doi: 10.1016/j.ygyno.2016.09.024

18. Goulding H, Pinder S, Cannon P, Pearson D, Nicholson R, Snead D, et al. A new immunohistochemical antibody for the assessment of estrogen receptor status on routine formalin-fixed tissue samples. *Hum Pathol* (1995) 26(3):291–4. doi: 10.1016/0046-8177(95)90060-8

19. Huang T, Tworoger SS, Hecht JL, Rice MS, Sood AK, Kubzansky LD, et al. Association of ovarian tumor β2-adrenergic receptor status with ovarian cancer risk factors and survival. *Cancer Epidemiol Biomarkers Prevention: Publ Am Assoc Cancer Res Cosponsored Am Soc Prev Oncol* (2016) 25(12):1587–94. doi: 10.1158/1055-9965.EPI-16-0534

20. Barnard ME, Hecht JL, Rice MS, Gupta M, Harris HR, Eliassen AH, et al. Anti-inflammatory drug use and ovarian cancer risk by COX1/COX2 expression and infiltration of tumor-associated macrophages. *Cancer Epidemiol Biomarkers Prev* (2018) 27(12):1509–17. doi: 10.1158/1055-9965.EPI-18-0346

21. Hecht JL, Kotsopoulos J, Hankinson SE, Tworoger SS. Relationship between epidemiologic risk factors and hormone receptor expression in ovarian cancer: results from the nurses' health study. *Cancer Epidemiol Biomarkers Prev* (2009) 18(5):1624–30. doi: 10.1158/1055-9965.Epi-08-1214

22. Shafrir AL, Babic A, Gates Kuliszewski M, Rice MS, Townsend MK, Hecht JL, et al. Estrogen receptor-β expression of ovarian tumors and its association with ovarian cancer risk factors. *Cancer Epidemiol Biomarkers Prev* (2020) 29(11):2211–9. doi: 10.1158/1055-9965.Epi-20-0618

23. Harris HR, Rice MS, Shafrir AL, Poole EM, Gupta M, Hecht JL, et al. Lifestyle and reproductive factors and ovarian cancer risk by p53 and MAPK expression. *Cancer Epidemiol Biomarkers Prev* (2018) 27(1):96–102. doi: 10.1158/1055-9965.EPI-17-0609

24. Kurman RJ, Shih Ie M. The origin and pathogenesis of epithelial ovarian cancer: a proposed unifying theory. *Am J Surg Pathol* (2010) 34(3):433–43. doi: 10.1097/PAS.0b013e3181cf3d79

25. Hoeting JA, Madigan D, Raftery AE, Volinsky CT. Bayesian Model averaging: A tutorial. *Stat Sci* (1999) 14(4):382–417.

26. Trabert B, Poole EM, White E, Visvanathan K, Adami HO, Anderson GL, et al. Analgesic use and ovarian cancer risk: An analysis in the ovarian cancer cohort consortium. *J Natl Cancer Institute* (2019) 111(2):137–45. doi: 10.1093/jnci/djy100

27. Dixon SC, Nagle CM, Wentzensen N, Trabert B, Beeghly-Fadiel A, Schildkraut JM, et al. Use of common analgesic medications and ovarian cancer survival: results from a pooled analysis in the ovarian cancer association consortium. *Br J Cancer* (2017) 116 (9):1223–8. doi: 10.1038/bjc.2017.68

28. Poole EM, Merritt MA, Jordan SJ, Yang HP, Hankinson SE, Park Y, et al. Hormonal and reproductive risk factors for epithelial ovarian cancer by tumor aggressiveness. *Cancer Epidemiol Biomarkers Prev* (2013) 22(3):429–37. doi: 10.1158/1055-9965.Epi-12-1183-t

29. Fortner RT, Poole EM, Wentzensen NA, Trabert B, White E, Arslan AA, et al. Ovarian cancer risk factors by tumor aggressiveness: An analysis from the ovarian cancer cohort consortium. *Int J Cancer* (2019) 145(1):58–69. doi: 10.1002/ijc.32075

30. Praestegaard C, Jensen A, Jensen SM, Nielsen TS, Webb PM, Nagle CM, et al. Cigarette smoking is associated with adverse survival among women with ovarian cancer: Results from a pooled analysis of 19 studies. *Int J Cancer* (2017) 140(11):2422–35. doi: 10.1002/ijc.30600

31. Shiels MS, Katki HA, Freedman ND, Purdue MP, Wentzensen N, Trabert B, et al. Cigarette smoking and variations in systemic immune and inflammation markers. *J Natl Cancer Institute* (2014) 106(11). doi: 10.1093/jnci/dju294

32. Jeon SY, Go RE, Heo JR, Kim CW, Hwang KA, Choi KC. Effects of cigarette smoke extracts on the progression and metastasis of human ovarian cancer cells *via* regulating epithelial-mesenchymal transition. *Reprod Toxicol* (2016) 65:1–10. doi: 10.1016/j.reprotox.2016.06.012

33. Goode EL, Block MS, Kalli KR, Vierkant RA, Chen W, Fogarty ZC, et al. Dose-response association of CD8+ tumor-infiltrating lymphocytes and survival time in high-grade serous ovarian cancer. *JAMA Oncol* (2017) 3(12):e173290. doi: 10.1001/jamaoncol.2017.3290

34. Zhang AW, McPherson A, Milne K, Kroeger DR, Hamilton PT, Miranda A, et al. Interfaces of malignant and immunologic clonal dynamics in ovarian cancer. *Cell* (2018) 173(7):1755–1769.e22. doi: 10.1016/j.cell.2018.03.073

35. Sieh W, Köbel M, Longacre TA, Bowtell DD, deFazio A, Goodman MT, et al. Hormone-receptor expression and ovarian cancer survival: an ovarian tumor tissue analysis consortium study. *Lancet Oncol* (2013) 14(9):853–62. doi: 10.1016/s1470-2045(13)70253-5

36. Carter LE, Cook DP, Collins O, Gamwell LF, Dempster HA, Wong HW, et al. COX2 is induced in the ovarian epithelium during ovulatory wound repair and promotes cell survival†. *Biol Reprod* (2019) 101(5):961–74. doi: 10.1093/biolre/ioz134

37. Nagaraja AS, Dorniak PL, Sadaoui NC, Kang Y, Lin T, Armaiz-Pena G, et al. Sustained adrenergic signaling leads to increased metastasis in ovarian cancer *via* increased PGE2 synthesis. *Oncogene* (2016) 35(18):2390–7. doi: 10.1038/onc.2015.302

38. Fagotti A, Ferrandina G, Vizzielli G, Fanfani F, Gallotta V, Chiantera V, et al. Phase III randomised clinical trial comparing primary surgery versus neoadjuvant chemotherapy in advanced epithelial ovarian cancer with high tumour load (SCORPION trial): Final analysis of peri-operative outcome. *Eur J Cancer* (2016) 59:22–33. doi: 10.1016/j.ejca.2016.01.017

39. Stewart SL, Cooney D, Hirsch S, Westervelt L, Richards TB, Rim SH, et al. The effect of gynecologic oncologist availability on ovarian cancer mortality. *World J Obstet Gynecol* (2014) 3(2):71–7. doi: 10.5317/wjog.v3.i2.71

40. Engbersen MP, Lahaye MJ, Lok CAR, Koole SN, Sonke GS, Beets-Tan RGH, et al. Peroperative scoring systems for predicting the outcome of cytoreductive surgery in advanced-stage ovarian cancer - a systematic review. *Eur J Surg Oncol* (2021) 47(8):1856–61. doi: 10.1016/j.ejso.2021.03.233

Frontiers in Oncology

Advances knowledge of carcinogenesis and tumor progression for better treatment and management

The third most-cited oncology journal, which highlights research in carcinogenesis and tumor progression, bridging the gap between basic research and applications to imrpove diagnosis, therapeutics and management strategies.

Discover the latest Research Topics

See more →

Frontiers

Avenue du Tribunal-Fédéral 34
1005 Lausanne, Switzerland
frontiersin.org

Contact us

+41 (0)21 510 17 00
frontiersin.org/about/contact